Phytoplankton ecology and biogeochemistry of the warming Antarctic sea-ice zone

Amber Luella Annett

A dissertation submitted for the degree of

Doctor of Philosophy

School of GeoSciences

The University of Edinburgh

2013

Declaration

I certify that the work described in this thesis is my own, except where otherwise stated, and has not been previously submitted for any other degree at this, or any other university.

Amber Luella Annett

Abstract

Marine productivity along the western Antarctic Peninsula (WAP) is declining. The WAP is site of the fastest regional warming in the southern hemisphere, and has experienced atmospheric and oceanic temperature increases leading to increased glacial inputs and reduced winter sea-ice cover. Sea-ice is a key link between climate and phytoplankton production, as melting sea-ice stratifies the water column and provides a source of micronutrients to surface waters. Reductions in ice cover have been accompanied by declining chlorophyll (chl; a proxy for phytoplankton biomass), and a shift to smaller cell sizes in phytoplankton communities. These reductions have implications for carbon drawdown and production available to higher trophic levels. However, little is known about phytoplankton shifts at the community level, as existing studies are based on satellite records and photosynthetic pigment analyses.

To elucidate the nature of the changes within phytoplankton assemblages, high-resolution time-series data of diatom speciation are coupled to environmental data from five years in Ryder Bay (Adelaide Island, WAP). Long-term monitoring at this site by the British Antarctic Survey has identified a strong relationship between chl and water column stratification, and this study spans a wide range of physical conditions and biological production. By comparing high- and low-chl phytoplankton assemblages, this study investigates the mechanisms underlying productivity changes and the manner in which these changes impact nutrient cycling, drawdown and trophic transfer.

The results presented here are the first full season *in-situ* records documenting differences in phytoplankton and diatom assemblages between high- and low-chl years. The primary difference between chl conditions is a dramatic

decline in diatom abundance. This analysis indicates that the mechanism producing low-chl seasons is less stratified surface waters, where light levels are much more variable than in high-chl years. Overall production is reduced, and small increases are seen in biomass of prymnesiophytes, which are better adapted to variable light. These shifts in phytoplankton composition and size structure are consistent with a southward propagation of observed climate change effects. Within the diatom community, changes in seasonal succession and a decrease in species richness occurred following low winter sea-ice. As the main component of high productivity and that most efficiently transferred to higher trophic levels, variation in diatom production due to environmental conditions is a mechanism to explain the observed WAP ecosystem changes and chl decline.

Changes in phytoplankton stocks and composition also affect nutrient use, and here the use of silicon and iron (Si and Fe, respectively, which limit productivity in large areas of the Southern Ocean) is investigated. Seasonal Si budgets estimated from Si isotopes indicate a 40 – 70% decline in Si use between high-chl and intermediate-chl years, in agreement with other indices of productivity. The consequences of reduced demand and changing supply suggest future accumulation of Si in WAP surface waters. This should increase Si export away from the WAP shelf, which may act as a mechanism to enhance productivity and carbon drawdown in the wider Southern Ocean.

Sources of Fe were assessed by direct measurement and naturally occurring radioisotopes of radium. These reveal significant inputs at the surface (due to glacial sources) and to deep waters (from shelf/slope sediments), which dominate supply to the surface mixed layer at different times. Iron availability and nutrient drawdown indicate that Fe is supplied to WAP surface waters in excess of biological demand. Projected changes to Fe sources and sinks indicate that continued warming will increase the WAP Fe inventory. As for Si, this excess Fe may also be advected away from the shelf, making this region a net Fe source to the Southern Ocean.

Acknowledgements

First and foremost, I am indebted to my supervisor, Dr. Raja Ganeshram for giving me the opportunity to pursue a PhD on such an interesting project. His support, guidance and enthusiasm over the past four years have been invaluable and inspiring. Recent, long hours of unfailingly helpful critiques of my writing have been especially helpful, and I could not wish for a better supervisor. Also at the University of Edinburgh, I would like to thank my second supervisor Dr. Kate Darling and advisor Dr. Simon Jung.

The fieldwork for this project was made possible by the British Antarctic Survey. I very much appreciate all the help from both Cambridge and Rothera Research Station staff in logistical support and planning, sampling, access to BAS data, and helpful discussions. Special mention is due to the Marine (Dream) Team at Rothera: boating officers Jim Elliott and Danny Edmunds, Bonner Lab managers John Loines and Matthew Von Tersch, and especially the marine assistants Ali Massey and Terri Souster for their long hours and tireless winching in the quest for samples. I would like to gratefully acknowledge Prof. Andy Clarke, Prof. Mike Meredith and Dr. Hugh Venables at BAS Cambridge for their oceanographic expertise and guidance at all stages of the project.

Many thanks to the Masters, Officers and the crew of the RV Lawrence M Gould for help collecting samples in January 2010, and those of the RSS James Clark Ross and Ernest Shackleton for getting me, equipment and samples safely across the Drake Passage on three occasions.

Completing the laboratory analysis for this project would not have been possible without the help of many people. My sincere gratitude to Dr. Ben Reynolds, at ETH-Zurich, Prof. Peter Statham at the National Oceanography Centre Southampton, Dr. Pieter van Beek and Marc Souhaut at LEGOS, Toulouse, Dr. Jan

Scholten at IAEA in Monaco, and Dr. Laetitia Pichevin at the University of Edinburgh.

I am very grateful to Dr. Walter Geibert at the University of Edinburgh for introducing me to the world of radium. He was instrumental in designing, planning and funding this radium work, and extremely helpful in preparing the first publication to come out of it.

During this project, I have been funded by a University of Edinburgh Overseas Research Student Awards Scheme scholarship, a Doctorate Studies Scholarship, from the School of Geosciences College Endowment Funds, and a Postgraduate Scholarship from NSERC (Canada). The project was supported by two Collaborative Gearing Scheme bids from the National Environmental Research Council (UK) through the Antarctic Funding Initiative. Additional project support has come from an Antarctic Science Bursary and the GeoTRACES/CostAction STSM programme.

Throughout this project, I have had the pleasure of working alongside Sian Henley, who has been a constant source of energy and enthusiasm. Many thanks to my partner in oceanographic crime! Special thanks to the other oceanophiles Luke Ridley, Robyn Tuerena and Dr. Tom Russon, and the GeoSciences postgraduate contingent who are too many to name.

I cannot thank all of my friends and family, both in the UK and Canada, enough. The support of my parents Lorraine McKinnon and Dick Annett, as well as their encouragement and tolerance of my continent-hopping habit, will be eternally appreciated. Finally, I am deeply grateful to Alan Homer for his decidedly average support.

This thesis is dedicated to my grandmother, Iris Maureen McKinnon, who never needed to see results before telling me she was proud of me.

Table of Contents

Chapter 1: Introduction

In light of rising carbon dioxide (CO_2) levels in the atmosphere due to anthropogenic activity (Keeling *et al*. 1995), increasing attention has been paid to the marine realm in the cycling of carbon (C) through the earth system. Studies have estimated that 1.5 – 2.0 Pg C y^{-1}, or 25% of CO_2 emissions, are being taken up by the oceans (Sarmiento *et al*. 2000, Gruber & Sarmiento 2002, Keeling & Garcia 2002, Takahashi *et al*. 2002, Sabine *et al*. 2004, Bender *et al*. 2005, Canadell *et al*. 2007, Le Quéré *et al*. 2010). One of the most important areas of the ocean in this regard is the Southern Ocean, which surrounds the Antarctic continent (Metzl *et al*. 1999, McNeil *et al*. 2007, Boutin *et al*. 2008, Gruber *et al*. 2009).

1.1 The Southern Ocean

1.1.1 Physical setting

As a result of its size (~20% of ocean surface) and low temperature surface waters, the Southern Ocean plays a disproportionately large role in regulating atmospheric (CO_2) levels and thus global climate. As the main point of gas exchange between the deep ocean and the atmosphere (Sarmiento & Toggweiler 1984), it has been postulated that on glacial-interglacial time scales it is the Southern Ocean which is primarily responsible for the observed 80-100 ppm variation in atmospheric CO_2 (Knox & McElroy 1984, Sarmiento & Toggweiler 1984, Siegenthaler & Wenk 1984, Toggweiler 1999, Kohler *et al*. 2005), demonstrating the significance of this region to global carbon (C) cycling. This strong link to global climate has both physical and biological foundations.

The bathymetry and atmospheric circulation surrounding the Antarctic continent facilitate the presence of the Antarctic Circumpolar Current (ACC), an unbroken eastward flowing current that creates strong gradients in physical parameters. Cold waters are isolated south of the ACC; this aids in maintaining the cold Antarctic climate and is believed to be a key factor which lead to the

establishment of the Antarctic ice sheets (Katz *et al*. 2011). These cold southern waters are less thermally stratified than most of the world's oceans, allowing exchange between the deep ocean and the atmosphere due to very deep mixing (Fig. 1.1). The importance of this exchange is highlighted by estimates that ~40% of the oceanic uptake of anthropogenic CO_2 emissions has occurred into the ACC (Sabine *et al*. 2004, Boning *et al*. 2008).

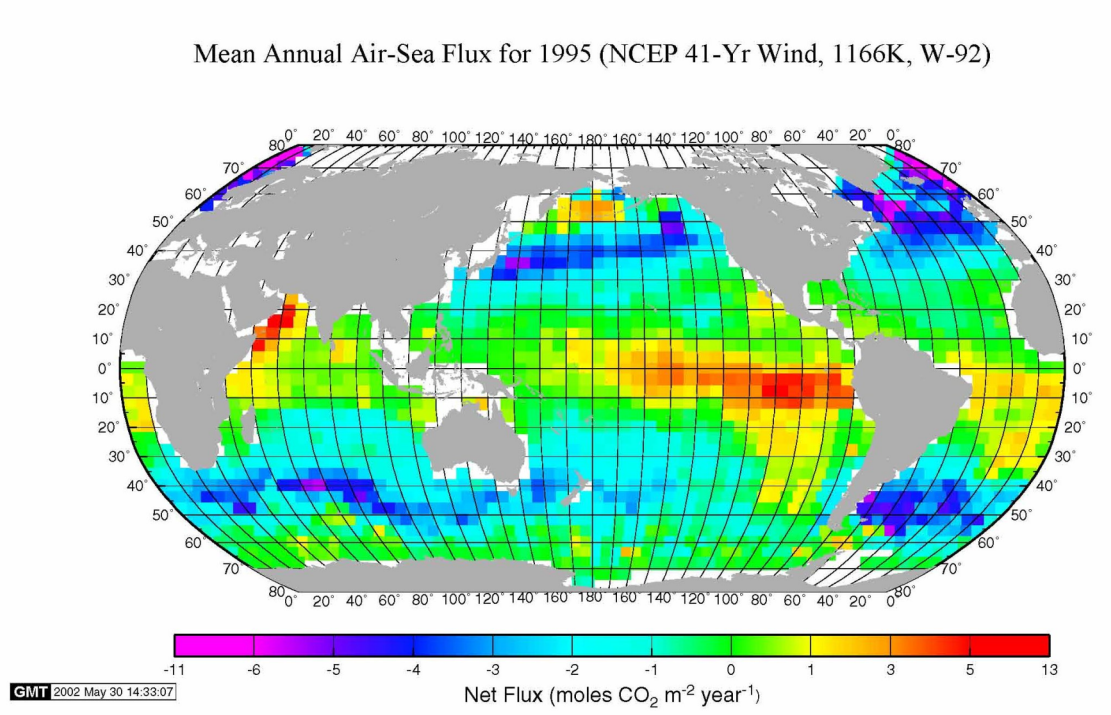

Figure 1.1: Air-sea gas exchange in the global oceans. There is a very strong flux from the atmosphere to seawater in the Southern Ocean. From Takahashi et al. (2009).

Near the continent, cooling and salinification due to winds and brine rejection during the freezing of sea-ice results in the formation of Antarctic Bottom Water, a key process in thermohaline circulation. Upwelling of nutrient-rich deep waters supports very productive surface waters, and as these waters move northwards they form Antarctic Intermediate Water. This is a key mechanism redistributing nutrients throughout the oceans, influencing biological productivity in low-latitudes (Sarmiento *et al*. 2004, 2007).

A key feature of the Southern Ocean is the seasonal expansion and retreat of sea-ice. Sea-ice refers to any of the many different forms of ice (pack ice, fast ice,

congelation ice, grease ice, etc.) which are sourced from frozen seawater. Sea-ice in the Antarctic is unconstrained by land, thus reaches a far greater areal extent than in the Arctic. Total sea-ice extent varies annually, averaging a minimum 4×10^6 km^2 in February to 19×10^6 km^2 in September (Gloersen *et al*. 1993, Cavalieri *et al*. 2003).

Sea-ice affects the atmosphere and ocean in myriad ways, including affecting circulation and weather conditions on regional and global scales (King 1994, King & Harangozo 1998, Smith & Stammerjohn 2001, Turner *et al*. 2005). Sea ice acts to increase albedo, cooling the surrounding area (Budyko 1959). Sea-ice physically restricts thermal and gas exchange between surface waters and the atmosphere, and limits wind-mixing, enhancing stratification during the following spring (Venables *et al*. *In press*). During the seasonal cycle of formation and melt, sea-ice plays a role in driving salinity changes (thereby influencing thermohaline circulation) via salt rejection or brine formation and transport of freshwater (Martinson & Iannuzzi 2001). Biologically, sea ice dynamics play a significant role in influencing primary production (Ablemann *et al*. 2006; Arrigo *et al*. 1997; Riebesell *et al*. 1991) and therefore the rest of the food chain (Eicken, 1992, Ducklow *et al*. 2007). The effects of sea ice dynamics on Antarctic marine ecosystems are largely a result of the relationship between sea ice and phytoplankton productivity, which is detailed below (section 1.2.3).

1.1.2 The biological pump in the Southern Ocean

The Southern Ocean also plays a significant role in the biological pump. This is the process by which C in the surface ocean is fixed into organic C via photosynthesis. A portion of this fixed C is exported to deep waters and sediments where it is effectively sequestered over long time-scales. This Southern Ocean export is believed to be a key process regulating atmospheric CO_2 levels over glacial-interglacial time scales (*e.g*. Knox & McElroy 1984, Sarmiento & Toggweiler 1984, Siegenthaler & Wenk 1984, Martin 1990, Sigman & Boyle 2000, Brzezinski *et al*. 2002, Sigman *et al*. 2004). Biological productivity in the Southern Ocean is mediated primarily by diatoms, single-celled algae (phytoplankton) that construct ornate cell walls out of silica. Diatoms account for up to 40% of global marine productivity

(Nelson *et al*. 1995), and up to 75% of Southern Ocean production (Nelson *et al*. 1995). This high diatom production has led to the accumulation of large sedimentary opal (biogenic silica) deposits beneath the Southern Ocean (Broecker 1982, Burckle & Cirilli 1987).

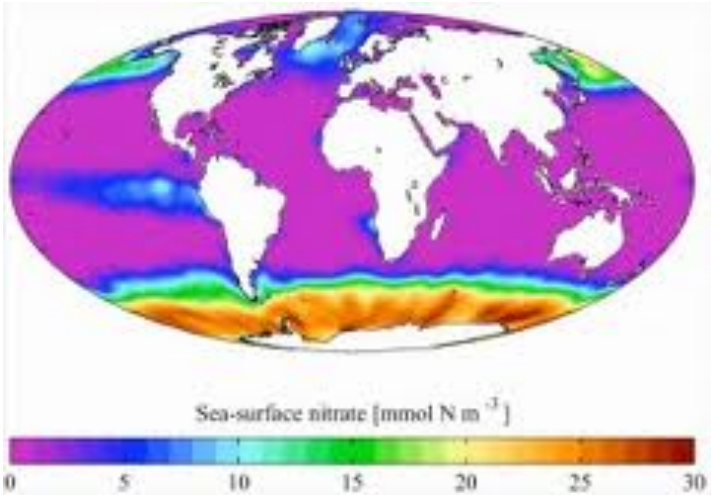

Figure 1.2: Annual mean sea surface nitrate from the World Ocean Atlas 2001. High surface concentrations of nitrate are present in the Southern Ocean, indicating incomplete utilisation of nutrients by phytoplankton in this region. (Image available at http://en.wikipedia.org/wiki/File:AYool_WOA_surf_NO3.png, Data from http://www.nodc.noaa.gov/OC5/WOA01/ World Ocean Atlas 2001 and plotted here using a Mollweide projection, using MATLAB and the [http://www.eos.ubc.ca/~rich/private/ M_Map] package.)

However, the Southern Ocean is not uniformly productive, with large areas classified as high-nutrient, low-chlorophyll (HNLC) regions (Fig 1.2). In these areas, phytoplankton growth is limited, and nutrients levels remain high due to incomplete utilisation. In the Southern Ocean, lack of iron (Fe) is the main factor inhibiting primary productivity. Iron is an essential micronutrient, required by all phytoplankton. It is primarily used for electron transport in photosynthesis (Raven 1990), but is also important for chlorophyll synthesis (Raven *et al.* 1999), nitrogen metabolism (Milligan & Harrison 2000) and detoxification of superoxide radicals (Chadd *et al.* 1996). Iron supply to the open ocean comes primarily from atmospheric dust deposition, which is very low in the Southern Ocean (Mahowald *et al*. 2009). Under oceanic conditions, most dissolved Fe is present as the oxidised ion Fe^{3+}, although > 99% of this is bound to organic ligands. These ligands help to keep Fe in

the dissolved phase, as Fe^{3+} is only sparingly soluble in seawater, and is rapidly scavenged onto particles. Both free Fe^{3+} and organically bound Fe are bioavailable to phytoplankton (Maldonado & Price 1999, 2001), but total Fe concentrations in the open Southern Ocean are typically very low (<0.1 nM; Johnson *et al*. 1997).

Low availability of the macronutrient silicon (Si) also affects diatoms in certain areas of the Southern Ocean. In addition to strong gradients in temperature, the presence of the ACC also leads to strong nutrient gradients across the Polar Front Zone (PFZ; Figure 1.3). North of the PFZ, concentrations of Si are low enough to limit diatom growth (Nelson *et al*. 2001; Coale *et al*. 2004; Brzezinski *et al*. 2005). Even south of the PFZ, co-limitation of diatom production by Fe and Si has been hypothesised by Leblanc *et al*. (2005), and supported by laboratory work (Hoffmann *et al*. 2008). The gradient in nutrients across the PFZ are relevant on very large spatial scales, as these waters redistribute nutrients to much of the world's surface oceans (via Sub-Antarctic Mode Water formation and meridional circulation; Rintoul *et al*. 2001, Brzezinski *et al*. 2002, Sarmiento *et al*. 2004, 2007). The reduced supply of Si relative to other nutrients limits diatoms to a relatively minor role in most other oceanic provinces (Yool & Tyrrell 2003). Changes in the export of Si from the Southern Ocean and resulting increases in diatoms at low latitudes have been proposed as a mechanism to reduce atmospheric CO_2 during glacial periods (Brzezinski *et al*. 2002, Matsumoto *et al*. 2002, 2007) highlighting the significance of this process.

A third factor regulating productivity in the Southern Ocean is availability of light (*e.g*. Mitchell & Holm-Hansen 1991, Lancelot *et al*. 2000). In addition to strong annual seasonality in light availability due to day length, the very deep mixed layers of the Southern Ocean result in phytoplankton assemblages being light or light/iron co-limited (Nelson & Smith 1991, Boyd *et al*. 1999, 2000). The depth at which vertically integrated photosynthesis and respiration are equal is known as the critical depth (z_c), indicating that above z_c, net photosynthesis can occur. Light limitation occurs when the mixed layer is below z_c. In addition to deep mixing, phytoplankton blooms themselves can reduce light levels within the water column; this "self-

shading" can result in light limitation even when mixed layers are relatively shallow (Nelson & Smith 1991).

The combination of these three main limiting factors means that coastal areas of the Southern Ocean exhibit the highest productivity. In these regions, shelf and coastal inputs of Fe are likely to be high, upwelling of deeper waters provides Si and other macronutrients, and stratified summer conditions allow for mixed layer depths above the critical depth. Thus the highest chlorophyll *a* concentrations (chl; a proxy for phytoplankton biomass) are typically found in the coastal regions. The western Antarctic Peninsula (WAP) in particular is a highly productive region (182 ±107 g C m^{-2} y^{-1}; Vernet *et al*. 2008) that supports a robust ecosystem (Ducklow *et al*. 2007) and is currently undergoing rapid warming as a result of climate change.

1.2 The western Antarctic Peninsula region

The WAP itself reaches from the Antarctic continent to ~62° S. The WAP is separated from South America by Drake Passage, although the volcanic arc islands of the South Orkney Islands, the South Sandwich Islands and South Georgia, and the Scotia Ridges between them provide some degree of topographic link between the WAP and South America (Fig 1.3). To the east of the WAP is the Weddell Sea, and the high topography of the WAP mountains (~3500 m above sea level) together with atmospheric and oceanic circulation create distinct east-west differences along the WAP (in ice, winds, temperatures; Schwerdtfeger 1975, 1979). The focus of this study is the western shelf of the WAP, with relevance to the volcanic arc region to the north influenced by WAP oceanography. This section introduces the changing oceanographic and biological setting in this area.

1.2.1 Oceanographic setting

The oceanography of the WAP region differs from other Antarctic shelf regions in its proximity to the ACC, as well as to large quantities of glacial meltwater from land (Clarke *et al*. 2008). The ACC is composed of Circumpolar Deep Water (CDW), a warm, saline water mass characterised by high nutrient and low oxygen concentrations (Sievers & Nowlin 1984), which is the ultimate source for all WAP shelf waters. Due to the absence of an Antarctic Slope Front here, CDW arrives on

the WAP shelf in a less modified form than in other regions (Klinck *et al*. 1998, Clarke *et al*. 2008, Meredith *et al*. 2008).

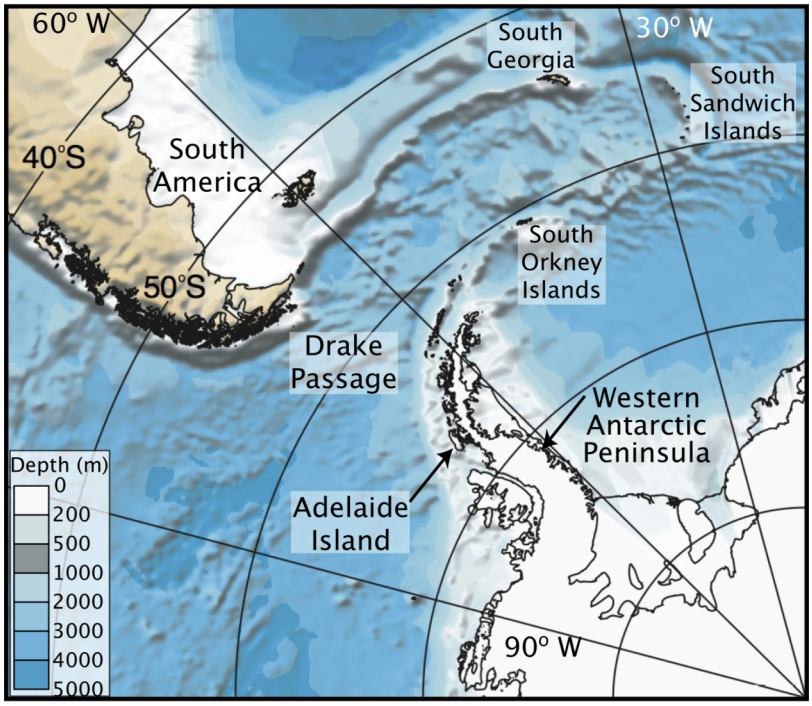

Figure 1.3: Bathymetry of the Western Antarctic Peninsula region. From the WOCE Southern Ocean Atlas (Orsi & Whitworth), available at: http://wocesoatlas.tamu.edu/.

Inputs of CDW are most pronounced near deep, glacially carved canyons such as Marguerite Trough (Moffat *et al*. 2009). There are two primary modes of CDW intrusion onto the shelf, with more dense, Lower CDW (LCDW) flowing into deep depressions, and Upper CDW (UCDW) moving onto the shelf via horizontal eddies (Moffat *et al*. 2009; depicted in Figure 1.4). This CDW transports heat, salt and nutrients (Klinck *et al*. 1998) onto the shelf, thereby influencing water mass properties and productivity along the WAP.

As mentioned above, glacial inputs are a significant and indeed dominant source of freshwater to the WAP region (Meredith *et al*. *In press*). Surface waters over the WAP shelf typically contain 2% meteoric water (mainly glacial with some precipitation), with this proportion rising to 5% adjacent to the coast (Figure 1.5). The influence of freshwater is a key component driving the Antarctic Peninsula

Coastal Current (APCC; Moffat *et al*. 2008), a southward moving current inshore of the ACC (Beardsley *et al*. 2004, Klinck *et al*. 2004, Moffat *et al*. 2008).

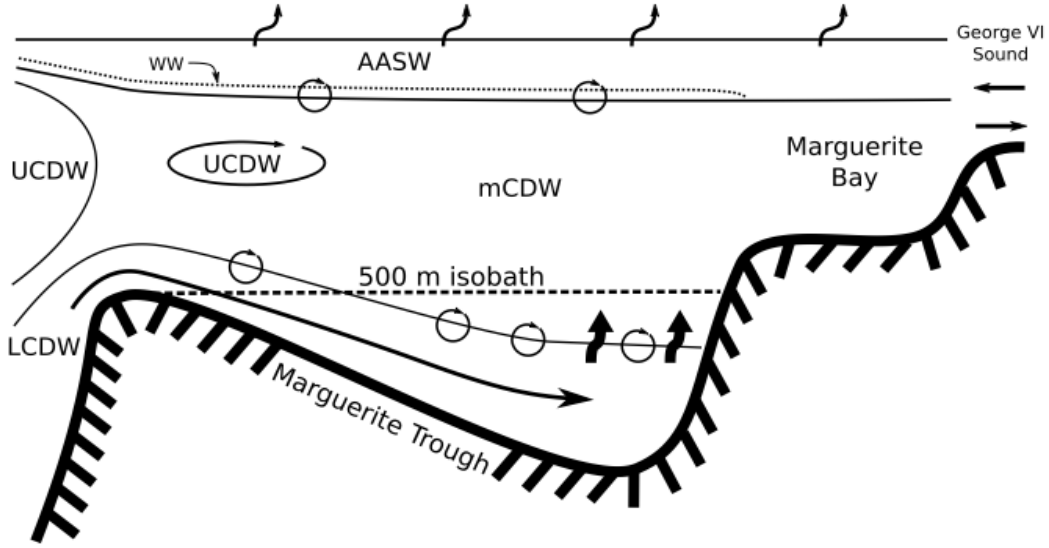

Figure 1.4: Schematic of UCDW and LCDW incursions onto the WAP shelf, from Moffat *et al*. (2009).

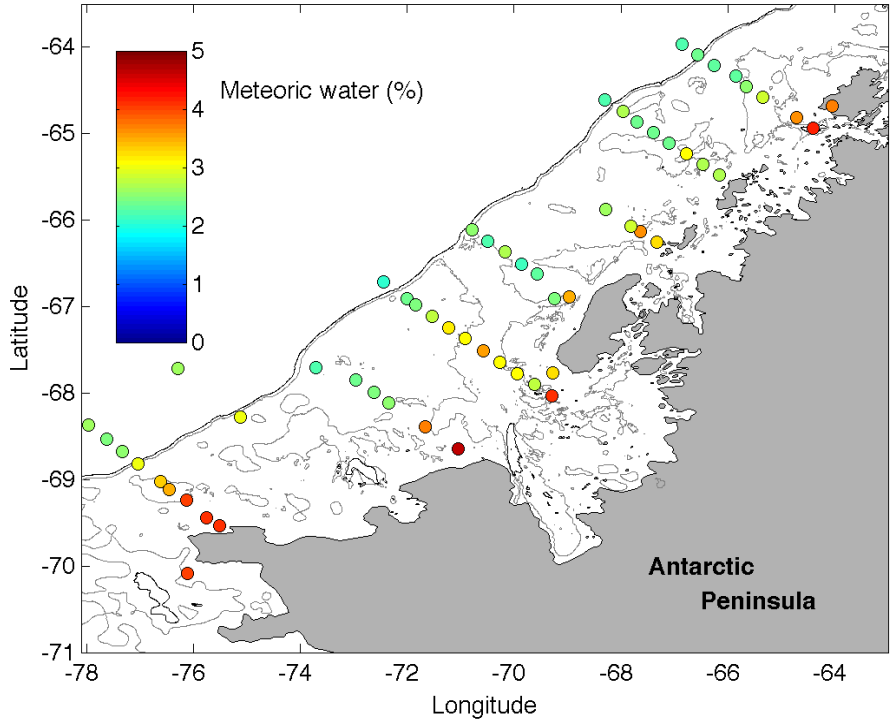

Figure 1.5: Spatial differences in proportions of meteoric (predominantly glacial and some snow) water above the WAP shelf, based on data from oxygen isotopes.

While meteoric inputs are greatest near the coast, even water above the shelf break contains measurable contributions from meteoric sources. From Meredith *et al*. (*In press*).

The low-salinity melt water from glaciers has a very strong influence on Southern Ocean seawater density, because water density is almost entirely dependent on salinity at low temperatures. Accordingly, glacial melt water at the surface can greatly affect stratification, with this effect persisting up to 100 km offshore (Dierssen *et al*. 2002). Additionally, meltwater from glaciers and icebergs can be a source of land-derived micronutrients (most notably Fe) to surface waters (Raiswell *et al*. 2006, 2008, Statham *et al*. 2008, Raiswell 2011, Shaw *et al*. 2011).

1.2.2 Recent rapid regional warming along the Antarctic Peninsula

The WAP is currently undergoing the most pronounced recent rapid regional warming in the Southern hemisphere (Hansen *et al*. 1999, Vaughan e*t al*. 2003). Since 1950, July air temperatures at Faraday Station (northern WAP) have risen by 6 °C (Stammerjohn *et al*. 2008a), while average air temperature on the WAP as a whole has increased at a rate of 3.6 ± 1.4 °C per century, several times the global average (Vaughan *et al.* 2003). Annual air temperature trends at five WAP research stations are shown in Figure 1.6.

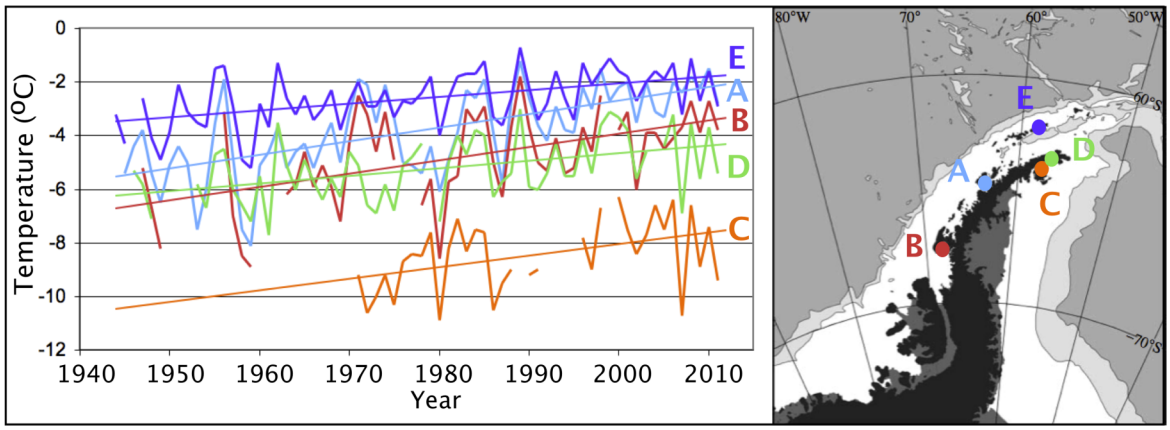

Figure 1.6: Mean annual air temperature trends at five WAP research stations: (A) Faraday-Vernadsky, (B) Rothera, (C) Marambio, (D) Esperanza, (E) Bellingshausen stations. Station locations are shown on map at right. Data available online at: http://www.antarctica.ac.uk/met/gjma/-temps.html.

At sea, increases of ~1 °C have been recorded in the surface waters (Meredith & King 2005) surrounding the WAP. Warming trends in the ocean are not restricted to the WAP; analysis by Gille (2002, 2008) found significant warming throughout the top 1000 m of the Southern Ocean since the 1930s, with the temperature increase greatest towards the surface (Fig. 1.7). This study further suggested a southward shift of the ACC since the 1930s, which would lead to greater contact of warm CDW with the WAP shelf. Martinson *et al*. (2008) have documented increasing trends in ocean heat content over the shelf over the period 1993–2004. This trend is consistent with an increase in frequency of CDW incursions, which are believed to be at least partially driven by changes in atmospheric circulation (Martinson *et al*. 2008, Meredith *et al*. 2010).

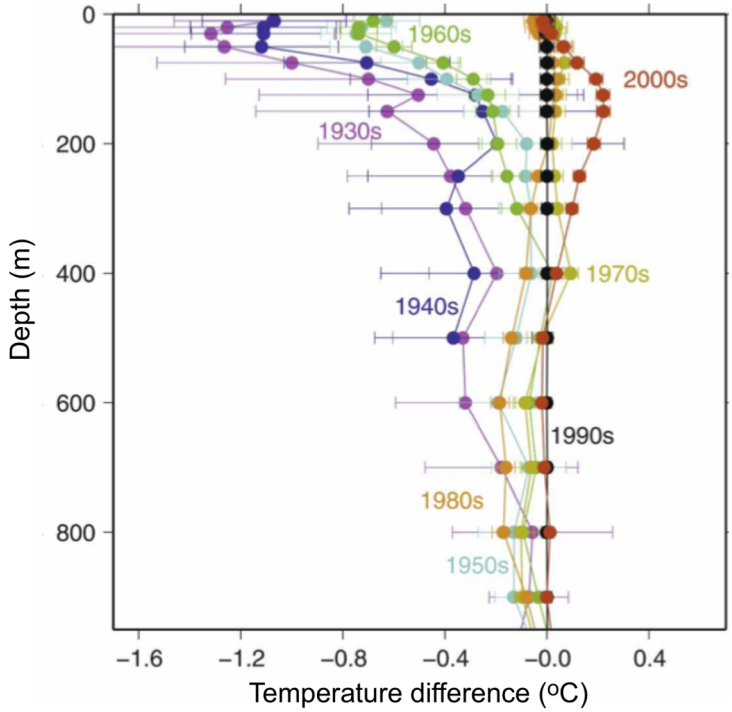

Figure 1.7: Ocean temperature changes in the top 800 m throughout the Southern Ocean. Shown are the differences relative to 1990 mean. From Gille (2008).

Warmer waters can influence glaciers, as it has been shown that the temperature of marine waters can significantly impact the melt rates of marine-terminating glaciers, both along the WAP and around Antarctica as a whole (Pritchard *et al*. 2012). In agreement with both seawater and air temperature increases, some ice shelves (Pritchard & Vaughan 2007) and the majority of glaciers

(Cook *et al*. 2005; Fig. 1.8) in the region are retreating, and the rate of this retreat is accelerating. While melting is occurring throughout the WAP, melting is more pronounced in the north, in keeping with the latitudinal temperature gradient (Vaughan & Doake 1996). Retreat of the Western Antarctic Ice Sheet in recent decades is well documented, and ice shelf collapses such as the Larsen A in 1995, the Larsen B in 2002, and the Wilkins in 2008-2009, have been widely publicised. It is estimated that losses to ice shelves along the WAP and Amundsen Sea account for more than half of the total floating ice loss in Antarctic between 1994 and 2004 (481 ± 38 km^3 y^{-1}, versus 746 ± 127 km^3 y^{-1} for Antarctica as a whole; Shepherd *et al*. 2010).

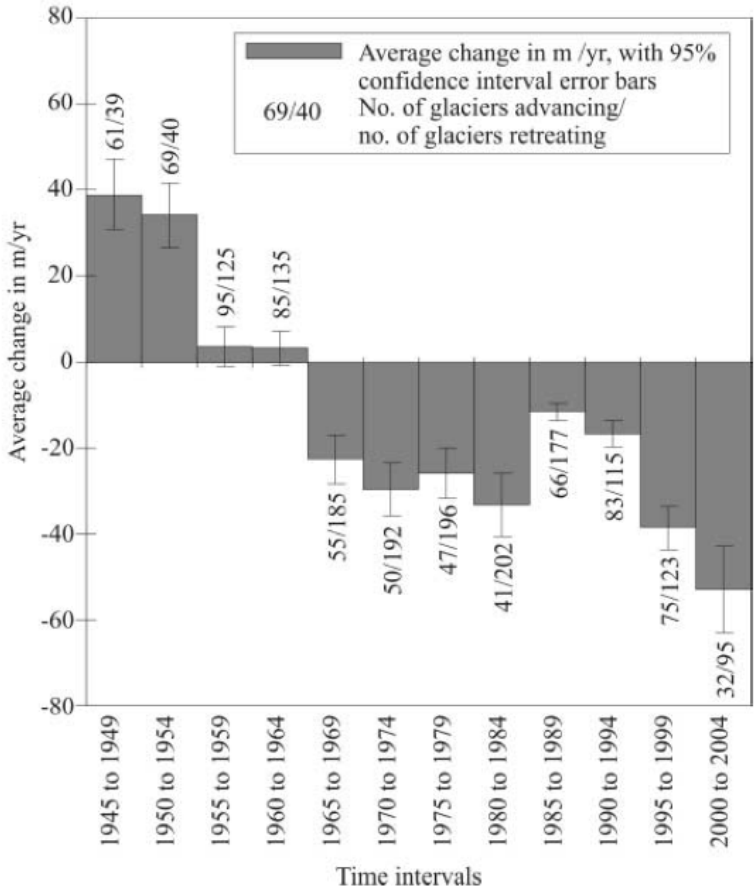

Figure 1.8: Glacial advance across the WAP, where negative values denote retreat. A long-term trend to more rapid retreat is apparent, from Cook *et al*. (2005).

Since 1979, monitoring from the Palmer Long Term Ecological Research (Pal-LTER) project has documented a 40% decrease in mean sea-ice duration (Smith & Stammerjohn, 2001). This contrasts with the overall slight increase in Antarctic

sea-ice extent, which is due to positive changes in sea-ice cover in East Antarctica (Stammerjohn & Smith 1997, Cavalieri & Parkinson 2008). The main changes to sea-ice dynamics are later (mean 54 days) advance and earlier (mean 31 days) retreat (Stammerjohn *et al*. 2008a). The delayed advance of sea-ice is linked to both warmer winter (July) temperatures (Vaughan *et al*. 2003) and changes in atmospheric circulation (Stammerjohn *et al*. 2008a). This results in a mean 85 day shorter sea-ice season for the WAP/southern Bellingshausen Sea (Stammerjohn *et al*. 2008a), although there is some regional variability along the WAP (Stammerjohn *et al*. 2008b; Fig. 1.9). Seasonal sea-ice dynamics are a key feature of the WAP system which can impact the regional biology in many ways, thus the changes in sea-ice have multiple potential ecosystem effects.

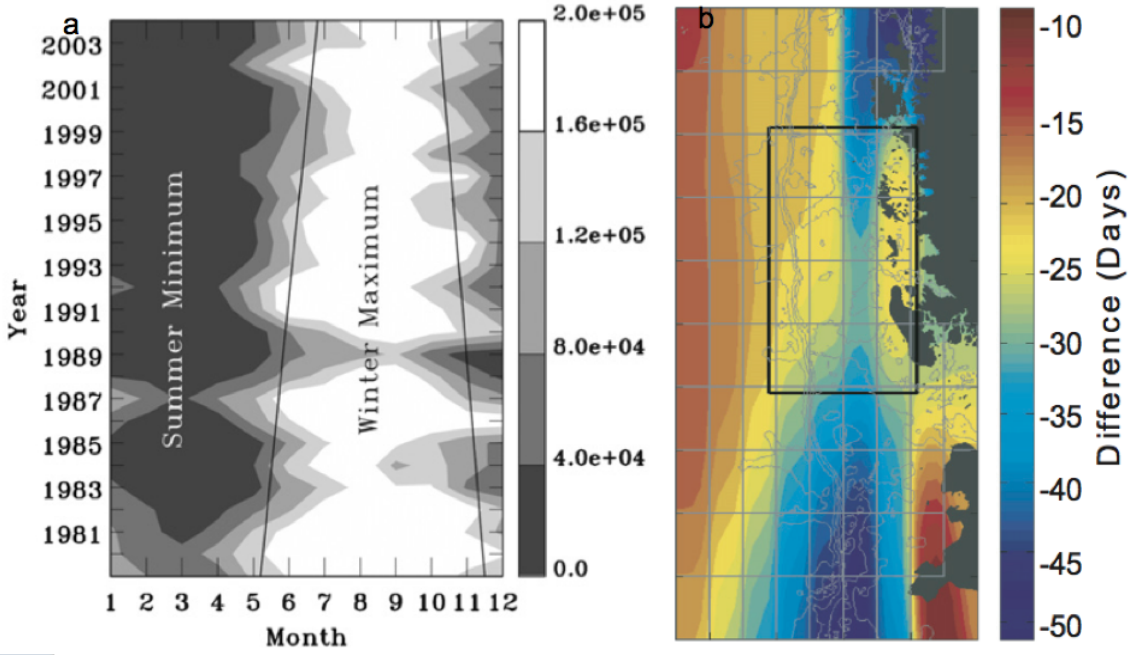

Figure 1.9: Sea-ice trends from the Pal-LTER grid. A trend towards later advance and earlier retreat is shown in (a), where interannual variability is strongly influenced by ENSO conditions. Also shown is a map of spatial variability in the difference (in days) of winter sea-ice duration between (1992 and 2004) minus (1979 to 1991). Note that even regions showing the least change (red areas) display a trend to shorter sea-ice cover. From Stammerjohn *et al*. (2008).

1.2.3 Biological processes in the seasonal sea-ice zone

Seasonal ice zones (SIZs), such as the sea-ice dominated WAP region, support large populations of mammals and seabirds (Ducklow *et al*. 2007). Sea-ice is an area of concentrated food for grazers, from heterotrophic nanoplankton to krill

(Donnelly *et al.* 2006; Eicken 1992), but can also impact the ecosystem at the level of primary producers.

A key influence on primary productivity along the WAP shelf is stratification, which is closely linked to sea-ice processes. Winter sea-ice promotes deep mixing of the water column via brine rejection during ice formation. This mixing with nutrient-rich deep waters replenishes surface nutrient inventories during the period when photosynthesis is already limited by low light availability. During late winter, sea-ice acts as a physical barrier to wind-driven mixing, which contributes to stable spring/summer conditions (Venables *et al*. *In press*). As day length increases, sea-ice provides a platform for photosynthesis where phytoplankton are subject to more constant light levels (Arrigo & Thomas 2004; Eicken 1992; Riebesell *et al.* 1991), which can lead to chl concentrations in platelet ice being among the highest in any marine setting (Arrigo & Thomas 2004). In spring and summer when the sea-ice retreats, meltwater creates a thin, freshwater lens. This limits vertical mixing, promotes high biomass by concentrating phytoplankton within the well-lit surface layer, and reduces sedimentation (Garibotti *et al*. 2003; Smith & Sakshaug 1990). As a result, sea-ice cover plays a crucial role in creating favourable conditions for primary productivity in SIZs.

Accordingly, chl data from coastal Antarctic regions generally show high concentrations in the upper water column (Garibotti *et al*. 2003b, Smith *et al*. 1998, Holm-Hansen *et al.* 1989). Throughout the WAP and the Antarctic marginal sea-ice zone as a whole, many studies have found significant correlations between water column stability and overall primary production (Garibotti *et al*. 2003, Smith *et al*. 2000, Smith *et al*. 1998, Kang & Lee 1995, Mitchell & Holm-Hansen 1991, Holm-Hansen *et al*. 1989, Smith & Nelson, 1985). While surface stability has been classically considered a result of sea-ice processes, studies have also suggested that in coastal areas glacial run-off can significantly affect stratification up to 100 km offshore (Dierssen *et al*. 2002).

In addition to light, growth of phytoplankton in Southern Ocean waters can be further limited by Fe, as noted above (Hoffmann *et al.* 2008, Gall *et al.* 2001). Freshwater inputs are clearly important to biological production due to their role in

stratification, but are also a potential source of micronutrients such as Fe (in run-off, glacial meltwater and associated glacial material; Edwards & Sedwick 2001, Raiswell 2011, Gerringa *et al*. 2012). Sea-ice has also been shown to accumulate Fe over the winter, and can thus act as a source of Fe (Sedwick & DiTullio 1997) and other nutrients when it melts in spring.

1.2.4 Biological changes in the WAP region

Sea-ice can influence biological processes in several ways, and physical changes in sea-ice cover are therefore expected to impact the regional food web. Along the WAP, krill are a dominant grazer (Garibotti *et al*. 2003) and a primary food source for many seabirds and mammals (Everson 2000). Historically considered a key species in the WAP region (Ducklow *et al*. 2007), observations suggest that krill stocks have declined over the 1976-2004 period as a result of changes in sea-ice cover, a crucial factor in spawning and grazing for these organisms (Atkinson *et al*. 2004, Wiedenmann *et al*. 2009). In addition to pelagic consumers, deep dwelling organisms rely on the sinking remains of surface-growing phytoplankton for food sources during the short but intense summer growing period (Clarke & Arntz 2006). Changes in phytoplankton community structure in response to sea-ice conditions will play a crucial role in determining the deep-sea export of organic detritus in these areas, due to large differences in export potential between taxonomic groups (Arrigo *et al*. 2002).

Changes in freshwater inputs as well as sea-ice cover can affect stratification and therefore productivity in this region, and the balance between sea-ice versus glacial meltwater induced stratification is likely to change as warming progresses Indeed, phytoplankton dynamics already show changes linked to sea-ice cover and stratification in both the northern and southern regions of the WAP (Montes-Hugo *et al*. 2009), although these changes differ in both direction and magnitude.

Observations of lower krill stocks in the northern WAP region agree well with a recent analysis of satellite-derived chl where sea-ice decline has reduced areas of seasonal ice over and led to chl levels 95-99% lower than pre-1970 levels (Montes-Hugo *et al*. 2009). In contrast, the changes in sea-ice dynamics in the southern WAP region have largely been associated with permanently ice-covered

areas becoming seasonal sea-ice zones (SIZs), causing an overall increase in the areal extent of SIZs, which has been accompanied by increasing chl levels (Montes-Hugo *et al*. 2009).

The increase in sea surface temperatures may also play a role in productivity changes, and hence the stocks of higher trophic organisms such as krill. Mesocosm experiments from the Baltic Sea showed that while temperature was not a significant factor in bloom timing, peak biomass was sensitive to temperature, with warmer conditions leading to lower biomass (Sommer & Lengfellner 2008). Phytoplankton community structure was also affected by warmer waters, showing a shift towards lower relative abundances of large (> 20 μm) diatoms; this shift is likely to result in reduced transfer of energy to higher trophic levels due to poorer feeding conditions for grazers such as copepods and krill (Sommer & Lengfellner 2008).

As the coastal regions have the greatest impact on overall WAP primary production (Smith *et al.* 1998, Smith *et al.* 2000, Smith *et al.* 1996), elucidating the interactions between sea-ice coverage, glacial melt, and productivity is crucial to understanding future changes in phytoplankton dynamics and the implications this may have for higher trophic levels and carbon fluxes in near-shore regions of the WAP.

1.3 Thesis overview

This thesis brings together two very important aspects of the WAP region: its high biological productivity and importance to the Southern Ocean biological pump, and the most rapid regional warming in the Southern hemisphere. As the interactions between environmental conditions and primary production are the key link between climate and biosphere in this region, the key focus is the impact of environmental variability on phytoplankton.

Here, the effects of interseasonal variability in the physical marine environment on phytoplankton assemblages are investigated at a coastal WAP location. **Chapter 2** introduces the study site and methods, ongoing monitoring and provides the context of seasonal variation in physical and biological processes which

frames the research questions addressed in data chapters. The main aims of this thesis are as follows:

1. To characterise phytoplankton and diatom assemblages from the coastal Antarctic sea-ice zone across a wide range of environmental conditions.
2. To evaluate the mechanisms linking these assemblage changes to water column conditions.
3. To better constrain silicon cycling by diatom communities on the WAP shelf and derive a silicon budget at the study site.
4. To investigate the relative importance of different micronutrient sources to the coastal sea-ice zone, and evaluate these sources relative to biological demand.
5. To consider the potential impacts to all of the above in the context of current and future climate change.

Phytoplankton assemblages are presented in **Chapter 3**, and the mechanisms linking microalgal composition with environmental conditions are explored. **Chapter 4** documents species-level composition of diatom communities throughout the study period, to identify new indicator species/assemblages useful for modern and sedimentary studies. Biogeochemistry of Si is considered in **Chapter 5**, characterising the biological use of Si by diatom production. A Si budget is derived for the study site by combining hydrographic records and Si isotopic data, and factors affecting Si isotopic fractionation in this region are evaluated. A significant route of micronutrient supply is from terrestrial sediments, and **Chapter 6** uses naturally occurring isotopes of radium to quantify potential sediment inputs to coastal surface waters. **Chapter 7** relates micronutrient fluxes specifically to dissolved measurements of Fe and aluminium, building on the Si budget from Chapter 5 to assess biological Fe demand. Finally, **Chapter 8** considers the implications of climate-induced changes in sea-ice, glacial retreat, water column stratification and deep water nutrient supply for the results presented here.

1.4 References

ABELMANN, A., GERSONDE, R., CORTESE, G., KUHN, G. & SMETACEK, V. 2006. Extensive phytoplankton blooms in the Atlantic sector of the glacial Southern Ocean. *Paleoceanography*, **21**, 10.1029/2005PA001199.

ARRIGO, K.R. & THOMAS, D.N. 2004. Large scale importance of sea ice biology in the Southern Ocean. *Antarctic Science*, **16**, 471–486, 10.1017/S0954102004002263.

ARRIGO, K.R., DUNBAR, R.B., LIZOTTE, M.P. & ROBINSON, D.H. 2002. Taxon-specific differences in C/P and N/P drawdown for phytoplankton in the Ross Sea, Antarctica. *Geophysical Research Letters*, **29**, 1938, 10.1029/2002GL015277.

ARRIGO, K.R., WORTHEN, D.L., LIZOTTE, M.P., DIXON, P. & DIECKMANN, G. 1997. Primary Production in Antarctic Sea Ice. *Science*, **276**, 394–397.

ATKINSON, A., SIEGEL, V., PAKHOMOV, E. & ROTHERY, P. 2004. Long-term decline in krill stock and increase in salps within the Southern Ocean. *Nature*, **432**, 100–103.

BEARDSLEY, R.C., LIMEBURNER, R. & OWENS, W.B. 2004. Drifter measurements of surface currents near Marguerite Bay on the western Antarctic Peninsula shelf during austral summer and fall, 2001 and 2002. *Deep-Sea Research II*, **51**, 1947–1964, 10.1016/j.dsr2.2004.07.031.

BENDER, M.L., HO, D.T., HENDRICKS, M.B., MIKA, R., BAZTTLE, M.L., TANS, P.P., CONWAY, T.J., STURTEVANT, B. & CASSAR, N. 2005. Atmospheric O_2/N_2 changes, 1993–2002: implications for the partitioning of fossil fuel CO_2 sequestration. *Deep-Sea Research I*, **51**, 793–808.

BONING, C.W., DISPERT, A., VISBECK, M., RINTOUL, S.R. & SCHWARZKOPF, F.U. 2008. The response of the Antarctic Circumpolar Current to recent climate change. *Nature Geoscience*, **1**, 1–6, 10.1038/ngeo362.

BOUTIN, J., MERLIVAT, L., HÉNOCQ, C., MARTIN, N. & SALLÉE, J.B. 2008. Air-sea CO_2 flux variability in frontal regions of the Southern Ocean from carbon interface ocean atmosphere drifters. *Limnology and Oceanography*, **53**, 2062–2079.

BOYD, P., LAROCHE, J., GALL, M., FREW, R. & MCKAY, R.M.L. 1999. Role of iron, light, and silicate in controlling algal biomass in subantarctic waters SE of New Zealand. *Journal of Geophysical Research*, **104**, 13395–13408.

BOYD, P.W., WATSON, A.J., LAW, C.S., ABRAHAM, E.R., TRULL, T., MURDOCH, R., BAKKER, D.C.E., BOWIE, A.R. & AL, E. 2000. A mesoscale phytoplankton bloom in the polar Southern Ocean stimulated by iron fertilization. *Nature*, **407**, 695–702.

BROECKER, W.S. & PENG, T.-H. 1982. *Tracers in the Sea*. Palisades: Eldigio Press.

BRZEZINSKI, M., JONES, J.L. & DEMAREST, M.S. 2005. Control of silica production by iron and silicic acid during the Southern Ocean Iron Enrichment Experiment (SOFeX). *Limnology and Oceanography*, **50**, 810–824.

BRZEZINSKI, M.A., PRIDE, C.J., FRANCK, V.M., SIGMAN, D.M., SARMIENTO, J.L. & MATSUMOTO, K. 2002. A switch from $Si(OH)_4$ to NO_3 depletion in the glacial Southern Ocean. *Geophysical Research Letters*, **29**, 10.1029/2001GL014349.

BUDYKO, M.I. 1959. The effect of solar radiation on the climate of the earth. *Tellus*, **21**, 611–619.

BURCKLE L.H. & CIRILLI, J. 1987. Origin of diatom ooze belt in the Southern Ocean: implications for late Quaternary paleoceanography. *Micropaleontology*, **33**, 82–86.

CANADELL, J.G., LE QUÉRÉ, C., RAUPACH, M.R., FIELD, C.B., BUITENHUIS, E.T., CIAIS, P., CONWAY, T.J., GILLETT, N.P., HOUGHTON, R.A. & MARLAND, G. 2007. Contributions to accelerating atmospheric CO_2 growth from economic activity, carbon intensity, and efficiency of natural sinks. *Proceedings of the US National Academy of Sciences*, **104**,

18866–18870.

CAVALIERI, D.J., PARKINSON, C.L. & VINNIKOV, K.Y. 2003. 30-Year satellite record reveals contrasting Arctic and Antarctic decadal sea ice variability. *Geophysical Research Letters*, **30**, 1–4, 10.1029/2003GL018031.

CHADD, H.E., NEWMAN, J., MANN, H. & CARR, N.G. Identification of iron superoxide dismutase and a copper/zinc superoxide dismutase enzyme activity with the marine cyanobacterium *Synechococcus* sp. WH 7803. *Fed. Eur. Miccrobiology Society Microbiological Letters*, **138**, 161–165.

CLARKE, A. & ARNTZ, W.E. 2006. An introduction to EASIZ (Ecology of the Antarctic Sea Ice Zone): An integrated programme of water column, benthos and bentho-pelagic coupling in the coastal environment of Antarctica. *Deep Sea Research Part II: Topical Studies in Oceanography*, **53**, 803–814, 10.1016/j.dsr2.2006.05.001.

CLARKE, A., MEREDITH, M.P., WALLACE, M.I., BRANDON, M.A. & THOMAS, D.N. 2008. Seasonal and interannual variability in temperature, chlorophyll and macronutrients in northern Marguerite Bay, Antarctica. *Deep Sea Research Part II: Topical Studies in Oceanography*, **55**, 1988–2006, 10.1016/j.dsr2.2008.04.035.

COALE, K.H. & AL, E. 2004. Southern Ocean iron enrichment experiment: carbon cycling in high- and low-Si waters. *Science*, **304**, 408–414.

COOK, A.J., FOX, A.J., VAUGHAN, D.G. & FERRIGNO, J.G. 2005. Retreating Glacier Fronts on the Antarctic Peninsula over the Past Half-Century. *Science*, **308**, 541–544, 10.1126/science.1109164.

DIERSSEN, H.M., SMITH, R.C. & VERNET, M. 2002. Glacial Meltwater Dynamics in Coastal Waters West of the Antarctic Peninsula. *Proceedings of the National Academy of Sciences of the United States of America*, **99**, 1790–1795.

DUCKLOW, H.W., BAKER, K., MARTINSON, D.G., QUETIN, L.B., ROSS, R.M., SMITH, R.C., STAMMERJOHN, S.E., VERNET, M. & FRASER, W. 2007. Marine pelagic ecosystems: the West Antarctic Peninsula. *Philosophical Transactions of the Royal Society B: Biological Sciences*, **362**, 67–94, 10.1098/rstb.2006.1955.

EICKEN, H. 1992. The role of sea ice in structuring Antarctic ecosystems. *Polar biology*, **12**, 3–13.

EVERSON, I. 2000. Role of Krill in marine food webs: The Southern Ocean. *In* Everson, I., *ed. Krill: biology, ecology and fisheries*. London: Blackwell Science, 194–201.

GARIBOTTI, I.A., VERNET, M., FERRARIO, M.E., SMITH, R.C., ROSS, R.M. & QUENTIN, L.B. 2003a. Phytoplankton spatial distribution patterns along the western Antarctic Peninsula (Southern Ocean). *Marine Ecology Progress Series*, **261**, 21–39.

GARIBOTTI, I.A., VERNET, M., KOZLOWSKI, W.A. & FERRARIO, M.E. 2003b. Composition and biomass of phytoplankton assemblages in coastal Antarctic waters: a comparison of chemotaxonomic and microscopic analysis. *Marine Ecology Progress Series*, **247**, 27–42.

GERRINGA, L.J.A., ALDERKAMP, A.-C., LAAN, P., THURÓCZY, C.-E., DE BAAR, H.J.W., MILLS, M.M., VAN DIJKEN, G.L., VAN HAREN, H. & ARRIGO, K.R. 2012. Iron from melting glaciers fuels the phytoplankton blooms in Amundsen Sea (Southern Ocean) Iron biogeochemistry. *Deep-Sea Research Part II*, **71-76**, 16–31, 10.1016/j.dsr2.2012.03.007.

GILLE, S.T. 2008. Decadal-Scale Temperature Trends in the Southern Hemisphere Ocean. *Journal of Climate*, **21**, 4749–4765, 10.1175/2008JCLI2131.1.

GILLE, S.T. 2002. Warming of the Southern Ocean since the 1950s. *Science*, **295**, 1275–1277.

GLOERSEN, P., CAMPBELL, W.J., CAVALIERI, D.J., COMISO, J.C., PARKINSON, C.L. & ZWALLY, H.J. 1993. Satellite passive microwave observations and analysis of Arctic and Antarctic

sea ice, 1978-1987. *Annals of Glaciology*, **17**, 149–154.

GRUBER, N. & SARMIENTO, J.L. 2002. Large-scale biogeochemical-physical interactions in elemental cycles. *In* Robinson, A.R., McCarthy, J. & Rothschild, B.J., *eds. The Sea*. New York: Wiley, 337–399.

GRUBER, N., GLOOR, M., MIKALOFF FLETCHER, S.E., DONEY, S.C., DUTKIEWICZ, S., FOLLOWS, M.J., GERBER, M., et al. 2009. Oceanic sources, sinks, and transport of atmospheric CO_2. *Global Biogeochemical Cycles*, **23**, 10.1029/2008GB003349.

HANSEN, J., RUEDY, R., GLASCOE, J. & SATO, M. 1999. GISS analysis of surface temperature change. *Journal of Geophysical Research - Atmospheres*, **104**, 30997–31022.

HOFFMANN, L.J., PEEKEN, I. & LOCHTE, K. 2008. Iron, silicate, and light co-limitation of three Southern Ocean diatom species. *Polar biology*, **31**, 1067–1080, 10.1007/s00300-008-0448-6.

HOLM-HANSEN, O., MITCHELL, B.G., HEWES, C.D. & KARL, D.M. 1989. Phytoplankton blooms in the vicinity of Palmer Station, Antarctica. *Polar biology*, **10**, 49:57.

JOHNSON, K.S., GORDON, M. & COALE, K.H. 1997. What controls dissolved iron concentrations in the world ocean? *Marine Chemistry*, **57**, 137–161.

KATZ, M.E., CRAMER, B.S., TOGGWEILER, J.R., ESMAY, G., LIU, C., MILLER, K.G., ROSENTHAL, Y., WADE, B.S. & WRIGHT, J.D. 2011. Impact of Antarctic Circumpolar Current Development on Late Paleogene Ocean Structure. *Science*, **332**, 1076–1079, 10.1126/science.1202122.

KEELING, C.D., WHORF, T.P., WAHLEN, M. & VAN DER PLICHT, J. 1995. Interannual extremes in the rate of rise of atmospheric carbon dioxide since 1980. *Nature*, **375**, 666–670.

KEELING, R.F. & GARCIA, H. 2002. The change in oceanic CO_2 inventory associated with recent global warming. *Proceedings of the US National Academy of Science*, **99**, 7848–7853.

KING, J.C. 1994. Recent climate variability in the vicinity of the Antarctic Peninsula. *Journal of Climatology*, **14**, 357–369.

KING, J.C. & HARANGOZO, S.A. 1998. Climate change in the western Antarctic Peninsula since 1945: observations and possible causes. *Annals of Glaciology*, **27**, 571–575.

KOHLER, P., JOOS, F., GERBER, S. & KNUTTI, R. 2005. Simulated changes in vegetation distribution, land carbon storage, and atmospheric CO_2 in response to a collapse of the North Atlantic thermohaline circuation. *Climate Dynamics*, **25**, 689-708. 10.1007/s00382-005-0058-8.

KLINCK, J.M. 1998. Heat and salt changes on the continental shelf west of the Antarctic Peninsula between January 1994 and January 1994. *Journal of Geophysical Research*, **103**, 7617–7636.

KLINCK, J.M., HOFMANN, E.E., BEARDSLEY, R.C., SALIHOGLU, B. & HOWARD, S. 2004. Water-mass properties and circulation on the west Antarctic Peninsula Continental Shelf in Austral Fall and Winter 2001. *Deep Sea Research Part II: Topical Studies in Oceanography*, **51**, 1925–1946, 10.1016/j.dsr2.2004.08.001.

KNOX, F. & MCELROY, M.B. 1984. Changes in atmospheric CO_2 - Influence of the marine biota at high latitude. *Journal of Geophysical Research - Atmospheres*, **89**, 4629–4637.

LANCELOT, C., HANNON, E., BECQUEVORT, S., VETH, C. & DE BAAR, H.J.W. 2000. Modeling phytoplankton blooms and carbon export production in the Southern Ocean: dominant controls by light and iron in the Atlantic sector in Austral spring 1992. *Deep-Sea Research I*, **47**, 1621–1662.

LE QUÉRÉ, C., RAUPACH, M.R., CANADELL, J.G. & AL, G.M.E. 2009. Trends in the sources and sinks of carbon dioxide. *Nature Publishing Group*, **2**, 831–836, 10.1038/ngeo689.

LEBLANC, K., HARE, C.E., BOYD, P.W., BRULAND, K.W., SOHST, B., PICKMERE, S., LOHAN,

M.C., BUCK, K., ELLWOOD, M. & HUTCHINS, D.A. 2005. Fe and Zn effects on the Si cycle and diatom community structure in two contrasting high and low-silicate HNLC areas. *Deep Sea Research Part I: Oceanographic Research Papers*, **52**, 1842–1864, 10.1016/j.dsr.2005.06.005.

MAHOWALD, N.M., ENGELSTAEDTER, S., LUO, C., SEALY, A., ARTAXO, P., BENITEZ-NELSON, C., BONNET, S., et al. 2009. Atmospheric Iron Deposition: Global Distribution, Variability, and Human Perturbations. *Annual Review of Marine Science*, **1**, 245–278, 10.1146/annurev.marine.010908.163727.

MALDONADO, MARIA T. & PRICE, N.M. 2001. Reduction and transport of organically bound iron by Thalassiosira oceanica (Bacillariophyceae). *Journal of Phycology*, **37**, 298–309.

MALDONADO, MAITE T & PRICE, N.M. 1999. Utilization of iron bound to strong organic ligands by plankton communities in the subarctic Pacific Ocean. *Deep-Sea Research II*, **46**, 2447–2473.

MARTIN, J.H. 1990. Glacial-interglacial CO_2 change: The iron hypothesis. *Paleoceanography*, **5**, 1–13.

MARTINSON, D.G. & IANNUZZI, R.A. 2001. Antarctic ocean-ice interaction: Implications from ocean bulk property distributions in the Weddell Gyre. *Antarctic Research Series*, **74**, 243–271.

MARTINSON, D.G., STAMMERJOHN, S.E., IANNUZZI, R.A., SMITH, R.C. & VERNET, M. 2008. Western Antarctic Peninsula physical oceanography and spatio-temporal variability. *Deep-Sea Research II*, **55**, 1964–1987, 10.1016/j.dsr2.2008.04.038.

MATSUMOTO, K., SARMIENTO, J.L. & BRZEZINSKI, M.A. 2002. Silicic acid leakage from the Southern Ocean: A possible explanation for glacial atmospheric pCO_2. *Global Biogeochemical Cycles*, **16**, 1–23, 10.1029/2001GB001442.

MAYKUT, G.A. 1978. Energy exchange over young sea-ice in the central Arctic. *Journal of Geophysical Research*, **51**, 281–305.

MCNEIL, B.I., METZL, N., KEY, R.M., MATEAR, R.J. & CORBIERE, A. 2007. An empirical estimate of the Southern Ocean air-sea CO_2 flux. *Global Biogeochemical Cycles*, **21**, 10.1029/2007GB002991.

MEREDITH, M.P., BRANDON, M.A., WALLACE, M.I., CLARKE, A., LENG, M.J., RENFREW, I.A., VAN LIPZIG, N.P.M. & KING, J.C. 2008. Variability in the freshwater balance of northern Marguerite Bay, Antarctic Peninsula: Results from $\delta^{18}O$. *Deep Sea Research Part II: Topical Studies in Oceanography*, **55**, 309–322, 10.1016/j.dsr2.2007.11.005.

MEREDITH, M.P., VENABLES, H.J., CLARKE, A., DUCKLOW, H., ERIKSON, M., LENG, M.J., LENAERTS, J.T.M. & VAN DEN BROEKE, M.R. *In press*. The freshwater system west of the Antarctic Peninsula: spatial and temporal changes. Journal of Oceanography.

MEREDITH, M.P., WALLACE, M.I., STAMMERJOHN, S.E., RENFREW, I.A., CLARKE, A., VENABLES, H.J., SHOOSMITH, D.R., SOUSTER, T. & LENG, M.J. 2010. Changes in the freshwater composition of the upper ocean west of the Antarctic Peninsula during the first decade of the 21st century. *Progress In Oceanography*, **87**, 127–143, 10.1016/j.pocean.2010.09.019.

METZL, N., TILBROOK, B. & POISSON, A. 1999. The annual fCO_2 cycle and the air–sea CO_2 flux in the sub-Antarctic Ocean. *Tellus*, **51B**, 849–861.

MILLIGAN, A.J. & HARRISON, P.J. 2000. Effects of non-steady-state iron limitation on nitrogen assimilatory enzymes in the marine diatom *Thalassiosira weissflogii* (Bacillariophyceae). *Journal of Phycology*, **36**, 78–86.

MITCHELL, B.G., BRODY, E.A., HOLM-HANSEN, O., MCCLAIN, C. & BISHOP, J. 1991. Light Limitation of Phytoplankton Biomass and Macronutrient Utilization in the Southern Ocean. *Limnology and Oceanography*, **36**, 1662–1677.

MOFFAT, C., BEARDSLEY, R.C., OWENS, B. & VAN LIPZIG, N. 2008. A first description of the

Antarctic Peninsula Coastal Current. *Deep-Sea Research Part II*, **55**, 277–293, 10.1016/j.dsr2.2007.10.003.

MOFFAT, C., OWENS, B. & BEARDSLEY, R.C. 2009. On the characteristics of Circumpolar Deep Water intrusions to the west Antarctic Peninsula Continental Shelf. *Journal of Geophysical Research*, **114**, 10.1029/2008JC004955.

MONTES-HUGO, M., DONEY, S.C., DUCKLOW, H.W., FRASER, W., MARTINSON, D., STAMMERJOHN, S.E. & SCHOFIELD, O. 2009. Recent Changes in Phytoplankton Communities Associated with Rapid Regional Climate Change Along the Western Antarctic Peninsula. *Science*, **323**, 1470–1473, 10.1126/science.1164533.

NELSON, D.M. & SMITH, W.O.J. 1991. Sverdrup Revisited: Critical Depths, Maximum Chlorophyll Levels, and the Control of Southern Ocean Productivity by the Irradiance-Mixing Regime. *Liminology and Oceanography*, **36**, 1650–1661.

NELSON, D.M., BRZEZINSKI, M.A., SIGMAN, D.E. & FRANCK, V.M. 2001. A seasonal progression of Si limitation in the Pacific sector of the Southern Ocean. *Deep-Sea Research II*, **48**, 3973–3995.

NELSON, D.M., TRÉGUER, P., BRZEZINSKI, M.A., LEYNAERT, A. & QUÉGUINER, B. 1995. Production and dissolution of biogenic silica in the ocean: Revised global estimates, comparison with regional data and relationship to biogenic sedimentation. *Global Biogeochemical Cycles*, **9**, 359–372.

PRITCHARD, H.D. & VAUGHAN, D.G. 2007. Widespread acceleration of tidewater glaciers on the Antarctic Peninsula. *Journal of Geophysical Research*, **112**, 10.1029/2006JF000597.

PRITCHARD, H.D., LIGTENBERG, S.R.M., FRICKER, H.A., VAUGHAN, D.G., VAN DEN BROEKE, M.R. & PADMAN, L. 2012. Antarctic ice-sheet loss driven by basal melting of ice shelves. *Nature*, **484**, 502–505, 10.1038/nature10968.

RAVEN, J. 1988. The iron and molybdenum use efficiencies of plant growth with different energy, carbon and nitrogen sources. *New Phytologist*, **109**, 279–287.

RAVEN, J.A., EVANS, M.C.W. & KORB, R.E. 1999. The role of trace metals in photosynthetic electron transport in O_2-evolving organisms. *Photosynthesis Research*, **60**, 111–149.

RIEBSELL, U., SCHLOSS, I. & SMETACEK, V. 1991. Aggregation of algae released from melting sea ice: implications for seeding and sedimentation. *Polar biology*, **11**, 239–248.

RINTOUL, S.R. & TRULL, T.W. 2001. Seasonal evolution of the mixed layer in the Subantarctic Zone south of Australia. *Journal of Geophysical Research*, **106**, 31447–31462.

SABINE, C.L., FEELY, R.A., GRUBER, N., KEY, R.M., LEE, K., BULLISTER, J.L., WANNINKHOF, R., et al. 2004. The oceanic sink for anthropogenic CO_2. *Science*, **305**, 376–371.

SARMIENTO, J.L. & TOGGWEILER, J.R. 1984. A new model for the role of the oceans in determining atmospheric pCO_2. *Nature*, **308**, 621–624.

SARMIENTO, J.L., GRUBER, N., BRZEZINSKI, M.A. & DUNNE, J.P. 2004. High-latitude controls of thermocline nutrients and low latitude biological productivity. *Nature*, **427**, 56–60.

SARMIENTO, J.L., MONFRAY, P., MAIER-REIMER, E., AUMONT, O., MURNANE, R.J. & ORR, J.C. 2000. Sea–air CO_2 fluxes and carbon transport: a comparison of three ocean general circulation models. *Global Biogeochemical Cycles*, **14**, 1267–1281.

SARMIENTO, J.L., SIMEON, J., GNANADESIKAN, A., GRUBER, N., KEY, R.M. & SCHLITZER, R. 2007. Deep ocean biogeochemistry of silicic acid and nitrate. *Global Biogeochemical Cycles*, **21**, 10.1029/2006GB002720.

SCHWERDTFEGER, W. 1979. Meteorological Aspects of the Drift of Ice From the Weddell Sea Toward the Mid-Latitude Westerlies. *Journal of Geophysical Research*, **84**, 6321–6328, 10.1029/JC084iC10p06321.

SCHWERDTFEGER, W. 1975. The Effect of the Antarctic Peninsula on the Temperature

Regime of the Weddell Sea. *Monthly Weather Review*, **103**, 45–51.

SEDWICK, P.N. & DITULLIO, G. 1997. Regulation of algal blooms in Antarctic shelf waters by the release of iron from melting sea ice. *Geophysical Research Letters*, **24**, 2515–2518.

SHEPHERD, A., WINGHAM, D. & RIGNOT, E. 2004. Warm ocean is eroding West Antarctic Ice Sheet. *Geophysical Research Letters*, **31**, 10.1029/2004GL021106.

SHEPHERD, A., WINGHAM, D., WALLIS, D., GILES, K., LAXON, S. & SUNDAL, A.V. 2010. Recent loss of floating ice and the consequent sea level contribution. *Geophysical Research Letters*, **37**, 1–5, 10.1029/2010GL042496.

SIEGENTHALER, U. & WENK, T. 1984. Rapid atmospheric CO_2 variations and ocean circulation. *Nature*, **308**, 624–626.

SIEVERS, H.A. & NOWLIN, W.D., Jr. 1984. The Stratification and Water Masses at Drake Passage. *Journal of Geophysical Research*, **89**, 10489–10514.

SIGMAN, D.M. & BOYLE, E.A. 2000. Glacial/interglacial variations in atmospheric carbon dioxide. *Nature*, **407**, 859–869.

SMITH, R.C. & STAMMERJOHN, S.E. 2001. Variations of surface air temperature and sea-ice extent in the western Antarctic Peninsula region. *Annals of Glaciology*, **33**, 493–500.

SMITH, R.C., BAKER, K.S. & STAMMERJOHN, S.E. 1998. Exploring sea ice indexes for polar ecosystem studies. *BioScience*, **48**, 83–93.

SMITH, R.C., STAMMERJOHN, S.E. & BAKER, K.S. 1996. Surface air temperature variations in the western Antarctic Peninsula region. *Antarctic Research Series: Foundations for ecological research west of the Antarctic Peninsula*, **70**, 105–121.

SMITH, W.O.J., MARRA, J., HISCOCK, M.R. & BARBER, R.T. 2000. The seasonal cycle of phytoplankton biomass and primary productivity in the Ross Sea, Antarctica. *Deep-Sea Research II*, **47**, 3119–3140.

SOMMER, U. & LENGFELLNER, K. 2008. Climate change and the timing, magnitude, and composition of the phytoplankton spring bloom. *Global Change Biology*, **14**, 1199–1208.

STAMMERJOHN, S.E. & SMITH, R.C. 1997. Opposing Southern Ocean climate patterns as revealed by trends in regional sea ice coverage. *Climatic Change*, **37**, 617–639.

STAMMERJOHN, S.E., MARTINSON, D.G., SMITH, R.C. & IANNUZZI, R.A. 2008a. Sea ice in the western Antarctic Peninsula region: Spatio-temporal variability from ecological and climate change perspectives. *Deep Sea Research Part II: Topical Studies in Oceanography*, **55**, 2041–2058, 10.1016/j.dsr2.2008.04.026.

STAMMERJOHN, S.E., MARTINSON, D.G., SMITH, R.C., YUAN, X. & RIND, D. 2008b. Trends in Antarctic annual sea ice retreat and advance and their relation to El Niño–Southern Oscillation and Southern Annular Mode variability. *Journal of Geophysical Research*, **113**, 10.1029/2007JC004269.

TAKAHASHI, T., SUTHERLAND, S.C., SWEENEY, C., POISSON, A., METZL, N., TILBROOK, B., BATES, N., et al. 2002. Global sea–air CO_2 flux based on climatological surface ocean pCO_2, and seasonal biological and temperature effects. *Deep-Sea Research II*, **49**, 1601–1622.

TOGGWEILER, J.R. 1999. Variation of atmospheric CO_2 by ventilation of the ocean's deepest water. *Paleoceanography*, **14**, 571-588.

TURNER, J., COLWELL, S.R., MARSHALL, G.J., LACHLAN-COPE, T.A., CARLETON, A.M., JONES, P.D., LAGUN, V., REID, P.A. & IAGOVKINA, S. 2005. Antarctic climate change during the last 50 years. *International Journal of Climatology*, **25**, 279–294, 10.1002/joc.1130.

VAUGHAN, D.G. & DOAKE, C.S.M. 1996. Recent atmospheric warming and retreat of ice shelves on the Antarctic Peninsula. *Nature*, **379**, 328–331.

VAUGHAN, D.G., MARSHALL, G.J., CONNOLLEY, W.M., PARKINSON, C., MULVANEY, R., HODGSON, D.A., KING, J.C., PUDSEY, C.J. & TURNER, J. 2003. Recent rapid regional climate warming on the Antarctic Peninsula. *Climatic Change*, **60**, 243–274.

VENABLES, H.J., CLARKE, A. & MEREDITH, M.P. *In press*. Wintertime controls on summer stratification and productivity at the western Antarctic Peninsula. *Limnology and Oceanography*, 1–30.

VERNET, M., MARTINSON, D., IANNUZZI, R., STAMMERJOHN, S., KOZLOWSKI, W., SINES, K., SMITH, R. & GARIBOTTI, I. 2008. Primary production within the sea-ice zone west of the Antarctic Peninsula: I—Sea ice, summer mixed layer, and irradiance. *Deep Sea Research Part II: Topical Studies in Oceanography*, **55**, 2068–2085, 10.1016/j.dsr2.2008.05.021.

WIEDENMANN, J., CRESSWELL, K.A. & MANGEL, M. 2009. Connecting recruitment of Antarctic krill and sea ice. *Limnology and Oceanography*, **54**, 799–811.

YOOL, A. & TYRELL, T. 2003. Role of diatoms in regulating the ocean's silicon cycle. *Global Biogeochemical Cycles*, **17**, 10.1029/2002GB002018.

Chapter 2: Study area

2.1 Introduction

This chapter serves as an introduction to the study area and ongoing monitoring at this site. The general methods of sample collection and analysis of parameters common to subsequent chapters are outlined here. Methodology for parameters discussed extensively will be presented in the relevant chapters.

In addition, the physical and hydrographical conditions of the study period are presented here, and related to regional climate trends and local biological processes. This chapter introduces the context of variation in biological production during the study period which the rest of this dissertation builds upon.

2.2 The Rothera Oceanographic and Biological Time Series Program

Ryder Bay is a seasonally ice-covered embayment of Marguerite Bay on the southern coast of the WAP (Fig 2.1). It is the site of the Rothera Oceanographic and Biological Time Series (RaTS), the longest running year-round oceanographic monitoring station in coastal Antarctica (Clarke *et al*. 2008). The long-term data from this monitoring scheme have established important regional hydrographic features, local El Niño Southern Oscillation (ENSO) effects and freshwater budgets (Meredith *et al*. 2004, 2010, *In press*), effects of polar temperature on benthic invertebrates (*e.g*. Brokington & Clarke 2001, Peck *et al*. 2004), and biological oceanographic processes including impacts of stratification on seasonal productivity dynamics and the annual importance of different size fractions to total chl concentrations (Clarke *et al*. 2008; Venables *et al*. *In press*).

The RaTS programme systematically monitors a wide variety of variables. Water column conditions are monitored ~biweekly (~monthly during winter) by CTD casts (conductivity, temperature, density), and additional sensors also measure pH, photosynthetically active radiation (PAR) and fluorescence. Water samples are

collected for chl, oxygen isotopes, macronutrients and ammonia. This programme has been operating in its current location since 1997, and this 16-year dataset allows a unique opportunity to contextualise results from this shorter-term study within the considerable interannual variability that characterises the Antarctic sea-ice zone.

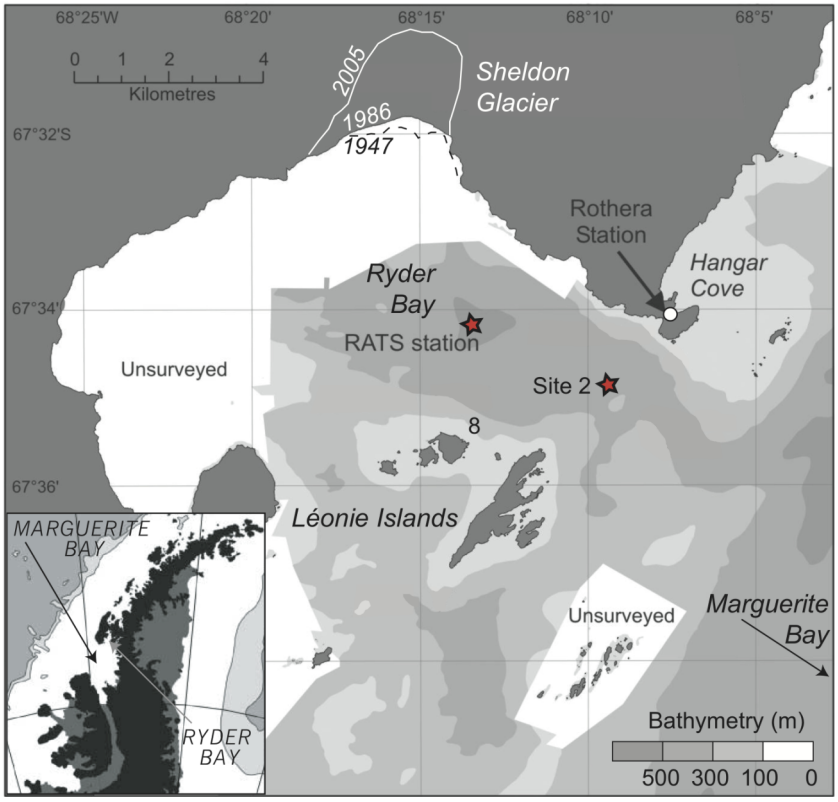

Figure 2.1: Map of the study area in Ryder Bay. The RaTS station (= Site 1) and Site 2 are shown, and Rothera Station on Rothera Point. The changes in the edge of Sheldon Glacier since 1947 are also shown.

2.2.1 Study period

The period sampled for this study was the austral summers (December to March) of 2008-09 and 2009-10. Previous work at the RaTS site on many of the same parameters examined here (particulate elemental composition, phytoplankton/diatom assemblages) extends the time series over three additional austral summers (2004 to 2007; Carson 2008, Annett 2008, Annett *et al*. 2010). Thus, wherever possible, data from five full seasons will be presented, over the 6-year period from 2004 to 2010 (note that the summer of 2007-08 was not sampled as part of these studies). Data from the RaTS sampling programme is available for the full 6 years, and hereafter "study period" refers to all six summers and intervening

winters which are considered based on available RaTS data to provide context for the high-resolution summer time-series data analysed here. Summer seasons will be referred to by the calendar year in which they start (*i.e*. the summer of 2004-2005 is hereafter "summer 2004"), thus the study period covers the austral summers of 2004, 2005, 2006, 2007 (RaTS data only), 2008 and 2009.

2.2.2 Local physical oceanography

The main source water for Marguerite Bay water is UCDW. Lower CDW is also found above the WAP shelf, although it is restricted to deep troughs (such as the Marguerite Trough) and is thought to mix only slowly with overlying UCDW (Howard *et al*. 2004, Martinson *et al*. 2008, Moffat *et al*. 2009).

In the summer, AASW occupies the top of the water column, which is a warm, fresh layer resulting from increased summer insolation and ice melt (commonly $\geq 0°C$, salinity ≤ 33.5; Meredith *et al*. 2004). During the winter months, AASW mixes with underlying water, creating WW, a very cold, relatively fresh water mass (commonly $\leq -1°C$, salinity 33.4 – 34 psu) extending to a typical depth of 40 – 60 m (Clarke *et al*. 2008). In late winter, this water mass can mix with underlying UCDW to near homogeneity (Clarke *et al*. 2008), but during the summer is present as a sub-surface temperature minimum where AASW forms above it (Meredith *et al*. 2004).

General patterns of circulation on the WAP shelf have been well studied (Hofmann *et al*. 1996, Hofmann & Klinck 1998, Klinck *et al*. 2004, Beardsley *et al*. 2004, Moffat *et al*. 2008, Savidge & Amft 2009), but local patterns within Ryder Bay and larger Marguerite Bay are not yet fully resolved. Circulation inshore of the ACC includes the southwestward flowing APCC which is thought to enter Marguerite Bay at the northern end and exit near Alexander Island, with cyclonic circulation occurring at the surface within Marguerite Bay (Moffat *et al*. 2008, Savidge & Amft 2009; Fig 2.2). Current data indicate some interaction with ACC waters via CDW incursions, and seaward movement of nearshore waters roughly above the Marguerite Trench (Savidge & Amft 2009).

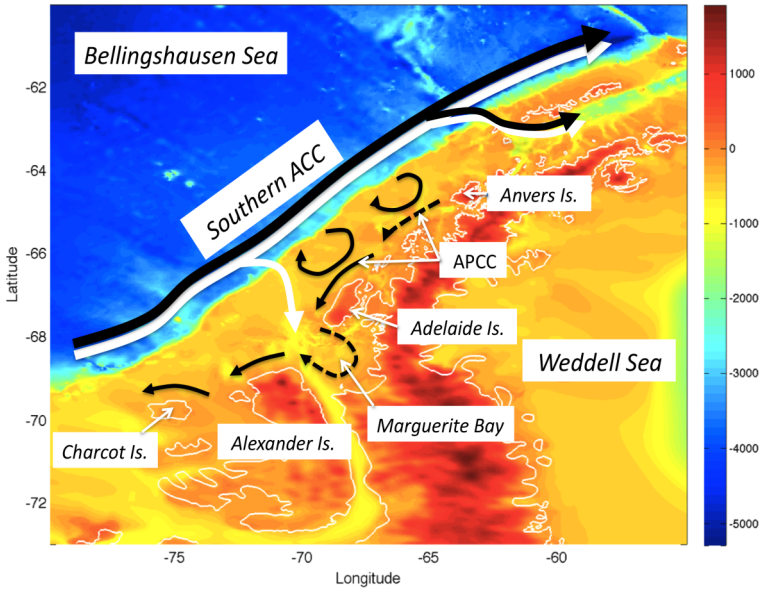

Figure 2.2: Schematic of local oceanographic circulation patterns and shelf bathymetry. White arrows represent deep currents, and black arrows show surface currents. Solid arrows denote flow patterns for which there is strong observational evidence; dashed arrows show flows that are presumed/inferred to exist. The Antarctic Peninsula Coastal Current (APCC) is shown following Moffat *et al*. (2008). From Meredith *et al*. (*In press*).

2.2.3 Local biological oceanography

In Ryder Bay, chl levels exhibit typical polar-region dynamics of a spring-summer productivity event and very low winter levels of photosynthetic biomass, but historically display considerable interannual variability (Clarke *et al*. 2008). Studies throughout the WAP region have established the importance of small phytoplankton classes (*i.e*. nanoflagellates) to annual production especially during winter, while the summer blooms are primarily dominated by larger algae, chiefly diatoms (Varela *et al*. 2002, Garibotti *et al*. 2005, Clarke *et al*. 2008). Throughout this region and the Antarctic marginal ice zone as a whole, many studies have found significant correlations between water column stability, often resulting from the freshwater lens produced by sea-ice melt and glacial runoff, and overall primary productivity (Holm-Hansen *et al*. 1989, Mitchell & Holm-Hansen 1991, Smith *et al*. 1998, Garibotti *et al*. 2003b, Vernet *et al*. 2008). Recent work in Ryder Bay has identified winter sea-

ice cover as a strong influence on water column stratification during the following summer (Venables *et al*. *In press*). The link between stratified conditions and high productivity may be a result of the diatom-dominated algal communities, as diatoms are associated with well-stratified conditions (Arrigo *et al*. 1999), and commonly associated with the retreating sea-ice edge (Smith *et al*. 1998).

2.3 Methods

2.3.1 Environmental/hydrographic conditions and sample collection

The RaTS programme makes frequent measurements of water column conditions, both physical and biological, in Ryder Bay. A CTD cast is performed on each sampling occasion, to monitor temperature, salinity, and density using a Sea Bird Electronics 19 Plus SEACAT CTD module. A Wet Labs Wetstar module was used for in situ fluorescence detection. Water samples are collected on each sampling event from 15 m depth, which corresponds to the long-term average depth of the chl maximum (Clarke *et al*. 2008). This sampling is done using a 2 L Niskin bottle, and samples are collected for chl, dissolved nutrients, and ammonium. Water samples are frozen for nutrient analysis in the UK (following standard autoanalyser protocols), and assays for ammonium concentration measurements and size-fractionated chl are performed on-site. Water samples for chl are filtered through a series of filters of pore sizes 20 µm, 5 µm, 2 µm and 0.2 µm, to measure chl in the >20 µm, 5-20 µm, 2-5 µm and 0.2-2 µm size-fractions, respectively. Filters are then placed in chloroform/methanol to extract chl, and concentrations determined based on fluorescence measurements. Ammonium concentrations are determined by *ortho*-phthaldialdehyde and fluorometry. Full details of RaTS programme sampling, analyses and calibration procedures are given in Clarke *et al*. (2008). All CTD and chl data presented here were provided by the RaTS programme database (British Antarctic Survey, Cambridge, UK).

Additional samples for this study were collected on two field campaigns during the austral summers (December to March) of 2008-2009 and 2009-2010. Biweekly sampling was carried out from a rigid inflatable boat as often as weather,

ice and logistics permitted, at the same time as RaTS sampling. Large-volume water samples for this study were collected using a 12 V Dolphin pump connected to weighted, acid-washed (5% v/v HCl, Analar-grade) silicon tubing, stored in 20 L acid washed (10% v/v HCl Analar-grade) HDPE carbuoys, and covered to limit exposure to sunlight until return to the laboratory for processing. Depth profile samples were collected on a ~weekly basis, when conditions allowed, at 5 depths: 0, 5, 10, 15 and 25 m. These depths were chosen to provide additional information throughout the productive surface waters, as chl concentrations are often high throughout a portion of the top 25 m (*i.e*. between 5 and 20 m depth), and MLD is often shallower than 25 m, such that parameters could potentially vary across a pycnocline within the photic zone. Samples were collected for the determination of multiple parameters: dissolved and particulate C, nitrogen (N), and phosphorus (P), isotopic composition of dissolved and particulate C and N, and radiocarbon, all of which are presented and discussed in Henley (2012). This study collected samples for phytoplankton biomass (Chapter 3), diatom composition and biomass (Chapter 4), dissolved and particulate Si and isotopic composition (Chapter 5), and dissolved iron (Chapter 7). Additional sampling was undertaken to investigate radium distributions, and is detailed in Chapter 6. A detailed list of dates and samples collected is given in Appendix A2.1.

Data on local sea-ice extent is also collected by BAS on a ~daily basis. Visual observations of Ryder Bay are made of the percent ice cover as well as ice type. These data are converted to weighted ice-type scores, as detailed in Meredith *et al*. (2010).

2.3.2 Dissolved and particulate elemental analyses

Samples are collected at the RaTS site for dissolved nutrient concentrations (N, P, Si) on each sampling event, as part of the RaTS sampling regime. Nutrient data from summer seasons and intervening winters, analysed using methods detailed in Clarke *et al*. (2008), were obtained from the RaTS database (British Antarctic Survey, Cambridge, UK).

Particulate organic C and particulate N (POC and PN, respectively) data are courtesy of Henley (2012), determined from from the material collected from pump

samples. In the lab, particulate material was collected onto pre-combusted, glass fibre filters (pore size ~0.7 μm), dried at ~37 °C, and stored frozen until analysis. Measurements were made following acidification to remove any inorganic C, on a Carlo Erba NA 2500 elemental analyser. Full details of these methods are presented in Henley (2012).

Particulate opal (biogenic silica; BSi) analysis was performed on separate, acid-clean polycarbonate filter samples. Full methodology of BSi analysis is outlined in Chapter 5 (and *Appendix A5.1*).

2.4 Results

2.4.1 Physical conditions

Ryder Bay displays a seasonal cycle typical of marginal sea-ice zones: sea-ice melt or break up occurs in spring (usually November/December), a spring phytoplankton bloom forms (which may begin under the ice just prior to break up), senescence of the bloom usually coincides with deterioration of the mixed layer, and finally formation of winter sea-ice. Summer conditions are predominantly open water, with ice bergs and intermittent presence of brash ice. While the timing and duration of these open water conditions varies annually, the duration of the summer bloom period (used here to refer to the first date where [chl] exceeds 2 mg m^{-3}, through the last date that [chl] remains above 1 mg m^{-3}) as assessed by chl concentrations is relatively consistent (90 to 125 days; for the period 2004-2010).

In contrast, winter sea-ice cover displays much greater interannual variation, ranging from < 20 to > 200 days of full fast-ice cover (RaTS data). Additionally, the pattern of ice cover may also vary, from several formation events followed by wind-induced break-up or blow-out, to winters of uninterrupted ice cover.

Temperature, salinity and density data are available from CTD casts throughout the study period, and are shown in Figure 2.3. Records are shown for 15 m water depth as well as deeper in the water column (100 and 200 m). Lower density summer surface waters reflect the input of meltwater, which is primarily derived from glaciers rather than sea-ice (as evidenced by oxygen isotopes, *in* Meredith *et al*. 2010). This warmer, less saline signal can also be seen in the temperature and

salinity records. These trends are also apparent, although to a much lesser extent, in the 100 and 200 m data.

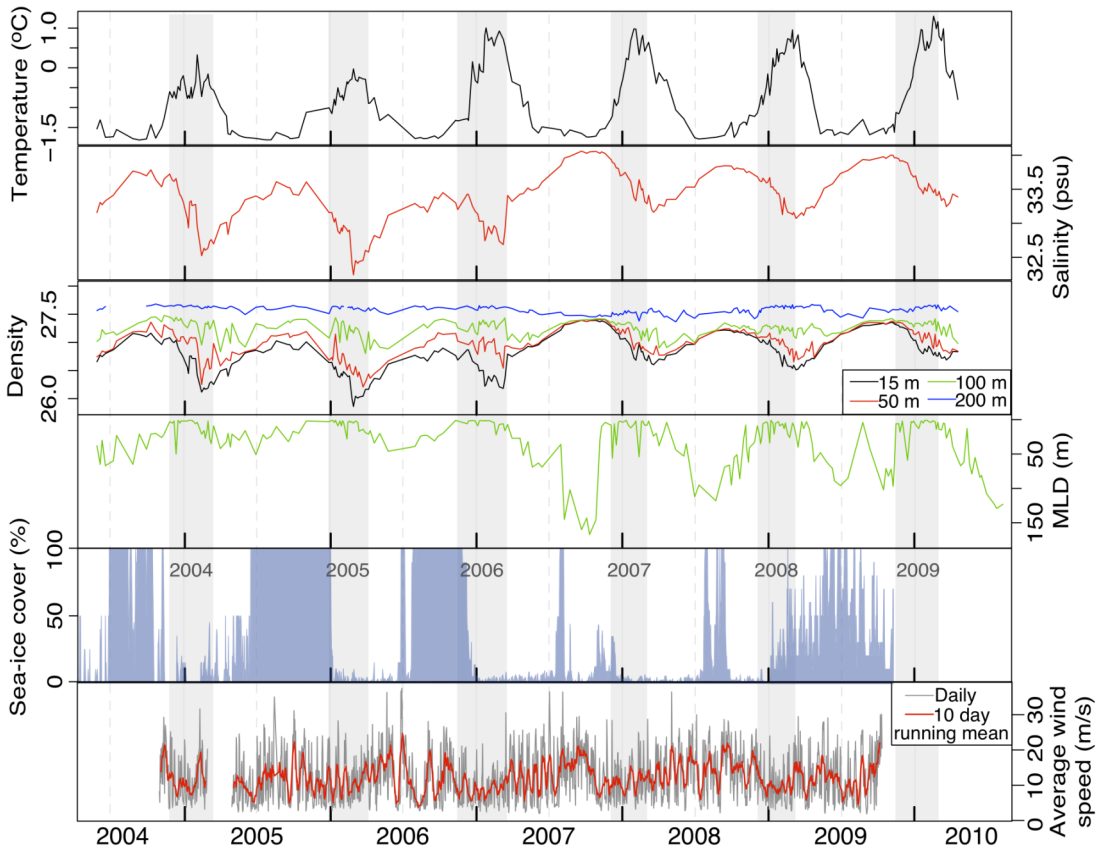

Figure 2.3: Physical conditions at the RaTS site during the study period. Temperature and salinity are from 15 m depth. Density is shown for four depths: 15, 50, 100 and 200 m. Mixed layer depth is shown in panel (d), and sea-ice cover for Ryder Bay is scored and weighted as per Meredith *et al*. (2010). Average wind speeds are shown in the bottom panel, both daily average (grey line) and a 10-day running mean of daily averages (red line). Grey shading denotes the summer bloom periods (see text), and are labelled by year in the sea-ice cover panel. All data courtesy of BAS.

Noteworthy in these data sets is a marked shift in conditions between the 2006 and 2007 summers. In the case of salinity and density both summer and winter averages change significantly only after the 2006 season, with winter averages increasing from <33.4 to >33.6 psu (<26.96 to >27.03 kg m^{-3} for density) and summer averages increasing from ~32.9 to ~33.5 psu (26.5 to ~26.9 kg m^{-3} for density) relative to the period June 2004 – Sept 2006. The shift appears to occur earlier in the case of temperature, during summer 2006, and results in a warmer

summer than the two previous years (by ~1.0 °C), although winter levels return to ~ -1.6 °C, very close to previous winter temperatures of -1.7 to -1.8 °C. From 2006 onwards, these warmer summer conditions persist. This event is also seen as a decrease in salinity and density, although these shifts are less extreme, suggesting that the earlier temperature signal may be linked to an input of warm meltwater, which preceded the main shift in water column conditions but is not linked to the main changes in density.

Changes are also seen in the mixed layer depth (MLD). We employ here the definition used by the RaTS programme, where MLD is the depth at which the density exceeds that at the surface by 0.05 kg m^{-3}. Winter 2007 displayed anomalously deep mixing down to >150 m, and the water column in winter 2008 and 2009 was mixed to ~100 m. This is in sharp contrast to the three earlier winters when mixing depth did not exceed 60 m. Summer MLD was also generally deeper in the last 3 years relative to the first 3 years of the study period. Average summer MLD for 2004-2006 was ~6.6 m, but ~11 m over the summer periods 2007-2009. While these differences are not statistically significant due to the large variance within each season caused by mixing events, the periods of stratification show a clear difference between the three early and later years of the study. The longest continous period of well stratified water (MLD <10 m) in each season was 48, 93, 96, and 25, 17, 35 days in 2004 to 2009, respectively. The periods of stratified conditions in the early years are statistically longer (p – value = 0.0156, 1-tailed t-test), contributing to the shallower average depth (6.6 m) in these years versus the average 11 m MLD for 2007-2009. Further, mixing events during the bloom period were less frequent (1 or 2 per season) in the early three years, compared to 4 or 5 events in the final three years of the study.

Overall, CTD data show a clear transition in winter 2007 to increasing salinity, density, and deeper MLDs. The transition in conditions coincides with an extended period of high average wind speeds and low ice cover in late winter 2007, when MLD first deepens to >100 m. The warmer, more saline and less stratified conditions persist through the end of the study interval. These changes can be easily seen in the much reduced range of density anomaly values in the upper water column

from winter 2007 onwards. While this signal is most pronounced in magnitude at the surface, the changes become apparent and significant at depth when considered relative to the much lesser extent of typical seasonal variation deeper in the water column (to 200 m; Fig. 2.4).

Data from oxygen isotopes show an uncommonly large range over winter 2007, concurrent with the physical changes noted above. The unprecedented increase in winter 2007 isotopic signatures, and high average values in 2008, reflect increased inputs of CDW to surface water (Meredith *et al*. 2010). These two years are the winters with extremely low sea-ice coverage, and Meredith *et al*. (2010) suggests that this low coverage is a result of high winds, which in turn results in high wind-mixing of the water column. This scenario explains the less stratified conditions due to higher wind mixing over winter, and wind-driven offshore movement of water would also account for more upwelling of CDW into Ryder Bay. Interestingly, oxygen isotope data also identify these two winters as years of high sea-ice production – seemingly at odds with the low sea-ice coverage, but reconciled by the tendency of Ryder Bay to act as a polynya. Thus high amounts of sea-ice begin to form in Ryder Bay, but are blown out into Marguerite Bay, leaving Ryder Bay as predominantly open water where more ice can form.

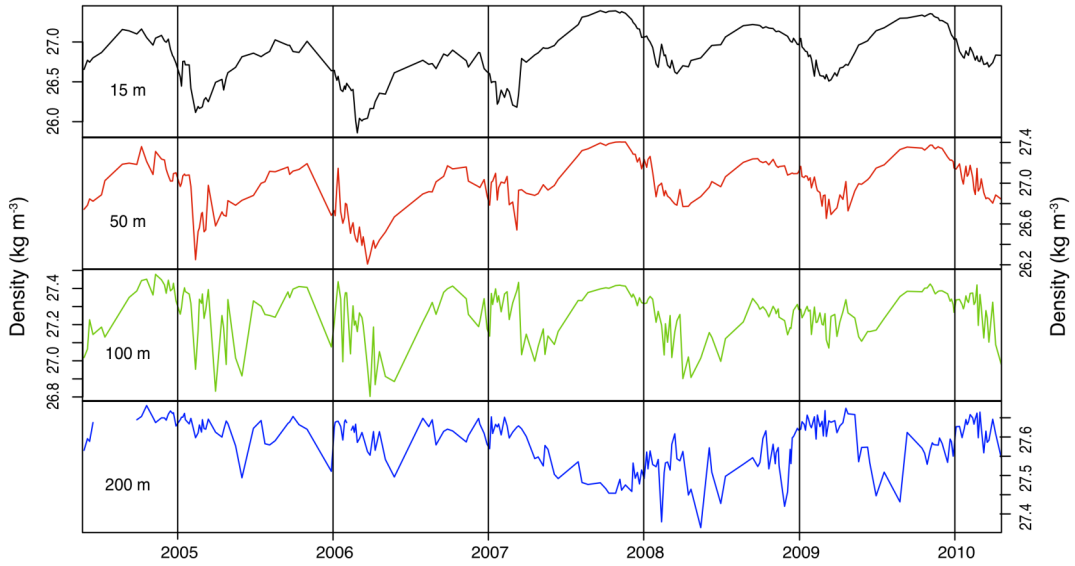

Figure 2.4: Density anomaly (σ_θ) at four depths in the water column: 15, 50, 100 and 200 m (top to bottom). Data from BAS.

The deep MLDs are a "recurrent but aperiodic" feature of northern Marguerite Bay and the WAP, resulting from a shift to a more northerly prevailing wind direction, which drives ice out of Ryder Bay (Meredith *et al*. 2010). These wind conditions are thought to be forced by periods of sustained positive southern annular mode and/or La Nina conditions.

2.4.2 Biological parameters

As with environmental conditions, chl concentrations ([chl]) showed considerable interannual variability across the six austral summers of the study period. As shown in Fig. 2.5, the first two summers exhibited high average [chl], with mean values in excess of 10 mg m^{-3}. Summer 2006 had somewhat lower concentrations, although still well above background, winter levels. The following two summer seasons (2007 and 2008) had much lower [chl], with concentrations not exceeding 4 and 7 mg m^{-3}, and averages of 1.7 and 1.9 mg m^{-3}, respectively. The final year of the study had relatively low [chl] early in the season, although during the second half of the season there was some recovery to higher concentrations with a maximum of ~22 mg m^{-3}.

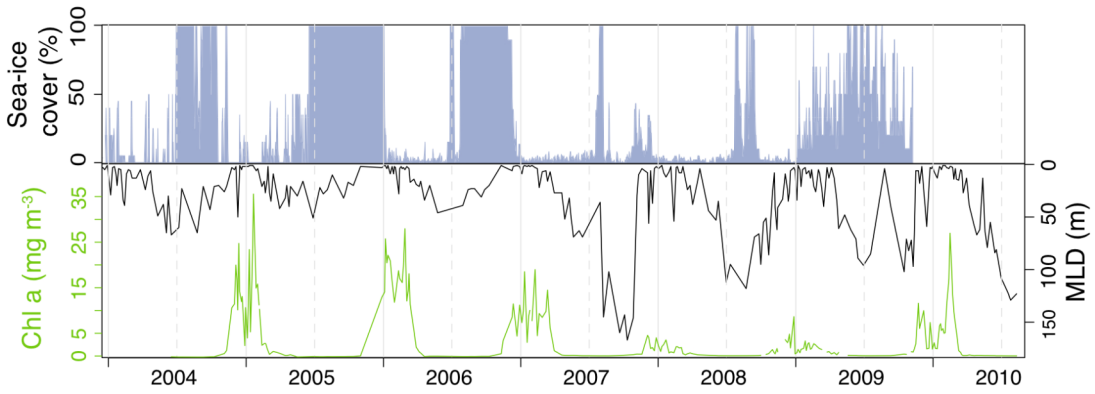

Figure 2.5: Chlorophyll concentrations at 15 m at the RaTS site during the study period, in relation to sea-ice cover and mixed layer depth. Data from BAS.

The relationship between sea-ice cover, MLD and [chl] is apparent in the time-series data in Fig. 2.5, where low sea-ice cover is followed by deeper MLD and low [chl]. As a first-order index of chl trends, seasonally integrated chl was calculated for each season. This index was calculated as the integrated area under the

15 m [chl] curve over the duration of the summer bloom period (as defined in 2.4.1). Thus this index will reflect both the magnitude and duration of the bloom. Summer peak concentrations ranged nearly 8-fold (3.7 to 28 mg m^{-3}) with integrated seasonal averages varying ~ 10-fold (150 to 1440), summarised in Table 2.1.

The first two summers of this time period (2004 and 2005) are easily identified as high-chl years, while 2007 and 2008 were low-chl years. Statistical analysis of variance (ANOVA) treatment indicates that the distribution of chl concentrations varies seasonally across the six-year stuy period (see Appendix A2.2), with both high-chl seasons exhibiting distributions distinct from the low-chl seasons. The remaining two seasons (2006 and 2009) exhibit intermediate [chl], and will be considered "intermediate" seasons (see also section 3.4.2.1). When grouped into seasonal chl type (*i.e.* high-, intermediate- or low-chl), the differences between the seasonal distributions of [chl] are highly statistically significant (ANOVA *p*-value = 2.2×10^{-16}; shown fully in Appendix A2.2).

In the context of longer-term variability at the RaTS site, records of sea-ice cover and [chl] at this location since 1997 are shown in Fig. 2.6. While there are considerable interseasonal variations in [chl], the two low-chl years identified during the study period are anomalously low, both in terms of chl and preceding winter sea-ice. The high and intermediate-chl seasons are much more in keeping with typical conditions in Ryder Bay.

Table 2.1: Seasonal chl measurements from samples at 15m water depth. Averages are listed ± 1 standard deviation. Integrated [chl] refers to the area under the [chl] curve during the summer bloom, as defined in the text, assuming a linear change between samples. Units are not given as this is a relative measure of seasonal productivity, and values are not corrected for length of the summer bloom period, nor integrated over the water column. Raw data from BAS.

Summer:	2004	2005	2006	2007	2008	2009
Average [chl] (mg m^{-3})	10.3±7.4	15±6.7	8.5±4.0	1.7±0.95	1.9±1.3	6.3±5.0
Max [chl] (mg m^{-3})	34.1	27.9	18.6	3.65	6.96	21.7
Integrated [chl]	1380	1440	1080	150	260	680

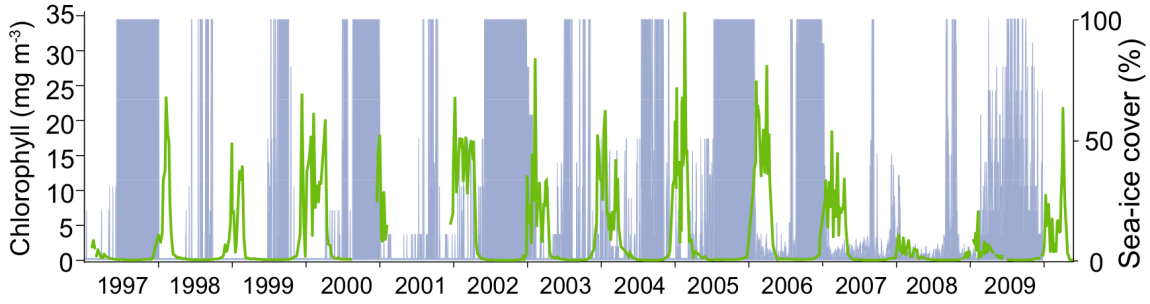

Figure 2.6: Chlorophyll concentrations (green line) and sea-ice cover (blue shading) at the RaTS site since monitoring began in 1997. Chlorophyll measurements are from 15 m. Data courtesy of BAS.

These uncharacteristically low chl concentrations occur following the change in physical conditions. Less stratified winter (and summer) conditions occurred during the winters of 2007 and 2008, and were followed by summer [chl] dynamics considerably below those recorded previously in the RaTS record. Thus in terms of high- and low-chl seasons, the physical changes in the water column are coupled to changes in biological productivity in surface waters. More difficult to distinguish based on environmental conditions are high-chl and "intermediate" years: there are no obvious physical reasons why [chl] was lower in summer 2006 than the preceding years. While temperatures were high, they were no higher than in late summer 2009 when [chl] reached ~23 μg L^{-1}. The other "intermediate" season, summer 2009/10, showed a partial recovery of chl late in the season, although this elevated chl level was short-lived. This late-2009 chl pulse might be explained by a short period of stable surface waters, as evidenced by shallow MLD during this period. In comparison to the full RaTS chl records, summer 2006 and likely 2009 as well, appear to be within the range of interannual variability. When considering POC, there is less difference between high and "intermediate" seasons than seen in chl records, thus the intermediate-chl seasons are likely to resemble high-chl season in terms of physical parameters.

The study period covered here comprises two high-chl seasons, two low-chl seasons, and two intermediate-chl seasons (Fig. 2.7). Following chapters will refine this characterisation by documenting and explaining differences in phytoplankton assemblages, diatom species composition, Si dynamics and Fe supply.

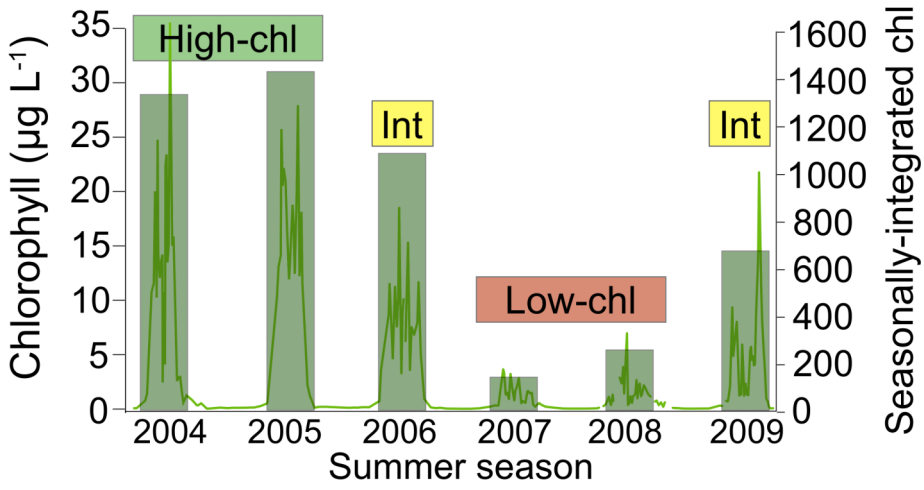

Figure 2.7: Classification of chl conditions for the study period presented here. Seasons are labelled by the calendar year in which they start on the x-axis. Shaded vertical bars denote seasonally-integrated chl, and is shown without units (see section 2.4.2 for details). Data courtesy of BAS.

2.5 References

ARRIGO, K.R., WEISS, A.M. & SMITH, W.O., Jr. 1998. Physical forcing of phytoplankton dynamics in the southwestern Ross Sea. *Journal of Geophysical Research*, **103**, 1007–1021.

BROKINGTON, S. & CLARKE, A. 2001. The relative influence of temperature and food on the metabolism of a marine invertebrate. *Journal of Experimental Marine Biology and Ecology*, **258**.

GARIBOTTI, I.A., VERNET, M. & FERRARIO, M.E. 2005. Annually recurrent phytoplanktonic assemblages during summer in the seasonal ice zone west of the Antarctic Peninsula (Southern Ocean). *Deep Sea Research Part I: Oceanographic Research Papers*, **52**, 1823–1841, 10.1016/j.dsr.2005.05.003.

GARIBOTTI, I.A., VERNET, M., FERRARIO, M.E., SMITH, R.C., ROSS, R.M. & QUENTIN, L.B. 2003. Phytoplankton spatial distribution patterns along the western Antarctic Peninsula (Southern Ocean). *Marine Ecology Progress Series*, **261**, 21–39.

HENLEY, S.F. 2012. *Climate-induced changes in carbon and nitrogen cycling in the rapidly warming Antarctic coastal ocean*. PhD Thesis. University of Edinburgh.

HOFMANN, E.E. & KLINCK, J.M. 1998. Thermohaline variability of the waters overlying the west Antarctic Peninsula continental shelf. *Antarctic Research Series*, **75**, 67–81.

HOFMANN, E.E., KLINCK, J.M., LASCARA, C.M. & SMITH, D.A. 1996. Water mass distribution and circulation west of the Antarctic Peninsula and including Bransfield Strait. *Antarctic Research Series: Foundations for ecological research west of the Antarctic Peninsula*, **70**, 61–80.

HOLM-HANSEN, O., MITCHELL, B.G., HEWES, C.D. & KARL, D.M. 1989. Phytoplankton blooms in the vicinity of Palmer Station, Antarctica. *Polar biology*, **10**, 49:57.

HOWARD, S.L., HYATT, J. & PADMAN, L. 2004. Mixing in the pycnocline over the western Antarctic Peninsula shelf during Southern Ocean GLOBEC. *Deep-Sea Research II*, **51**, 1965–1979, 10.1016/j.dsr2.2004.08.002.

KLINCK, J.M., HOFMANN, E.E., BEARDSLEY, R.C., SALIHOGLU, B. & HOWARD, S. 2004. Water-mass properties and circulation on the west Antarctic Peninsula Continental Shelf in Austral Fall and Winter 2001. *Deep Sea Research Part II: Topical Studies in Oceanography*, **51**, 1925–1946, 10.1016/j.dsr2.2004.08.001.

MARTINSON, D.G., STAMMERJOHN, S.E., IANNUZZI, R.A., SMITH, R.C. & VERNET, M. 2008. Western Antarctic Peninsula physical oceanography and spatio-temporal variability. *Deep-Sea Research II*, **55**, 1964–1987, 10.1016/j.dsr2.2008.04.038.

MEREDITH, M.P., RENFREW, I.A., CLARKE, A., KING, J.C. & BRANDON, M.A. 2004. Impact of the 1997/98 ENSO on upper ocean characteristics in Marguerite Bay, western Antarctic Peninsula. *Journal of Geophysical Research*, **109**, 10.1029/2003JC001784.

MEREDITH, M.P., VENABLES, H.J., CLARKE, A., DUCKLOW, H., ERIKSON, M., LENG, M.J., LENAERTS, J.T.M. & VAN DEN BROEKE, M.R. *In press*. The freshwater system west of the Antarctic Peninsula: spatial and temporal changes. Journal of Oceanography.

MEREDITH, M.P., WALLACE, M.I., STAMMERJOHN, S.E., RENFREW, I.A., CLARKE, A., VENABLES, H.J., SHOOSMITH, D.R., SOUSTER, T. & LENG, M.J. 2010. Changes in the freshwater composition of the upper ocean west of the Antarctic Peninsula during the first decade of the 21st century. *Progress In Oceanography*, **87**, 127–143, 10.1016/j.pocean.2010.09.019.

MITCHELL, B.G. & HOLM-HANSEN, O. 1991. Observations and modeling of the Antarctic phytoplankton crop in relation to mixing depth. *Deep Sea Research*, **38**, 981–1007.

MOFFAT, C., BEARDSLEY, R.C., OWENS, B. & VAN LIPZIG, N. 2008. A first description of the

Antarctic Peninsula Coastal Current. *Deep-Sea Research Part II*, **55**, 277–293, 10.1016/j.dsr2.2007.10.003.

MOFFAT, C., OWENS, B. & BEARDSLEY, R.C. 2009. On the characteristics of Circumpolar Deep Water intrusions to the west Antarctic Peninsula Continental Shelf. *Journal of Geophysical Research*, **114**, 10.1029/2008JC004955.

PECK, L.S., WEBB, K.E. & BAILEY, D.M. 2004. Extreme sensitivity of biological function to temperature in Antarctic marine species. *Functional Ecology*, **18**, 625–630.

SAVIDGE, D.K. & AMFT, J.A. 2009. Circulation on the West Antarctic Peninsula derived from 6 years of shipboard ADCP transects. *Deep Sea Research Part I: Oceanographic Research Papers*, **56**, 1633–1655, 10.1016/j.dsr.2009.05.011.

SMITH, R.C., BAKER, K.S. & STAMMERJOHN, S.E. 1998. Exploring sea ice indexes for polar ecosystem studies. *BioScience*, **48**, 83–93.

VARELA, M., FERNANDEZ, E. & SERRET, P. 2002. Size-fractionated phytoplankton biomass and primary production in the Gerlache and south Bransfield Straits (Antarctic Peninsula) in Austral summer 1995-1996. *Deep-Sea Research II*, **49**, 749–768.

VENABLES, H.J., CLARKE, A. & MEREDITH, M.P. *In press*. Wintertime controls on summer stratification and productivity at the western Antarctic Peninsula. *Limnology and Oceanography*, 1–30.

VERNET, M., MARTINSON, D., IANNUZZI, R., STAMMERJOHN, S., KOZLOWSKI, W., SINES, K., SMITH, R. & GARIBOTTI, I. 2008. Primary production within the sea-ice zone west of the Antarctic Peninsula: I—Sea ice, summer mixed layer, and irradiance. *Deep Sea Research Part II: Topical Studies in Oceanography*, **55**, 2068–2085, 10.1016/j.dsr2.2008.05.021.

Chapter 3: Causes and characteristics of environmentally-linked community-level phytoplankton changes in Ryder Bay

3.1 Abstract

Environmental changes along the WAP have the potential to significantly impact the marine ecosystem in this region. Changes in sea surface temperature, atmospheric circulation and sea-ice cover have been accompanied by changes in chl concentrations and phytoplankton size distribution (*e.g*. Montes-Hugo *et al*. 2009). However, evidence for these biological changes is indirect, with results inferred from satellite records and comparison to historical studies. Thus relatively little is known about the nature of biological changes at the phytoplankton level. To address this issue, this study presents high-resolution phytoplankton counts from a coastal WAP site spanning five austral growing seasons and a range of environmental conditions and biological production. Standing stocks are linked to environmental conditions, in particular water column stratification, which has previously been shown to play a key role in summer productivity at this site (Venables *et al*. *In press*). Phytoplankton assemblages from high-chl conditions are dominated by the largest (>20 μm) chl size fraction and high diatom abundances. Low-chl conditions display much greater contributions from smaller chl fractions and are characterised by proportionally higher non-diatom biomass, which is suggested to be primarily prymnesiophytes at this location. Here potential top-down and bottom-up mechanisms driving the changes are considered, and light levels are suggested to be a primary factor in structuring community composition and determining overall seasonal productivity.

3.2 Introduction

The WAP is the fastest-warming region of the southern hemisphere, with average annual air temperatures increasing at three times the global average rate (3.4 versus 0.7 °C century^{-1}; Vaughan *et al*. 2003). Atmospheric changes also include

changes in wind patterns, which are believed to be a cause of increased UCDW incursions onto the WAP shelf (Martinson *et al*. 2008, Meredith *et al*. 2010). Consistent with the intrusion of more warm UCDW, ocean heat content on the shelf has also increased in recent decades (Martinson *et al*. 2008). Warming of both the atmosphere and ocean are expected to impact glacial melt rates from above and below, respectively, and indeed over 85% of WAP glaciers were in retreat as of 2005, with the rates of this retreat accelerating (Cook *et al*. 2005).

The WAP is a highly productive region and has undergone significant changes in the past, from extremely high fishing (Ainley & Blight 2009) and whaling pressure (Croxall *et al*. 1992), to the more recent climatic changes outlined above. Both biological and physical factors can strongly impact productivity, but environmental conditions have been identified as an especially important factor regulating the structure and seasonal succession of phytoplankton communities in WAP waters (Prézelin *et al*. 2004). Stratification of the water column via sea-ice cover (Stammerjohn *et al*. 2008), sea-ice meltwater lenses (Vernet *et al*. 2008) and glacial meltwater lenses (Moline *et al*. 2001, Dierssen *et al*. 2002) are of particular importance, as are nutrient supplies via UCDW inputs (Prézelin *et al*. 2004). Given the climatic changes in recent decades, it is perhaps not surprising that changes in primary production have also been observed.

Changes at the phytoplankton level are less well-established, owing partly to the scarcity and length of water column monitoring records. Monitoring programs (e.g. Palmer LTER, RaTS) have only been operating since 1990 and 1997, respectively. Of the ship-based studies where stations are sampled repeatedly, data are rarely available for more than one sampling event per season and often occur at different points during the austral summer, owing to the short ice-free season, interannual variability in ice-cover and thus both seasonal timing and accessibility. As a result, multi-year comparisons of phytoplankton data are not always applicable between different cruises.

Recently, a comparison of satellite data has indicated drastic changes in [chl] along the WAP since 1978 (Montes-Hugo *et al*. 2009; Fig. 3.1). Although there is some debate concerning the ability of satellites to assess water column [chl] where blooms often occur below the optical depth of satellite detection, Dierssen & Smith

(2000) used a large data set to calibrate remote sensing methods for the WAP region specifically. Montes-Hugo *et al*. (2008a, 2008b) further refined these methods using extensive field data to provide information on phytoplankton community size structure and composition, especially with regards to diatom cells which are distinguishable from other phytoplankton groups by the pigment fucoxanthin.

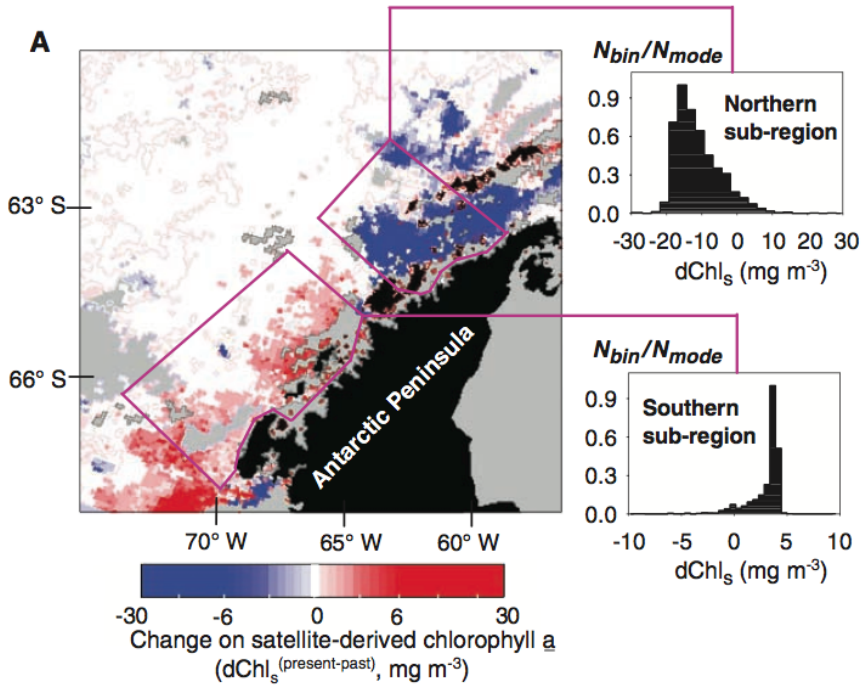

Figure 3.1: Satellite-derived chlorophyll analysis by Montes-Hugo *et al.* (2009) of changes in productivity in the WAP region. Shown are the differences in [chl]: past (1978-1986) minus present (1998-2006) as calculated from satellite data. Also shown are histograms of the pixel-by-pixel data where N_{bin}/N_{mode} is the relative frequency of observations per bin, normalized by the mode. Figure from Montes-Hugo *et al*. (2009).

The analyses by Montes-Hugo *et al*. (2009) compared the period 1978-1986, before the initiation of current monitoring programmes, with a period twenty years later (1998-2006). Based on the different system responses at the regional level, they divided the WAP into northern and southern subregions, where the division between the two occurs at roughly 64° S (*see* Figure 3.1). In the northern subregion, they found a trend towards stronger winds, which in combination with decreased sea-ice has led to more deeply mixed waters and in turn a very strong reduction in [chl]. Their data indicate that the average seasonal [chl] within this northern subregion has

declined by 89% relative to the 1978-1986 period, an even greater extent than the few available in situ ship-based data suggest (25–74% decline in January and February, respectively; Montes-Hugo *et al*. 2009 *and supporting online material*).

The changes seen in the southern subregion are very different, but consistent with the considerable latitudinal gradient present along the WAP. In the southern region, the decline in sea-ice coverage has occurred predominantly in areas that were covered year round by sea-ice during the earlier period, such that they have transitioned from permanent sea-ice zones to seasonal sea-ice zones. Consequently, the resulting ice-free summer conditions have enhanced phytoplankton productivity, and [chl] in this area has increased ~66% relative to the earlier study period (Montes-Hugo *et al*. 2009). In concert with these chl changes, the satellite-derived size-structure of phytoplankton communities has been seen to change.

High chl, where detected by satellite data, is characterised in both subregions by changes in backscattering which indicate larger phytoplankton cells (>20 μm), and higher fucoxanthin, an indicator pigment for diatoms (Montes-Hugo *et al*. 2009). In contrast, lower [chl] corresponds to communities with greater proportions of small cells and less fucoxanthin (= diatoms). Thus the northern region has experienced a decline in both [chl] and average cell sizes, while these parameters have increased south of 64° S. The inferred switch from high-chl diatom communities to low-chl non-diatom assemblages is supported by comparing sparse plankton studies from the early (1978-1986) period to more recent pigment analysis (*see section 3.5*).

In Ryder Bay, a shallow embayment at the northern tip of Marguerite Bay, records since 1997 show a regular seasonal dynamic of sea-ice break up, a spring phytoplankton bloom (sometimes beginning under the ice just prior to break up), senescence of the bloom and formation of winter sea-ice lasting ~4-8 months. Fed at depth by inputs from the Marguerite trench, water column profiles from previous investigations have shown that Ryder Bay is influenced by the same water masses as larger Marguerite Bay and displays the same seasonal dynamics in hydrographic and biological processes (Clarke *et al*. 2008). However, as outlined in Chapter 2, recent years of anomalously low winter sea-ice cover have been followed by very low summer [chl]. The study period here spans two years of high-chl conditions, two

years of intermediate [chl], and two years of extremely low winter sea-ice followed by low [chl] (Chapter 2).

This chapter presents a relatively long (5 years), high-resolution record of diatom and other phytoplankton assemblages from microscope counts in order to characterise changes associated with high- and low-chl seasons. This provides the first description of full season high- and low-chl phytoplankton communities from direct microscope investigation rather than pigment-based analysis. As Ryder Bay has been found to be representative of processes affecting the wider WAP region (Clarke *et al*. 2008), we look therefore at phytoplankton communities in Ryder Bay as a window into the changes occurring in Marguerite Bay, and along the WAP as a whole.

3.3 Methods

3.3.1 Study site

Surface water samples were obtained from the Rothera Oceanographic Time Series (RaTS) Sites 1 and 2, shown in Figure 2.1, in Ryder Bay (Adelaide Island, Antarctica) during the 2008 and 2009 summer field seasons. These sites are situated at a distance of ~4 km from the shore, over water of 520 and 400 m depth, respectively. RaTS Site 2 was used when ice or weather prevented access to Site 1, and both have previously been shown to be associated with the same water mass and display very similar properties (Clarke *et al*. 2008).

3.3.2 Sample collection

Water samples were collected as described in Chapter 2, approximately bi-weekly as conditions allowed, during the austral summers of 2008-09 and 2009-10. A list of sampling events is given in Table A2.1. For RaTS programme chl sampling, water was collected from a Niskin bottle and separated in the lab by filtration into four size fractions: 0.2–2 μm, 2-5 μm, 5-20 μm and >20 μm.

For electron microscope work and quantitative light microscope identification, water was collected from pump outflow, stored in 250 ml amber glass bottles, and preserved with 2.5% Lugol's fixative (iodine solution) which was

lowered to pH <7 to prevent dissolution of silica which can occur in alkaline conditions. Samples were stored in the dark at 4°C until they were filtered (~2–24 hours after collection). Replicate samples were collected on two types of 25 mm filter, Millipore® HAWG (0.45 μm) filters for light microscopy (LM), and isopore (0.2 μm) filters for scanning electron microscopy (SEM). Volumes filtered in most cases were 50 mL per filter, but near the end of the growing season, when suspended particulates in large-volume samples were visibly lower, volumes were increased to 100 mL per filter. Filtration was done under low vacuum, to minimise bursting of cells or breaking of chains. Both types of filters were then loosely covered and dried overnight in an oven at low temperature (37 °C). Filters for SEM were then stored in petrislides until analysis. Filters for LM were mounted on slides, following the methods detailed in Chapter 4.

3.3.3 Sample processing

3.3.3.1 Light microscopy

Filters were examined using a Leica microscope at 500x magnification. The filters are pre-printed with grid squares of 9.50 mm^2. Phytoplankton were counted and identified to the lowest taxonomic level possible in three randomly chosen grid squares. In the event that less than 300 cells were enumerated, counting continued until the cell count exceeded 300. Full details are provided in Chapter 4.

Previous samples (2006 season) were also analysed using LM. This analysis was performed using settling chambers and an inverted light microscope; full methodology can be found in Annett *et al.* (2010).

3.3.3.2 Scanning electron microscopy

Samples collected in previous seasons (2004-2005 and 2005-2006) were analysed using scanning electron microscopy. Full details of sample processing and counting methods can be found in Annett *et al.* (2010). Species abundances were obtained by assuming even distribution of cells on the filter, where the areal proportion of the filter examined was converted to the proportion of sample volume filtered. While the observed distribution of cells across the filter was not uniform, random choice in fields of view should minimise the effect of uneven distribution.

The diatom assemblage data from the summers of 2004 and 2005 have been previously described in Annett *et al*. (2010), but only in terms of relative species composition. To date, insufficient data has been available to establish the reliability of absolute concentration estimates. Appendix A3.1 compares the biomass estimates from all seasons to show that the data from the early two seasons are in keeping with those from later years. The strong correlation between measured POC and estimated diatom biomass (Fig. A3.1) suggests that any uneven distribution of cells on the filter had a negligible effect on the calculated cell abundances, and that the data presented here are robust reflections of biomass trends.

Although potential problems with preservation of cells - especially of taxa without siliceous or calcareous external structures (*i.e*. prymnesiophytes, choanophytes, dinoflagellates) - prevents comprehensive analysis of phytoplankton communities, the abundances of species observed by this method are believed to be robust (Annett *et al*. 2010).

3.3.3.3 Diatom biomass

In order to relate abundances to production and cycling of carbon (C), all diatom assemblage data presented here are expressed in terms of the C content calculated for each species. Cellular biomass of each species was estimated from cell biovolume, which was calculated using geometric formulae appropriate to the shape of the cell (Smayda 1978, Hillebrand *et al*. 1999). Full details of cell volume estimation and calculation of cellular biomass for each species are presented in Chapter 4.

3.4 Results

3.4.1 Physical setting

During the study period, winter sea-ice cover displayed considerable variability, which can be separated into two distinct types of coverage (Fig. 3.2). The first three winters were characterised by continuous or near-continuous cover, lasting 79, 201 and 148 days (2004, 2005, and 2006, respectively). Winter 2007 marked a shift to much lower ice cover. For the latter three years of the study (2007 to 2009) high concentrations of sea-ice occurred in short-lived events. For these three seasons

the number of sea-ice days of >80% ice cover were 11, 22, and 42 for 2007, 2008 and 2009, respectively.

Accompanying the shifts in sea-ice cover was a change to deeper mixing. This is apparent in the MLD (Fig. 3.2), and reflected by the much smaller differences in density between different depths within the water column. Increased mixing entrains more warm, salty water from depth (sourced ultimately from UCDW), and a marked change was apparent in temperature and salinity records at 15m depth. While the causes of these trends in stratification are discussed in Venables *et al*. (*In press*), the association is highlighted here between high (low) winter sea-ice cover and shallow (deep) summer MLD, as noted in section 2.4.1.

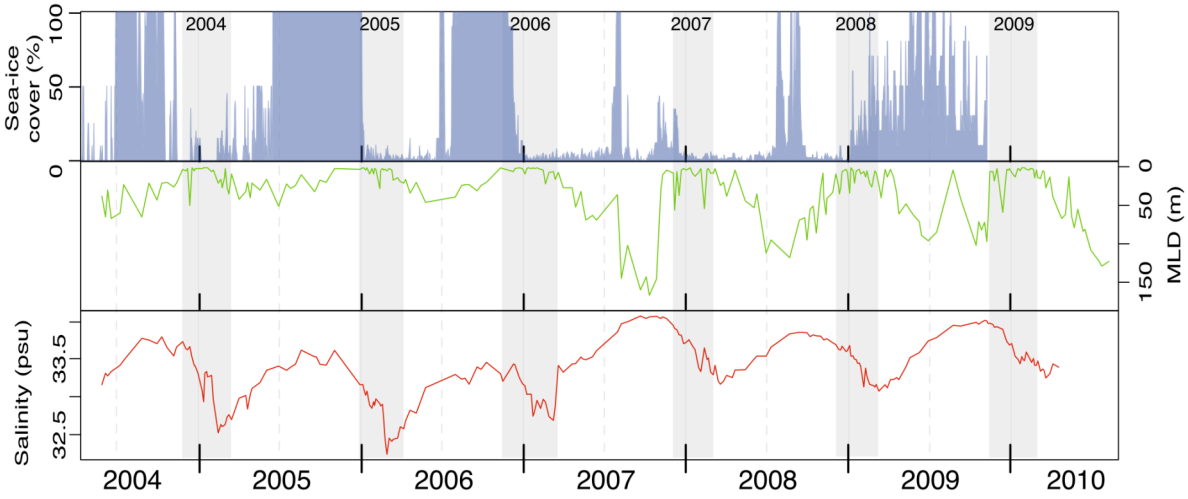

Figure 3.2: Environmental conditions during the study period (2004-2010). Shown from top to bottom are sea-ice cover, MLD and salinity at 15 m. Calendar years are labelled on the x-axis, and shaded sections denote the summer bloom period (as defined in Chapter 2), labelled at the top. Data courtesy of BAS.

3.4.2 Biological setting

3.4.2.1 Chlorophyll "regimes"

The first two summers of the study period (2004 and 2005) are easily identified as high-chl years, while 2007 and 2008 were low-chl years (see section 2.4.2). In addition to [chl], these "regimes" are also distinguishable on the basis of size-fractionated chl (Figure 3.3). High-chl seasons were almost wholly dominated by the >20 μm size fraction. While even the smallest chl size fractions (0.2-2 μm, 2-

5 μm) increased relative to winter levels (Figure 3.4), these increases were very modest, reaching concentrations much lower (<0.5 mg m^{-3}) than those of the >20 μm size fraction (>20 mg m^{-3}). In contrast, low-chl years showed contributions of up to 98% from the <20 μm size class.

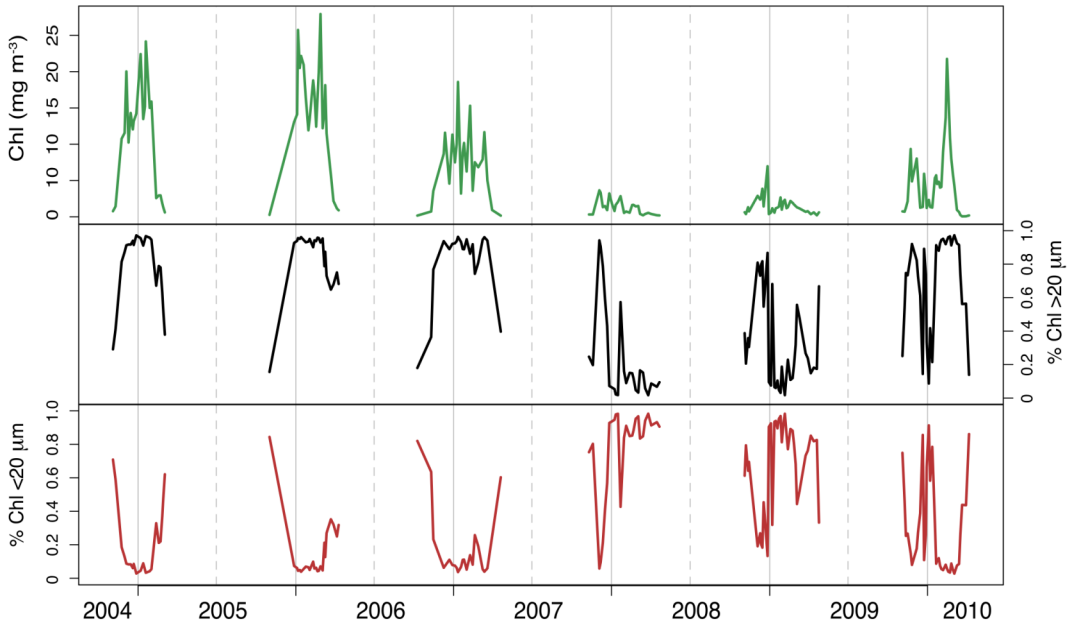

Figure 3.3: Total chlorophyll concentrations ([chl]) during the 6-year study period (top). Contributions of large (>20 μm) and small (<20 μm) fractions of chl relative to the total [chl] are shown in the middle and bottom panels respectively. A clear difference can be seen in the first 3 summers relative to the final 3 years. Records are from 15 m water samples, data shown for summer bloom periods (as defined in Chapter 2) only. Data courtesy of BAS.

The remaining two seasons (2006 and 2009) exhibit intermediate characteristics such as reduced chl levels, but significant contributions from the largest size class more typical of high-chl seasons. As such they will be considered "intermediate" seasons.

3.4.2.2 Diatom biomass estimates

Diatom community composition was assessed in this study for the two growing seasons 2008/09 and 2009/10. Comparisons focus on three previous seasons for which diatom community composition is also available (2004-2006; Annett *et al.* 2010), thus comparing two high-chl seasons, two intermediate seasons, and one low-chl year. Species-level results are presented in detail elsewhere (*see* Chapter 4). Each diatom species' abundance was converted to biomass based on estimated cellular carbon, and total diatom community biomass is presented in Figure 3.5.

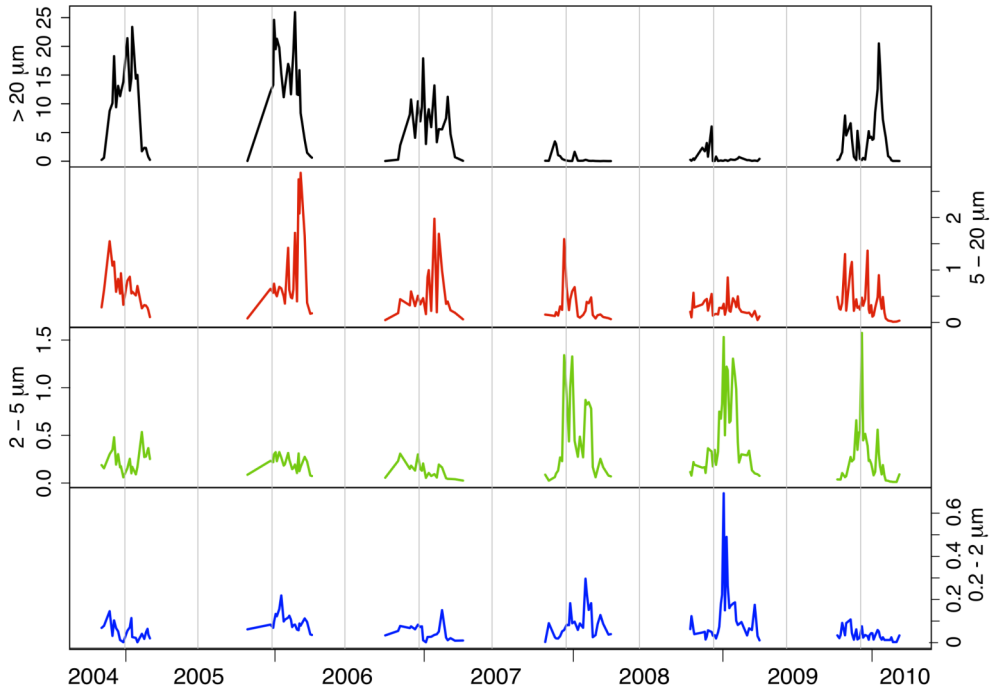

Figure 3.4: Absolute concentrations of the four size fractions of chl assessed by RaTS programme sampling at 15 m depth. The largest size fraction is shown at the top, smallest at the bottom. Size fractions are given on each y-axis (>20 µm, 5-20 µm, 2-5 µm, 0.2-2 µm), all data are [chl] in units of mg m^{-3}. Data courtesy of BAS.

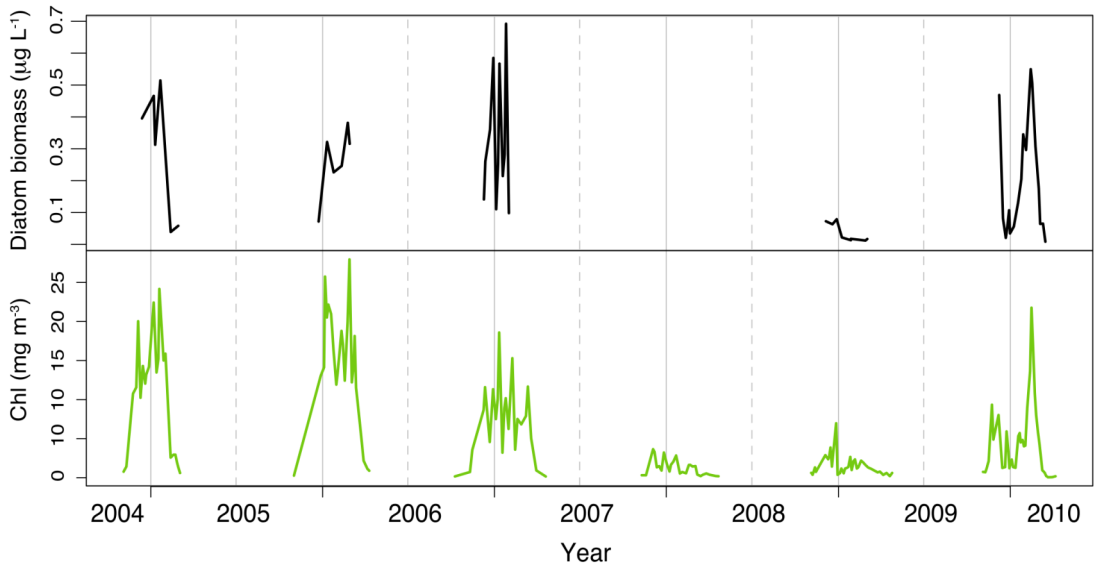

Figure 3.5: Diatom community biomass in black, as estimated from cell counts and species-specific biomass based on cell size measurements evaluated in this study. Diatom biomass is not available for summer 2007 as samples were not collected for diatom analysis in this season. Chlorophyll (green; from BAS data) is shown for comparison in lower panel.

3.4.2.3 Diatom biomass "regimes"

Estimates of diatom biomass largely follow the [chl] curve, including large fluctuations in summer 2006 and the mid-season low/late-season peak in summer 2009 (Fig. 3.5). Size-fractionated diatom biomass reflects similar trends as in chl data, although with smaller amplitude and notable temporal offsets (Fig. 3.6). In the two high-chl seasons, the percentage of chl attributable to small cells was initially very high and rapidly decreased as the summer bloom progressed, with larger cells then accounting for the majority of chl. Diatom biomass estimates are not available as early in the season as chl, but show a similar trend of initially high contributions from small cells, despite the small chl having already declined to very small proportions by this time. In the low-chl and intermediate seasons for which diatom analysis is available, the same high initial contribution of biomass from small cells was not seen. However the initiation of sampling during these seasons occurred later relative to the start of the bloom, and it is postulated that earlier samples may have shown greater contributions from smaller size fractions, as chl data from winter samples over the duration of the RaTS study consistently show a shift from small to large size fractions over the winter to summer transition (Clarke *et al*. 2008).

If the earliest samples in 2004 and 2005 where early sampling may bias the record compared to other seasons are not considered, the key compositional difference between the low-chl seasons and more productive years then becomes the higher relative amounts of small chl after the initial decline, which is absent in years of high chl. Rather than a sustained bloom of large diatom species, characteristic of high-chl seasons (large-cell biomass >80%), diatom biomass in the low-chl year shows markedly higher contributions from small cells (up to 60%) both mid- and late-bloom (2008). The intermediate years show less contrast with high-chl years, but exhibit several mid- or late- season samples with >20% of biomass contributions from small cells.

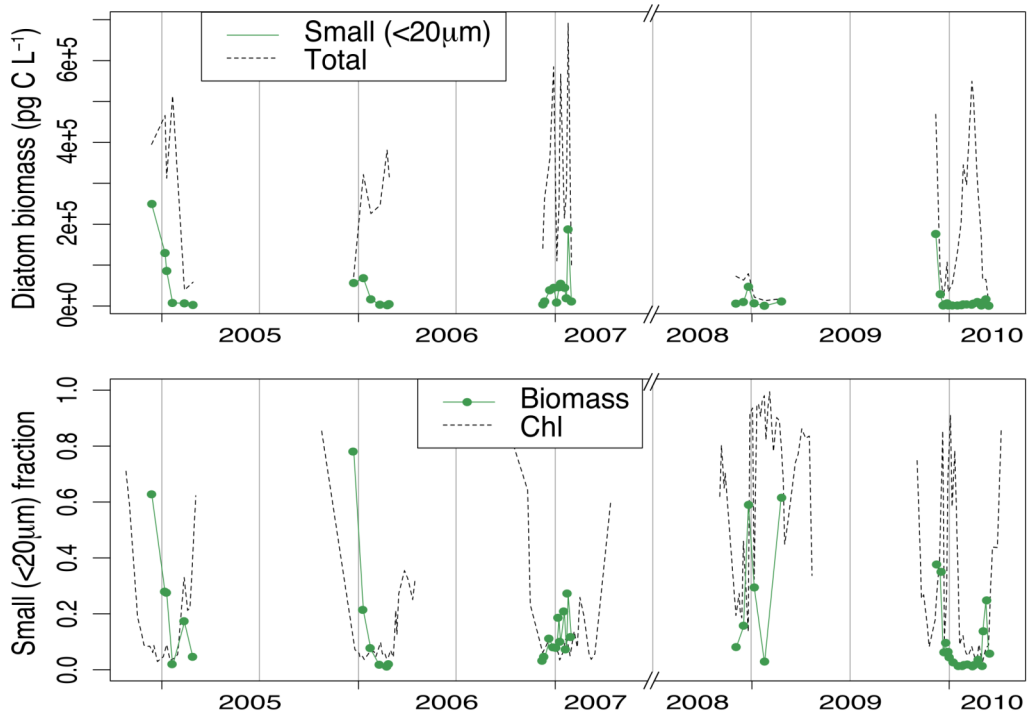

Figure 3.6: Total estimated diatom biomass and estimated small (<20 µm) diatom biomass (top). Bottom panel shows the fraction of biomass and of chl accounted for by small cells (bottom). Chl data from BAS.

Especially in the early season samples, there are instances where the biomass contribution of small diatoms appears to exceed the relative chl accounted for by the <20 µm size fraction. This is likely to occur when there are high abundances of chain-forming taxa (*e.g. Chaetoceros* spp., some *Fragiliariopsis* spp.), as these will largely be retained on a 20 µm filter, but are counted here as "small" diatoms

because individual cells are <20 μm. To compensate for this discrepancy, subsets of six samples per season were re-counted for chain forming diatom species (excluding summer 2006, for which samples were not available for re-analysis). Full explanation and analysis of these data are presented in *Chapter 4*, but diatom biomass size fractions, corrected to account for the percentage of small diatoms present in chains, are shown in Figure 3.7. This analysis shows that chains do indeed account for nearly all of the offsets where contributions of small chl are less than those of small biomass.

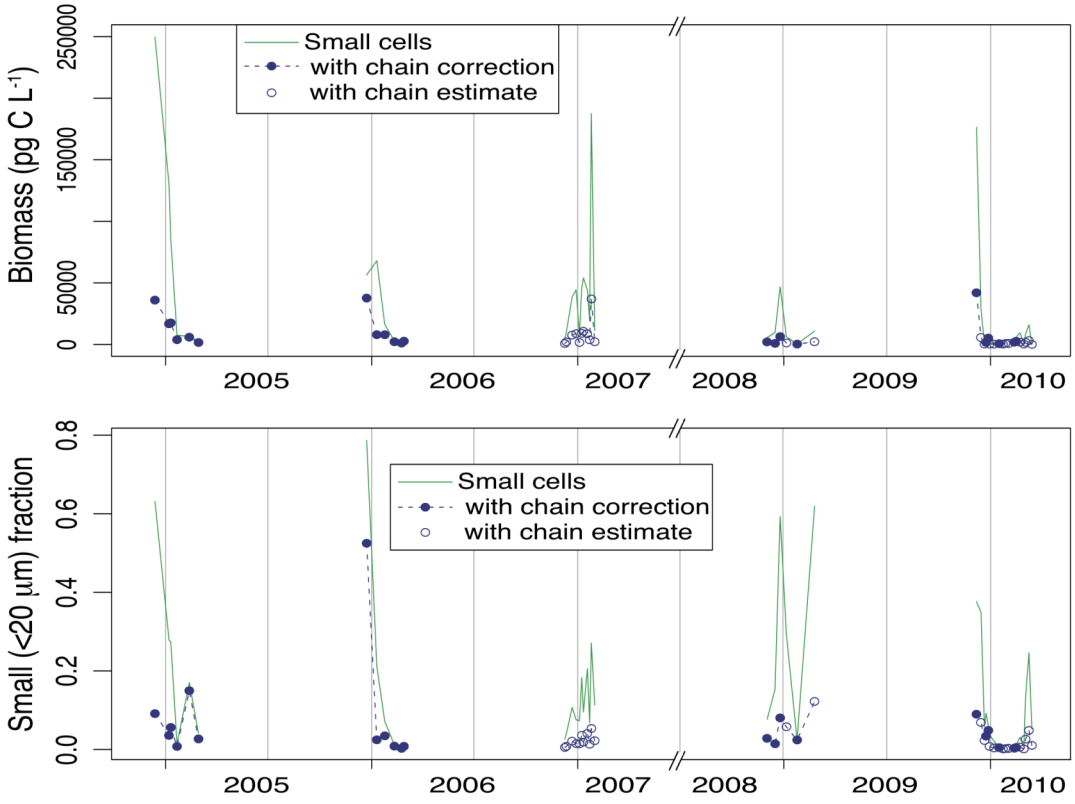

Figure 3.7: Total biomass (top) and fraction of total biomass (bottom) in small cells, with and without correction for chain-forming species. Six samples were analysed for chains in each season (except 2006), and average proportions used to estimate the chain-corrected biomass in other samples (see chapter 4).

3.4.2.4 Diatom community speciation

It should be emphasized here that no significant shifts in overall species composition were observed during this study. Full details of species-level analyses are presented in Chapter 4, but nearly all species were present in all seasons, albeit in

varying proportions and abundances. These data do not suggest any large-scale changes within the diatom community (*e.g*. regime shifts, or north to south displacement of communities) within the time frame of this study. While full non-diatom community data is not available across all seasons for comparison, it is likely that the same is true for other phytoplankton groups. Therefore no regime shift is implied, but rather that the seasonal balance of groups and/or species within local phytoplankton communities is highly plastic and responsive to environmental conditions.

3.5 Discussion

Trends in satellite-derived productivity data are described as a gradual southward relocation of phytoplankton assemblages containing abundant and large cells (Montes-Hugo *et al*. 2009). As the changes are characterised as a southward progression of phytoplankton communities, consistent with the geographic displacement seen in higher trophic levels (e.g. Chinstrap and Gentoo penguins; Ducklow *et al*. 2007), it can be hypothesised that as warming continues these shifts will continue to move southward. In this case, the divide between regions with small cells and low [chl] versus larger, high-chl communities would shift, with more of the WAP displaying the low-chl characteristics of the "northern" subregion.

Given the considerable interannual variability in [chl] and phytoplankton assemblages previously documented in this region (Garibotti *et al*. 2005, Clarke *et al*. 2008, Annett *et al*. 2010), it is unlikely that such a change would be manifested as either a gradual shift between high- and low- chl conditions, or an instant and permanent transition from one state to another. More likely such a shift would occur as a trend towards more numerous low-chl years compared to high-chl years, such as are exemplified by the different seasons observed here. Within the context of high regional variability, only longer-term records will be able to verify if such a shift is underway at the RaTS site, but it is consistent with the suggestion that the 2007 and 2008 seasons observed here are early low-chl conditions to which this region will progress.

3.5.1 Regional context

Shifts in phytoplankton size-structure coupled to overall productivity changes have been documented in multiple WAP studies. In addition to the satellite records analysed by Montes-Hugo *et al*. (2009), similar size shifts are suggested in data of the PalLTER study, at 64° 64' 27" S. Moline *et al*. (2001) document a seasonal pattern from 1991 through 1996 of late-spring diatom dominance followed by a transition to cryptophyte-dominated communities, linked to high input of glacial meltwater. This was in contrast to previous work by Krebs (1983) in 1972-1974, which had found diatom-dominated phytoplankton communities throughout the season, with diatom abundances strongly correlated to total [chl], indicative of very low proportions of non-diatom taxa. This suggests that between the early 1970's and 1990's, a transition has occurred from diatom-dominated communities to diatom-then-cryptophyte dominated communities, consistent with the satellite observations of Montes-Hugo *et al*. (2009).

Further documentation of size-structure changes come from Paradise Bay, at 64° 53' 42" S. Between 1970 and 1993 a decline in diatom communities was observed, along with increases of cryptophytes and other phytoflagellates (*see* Moline *et al*. 2001 *and references therein*). Paradise Bay and Palmer Station are located between the two subregions defined by Montes-Hugo *et al*. (2009), and are consistent with the changes seen in the northern sub-region during the period of satellite analysis.

However, existing assessments of community change are based primarily on satellite and pigment data, or comparisons to historical records. This study is the first to document differences at the phytoplankton level between high and low-chl seasons at a single location, identifying the primary mechanism for large fluctuations in [chl] under different environmental conditions.

The high- and low- chl conditions identified in previous studies have consequences for carbon drawdown and primary production available to higher trophic levels. Within the context of these productivity states, however, dynamics at the level of phytoplankton community must be taken into account, as they can act to amplify or dampen changes in nutrient cycling and production. This study presents

the first direct documentation of assemblage-level changes in phytoplankton communities between high- and low-chl seasons. These changes at the phytoplankton community level are considered further, to characterise the microalgal communities associated with high- and low- chl years, and assess some of the mechanisms which may drive these changes. Finally, the potential impacts of a sustained transition between high- and low- chl seasons will be explored in Chapter 8.

3.5.2 Phytoplankton-level aspects of chlorophyll step-changes

In addition to the overall differences in concentrations of chl (first observed by Venables *et al*. *In press*), the high and low-chl years can be differentiated by greatly enhanced contributions from the smaller size classes of chl in low-chl seasons (Figs. 3.3, 3.4). In Ryder Bay, the change to smaller size fractions is also reflected in diatom community records, although in diatom community biomass the difference is very slight compared to chl (mean 29% of biomass from chain-corrected small diatom biomass in 2008, compared with mean 11% (range 6–16%) in high- and intermediate-chl seasons). In comparison, the chl accounted for by the <20 μm size fraction is 68% in 2008 versus 22% (range 15–29%) in high/intermediate-chl seasons. This discrepancy (68% of chl but only 29% of diatom biomass in 2008) is of great importance, as it suggests that some of that increased contribution from small cells must come from non-diatom phytoplankton. Additionally, while this is an increase in the proportion of small diatom biomass, mean absolute biomass concentrations were lowest in the low-chl season, consistent with lower overall biomass. Thus increases in non-diatom phytoplankton groups must occur in order to explain the absolute increases (~1.0 μg L^{-1} (~3-fold) in the 2-5μm chl fraction) and higher relative small chl (up to 9-fold increase in the proportion of <20 μm chl).

As with periods of small diatom biomass contribution exceeding that of small chl, offsets also occur where the percentage of small chl is greater than that of small diatom biomass (Figure 3.6). When chains are taken into account, these discrepancies are even greater (Figure 3.7). As small cells present as chains will have been present in the >20 μm chl class, calculating the remaining fraction of diatom biomass that would have been measured in the smaller fractions leaves even lower small diatom biomass. Absolute biomass from the small diatom fraction is lower

overall in seasons 2008 and 2009, in keeping with the overall chl. The difference in trends between small diatom biomass and small [chl] offer strong evidence that the vast majority of the increase in <20 μm chl comes from non-diatom phytoplankton.

In the warming-induced regional trends from satellite data, the higher contribution of the small chl fraction is a key feature of low-chl seasons (Montes-Hugo *et al*. 2009). Diatom biomass estimates from this study show that the low-chl years documented by this study can be characterised by higher proportions of non-diatom phytoplankton. This reveals that the relationship between chl and diatoms in the WAP is very different to the Ross Sea. Along the WAP, this study and other published data suggest that low diatom abundances co-occur with low-chl conditions. In contrast, studies from the Ross Sea observe low diatoms in areas where chl is still high, due to high abundances of prymnesiophytes. Thus while the Ross Sea exhibits areas of either diatoms or *Phaeocystis*, both of which are associated with bloom events, in the WAP region low diatom abundance is not counteracted by high abundance of other phytoplankton, but rather chl remains low overall (although very slight increases in non-diatoms may occur, as in the case here).

3.5.2.1 Characteristics of phytoplankton assemblages in low-chl seasons

While the low-chl season non-diatom microalgae could be any of several groups, the prymnesiophyte *Phaeocystis antarctica* is likely one of the main species present during low-chl seasons. Elemental ratios in particulate organic matter (C, N data from Henley 2012; Si data see Chapter 5) indicate higher average Si:C and Si:N in the two early, high-chl years (Fig. 3.8). These parameters are consistent with diatom-dominated organic matter in the earlier years, and greater amounts of non-diatoms in the 2008 and 2009 seasons. Common non-diatom taxa in the Antarctic sea-ice zone include cryptophytes and prymnesiophytes; the former are commonly observed along the WAP where diatom abundances are low (Moline *et al.* 2001, 2004), while the latter are a key component in Ross Sea assemblages (Leventer & Dunbar 1996) and thought to be correlated with diatom abundances in areas including the WAP (Prézelin *et al*. 2004).

Several lines of evidence suggest increases in the abundance of *Phaeocystis antarctica*, a small prymnesiophyte common in many areas of the Southern Ocean. Cells can be solitary (3–9 μm in diameter), or form large colonies protected by a thick, gelatinous mucus. The solitary cells of *P. antarctica* would be in the appropriate size range for the non-diatom community, and nutrient and chl ratios are consistent with this phytoplankton group, as *P. antarctica* does not have the same frustule requirement for Si as diatoms, and has very high cellular carbon (C), in keeping with high production of organic mucus (Schoemann *et al.* 2005). This results in *P. antarctica* displaying much lower Si:C and chl:POC ratios than diatoms. Ratios of C:N are generally similar to that of the classic Redfield ratio (6.6 vs. 4–6 for *P. antarctica*), due to significant amounts of N-containing compounds in addition to carbohydrates (Solomon *et al.* 2003). However, cryptophytes also have similar C:N ratios, somewhat below Redfield ratio (4.4, Seixas e*t al*. 2009; <5.3, indirect estimate from data in Haberman *et al*. 2003). Particulate C:N ratios in Ryder Bay are typically 5-6 mol:mol, although some samples have higher ratios. This range of C:N values is consistent with either prymnesiophytes or cryptophytes.

The isotopic C signature of suspended particulate matter is also consistent with high abundances of *P. antarctica*. On average, the final two seasons of the study period have more depleted C signatures than the earlier seasons (*data presented and discussed in* Henley 2012). Previous studies in the Ross Sea have shown that assemblages dominated by *P. antarctica* (Leventer & Dunbar 1996) are associated with low C isotopic values in both suspended POC and sediment trap material (Villinski *et al*. 2000). In contrast, suspended and sinking material in areas of diatom-dominated communities displays much less depeleted isotopic signatures (Villinski *et al*. 2000). Recent work in Ryder Bay has shown that dramatic, late-season excursions to lower C isotopic values are associated with blooms of the rhizosolenoid diatoms of the genus *Proboscia* (Henley *et al*. 2012). However, as diatoms of this genus were very rare during summer 2008 and early 2009, another mechanism is needed to account for the overall more negative C signatures during these periods. High contributions of *P. antarctica* are consistent with both the depleted C isotopic values, and the low C:N and Si:C ratios of organic matter.

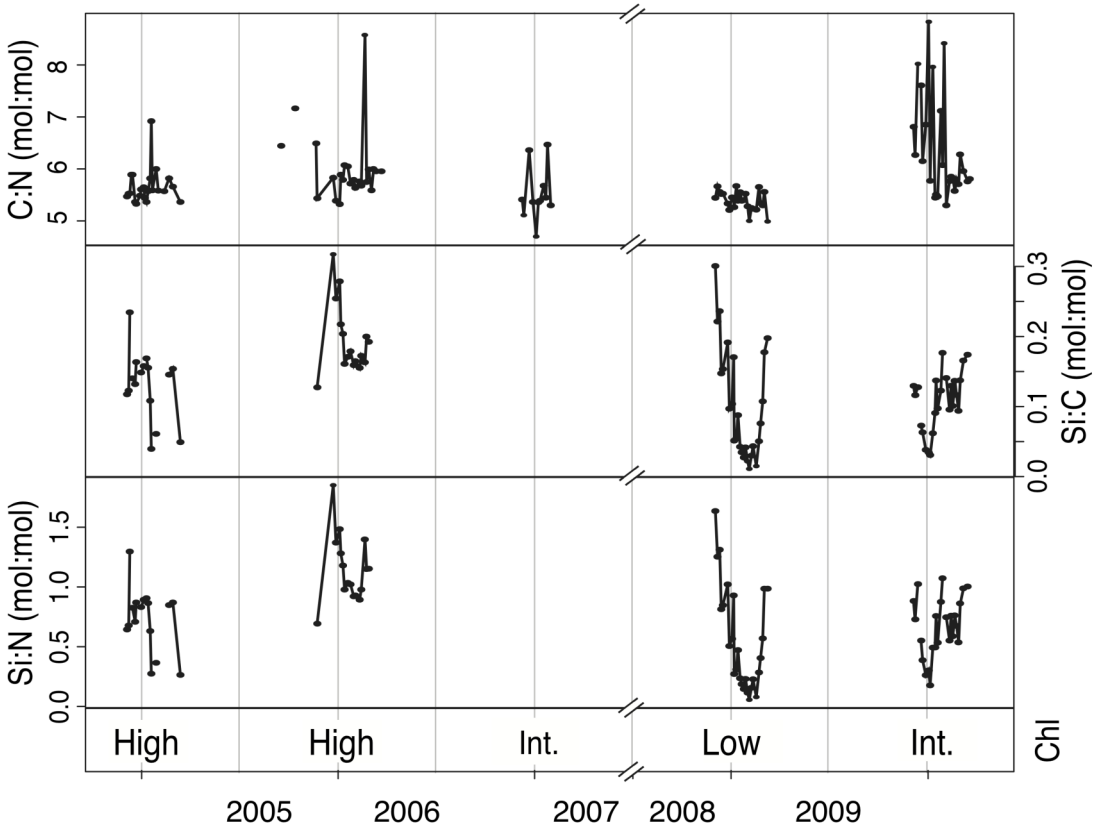

Figure 3.8: Elemental nutrient ratios determined in suspended particulate matter; C:N (top), Si:C (middle), and Si:N (lower). The seasons are classified based on chl dynamics, listed in the bottom panel. C and N analysis for organic material are outlined in Henley (2012), biogenic Si analysis is outlined in Chapter 5.

Most convincingly, *P. antarctica* synthesises characteristic star-shaped pentate thread structures, which are not known to be associated with any other phytoplankton (Buck & Garrison 1983, Fryxell 1989). Such "star-threads" were noticeably abundant in 2008 samples during SEM analysis, as shown in Figure 3.9. These threads were much less abundant, or not noticed at all in other seasons. Possibly due to their very small size, these star-threads were not noted in any of the SEM samples from the 2004 and 2005 seasons, although analysis was carried out primarily for diatom identification. However, as they were noticed in the 2008 samples it is assumed that had they been present in earlier seasons they would have similarly been observed. Additionally, the sample volumes filtered in the earlier seasons were much greater than in 2008-2009, so even lower concentrations should have been present on the filters in comparable abundances, thus the lack of observation is considered to reflect an absence of star-threads in the high-chl seasons.

As these structures are extremely small, and clearly visible only at very high magnification (>8000x), a fully quantitative assessment of their distribution would extremely time consuming. However, qualitatively it was noted that only a small area was scanned for star threads to be seen in 2008 samples, but much larger areas were searched before any were found on 2009 filters. The most star-thread structures were noted on 12 Feb 2009, with some observed very early in the season (28 Nov and 15 Dec 2008) and few in the 2 Mar 2009 sample. None were noted in the mid-season sample (26 Jan 2009), although this does not rule out very low abundances. In contrast, star-threads were only noted in two samples from summer 2009. They were relatively common in late Dec 2009, when small chl was very high (up to 90% of total), and were seen at low abundances on 12 Feb 2010, similar to the 2 Mar 2009 sample. In the following sample (15 Feb 2010), none were found, despite a targeted search.

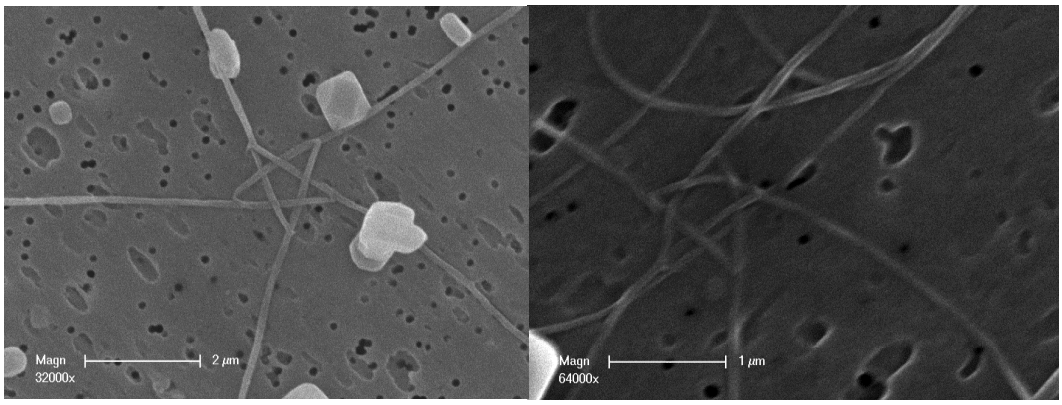

Figure 3.9: Scanning electron micrographs of pentate "star threads" associated with *Phaeocystis antarctica*, at 32000x and 64000x magnification. In some cases, salt crystals are visible on the threads, despite samples being rinsed with distilled water to remove the majority of salt. At lower magnification (such as that used for diatom identification) the small size of these structures and high susceptibility to small salt crystals make them difficult to differentiate from other fine thread-like structures (broken setae, choanoflagellates, etc.).

While cryptophytes, another common phytoplankton group in coastal WAP waters, are another possibility for the non-diatom biomass during low-chl seasons, the strong evidence here for *P. antarctica* combined with published cryptophyte dynamics make this unlikely. Cryptophyte abundances have been shown to vary inversely with surface salinity (Moline *et al.* 2001, 2004), associated with very high

glacial melt water inputs and highly stratified water columns. The higher salinities in the low-chl seasons in Ryder Bay would therefore suggest that cryptophyte abundance should have been lower rather than higher. Additionally, Garibotti *et al*. (2005) have repeatedly observed low or minimum cryptophyte abundance in Marguerite Bay.

3.5.3 Possible mechanisms for shifts in community size-structure/composition

Changes in water column conditions have a pronounced effect on overall productivity levels (*Chapter 2*; Venables *et al. In press*). The marked shift to two seasons of very low chl is associated with smaller cell sizes and more non-diatom phytoplankton. This section evaluates potential mechanisms which may drive both low productivity and non-diatom dominated community structure.

Limitations on primary production in marine systems can be divided into two main categories: bottom-up and top-down controls. Bottom-up factors are those such as light levels or nutrient availability, linked to physical processes, which set production limits. For example, minimum light requirements exist for net photosynthesis to take place, and macro- or micro-nutrients must be in adequate supply (via *e.g*. upwelling) for all necessary cellular reactions. In the Southern Ocean, iron (Fe) is often limiting, although this can be compounded by the availability of light and/or silicate (Hoffmann *et al*. 2008).

Conversely, top-down controls are biological factors, such as grazing pressure, which act to remove biomass from the system after the production step. In any system several factors may interact to limit productivity, or indeed limitations on levels of primary production may switch between factors as each becomes more or less important during the course of the season. Here, several possible governing mechanisms for the step changes in Ryder Bay productivity and community size-structure are evaluated and compared.

3.5.3.1 Bottom-up controls

One potential factor which might limit productivity and also drive a shift to smaller phytoplankton cells is nutrient availability. Supply of macronutrients (C, N,

P, Si) is generally high in Ryder Bay, due to the nutrient-rich deeper waters formed from circumpolar deep water (CDW) and the high solubility of CO_2 in cold water. In the context of interannual variation from high- to low-chl regimes, it can be seen that nutrients are not drawn down to low concentrations in low-chl seasons (Fig. 3.10). The most likely micronutrient to be a limiting factor in the marine system is iron (Fe), which limits productivity in several areas, including vast regions of the Southern Ocean. During the 2009 season, samples were collected for dissolved Fe analysis in Ryder Bay, to elucidate the role of Fe within the study area. These data are discussed in detail in Chapter 7, but over the seasonal scale of interest here, Fe can be discounted as a primary limitation on overall summer productivity.

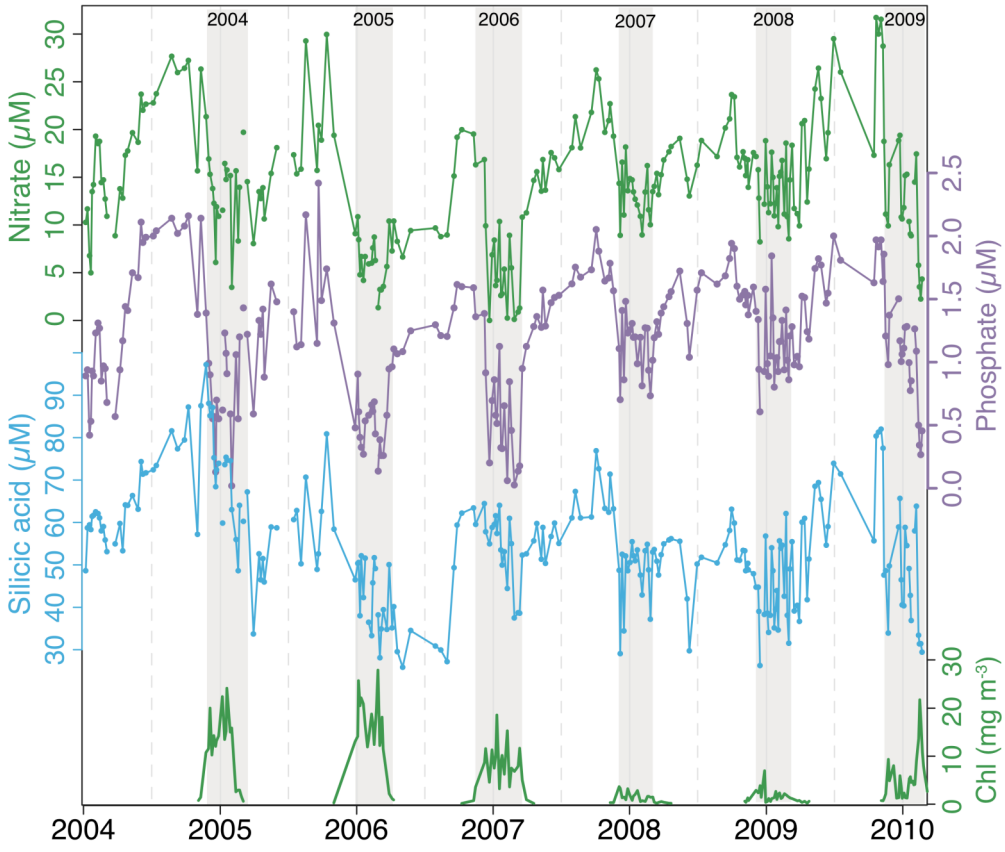

Figure 3.10: Macroutrient concentrations at 15 m during the study period. Shown from top to bottom are N, P, Si, and chl concentrations for comparison. Summer bloom periods are indicated by grey shading, and are labelled at the top of the plot. Note that in the two low-chl seasons, 2007 and 2008, nutrients are not drawn down to completion. Data courtesy of BAS.

Finally, light availability can control primary production in a bottom-up manner due to its role in photosynthesis. While light clearly sets limits on the length of the growing season, several factors can influence light levels in addition to the polar seasonal pattern. In general, coastal waters have higher suspended particulate matter, both organic and lithogenic, which reduces light availability. The depth of the mixed layer also plays a key role in determining the average light levels that phytoplankton are exposed to; if incident light remains relatively constant, a deeper mixed layer results in cells spending more time in deeper, low-light waters, reducing the average daily irradiance.

Given the negative correlation between mixed layer depth and average irradiance, it would be expected that lower stratification would result in lower [chl]. Indeed, this has been investigated in depth by Venables *et al*. (*In press*) and a strong relationship between these two variables was found in Ryder Bay. However, light can affect more than overall productivity, as different phytoplankton respond differently to high- and low- light conditions. In the Ross Sea, highly-stratified conditions have been correlated with higher abundances of diatoms, while more deeply mixed waters have been found to favour *Phaeocystis*-dominated communities (Leventer & Dunbar 1996, Arrigo *et al*. 1999). It was suggested by Arrigo *et al*. (1998) that differences in photosynthetic efficiency may be key in determining the distributions of these two algal groups. The photophysiology of *P. antarctica* is suggested to be very flexible, and capable of adapting to the wide range of light intensities experienced in conditions of deeper mixing ("shade conditions"; Schoemann *et al*. 2005). Tilzer *et al*. (1986) found that diatoms exhibit only 20-50% of the photosynthetic efficiency of *P. antarctica*, and as such may only outcompete *Phaeocystis* under high-light conditions ("sun adapted"). In agreement, a field study in the WAP found volumetric production rates in diatom-dominated communities were over twice those found in phytoflagellate-dominated communities (composed of a mix of *Phaeocystis* and cryptophytes; Prézelin *et al*. 2004), both under mid-day light regimes. In contrast, a study by van Hilst & Smith (2002) found only mild differences between the photosynthetic response of diatoms and *P. antarctica*, both cultured and *in situ*, indicating that light control alone is insufficient to explain distribution patterns in the Ross Sea. Additional factors (especially iron availability)

can modulate the effects of photosynthetic responses in Southern Ocean diatoms and *P. antarctica* (Strzepek *et al*. 2012).

The repeated pattern of more diatoms (*Phaeocystis*) in shallow- (deep-) mixed waters observed in coastal Antarctic regions agrees well with current understanding of diatom and *Phaeocystis* ecological preferences. Within the Antarctic circle during summer, light is constantly available, and the deepening of the average MLD from ~8 to ~13 m at the RaTS stie should result in a decrease in the average available light levels of ~30% (based on average PAR in the top 13 m vs. average in the top 8 m, from BAS data). However, when accounting for self-shading by phytoplankton, Venables *et al*. (*In press*) found that light availability within the mixed layer was higher overall in Ryder Bay during low chl seasons. In periods of abundant light, low growth rates were attributed to lower overall efficiency of phytoplankton cells over a greater range of light levels (Venables *et al*. *In press*). The wider light tolerance of *P. antarctica* would favour this species during unstable conditions (such as deep MLD), but the more frequent exposure to low-light conditions would concurrently restrict total biomass production. This suggests that the range of light levels experienced throughout the mixed layer, which is tightly linked to MLD, may be key in driving both phytoplankton assemblage changes and reductions in [chl], as lower average light levels are consistent with the overall lower productivity accompanying the phytoplankton compositional change. It has been suggested that these deeply mixed conditions are a result of changes in the prevailing wind patterns, which in turn are likely controlled by atmospheric variations in the Southern Annular Mode (SAM) and ENSO (Meredith *et al*. 2010).

3.5.3.2 Top-down controls

Primary consumers along the western Antarctic Peninsula include krill, salps, copepods, jellies, protists and many others (Ducklow *et al*. 2007). Although the dominant groups are krill, copepods and salps, krill are believed to be a particularly important group. Krill support higher trophic levels (Laws 1985), form the basis of a large fishing industry (Ichii 2000) and are a key component of carbon export in the Southern Ocean (Tarling & Johnson 2006). In the context of this investigation, Marguerite Bay is a krill-rich area (Marr 1962, Lawson *et al*. 2008) that has been

suggested by several studies to be a key overwintering ground and important source area for the highly-populated regions of Bransfield Strait and South Georgia (Brinton 1985, Atkinson *et al*. 2001, Fach *et al*. 2002).

Krill can affect both total phytoplankton biomass and composition, as they are known to prefer large diatoms (and/or longer chains of diatoms; Bergkvist *et a*l. 2012) and selectively graze on diatom communities (Haberman *et al*. 2003), including showing directed movement away from cryptophyte-dominated waters (Kanda *et al*. 1982). They are less efficient at grazing small particles (<20 μm; Quetin & Ross 1985, Weber & El-Sayed 1985), including Phaeocystis communities and cryptophytes (Haberman *et al*. 2003), nor are solitary cells efficiently consumed, due to their small size (Breton *et al*. 1999).

Salps are much more efficient at grazing smaller size fractions (Harbison *et al*. 1986, Kremer & Madin 1992, Madin & Kremer 1995), even down to 1-2 μm (Walsh *et al*. 2001), and in fact are thought to avoid areas of high diatom biomass, as diatoms can clog their filtering membranes (Quetin *et al*. 1996, Perissinotto & Pakhomov 1998a, b). Thus, zooplankton communities may respond to the phytoplankton community assemblage, where low chl concentrations and smaller size distributions favour grazing by salps (Quetin *et al*. 1996). However, Phaeocystis-dominated waters have been observed following high levels of krill abundance, likely as a result of the selective, high removal rates of diatoms by krill: Graneli *et al*. (1993) and Jacques & Panous (1991) observed that krill swarms can strip surface waters of diatoms in a matter of hours. As such, grazing can be either a result or a cause of phytoplankton assemblages in a way not directly related to total food availability as reflected in bulk [chl] measurements.

An evaluation of nutrient drawdown (and therefore a second index of production) compared to [chl] (representing standing stocks) allows a preliminary assessment of grazing impact. It is worth distinguishing here between chl (as a proxy for phytoplankton biomass) and production. Primary production refers to the production of new organic matter via photosynthesis. While chl is linked to this process, [chl] reflects standing stock, the amount of chl in the water column at the time of sampling and does not necessarily reflect the rate of productivity. Thus productivity may be low despite [chl] being high (as appears to be the case in 2005),

or productivity may be high even when standing stocks are low, although this case is more rare and usually reflects tightly coupled removal processes such as grazing. Between nutrient use (here based on nitrogen: "N-use") and [chl], N-use will be a more accurate estimate of production than [chl], as the latter only reflects phytoplankton standing stock.

Seasonal N-use from nutrient analysis (Fig. 3.11) was much lower in the summers of 2007 and 2008 compared to the maximum (2004), indicating that productivity was low overall, thus biomass drawdown by grazing cannot have been great. This therefore suggests that either light availability, or sustained and unusually tightly-coupled grazing pressure prevented the summer bloom from reaching typical [chl]. Interestingly, summer 2005 was a high-chl year but shows low N-use. This is likely due to periods of extended stratification where an initial pulse of production resulted in accumulated chl/biomass and some nutrient use, but lack of nutrient injections during the season prevented high cumulative drawdown, as has been suggested by Carson (2008), Annett *et al*. (2010), and Henley (2012).

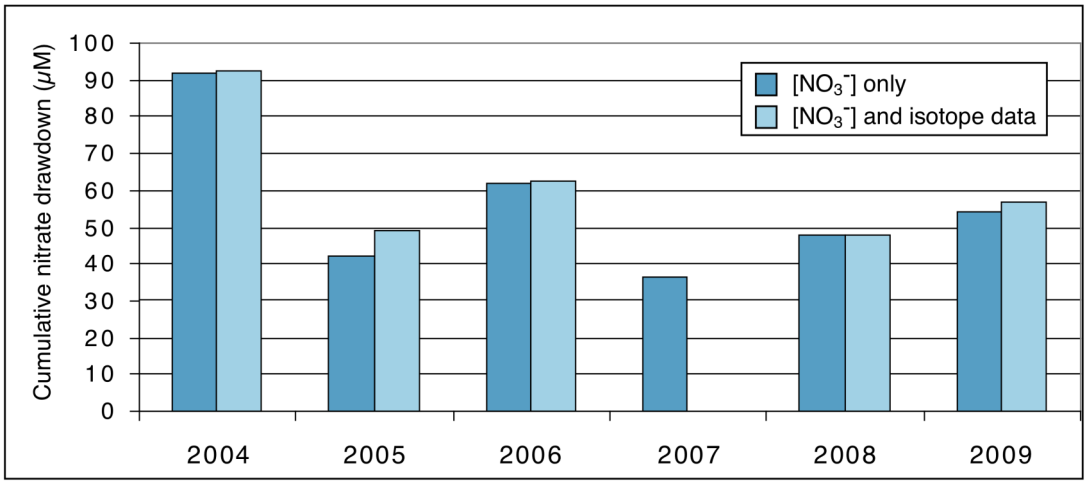

Figure 3.11: Seasonal nutrient (nitrate) use at the RaTS site. Concentration-only estimates calculated from BAS data (Cambridge, UK) using the difference in $[NO_3^-]$ between each sampling event. Increases in $[NO_3^-]$ (=negative drawdown) are assumed to represent input (upwelling/mixing) events and are not included in seasonal drawdown (calculated by summing all positive drawdown throughout the growing season). Estimates including nitrogen isotopic measurements, which were performed for five seasons, and are shown by light shading. These more robust N-use estimates taking isotopic data into account are presented and discussed in detail by Henley (2012), and are seen here to be very consistent with estimates from concentration alone.

The relationship between phytoplankton standing stock (integrated chl, *see* Chapter 2) and nutrient drawdown is shown in Figure 3.12, where high grazing would result in high N-use but low chl, and hence a horizontal or negative relationship. The resulting positive regression between N-use and chl is significant and highly linear (r^2 = 0.81, *p*-value = 0.024). As nutrient use and chl stocks are consistent between years, it follows that higher grazing does not correspond to lower chl, but instead occurs during periods of higher productivity, and vice-versa. This indicates that fluctuations in grazing pressure are tightly coupled to changes in production, in keeping with the ability of grazers to vary their clearance rates and seek out areas of higher prey density. This analysis strongly indicates that grazing is not a driver of phytoplankton compositional changes, but rather that grazers will respond to such changes. Thus the changes in phytoplankton from high-diatom, high-chl communities to low-diatom, low-chl communities are a plausible mechanism linking environmental trends to the observed changes in grazer dynamics.

Previous WAP studies have suggested that grazing is not a primary driver of community structure in this region (*e.g.* Moline *et al*. 2001, Prézelin *et al*. 2004 Vernet *et al*. 2008), and without direct quantification of grazing, the nutrient use analysis presented here is consistent with grazing being a minor forcing on phytoplankton communities. However, this study indicates that overall productivity accompanying shifts in structure are closely coupled to differences in grazing pressure. Thus the changes in phytoplankton composition are highly likely to impact food availability for higher trophic levels and favourable spawning conditions for krill, in addition to nutrient cycling, budgets and drawdown. These impacts are addressed in Chapter 8.

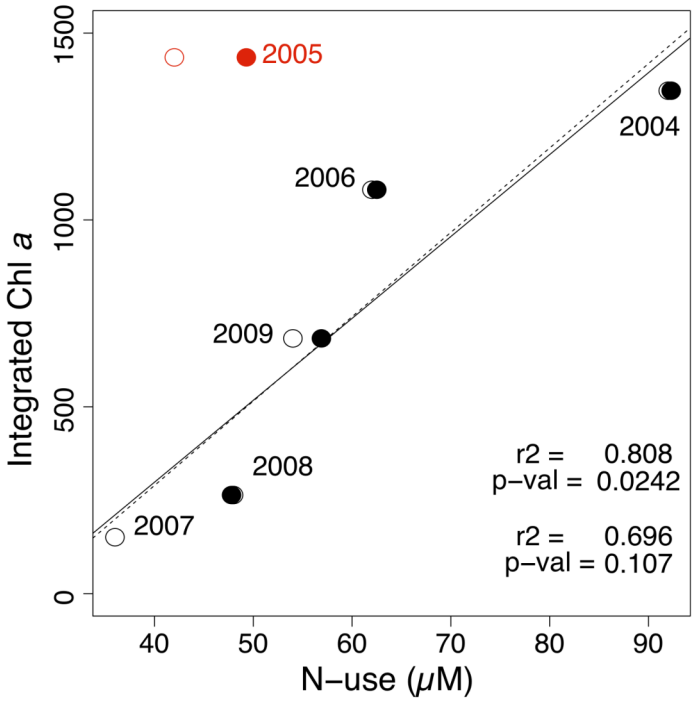

Figure 3.12: Time-integrated concentration of chl a (see section 2.4.2) versus N-use at 15 m depth for the six-year study period. Open symbols are calculated from $[NO_3^-]$ changes only, and the regression is shown by a dotted line. Filled symbols are N-use from concentrations and isotopic values as per Henley (2012), and no isotopic data is available for 2007, thus the correlation for this data set (solid line) is weaker owing to the smaller sample number. The very strongly stratified year of 2005, shown in red, is not included in the regressions, as in this case time-integrated [chl] does not represent high production, but rather that chl was physically retained at the surface (see text for discussion).

3.5.4 Production and community structure in low chlorophyll seasons

The strength of the relationship between N-use and annual integrated [chl] shown in Figure 3.12 is noteworthy. In addition to indicating relatively low grazing during low-chl seasons, these data imply that low-chl communities, with higher relative contributions of non-diatom phytoplankton, are characterised by low productivity. The converse is not universally true, as exemplified by 2005, where [chl] was very high and diatoms were dominant, but nutrient use (and by extension productivity) were low. This is explained by the very strong stratification in summer 2005 where phytoplankton cells were retained near the surface, thus while productivity was low, standing stock remained high.

The implication of this is that high [chl] cannot necessarily be interpreted to reflect high productivity. While high (and intermediate) [chl] did indeed reflect high (and intermediate) nutrient use in three of the four seasons presented here, effects such as stratification can decouple these processes (as in 2005). However, low [chl] does indicate low productivity. The trend seen in the southern WAP subregion of increasing [chl] suggests a trend to greater primary production, but this increase in productivity may not be as great as the change in [chl]. Equally, the decrease in [chl] in the northern subregion suggests that productivity there was higher in the past, although again potentially not to the same degree as [chl]. Current, low-chl conditions in the northern subregion can be confidently interpreted to reflect low primary productivity.

3.5.5 Sea-ice and chlorophyll conditions

While there are many factors linking sea-ice coverage with marine productivity, these are indirect mechanisms (*e.g.* light regulation, stratification). A strong link between water-column stratification and overall chl concentration has been shown in Ryder Bay (Venables *et al*. *In press*), and as sea-ice coverage is mechanistically linked to stratification in Ryder Bay due to its polynya-like behaviour, it follows that sea-ice cover will also be correlated to fluctuations in phytoplankton biomass. Indeed, seasonally-integrated chl, calculated as the area under the curve of [chl] at 15 m for the duration of the summer bloom period, shows a very strong correlation with days of >80% ice cover, below a threshold of ~80 days (r^2 = 0.83, *p*-value = 0.0027; Fig. 3.13). While sampling resolution was high (generally bi-weekly to weekly), this approach assumes a linear change in [chl] between sampling events, and may have missed or over-represented short-lived fluctuations in [chl]. This index does not integrate over the depth of the water column, although it has previously been shown that 15 m chl at the RaTS site is highly correlated to total water column chl (Clarke *et al*. 2008).

Despite these uncertainties, there is a very strong and significant association between our estimated seasonal chl and sea-ice cover above a threshold of ~80 days. Sea-ice cover is therefore proposed as an easily observable parameter with which to predict broad trends in phytoplankton standing stocks. It should be noted here that

standing stock ([chl]) does not correspond directly to productivity (*section 3.5.4*), but nonetheless provides important information regarding biological activity and is one of the most widely used parameters to assess marine production (via satellite records, etc.).

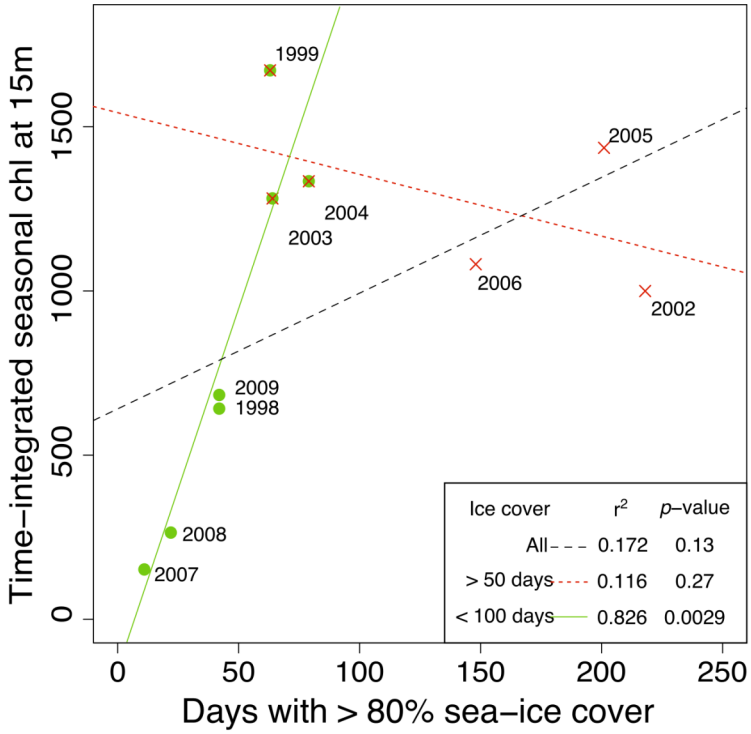

Figure 3.13: Time-integrated seasonal chl at 15m (see section 2.4.2) versus number of days with >80% sea-ice cover. Crosses (red) denote seasons used for the high ice-cover regression (dotted red line), and circles (green) show the seasons used in the low ice-cover regression (solid green line). Where both symbols are shown (1999, 2003 and 2004) these data were included in both regressions. The dashed black line shows the overall regression using all data.

This relationship is at odds with the model of Arrigo & Thomas (2004) which predicts an increase in Southern Ocean productivity with a decline in sea-ice cover. This prediction of greater production is based on the change in area of open ocean zones versus marginal ice zones and sea-ice zones, taking into account the timing of ice cover and typical rates of production for each zone. These opposing predictions may be reconciled by considering a threshold in sea-ice cover. A threshold for strongly declining productivity occurs in this study around 60-80 days of high (>80%) sea-ice cover (Fig. 3.13). Above this, there is a weak trend to lower

productivity with higher ice cover. Although this trend is not statistically significant, this may be an artefact of the low number of data points available, as such a trend is highly consistent with the Arrigo & Thomas (2004) model.

A reduction in sea-ice cover above the threshold value (which is suggested to be ~80 days for Ryder Bay, but may differ regionally) would increase primary production, as in the Arrigo & Thomas (2004) model. However, below the threshold, a severe decline in productivity would occur with reduced ice cover, as exemplified by the 2007 and 2008 seasons presented here. This strong evidence for decreased standing stock and production following lower sea-ice cover implies that at some threshold value, overall production will decline significantly along with sea-ice. This scenario is consistent with observations of decreased chl along the WAP (Montes-Hugo *et al*. 2009), and the strong link between winter stratification and summer productivity identified at the RaTS site (Venables *et al*. *In press*). This suggests therefore that productivity and timing of the annual phytoplankton bloom are significantly affected by factors such as stratification, such that longer periods of open water production are unable to compensate for productivity loss due to sea-ice decline in the Southern Ocean.

3.6 Conclusions

This chapter presents coupled, size-fractionated records of chl concentrations and diatom biomass, showing a strong relationship between diatom abundances, phytoplankton standing stocks and environmental conditions. The previously demonstrated relationship between stratification and total chlorophyll (Venables *et al*. *In press*) is shown to be accompanied by relatively higher non-diatom biomass, and smaller phytoplankton size distribution. This is in keeping with a continuation of the southward propagation of these trends observed along the WAP by satellite investigations.

These data indicate that low phytoplankton standing stocks in Ryder Bay are due to low primary production. Grazing may also contribute to low-chl conditions by removing biomass, but is not required to explain the observed changes. This analysis indicates that grazing in low-chl years is low, and higher in high-chl years. This is a key finding of this work, as it shows that production is low under low-chl conditions.

This is strong evidence that the established trends in satellite-derived chl along the WAP are accompanied by a decrease in marine productivity, likely with the same regional trends as seen in chl data.

The data presented here suggest that light levels are a very likely factor regulating community structure (including size structure) and biomass, a hypothesis consistent with changes in wind patterns, sea-ice cover, mixed layer depths and the interaction between them. Indices of nutrient drawdown and standing stock are all consistent with strong declines in the diatom population and lower productivity. There is strong evidence to suggest that a large component of non-diatom biomass in Ryder Bay comes from *Phaeocystis antarctica*, and the inferred increases of this taxon in less stratified waters is consistent with light-regulation of phytoplankton communities.

The higher relative proportion of *P. antarctica* in low-chl years at the WAP contrasts with current understanding of conditions in the Ross Sea. Ducklow *et al*. (2006) have described Ross Sea production as very similar between diatom-dominated and *Phaeocystis*-dominated communities. Conversely, the WAP shows high interannual variability in productivity (Ducklow *et al*. 2006), which this study shows is due to large fluctuations in diatom production. Small increases in *P. antarctica* do not compensate for the lower diatom production, resulting in overall productivity being determined primarily by diatoms.

3.7 References

AINLEY, D., BALLARD, G., ACKLEY, S., BLIGHT, L.K., EASTMAN, J.T., EMSLIE, S.D., LESCROËL, A., et al. 2007. Paradigm lost, or is top-down forcing no longer significant in the Antarctic marine ecosystem? *Antarctic Science*, **19**, 283, 10.1017/S095410200700051X.

AINLEY, D.G. & BLIGHT, L.K. 2009. Ecological repercussions of historical fish extraction from the Southern Ocean. *Fish and Fisheries*, **10**, 13–38, doi:10.1111/j.1467-2979.2008.00293.x

ANNETT, A.L., CARSON, D.S., CROSTA, X., CLARKE, A. & GANESHRAM, R.S. 2010. Seasonal progression of diatom assemblages in surface waters of Ryder Bay, Antarctica. *Polar biology*, **33**, 13–29, 10.1007/s00300-009-0681-7.

ARRIGO, K.R., ROBINSON, D.H., WORTHEN, D.L., DUNBAR, R.B., DITULLIO, G.R., VANWOERT, M. & LIZOTTE, M.P. 1999. Phytoplankton Community Structure and the Drawdown of Nutrients and CO_2 in the Southern Ocean. *Science*, **283**, 365–367.

ARRIGO, K.R., WEISS, A.M. & SMITH, W.O., Jr. 1998. Physical forcing of phytoplankton dynamics in the southwestern Ross Sea. *Journal of Geophysical Research*, **103**, 1007–1021.

ATKINSON, A., WHITEHOUSE, M.J., PRIDDLE, J., CRIPPS, G.C., WARD, P. & BRANDON, M.A. 2001. South Georgia, Antarctica: a productive, cold water, pelagic ecosystem. *Marine Ecology Progress Series*, **216**, 279–308.

BERGKVIST, J., THOR, P., JAKOBSEN, H.H., WANGBERG, S.-A. & SELANDER, E. 2012. Grazer-induced chain length plasticity reduces grazing risk in a marine diatom. *Limnology and Oceanography*, **71**, 318–324, 10.4319/lo.2012.57.1.0318.

BRETON, E., SAUTOUR, B. & BRYLINSKI, J.-M. 1999. No feeding on *Phaeocystis* sp. as solitary cells (post bloom period) by the copepod Temora Longicornis in the coastal waters of the English Channel. *Hydrobiologia*, **414**, 13–23.

BRINTON, E. 1985. The oceanographic structure of the eastern Scotia Sea. III. Distributions of euphausiid species and their developmental stages in 1981 in relation to hydrography. *Deep Sea Research*, **32**, 1153–1180.

BUCK, K.R. & GARRISON, D.L. 1983. Protists from the ice-edge region of the Weddell Seas. *Deep Sea Research*, **30**, 1261–1277.

CARSON, D.S. 2008. *Biogeochemical Dontrols on Productivity and Particle Flux in the Coastal Antarctic Sea Ice Environment*. PhD Thesis. University of Edinburgh.

CLARKE, A., MEREDITH, M.P., WALLACE, M.I., BRANDON, M.A. & THOMAS, D.N. 2008. Seasonal and interannual variability in temperature, chlorophyll and macronutrients in northern Marguerite Bay, Antarctica. *Deep Sea Research Part II: Topical Studies in Oceanography*, **55**, 1988–2006, 10.1016/j.dsr2.2008.04.035.

COOK, A.J., FOX, A.J., VAUGHAN, D.G. & FERRIGNO, J.G. 2005. Retreating Glacier Fronts on the Antarctic Peninsula over the Past Half-Century. *Science*, **308**, 541–544, 10.1126/science.1109164.

CROXALL, J.P. 1992. Southern ocean environmental changes: effects on seabird, seal and whale populations. *Philosophical Transactions of the Royal Society of London, Series B*, **338**, 319–328.

DIERSSEN, H.M. & SMITH, R.C. 2000. Bio-optical properties and remote sensing ocean color algorithms for Antarctic Peninsula waters. *Journal of Geophysical Research*, **105**, 26301–26312.

DIERSSEN, H.M., SMITH, R.C. & VERNET, M. 2002. Glacial Meltwater Dynamics in Coastal Waters West of the Antarctic Peninsula. *Proceedings of the National Academy of Sciences of the United States of America*, **99**, 1790–1795.

DUCKLOW, H.W., BAKER, K., MARTINSON, D.G., QUETIN, L.B., ROSS, R.M., SMITH, R.C., STAMMERJOHN, S.E., VERNET, M. & FRASER, W. 2007. Marine pelagic ecosystems: the West Antarctic Peninsula. *Philosophical Transactions of the Royal Society B: Biological Sciences*, **362**, 67–94, 10.1098/rstb.2006.1955.

FACH, B.A., HOFMANN, E.E. & MURPHY, E.J. 2002. Modeling studies of Antarctic krill Euphausia superba survival during transport across the Scotia Sea. *Marine Ecology Progress Series*, **231**, 187–203.

FRYXELL, G.A. 1989. Marine phytoplankton at the Weddell Sea ice edge: seasonal changes at the specific level. *Polar biology*, **19**, 1–18.

GARIBOTTI, I.A., VERNET, M. & FERRARIO, M.E. 2005. Annually recurrent phytoplanktonic assemblages during summer in the seasonal ice zone west of the Antarctic Peninsula (Southern Ocean). *Deep Sea Research Part I: Oceanographic Research Papers*, **52**, 1823–1841, 10.1016/j.dsr.2005.05.003.

GRANELI, E., GRANELI, W., RABBANI, M.M., DAUGBJERG, N., FRANSZ, G., CUZIN-ROUDY, J. & ALDER, V.A. 1993. The influence of copepod and krill grazing on the species composition of phytoplankton communities from the Scotia-Weddell Sea. *Polar biology*, **13**, 201–213.

HABERMAN, K.L., QUENTIN, L.B. & ROSS, R.M. 2003. Diet of the Antarctic Krill (*Euphausia superba* Dana): I. Comparisons of grazing on *Phaeocystis antarctica* (Karsten) and *Thalassiosira antarctica* (Comber). *Journal of Experimental Marine Biology and Ecology*, **283**, 79–95.

HARBISON, G.R., MCALISTER, V.L. & GILMER, R.W. 1986. The response of the salp, *Pegea confoederata,* to high levels of particulate material: starvation in the midst of plenty. *Limnology and Oceanography*, **31**, 371–382.

HENLEY, S.F. 2012. *Climate-induced changes in carbon and nitrogen cycling in the rapidly warming Antarctic coastal ocean*. PhD Thesis. University of Edinburgh.

HILLEBRAND, H., DURSELEN, C.-D., KIRSCHTEL, D., POLLINGHER, U. & ZOHARY, T. 1999. Biovolume calculation for pelagic and benthic macroalgae. *Journal of Phycology*, **35**, 403–424.

HOFFMANN, L.J., PEEKEN, I. & LOCHTE, K. 2008. Iron, silicate, and light co-limitation of three Southern Ocean diatom species. *Polar biology*, **31**, 1067–1080, 10.1007/s00300-008-0448-6.

ICHII, T. 2000. Krill harvesting. *In* Everson, I., *ed. Krill biology, ecology and fisheries*. London: Blackwell Science, 228–261.

JACQUES, G. & PANOUSE, M. 1991. Biomass and composition of size fractionated phytoplankton in the Weddell Sea confluence area. *Polar biology*, **11**, 315–328.

KANDA, K., TAKAGI, K. & SEKI, Y. 1982. Movement of the larger swarms of Antarctic krill, *Euphausia superba* off Enderby Land during 1976-77 season. *Journal of Tokyo University Fisheries*, **68**, 24–42.

KREBS, W.N. 1983. Ecology of neritic diatoms, Arthur Harbor, Antarctica. *Micropaleontology*, **29**, 267–297.

KREMER, P. & MADLIN, L.P. 1992. Particle retention efficiency of salps. *Journal of Plankton Research*, **14**, 1009–1015.

LAWS, R.M. 1985. The ecology of the Southern Ocean. *American Science*, **73**, 26–40.

LEVENTER, A. & DUNBAR, R.B. 1996. Factors influencing the distribution of diatoms and other algae in the Ross Sea. *Journal of Geophysical Research*, **101**, 18489–18500.

MADIN, L.P. & KREMER, P. 1995. Determination of the filter-feeding rates of salps (*Tunicata, Thaliacea*) ICES. *Journal of Marine Science*, **52**, 583.

MARTINSON, D.G., STAMMERJOHN, S.E., IANNUZZI, R.A., SMITH, R.C. & VERNET, M. 2008. Western Antarctic Peninsula physical oceanography and spatio-temporal variability. *Deep-Sea Research II*, **55**, 1964–1987, 10.1016/j.dsr2.2008.04.038.

MEREDITH, M.P., WALLACE, M.I., STAMMERJOHN, S.E., RENFREW, I.A., CLARKE, A., VENABLES, H.J., SHOOSMITH, D.R., SOUSTER, T. & LENG, M.J. 2010. Changes in the freshwater composition of the upper ocean west of the Antarctic Peninsula during the first decade of the 21st century. *Progress In Oceanography*, **87**, 127–143, 10.1016/j.pocean.2010.09.019.

MOLINE, M.A., CLAUSTRE, H., FRAZER, T.K., GRZYMSKI, J., SCHOFIELD, O. & VERNET, M. 2001. Changes in Phytoplankton Assemblages Along the Antarctic Peninsula and Potential Implications for the Antarctic Food Web. *In:* Davison, W., Howard-Williams, C., Brody, P., *eds. Antarctic ecosystems: model for wider ecological understanding.* Christchurch: Caxton Press, 263–271.

MOLINE, M.A., CLAUSTRE, H., FRAZER, T.K., SCHOFIELD, O. & VERNET, M. 2004. Alteration of the food web along the Antarctic Peninsula in response to a regional warming trend. *Global Change Biology*, **10**, 1973–1980, 10.1111/j.1365-2486.2004.00825.x.

MONTES-HUGO, M., DONEY, S.C., DUCKLOW, H.W., FRASER, W., MARTINSON, D., STAMMERJOHN, S.E. & SCHOFIELD, O. 2009. Recent Changes in Phytoplankton Communities Associated with Rapid Regional Climate Change Along the Western Antarctic Peninsula. *Science*, **323**, 1470–1473, 10.1126/science.1164533.

MONTES-HUGO, M.A., M, V., MARTINSON, D., SMITH, R. & IANNUZZI, R. 2008a. Variability on phytoplankton size structure in the western Antarctic Peninsula (1997-2006). *Deep-Sea Research II*, **55**, 2106–2117, 10.1016/j.dsr2.2008.04.036.

MONTES-HUGO, M.A., VERNET, M., SMITH, R. & CARDER, K. 2008b. Phytoplankton size-structure on the western shelf of the Antarctic Peninsula: a remote sensing approach. *International Journal of Remote Sensing*, **29**, 801–829, 10.1080/01431160701297615.

PERISSINOTTO, R. & PAKHOMOV, E.A. 1998a. Contribution of salps to carbon flux of marginal ice zone of the Lazarev Sea, Southern Ocean. *Marine Biology*, **131**, 25–32, 10.1007/s002270050292.

PERISSINOTTO, R. & PAKHOMOV, E.A. 1998b. The trophic role of the tunicate *Salpa thompsonii* in the Antarctic marine ecosystem. *Journal of Marine Systems*, **17**, 361–374.

PRÉZELIN, B.B., HOFMANN, E.E., MOLINE, M. & KLINCK, J.M. 2004. Physical forcing of phytoplankton community structure and primary production in continental shelf waters of the Western Antarctic Peninsula. *Journal of Marine Research*, **62**, 419–460.

QUENTIN, L.B. & ROSS, R.M. 1985. Feeding by Antarctic Krill, *Euphausia superba*: does size matter? *In* Siegfried, W.R., Condy, P.R. & Laws, R.M., *eds. Antarctic Nutrient Cycles and Food Webs*. Berlin: Springer-Verlag, 372–377.

QUENTIN, L.B., ROSS, R.M., FRAZER, T.K. & HABERMAN, K.L. 1996. Factors affecting distribution and abundance of zooplankton, with an emphasis on Antarctic krill, *Euphausia superba*. *In* Ross, R.M., Hofmann, E.E. & Quentin, L.B., *eds. Foundations for ecological research west of the Antarctic Peninsula*. Washington, DC: American Geophysical Union, 357–371.

SCHOEMANN, V., BECQUEVORT, S., STEFELS, J., ROUSSEAU, V. & LANCELOT, C. 2005a. *Phaeocystis* blooms in the global ocean and their controlling mechanisms: a review. *Journal of Sea Research*, **53**, 43–66, 10.1016/j.seares.2004.01.008.

SEIXAS, P., COUTINHO, P., FERREIRA, M. & OTERO, A. 2009. Nutritional value of the cryptophyte *Rhodomonas lens* for *Artemia* sp. *Journal of Experimental Marine Biology and Ecology*, **381**, 1–9.

SMAYDA, T.J. 1978. From phytoplankters to biomass. *In* Sournia, A., *ed. Monographs on oceanographic methodology*. Paris: UNESCO, 273–279.

SOLOMON, C.M., LESSARD, E.J., KEIL, R.G. & FOY, M.S. 2003. Characterization of extracellular polymers of *Phaeocystis globosa* and *P. antarctica*. *Marine Ecology Progress Series*, **250**, 81–89.

STAMMERJOHN, S.E., MARTINSON, D.G., SMITH, R.C. & IANNUZZI, R.A. 2008. Sea ice in the

western Antarctic Peninsula region: Spatio-temporal variability from ecological and climate change perspectives. *Deep Sea Research Part II: Topical Studies in Oceanography*, **55**, 2041–2058, 10.1016/j.dsr2.2008.04.026.

STRZEPEK, R.F., HUNTER, K.A., FREW, R.D., HARRISON, P.J. & BOYD, P.W. 2012. Iron-light interactions differ in Southern Ocean phytoplankton. *Limnology and Oceanography*, **57**, 1182–1200, 10.4319/lo.2012.57.4.1182.

TARLING, G.A. & JOHNSON, M.L. 2006. Satiation gives krill that sinking feeling. *Current Biology*, **16**, R83–84.

TILZER, M.M., ELBRACHTER, M., GIESKES, W.W. & BEESE, B. 1986. Light-Temperature interactions in the control of photosynthesis in Antarctic phytoplankton. *Polar biology*, **5**, 105–111.

VAN HILST, C.M. & SMITH, W.O., Jr. 2002. Photosynthesis/irradience relationships in the Ross Sea, Antarctica, and their control by phytoplankton assemblage composition and environmental factors. *Marine Ecology Progress Series*, **226**, 1–12.

VAUGHAN, D.G., MARSHALL, G.J., CONNOLLEY, W.M., PARKINSON, C., MULVANEY, R., HODGSON, D.A., KING, J.C., PUDSEY, C.J. & TURNER, J. 2003. Recent rapid regional climate warming on the Antarctic Peninsula. *Climatic Change*, **60**, 243–274.

VENABLES, H.J., CLARKE, A. & MEREDITH, M.P. *In press*. Wintertime controls on summer stratification and productivity at the western Antarctic Peninsula. *Limnology and Oceanography*, 1–30.

VERNET, M., MARTINSON, D., IANNUZZI, R., STAMMERJOHN, S., KOZLOWSKI, W., SINES, K., SMITH, R. & GARIBOTTI, I. 2008. Primary production within the sea-ice zone west of the Antarctic Peninsula: I—Sea ice, summer mixed layer, and irradiance. *Deep Sea Research Part II: Topical Studies in Oceanography*, **55**, 2068–2085, 10.1016/j.dsr2.2008.05.021.

VILLINSKI, J.C., DUNBAR, R.B. & MUCCIARONE, D.A. 2000. Carbon 13/Carbon 12 ratios of sedimentary organic matter from the Ross Sea, Antarctica: A record of phytoplankton bloom dynamics. *Journal of Geophysical Research*, **105**, 14163–14172.

WALSH, J.J., DIETERLE, D.A. & LENES, J. 2001. A numerical analysis of carbon dynamics of the Southern Ocean phytoplankton community: the roles of light and grazing in e!ecting both sequestration of atmospheric CO_2 and food availability to larval krill. *Deep-Sea Research I*, **48**, 1–48.

WEBER, L.H. & EL-SAYED, S.Z. 1985. Spatial variability of phytoplankton and the distribution and abundance of krill in the Indian sector of the Southern Ocean. *In* Siegfried, W.R., Condy, P.R. & Laws, R.M., *eds. Antarctic Nutrient Cycles and Food Webs*. Berlin: Springer-Verlag, 283–293.

Chapter 4: Species-level changes in diatom assemblages linked to environmental changes in Ryder Bay

4.1 Abstract

As warming and environmental change progress at the Antarctic Peninsula, changes are also being observed in phytoplankton communities. These changes reflect shifts in microalgal assemblages between high-chl conditions with large, predominantly diatom cells, and low-chl conditions characterised by smaller average cell sizes and less abundant diatoms. Thus, the difference between high- and low-chl conditions primarily reflects the changes in the diatom community. Productivity by diatoms is a key part of the Antarctic sea-ice zone; it is the main fraction transferred to higher trophic levels and a primary vector moving C from the atmosphere to deeper waters. Despite the importance of diatom communities, previous studies documenting changing chl dynamics have not looked at changes within diatom assemblages. Here, high-resolution records of diatom species composition are presented spanning five austral summers and a range of environmental conditions at a coastal Antarctic site. These data suggest a decrease in diatom species richness during low-chl conditions. Diatom size distributions show some trend towards smaller cells during the low-chl season, although this is within the seasonal range of variability. Several species and species ratios are identified which may be used to diagnose high-, intermediate- and low-chl conditions.

4.2 Introduction

Current climate changes along the WAP are well established. Both air (Vaughan *et al*. 2003) and surface waters (Meredith & King 2005) are warming, and ocean heat content on the WAP shelf is increasing (Martinson *et al*. 2008). The southern annular mode has intensified (Marshall *et al*. 2006), and more cyclonic atmospheric circulation and warm air convection has caused anomalously warm

winter conditions (Turner *et al*. 1997). Changes in the timing of sea-ice advance and retreat have resulted in markedly shorter winter sea-ice cover (Stammerjohn *et al*. 2008). Glacial retreat is accelerating (Cook *et al*. 2005, Pritchard & Vaughan 2007), and is expected to result in increased runoff (Vaughan 2006).

These environmental changes are demonstrably affecting marine productivity, largely via changes in sea-ice cover, cloudiness and wind-mixing (Montes-Hugo *et al*. 2009). A strong relationship has been found between winter water column stratification and primary productivity in the following summer (Venables *et al*. 2012). Chlorophyll concentrations along the WAP as a whole have declined since the 1960s, although there are strong regional differences in these trends. These changes are primarily a function of diatom assemblages, with low-chl conditions characterised by communities of smaller cells and fewer diatoms (Montes-Hugo *et al*. 2009). Low productivity phytoplankton communities fix less C into organic matter, which can result in a net flux of CO_2 from the ocean to the atmosphere.

Diatoms in the Southern Ocean are the key link between primary productivity and higher trophic levels. Diatoms are the group preferentially grazed by krill (Haberman *et al*. 2003), and thus the base of the very productive Antarctic marine food chain around the WAP. Diatoms are also grazed to some extent by other zooplankton, such as salps, but C routed through salps is not transferred to higher trophic levels, and salps avoid regions of high diatom abundance (Quentin *et al*. 1996, Perissinotto & Pakhomov 1998a, b). Krill are able to graze other phytoplankton groups (Quentin & Ross 1985, Haberman *et al*. 2003), but survival and reproduction are correlated to the abundance of a diatom food source (Quentin *et al*. 1996, Loeb *et al*. 1997, Quentin & Ross 2003). Studies have found a trend toward increasing salp abundances and decreasing krill, consistent with the decreases in diatom biomass (Atkinson *et al*. 2004).

Thus, the key link between environmental conditions and C drawdown and trophic transfer is diatoms. Despite the significant recent changes documented along the WAP, the decline in diatom populations has not yet been assessed at the species level. This study investigates how diatom communities change in response to environmental variability, and explores the potential impacts in diatom speciation

changes. Here, diatom assemblages from five Antarctic summer seasons spanning a nearly 10-fold range in chl concentrations are documented and characterised.

This study spans several years at high resolution and full seasonal coverage. The remoteness of Antarctica and logistical difficulties presented by sea-ice cover make this type of analysis unfeasible over larger areas or much longer time scales. Thus we seek to address how the information acquired here can be applied to other modern studies. For example, characteristic assemblages indicating high- or low-productivity conditions may be applied to samples along a ship's track, where full-season coverage is unavailable. Additionally, such assemblages can be applied to interpretations based on sediment records, to provide additional information about biological processes in addition to physical conditions.

4.3 Methods

4.3.1 Study site

Surface water samples were collected from the RaTS Sites 1 and 2, during the 2008 and 2009 summer field seasons. The RaTS sites are situated over the deepest part of Ryder Bay (northern Marguerite Bay, Antarctica), where water depth is 520 and 400 m for sites 1 and 2, respectively. Site 2 is used when ice or weather conditions prevent access to site 1. The locations of sampling stations are shown in Figure 2.1.

4.3.2 Sample collection and preparation

Water samples were collected ~twice weekly, as logistics and weather allowed, from 15 m depth (the long-term average depth of the chl maximum; Clarke *et al*. 2008). Collections were made as described in Chapter 1, and preserved with Lugol's fixative. Filtrations were done within 24 hours of collection. For light microscopy (LM), appropriate volumes (50–100 mL) were gently filtered onto 25 mm Millipore® HAWG (0.45 μm) filters and dried at low temperature (~37 °C) overnight. The dry filters were mounted on slides using microscope immersion oil and gentle heating, according to the methods in the Millipore® catalogue (Cat. No. LAB310/P). Samples for scanning electron microscopy (SEM) were filtered onto 25

mm isopore (0.2 μm) filters, dried and stored until analysis. While the filter pore sizes for SEM and LM analysis differ, these pore sizes were readily available and are much smaller than diatom sizes and will in both cases collect the full diatom community.

4.3.3 Sample processing

4.3.3.1 Light microscopy

Phytoplankton counts were performed using a Leica microscope at 500x magnification. The HAWG filters are pre-printed with grid squares of 9.50 mm^2, and phytoplankton were enumerated and identified in three randomly chosen grid squares. Cells were identified to species, genus or group level (as possible), using the taxonomic guidelines outlined in Hasle & Syvertsen (1997) for diatoms. Additional references, where needed, were Doucette & Fryxell (1985), Johansen & Fryxell (1985), Jordan *et al.* (1991) and Scott & Thomas (2005). A full list of all phytoplankton taxa observed in this study is given in A4.1. In the event that less than 300 cells were enumerated in three grid squares, additional squares were counted until the cell total exceeded 300. Counts were combined with the fraction of the filter area scanned and the volume filtered to convert these to cell concentrations per ml of seawater. For very large species (*e.g. Coscinodiscus* spp) or very rare taxa, additional squares were scanned and counted only for these species, and abundances for these species calculated for the larger filter area analysed. Cell measurements were performed on digital images taken using Leica Application Suite software, which is capable of making precise distance measurements on digital images based on the magnification used. Where possible, several (>3) measurements of cell diameter (or other axes) were made and averaged, to obtain more robust measurements where cells were not perfectly circular (or consistent).

Previous samples (2006 season) were also analysed using LM. This analysis was performed using settling chambers; full details can be found in Annett *et al.* 2010.

4.3.3.2 Scanning electron microscopy

For some diatoms, especially discoid centric species, identification to species level was not possible using the LM methods described above. Therefore a subset of samples was also analysed using SEM, primarily to aid in species-level identification. These samples were mounted on stubs and thinly sputter-coated with a layer of gold. Phytoplankton assemblages were imaged on a Philips XL 30 CP microscope using secondary electron imaging with a 20 keV beam and a 10 mm working distance. Slides were scanned in transects, and centric species imaged and identified at magnifications of 2000x (or higher where necessary). Cell sizes were measured digitally whenever possible. These sizes were used to relate species counts from SEM to absolute concentrations determined by LM analysis. For each size class (very small (<10 μm), small (10–20 μm), medium (20-50 μm) and large (>50 μm) cells), the percentage of each species relative to the total for that size class was determined from SEM analysis and applied to the absolute concentrations from LM. In some cases species size ranges spanned two size classes (*e.g. Thalassiosira antarctica*; 30-60 μm). In such an event, the portion of the medium size class cells identified as this species was converted to cell abundances, and added to the portion of large size class cells identified as *T. antarctica* (also converted to cell abundance), to yeild a total absolute abundance for the speices. As SEM analysis was not possible for all samples due to time and resource constraints, data on centric diatoms are presented in the first instance based on size fractions, as this data is available at the highest resolution.

Samples collected in previous seasons (2004-2005 and 2005-2006) for barium analysis also allowed assessment of diatom assemblages by SEM. Full sample processing and counting methods can be found in Annett *et al.* (2010). For both LM and SEM samples, following the procedure of Annett *et al*. (2010), individual species were grouped in some cases due to ecological preferences, low abundances or difficulties in distinguishing between species in the light microscope. The *Banquisia* group includes the *Banquisia belgicae* (van Heurk) Paddock, *Berkeleya spp.* (Trentep. ex Roth) Grunow, *Entomoneis kjellmanii* (Cleve) Poulin & Cardinal, *Haslea trompii* (Cleve) Simonsen, *Ephemera planamembranacea* (Hendey)

Paddock, related genera and members of the bottom ice community (Horner 1985), and *Membraneis challengeri* (Grunow) Paddock, a related sea-ice species (Scott & Thomas 2005). These species were counted individually, and biomass estimates (below) calculated for each species before being pooled. The *Chaetoceros* subgenus *Hyalochaeta* (Gran) includes *C. neglectus* Karsten, *C. simplex* Ostenfeld and *C. socialis* Lauder. The *Chaetoceros* subgenus *Phaeoceros* (Gran) includes the larger, less abundant species *C. atlanticus* Cleve, *C. convolutus* Castracane, *C. criophilus* Castracane, *C. dichaeta* Ehrenberg and *C. flexuosus* Mangin. Wherever possible, *Chaetoceros* cells were counted at the species level, and biomass estimates calculated for each species before being combined. The *Fragilariopsis curta* group here includes *F. curta* (van Heurck) Hustedt, *F. cylindrus* (Grunow) Krieger, and *F. vanheurkii* (Pergallo) Hustedt; as these species have been noted in Ryder Bay sea-ice samples (Annett 2008), or are commonly associated with sea-ice zones (*F. vanheurkii*; A. Leventer, *pers. comm.*). Other *Fragilariopsis* species were relatively rare, and were grouped with *Fragilariopsis kerguelensis* (O'Meara) Hustedt which is associated with more open water conditions, as other *Fragilariopsis* species (including *F. obliquecostata* (van Heurck) Heiden, *F. rhombica* (O'Meara) Heiden and Kolbe, *F. ritscheri* Hustedt, *F. separanda* Hustedt and *F. sublinearis* (van Heurck) Heiden) are rare or absent in Ryder Bay sea-ice samples. Again, most *Fragilariopsis* cells were identified to species level and grouped after biomass estimates were calculated. The *Proboscia* spp. group consists primarily of *P. inermis* (Castracane) Jordan & Ligowski, with very low abundance and biomass contributions from *P. alata* (Brightwell) Sundström and *P. truncata* (Karsten) Nöthig & Ligowski, except where specified. Both *Pseudonitzschia lineola* (Cleve) Hasle and *P. turgidula* (Hustedt) Hasle are included in the *Pseudo-nitzschia* group, with *P. lineola* being the dominant species (numerically >80%) in all samples.

In SEM samples, identification of discoid, centric diatoms ("Centrics") was possible to species level. Due to lower magnification, in LM (2006-2007) samples, counts were made on the basis of size ("very small," ~10 μm; "small," 10-20 μm; "medium," 20-50 μm; "large," >50 μm), and the biomass of each size range estimated to calculate total "Centric" biomass. This "Centrics" group includes members of the discoid genera *Actinocyclus*, *Asteromphalus*, *Porosira*, *Stellarima*

and *Thalassiosira*. Members of these genera, which are generally part of late summer phytoplankton (Denis *et al*. 2006, Maddison *et al*. 2006, Stickley *et al*. 2005) and have been identified by SEM, are the main "centric" species present across all seasons.

4.3.3.3 Diatom volume and biomass

Due to the large range in cell volumes (9.2 to 250000 μm^3 in this study), interspecific comparisons of cellular concentrations (cells L^{-1}) are an imprecise or even inadequate method of characterising phytoplankton communities (Smayda 1978). Cell volume estimates were made to facilitate estimates of biomass. Cell volumes were calculated using geometric formulae appropriate to the shape of the cell (Smayda 1978, Hillebrand *et al*. 1999). The geometric shapes used for each species are listed in Appendix A4.1. Areas and volumes were calculated individually from measurements of up to 30 cells of each species (where possible) from digital LM images and electron micrographs, and averaged to obtain the mean values listed in Appendix A4.1 (Smayda 1978).

As relating diatom community composition to overall productivity and potential paleoproxies based on bulk sediment analysis is a key focus of this study, assessment of the contribution of each species to the organic carbon pool requires determination of biomass rather than cell abundances or biovolume. Conversion to biomass was done by calculating plasma volume (PV) according to Equation 3 of Smayda (1978):

$$PV = (\text{surface area, } \mu m^2)(\text{cytosolic layer}) + 0.10 \times (\text{total cell volume, } \mu m^3) \quad (1)$$

The thickness of the cytosolic layer varied from 1–2 μm, depending on the ratio of surface area to volume, as outlined in Smayda (1978). These PV estimates were then converted to cellular carbon (in pg C $cell^{-1}$) from the equations of Strathmann (1967), where:

$$\log_{10}C = 0.892(\log_{10}PV) - 0.61 \quad (2)$$

for diatoms. A second equation:

$$\log_{10}C = 0.94(\log_{10}V) - 0.60 \quad (3)$$

was used for other phytoplankton groups based on total cell volume (V) rather than plasma volume (Eppley *et al*. 1970, corrected in Smayda 1978). These biomass estimates are given along with size data in Appendix A4.1.

The sizes of many common diatoms have been previously measured in Ryder Bay (Annett *et al*. 2010), and thus the cell sizes here were compared to this previous study. Where cell size ranges were consistent between studies, the previously determined values for biovolume and biomass were also used here.

Sizes of some species can vary even between samples from a given season. A detailed look at changes within the size distribution of a single species (*Corethron pennatum*) is given in section 4.4.5.1, including an assessment of how using sample-specific sizes for biomass calculations impacts trends in estimated diatom biomass at seasonal and intraseasonal time scales. As full size analysis of every enumerated diatom cell would be very time consuming or impossible for this or any other study, average values for biomass (Appendix A4.1) were used here to estimate species biomass, except in the case of *C. pennatum*, for which additional size measurements were performed. Intersample variability of this very large species is likely to be more significant for total diatom biomass estimates than for smaller diatoms, as discussed in section 4.4.5.1, and thus use of average biomass values should be robust in most cases.

4.3.3.4 Chain-forming species

Some diatom species are commonly found as chains. These include, but are not limited to, the genera *Chaetoceros*, *Eucampia*, *Fragilariopsis*, *Odontella*, and *Thalassiosira*. In order to better characterise the changes in these species, a subset of six samples from each of 4 seasons (2004, 2005, 2008 and 2009) were analysed for chains, focusing on the *Hyalochaeta* subgenus of *Chaetoceros*, *Fragilariopsis curta*, *Eucampia antarctica*, and *Odontella weissflogii*. The discoid centrics considered were *Thalassiosira antarctica*, and small (~20 μm) cells which could not be

positively identified to species level in LM counts, but are predominantly *T. gracilis* and *T. gravida* (from SEM observations). For the latter seasons, 3 filter squares were scanned by LM, and all cells from these genera were counted, noted whether they were solitary or in a chain, and the number of cells in each chain recorded. For the earlier seasons, all 30 SEM images at 500x magnification were examined, and again the proportions of cells found in chains and lengths of chains recorded. Chains which appeared to continue out of the field of view were included in proportions of cells as chains, but not in chain lengths, as the full number of cells in these chains could not be determined.

4.4 Results

Seasonal trends in ice cover, temperature, salinity, etc. have been outlined previously, and differences linked to overall productivity largely via stratification (*see* Chapters 1, 2). In terms of chlorophyll dynamics, the same high-, intermediate- and low-chl designations are employed as in Chapter 2, and diatom speciation is related to these broad-scale trends in environmental conditions and chl. Here the diatom community is presented in detail, and physical parameters detailed where they are relevant to the mechanisms and interpretation of biological processes.

To investigate differences between the study seasons, we characterise diatom assemblages at different scales of temporal resolution. First, results are presented for each season, to compare broad-scale differences between the growing seasons. Generally, this is the finest scale resolution that is applicable to sediment studies, as only a few regions display seasonally laminated sediments. To link diatom species dynamics to short-term environmental conditions, variations and trends within diatom assemblages are then shown across each season, highlighting differences in seasonal progression. Finally, patterns at the species level are presented, both within and between seasons.

The focus of this study is the variation in diatom species composition, relative to total diatom biomass, within and between seasons. Therefore, the results presented here are given in terms of biomass (C L^{-1}), estimated from measured cell sizes (cellular biovolume) and abundances (cells L^{-1}). Some other studies, especially those examining the sediment record, report cell abundances rather than biomass values,

thus for ease of comparison to other studies, cellular abundance data is given in Appendix A4.2. As biomass was determined based on average cell biovolume and abundances, trends in absolute biomass for a given species within or between seasons reflect changes in abundances, and thus the results and interpretation here of absolute biomass trends can be applied to that species' abundance as well.

4.4.1 Indices of diversity

To investigate community level changes, two indexes were calculated, species richness (Margalef's D) and species diversity (Shannon-Weiner index, H'). Some species were only identified to a group level (e.g. *Chaetoceros Hyalochaeta* subgenus, centrics size classes), and both indices reflect this level of grouping, so both will underestimate species richness to some extent. The use of these groups was to avoid any bias from higher proportions of SEM analysis in some years where more species-level identification was possible. Diversity here refers to the distribution of individuals across species or groups, for example a sample with high species richness but where 90% of individuals are of a single species would not be as diverse as a sample with fewer species present, but where each species contributed a similar number of individuals to the total. The index used here (H') calculates a species diversity index (H) for each sample, which is scaled relative to the theoretical maximum of H based on the number of species and individuals present in that sample.

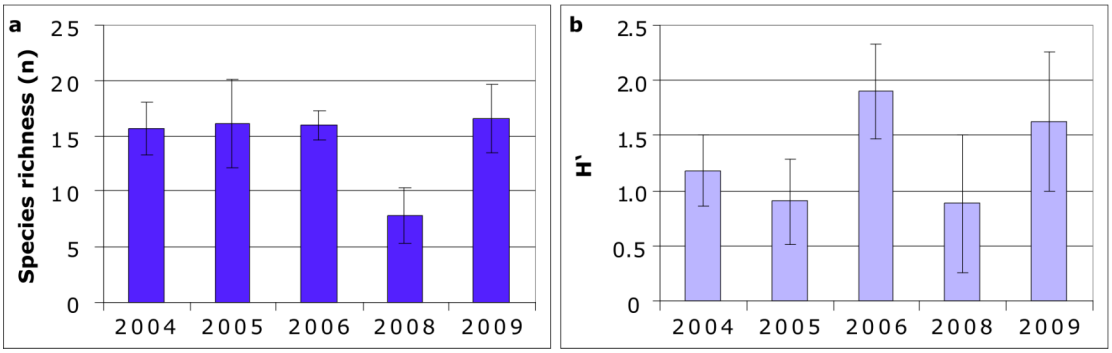

Figure 4.1: Richness (a) and diversity (H'; b). Richness reflects the number of species (or groups) present. Diversity reflects the evenness of individuals across richness. Bars are the averages of all samples in each season, error bars show standard deviation.

The results of these analyses are shown in Figure 4.1, while a full list of groups counted here (and their constituent species) is given in Appendix A4.3. A drop in richness of nearly 50% in the low-chl season is the striking feature apparent in this analysis. Diversity (H') was roughly equal in high and low years, and highest in intermediate seasons.

4.4.2 Patterns of interannual diatom biomass

To identify broad-scale changes between high-, intermediate- and low-chl seasons, we first investigate annual trends in absolute and relative biomass for different species and groups. As seasons were sampled at different temporal resolution (*e.g.* only 6 samples in 2004 and 2005) and coverage (no late season samples in 2006), these represent a qualitative assessment of diatom communities. In order to account for the different sampling regimes, absolute biomass estimates (cumulative from all samples in a given season) have been scaled to time-integrated chlorophyll for each season. This was done by dividing the cumulative species' biomass by the cumulative diatom biomass for each season and multiplying the result by the time-integrated seasonal chl. The goal was to represent the seasonal biomass of each species as the proportion of the integrated chl that could reasonably be expected to come from that species. These results are presented in Figure 4.2. This transformation reconciles the lower sampling resolution in the first two high-chl seasons, where otherwise these sample would appear to have lower biomass than the intermediate seasons. While this does assume that all species have similar chl:C ratios, because comparisons are only made for a given species between seasons, this assumption will not affect the resulting interannual differences provided the chl:C ratio does not vary greatly within that species. This method primarily reflects the assemblage composition of high-biomass samples, as the low-biomass samples have little effect on the total. However, it does incorporate the assumption that changes in species composition are linear between the samples counted. While this introduces some uncertainty if species composition changes rapidly between high-biomass samples, these estimates of annual biomass differences should be robust at the first order.

Trends in species biomass were relatively variable, with few species showing clear patterns between high-, intermediate- and low-chl seasons. For example, scaled biomass of *Banquisia* group species in the two high-chl seasons ranged both above and below the intermediate-season values. However, the scaled *Banquisia* group biomass in the low-chl season was ~5 times lower than in any other season. At this broad scale, several species exhibit a relationship to the overall chlorophyll trends.

Corethron pennatum had markedly higher biomass in the low-chl season, even though overall diatom biomass was much lower during this year. As such, it is a prime candidate for a low-productivity marker species. *Eucampia antarctica* (exclusively var. *recta*) were noticeably prevalent during the intermediate seasons, relatively rare during the high-chl seasons, and absent in the low-chl year. At the genus level, *Fragilariopsis* seemed to vary with overall chl trends, although there were slight differences at the species/group level. The *F. kerguelensis* group, although at lower biomass than the *F. curta* group, showed the clearest trend with integrated seasonal chl levels. The *F. curta* group (and *F. cylindrus* in particular) was relatively abundant in the high-chl seasons, and very rare in all other years.

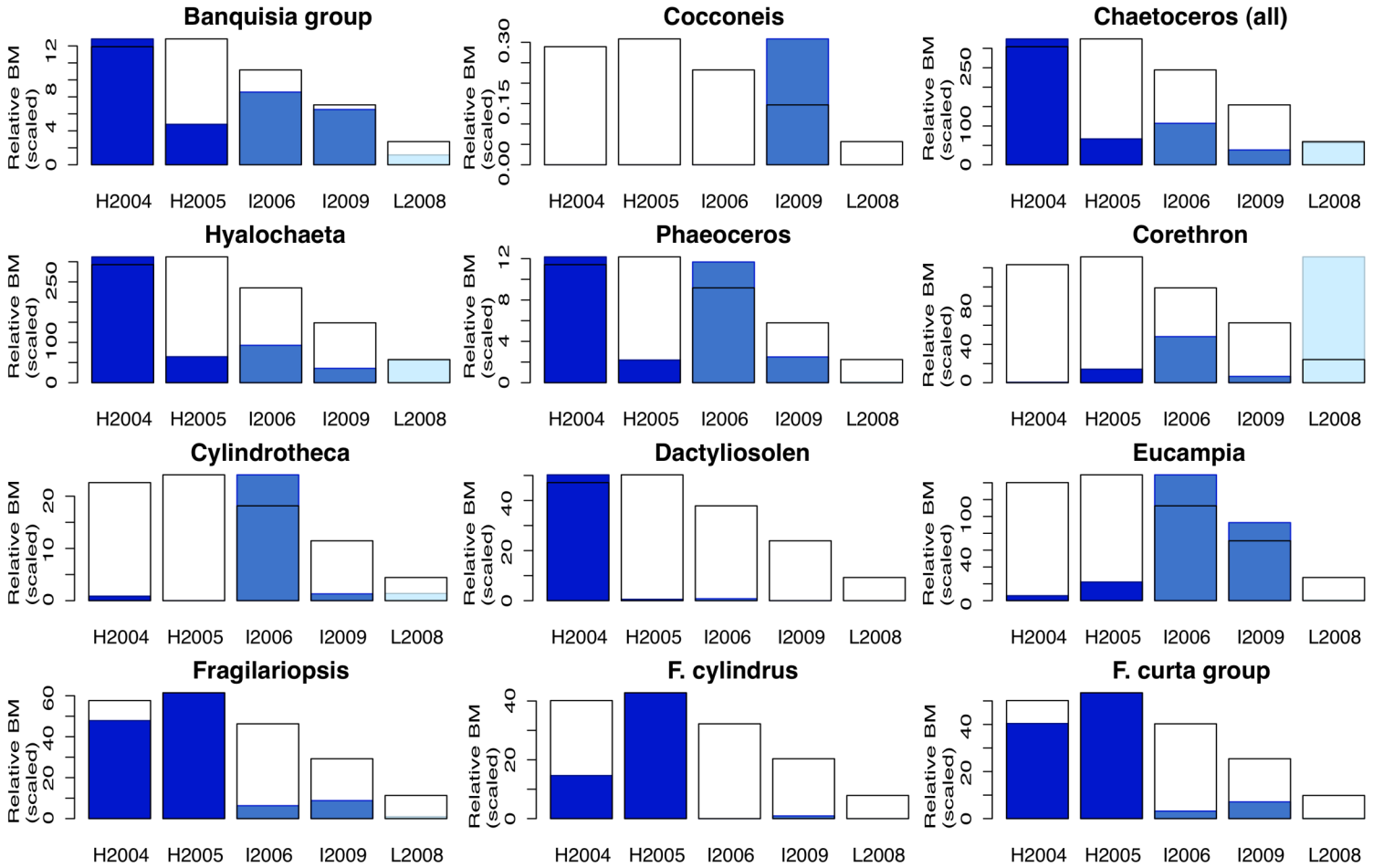

Figure: 4.2a: Seasonal index of species biomass (BM), scaled to seasonal chlorophyll concentrations. Seasons are shown from high- (left hand) to low-chl (right hand). Black boxes show total diatom biomass trends for comparison and are not to scale with the y-axis, (continued below).

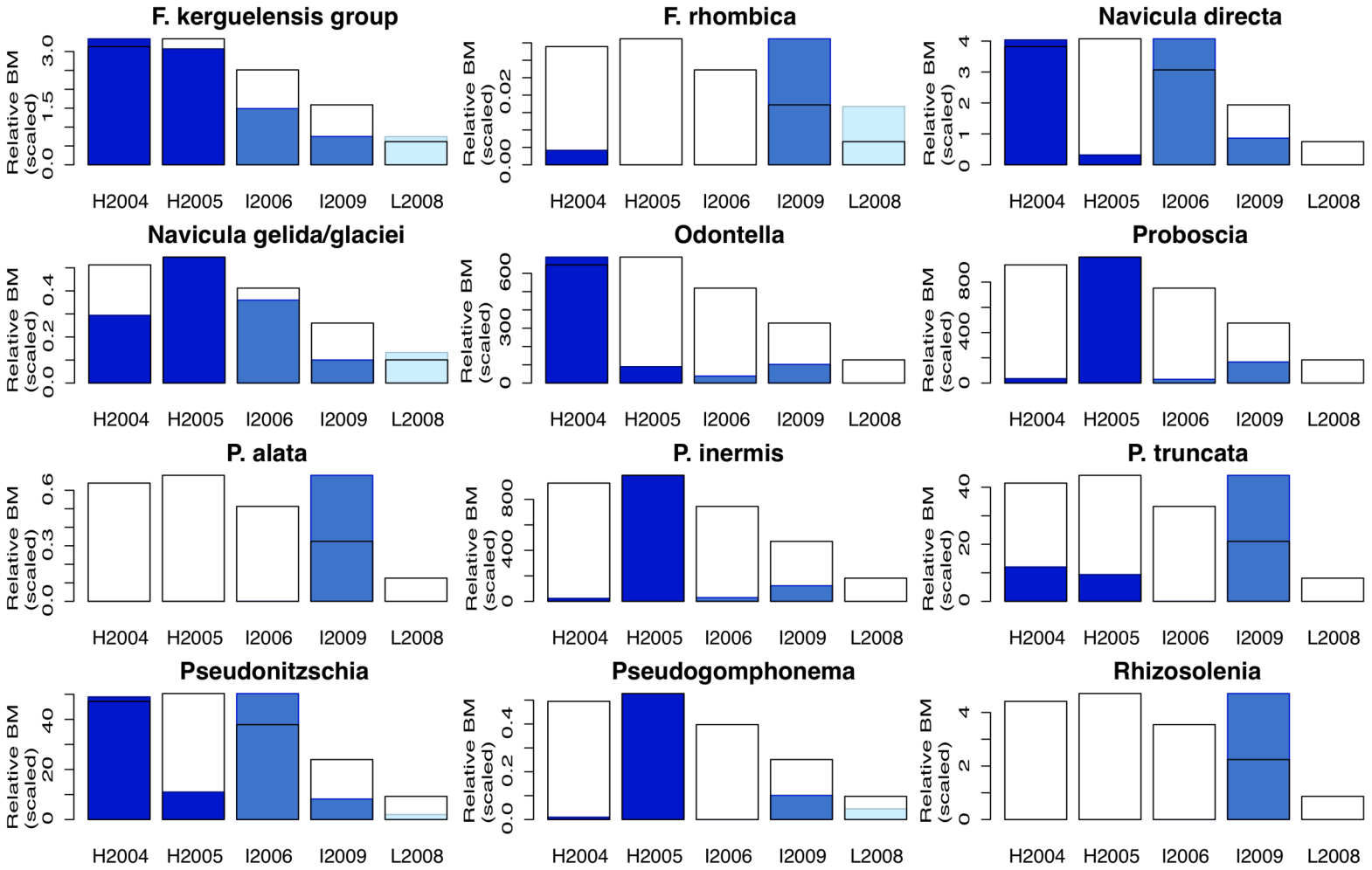

Figure: 4.2b: Seasonal index of species biomass (BM), scaled to seasonal chlorophyll concentrations. Seasons are shown from high- (left hand) to low-chl (right hand). Black boxes show total diatom biomass trends for comparison and are not to scale with the y-axis, (continued below).

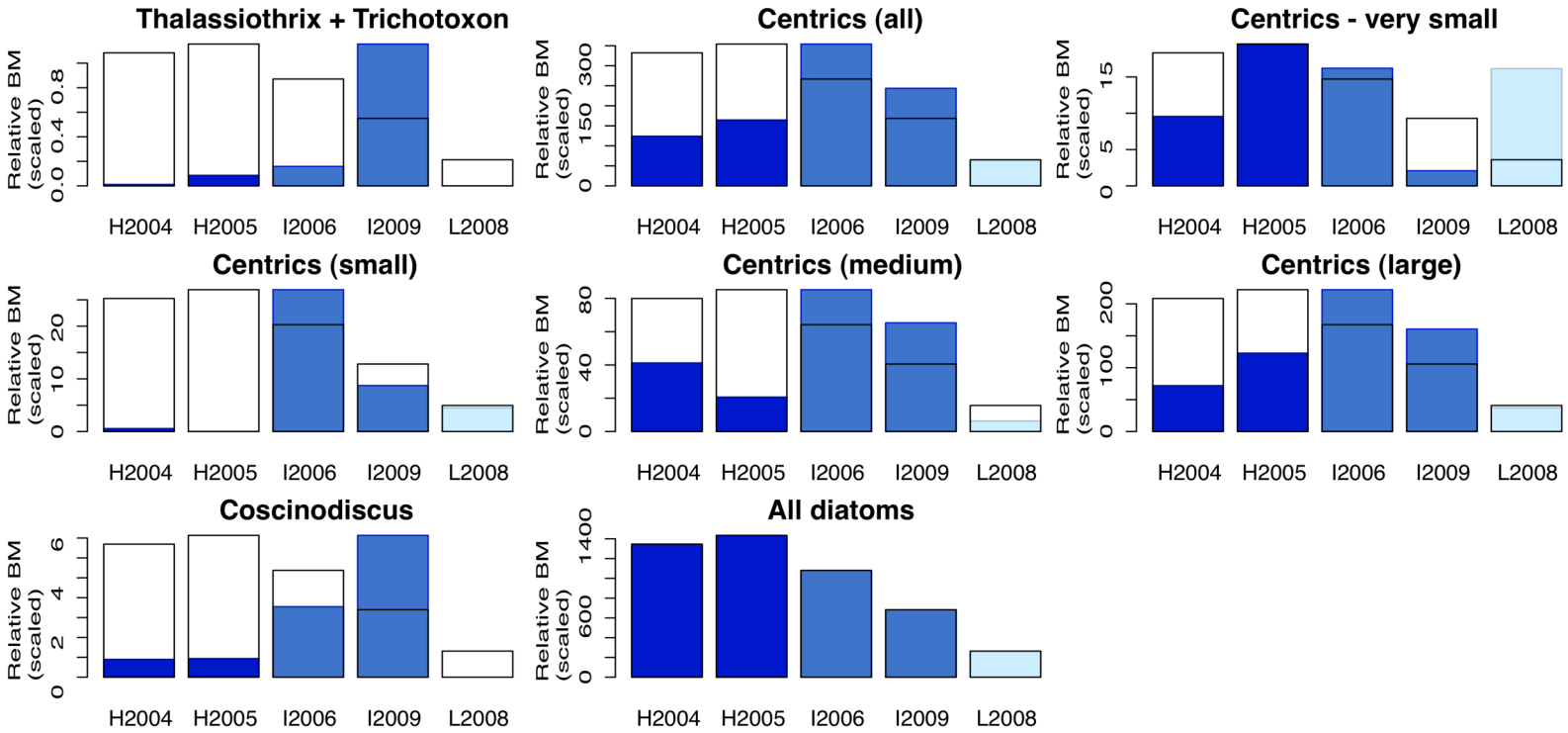

Figure: 4.2bc Seasonal index of species biomass (BM), scaled to seasonal chlorophyll concentrations. Seasons are shown from high- (left hand) to low-chl (right hand). Black boxes show total diatom biomass trends for comparison and are not to scale with the y-axis.

The centrics group was most prevalent in the intermediate seasons, which was true of all size classes save the smallest (~10 μm) which includes large proportions of *Minidiscus chilensis*, an early season diatom with no clear interannual pattern. The difference between high- and intermediate-chl years was greatest in the small centrics group, and smaller but still present in the large (>50 μm) group. *Coscinodiscus* spp. were also considerably more common in the intermediate-chl seasons.

4.4.3 Patterns in interannual diatom community composition

The relative biomass (percent of total diatom community, Fig. 4.3) for most species displays similar trends to absolute and scaled biomass, with the key difference being amplified trends for species common in the low-chl season.

Chaetoceros (predominantly the *Hyalochaeta* subgroup) were common across all seasons, ranging from ~5–15% of diatom biomass, although the variation between seasons shows no discernable pattern with total standing stocks. Centric species were also abundant in all years, contributing > 10% of community biomass in all years. This contribution was greatest in the low- and intermediate-chl years, where centrics accounted for >20% of biomass estimates, although this pattern shows some differences between the size classes. The very small size class (~10 μm) of centrics was much more prevalent in the low-chl season (~14%) than in any other year (<4%). The small (10–20 μm) class of centrics was found in the low- and intermediate- seasons, but very low in the high-chl seasons, although overall the total contribution to community biomass was very rare (<3%). A similar trend was seen in the large centric group, although at higher relative proportions (high-chl seasons: 5–10%; >15% in other years). Medium centrics (20–50 μm) were present to varying degrees in all seasons.

Corethron pennatum were dominant in the low-chl season, contributing over 50% of the estimated community biomass in summer 2008. *Eucampia antarctica* and *Coscinodiscus* were both more prevalent in the intermediate-chl years. In the case of *Coscinodiscus*, there was a 5-fold degree of variation between the two intermediate-chl seasons, while the relative contributions of *E. antarctica* were more consistent (13 and 19% in 2006 and 2009, respectively, versus <4% in other years).

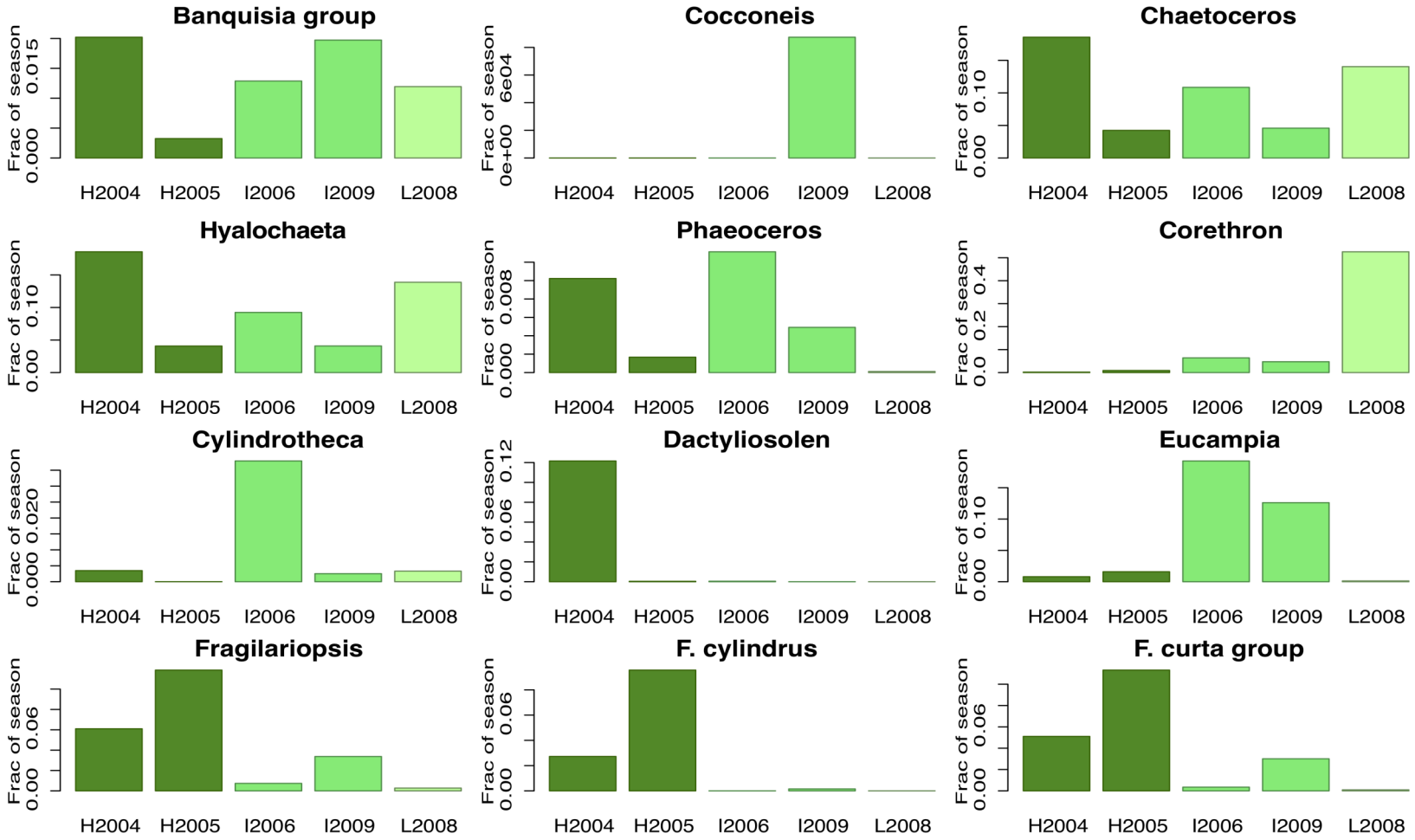

Figure: 4.3 a: Fractional contribution of each species to total estimated diatom biomass by year. Seasons are shown from high- (left hand) to low-chl (right hand). Note that the y-axes are not consistent between plots (so that very low species can still be seen: *e.g.* Proboscia max = 60%, Rhizosolenia max = 0.7%). (Continued below.)

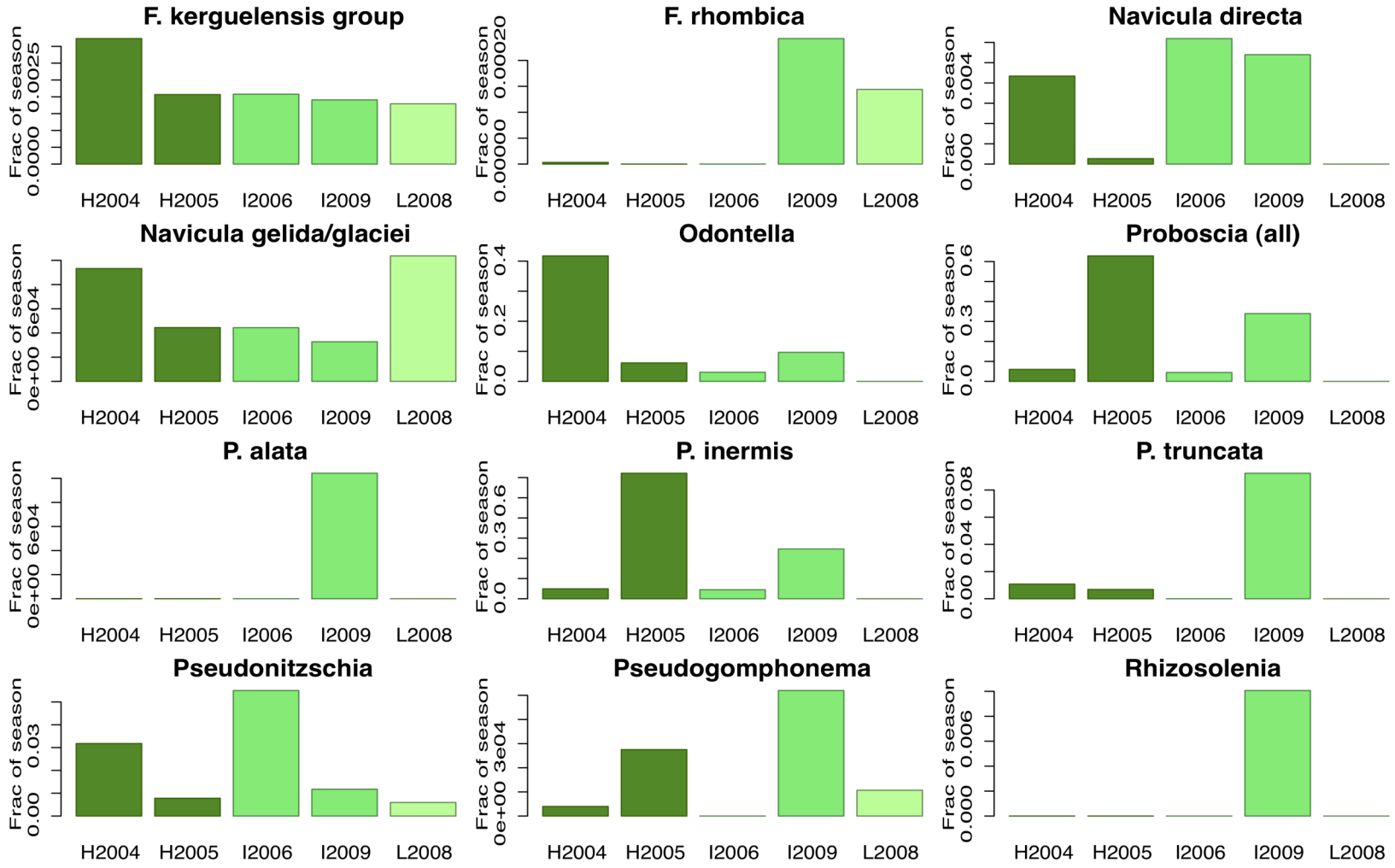

Figure: 4.3b: Fractional contribution of each species to total estimated diatom biomass by year. Seasons are shown from high- (left hand) to low-chl (right hand). Note that the y-axes are not consistent between plots (so that very low species can still be seen: *e.g.* Proboscia max = 60%, Rhizosolenia max = 0.7%). (Continued below.)

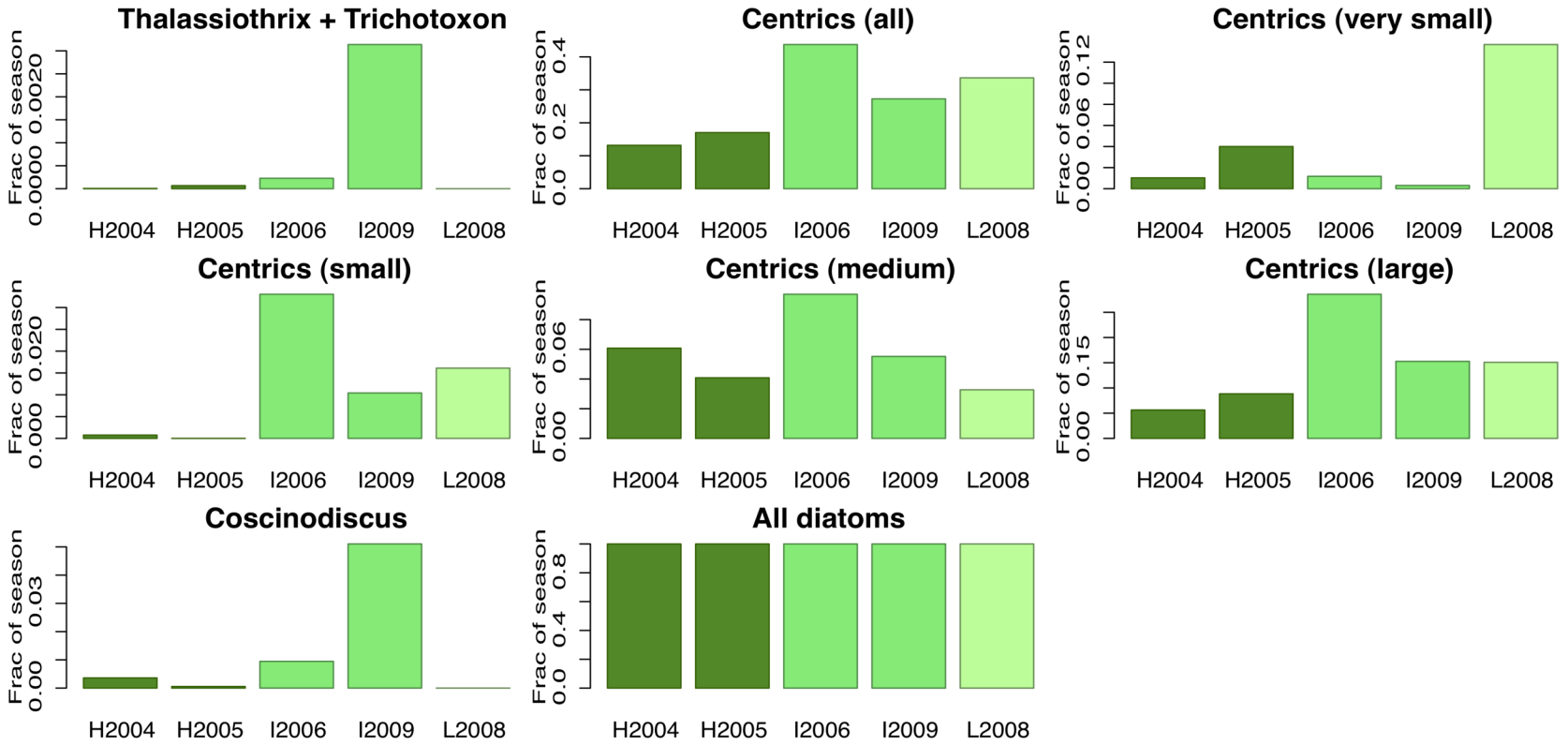

Figure: 4.3c: Fractional contribution of each species to total estimated diatom biomass by year. Seasons are shown from high- (left hand) to low-chl (right hand). Note that the y-axes are not consistent between plots (so that very low species can still be seen: *e.g.* Proboscia max = 60%, Rhizosolenia max = 0.7%).

4.4.4 Intraseasonal progression of diatom species

Diatom assemblages are not static, but vary in both absolute biomass and composition throughout the growing season. This section focuses on the progression of prominent species during each season. The summer bloom period has been divided into three functional periods: early-, mid- and late-season, following Annett *et al*. (2010). As the bloom in Ryder Bay often displays two distinct peaks, these periods cover the time period up to the first chl peak, the interval between peaks, and from the second peak through senescence. The low-chl season did not have a second chl peak, but as the final two samples are from early March, we consider these late season samples. Neither were there two distinct peaks in 2006, but sampling ended in late January of this summer, so no samples are available from late 2006.

Assemblages from 2004–2006 have been previously described in Annett *et al*. (2010), but only in relative terms. As analysis here has shown that absolute biomass concentration estimates from these seasons are also robust (*see* Appendix A3.1), this new data is presented in Figures 4.4 and 4.5, and includes two additional mid-season samples from summer 2004, in addition to the main trends from previous work.

In 2004, the early assemblage biomass had large contributions from the centrics group (primarily very small centrics, in this case largely *Minidiscus chilensis*) and some *Fragilariopsis curta* group. *Odontella weissflogii* then became the dominant diatom species (up to 80% of biomass; not previously observed to this extent in earlier analysis), although biomass of the *F. curta* group continued to increase. Towards the end of the season when biomass was low, dominance shifted to *Dactyliosolen* cf. *antarctica*, medium centrics, and *Proboscia inermis*.

In 2005, early samples contained very high proportions of *F. curta* group and very small centrics. Large centric species and *P. inermis* both initially increased mid-season, but growth of *P. inermis* continued, eventually coming to strongly dominate diatom biomass (>90%) by the second chl peak.

Assemblages in 2006 did not show such distinct seasonal progression, with early- and mid-season both samples having consistently large proportions of large centric diatoms. Medium centrics and *E. antarctica* were also commonly >20%

biomass, and *Chaetoceros* (*Hyalochaeta*) and *P. inermis* were similarly prevalent in a limited number of samples. Late season data is not available for this season.

The low-chl season (2008) had very large initial and late contributions from *Corethron pennatum*. There were small increases in the biomass of *Chaetoceros* (*Hyalochaeta*) and large centrics associated with the (very low) chl peak in late December. Later in the season, small and very small centric species (including *M. chilensis*, *Thalassiosira gracilis*, *T. dichotomica* and possibly *Thalassiosira* auxospores) contributed significant portions of the very low total biomass.

In the final season, chl peaked just prior to the initiation of sampling, but the first sample contained high proportions of *Chaetoceros* (*Hyalochaeta*) and medium centric species, which are likely to be the main contributors of early-season biomass. Mid-season assemblages were predominantly *P. inermis*. The second chl peak was mainly large centrics, along with *E. antarctica* and *O. weissflogii*. There was a pulse of the *F. curta* group in the penultimate sample from this season, and the very final sample on 15 March 2010 had a very high contribution from *Coscinodiscus*.

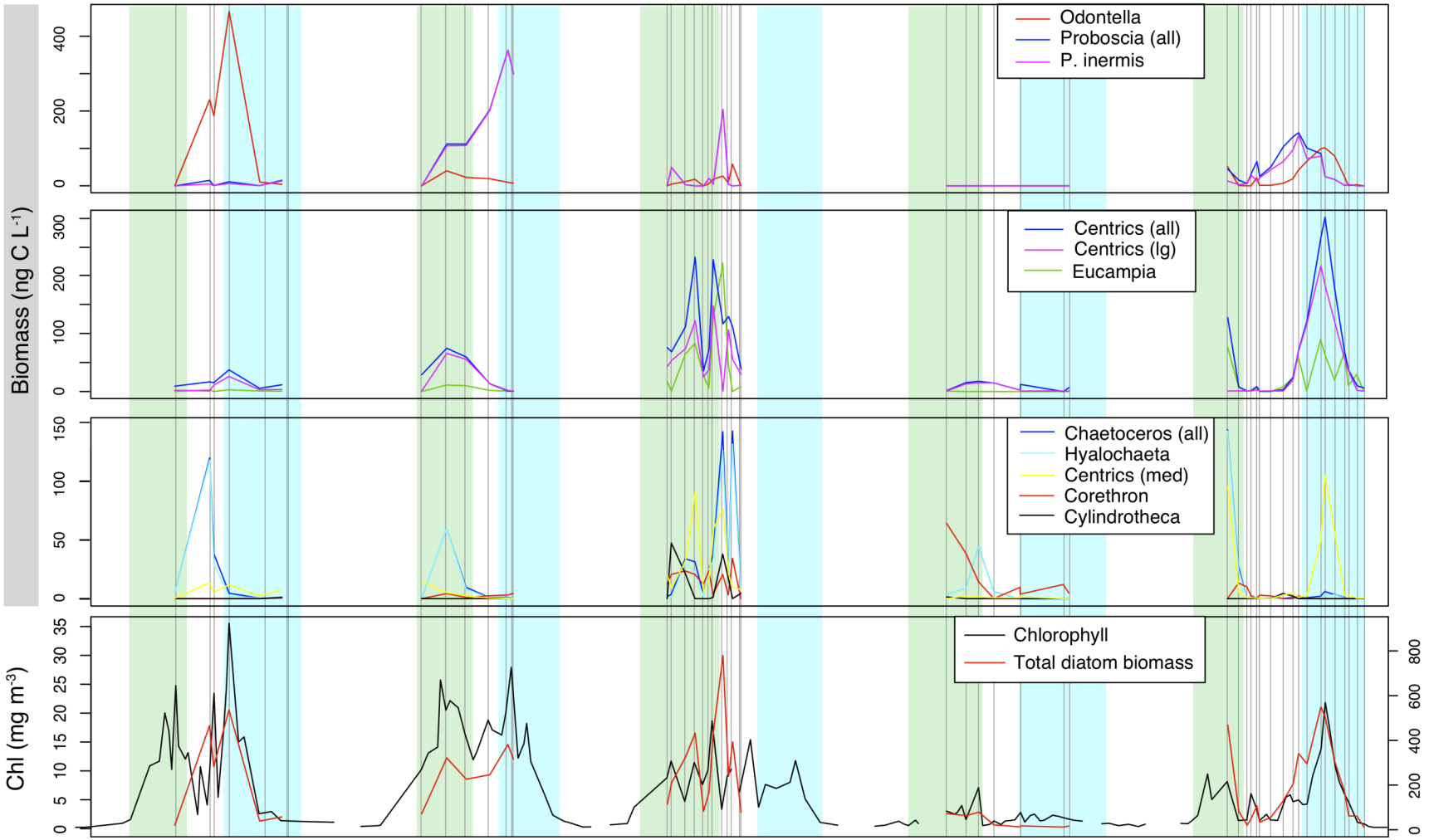

Figure 4.4a: Absolute biomass estimates of diatom species and groups in all five study seasons. Early and late seasons are identified by green and blue shading, respectively. Groups are listed by genus unless species names are also necessary. Vertical lines denote diatoms assemblage analysis dates. Shown for comparison is the chl concentration from BAS data (bottom panel).

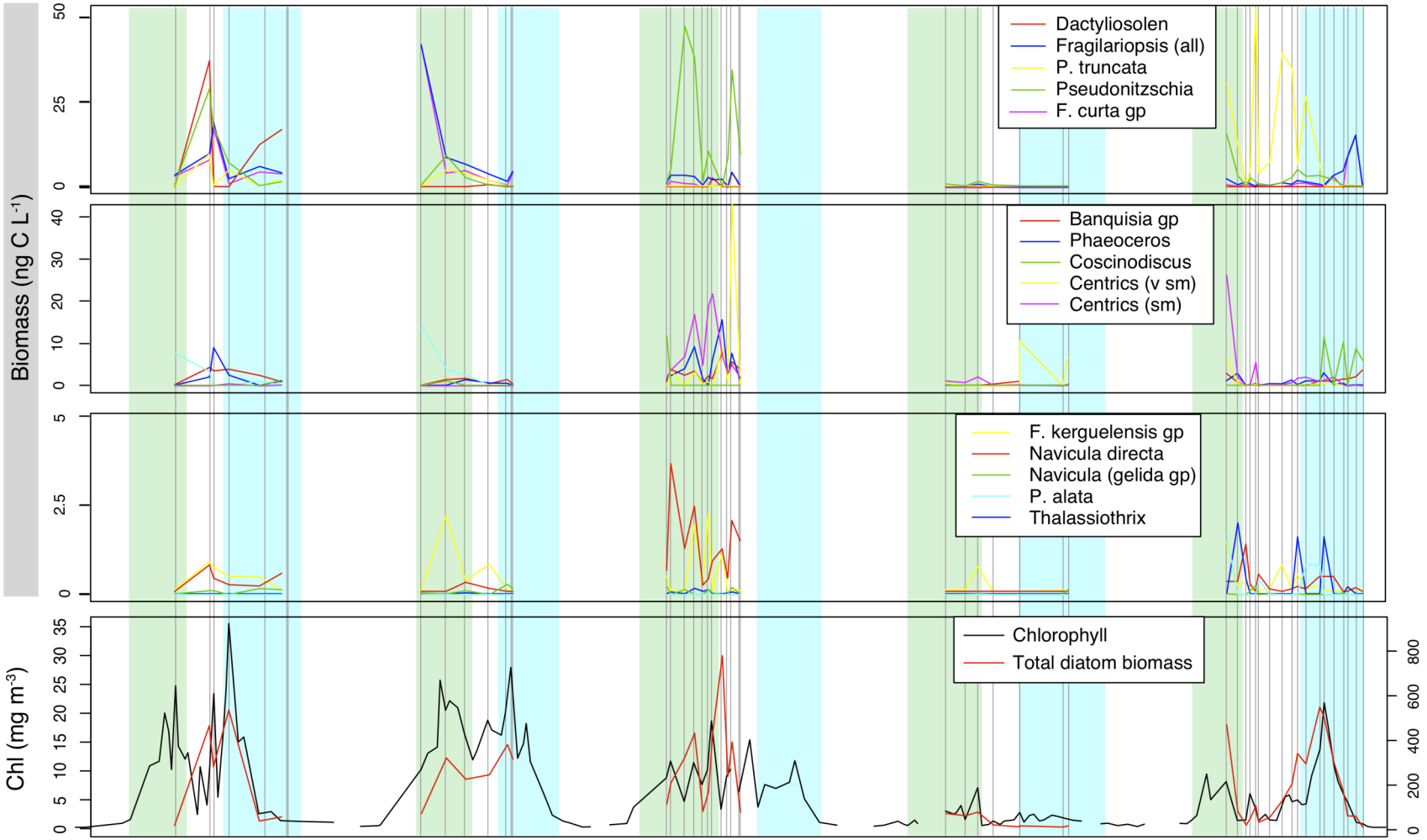

Figure 4.4b: Absolute biomass estimates of diatom species and groups in all five study seasons. Early and late seasons are identified by green and blue shading, respectively. Groups are listed by genus unless species names are also necessary. The total (sum) diatom biomass is scaled to the right-hand y-axis. Shown for comparison is the chl concentration from BAS data (bottom panel).

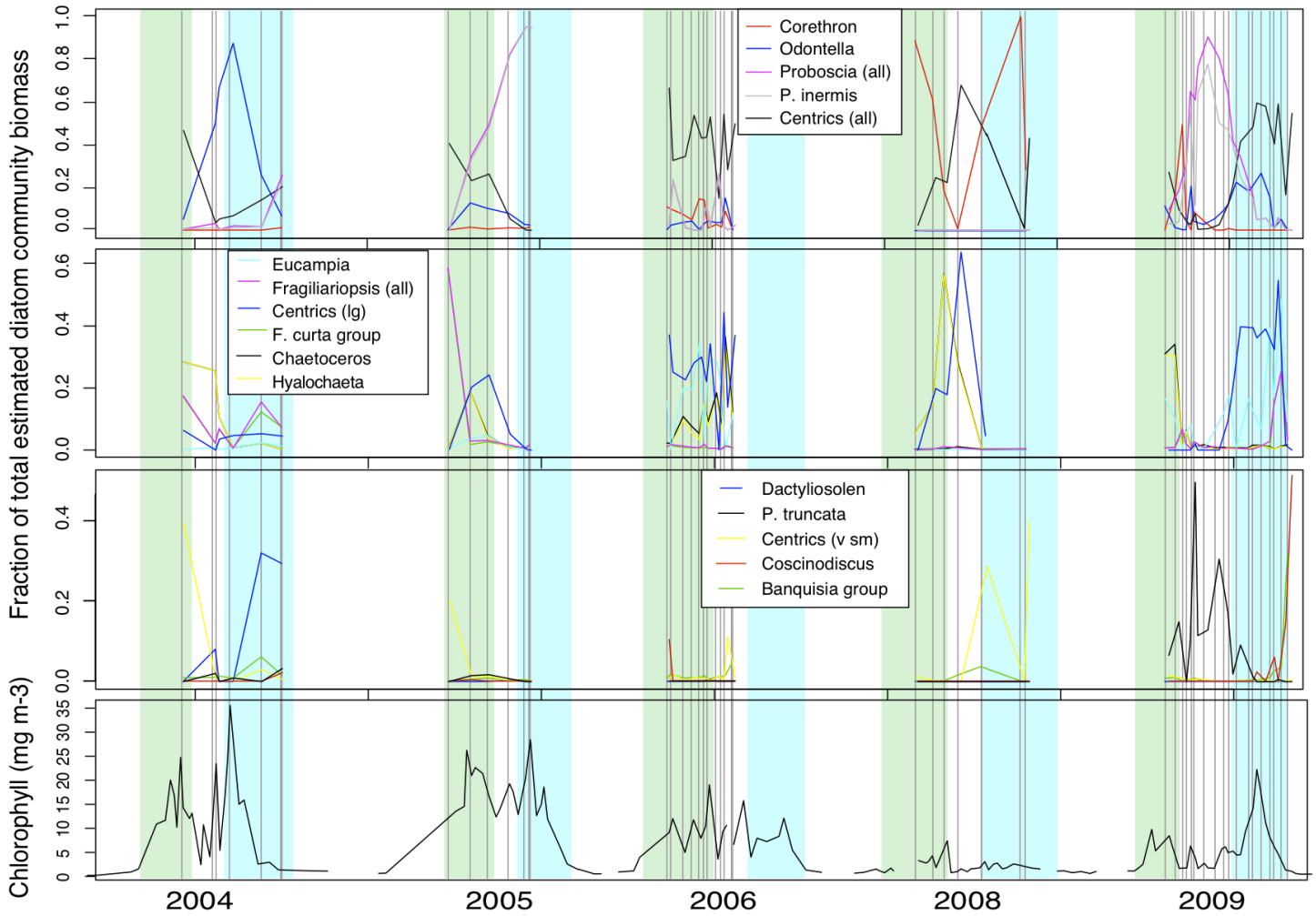

Figure 4.5a: Fractional contribution of each species to total estimated diatom community biomass. Green shading denotes early season, blue denotes late season, vertical lines show dates of diatom community analysis. Also shown for comparison is [chl] (bottom panel).

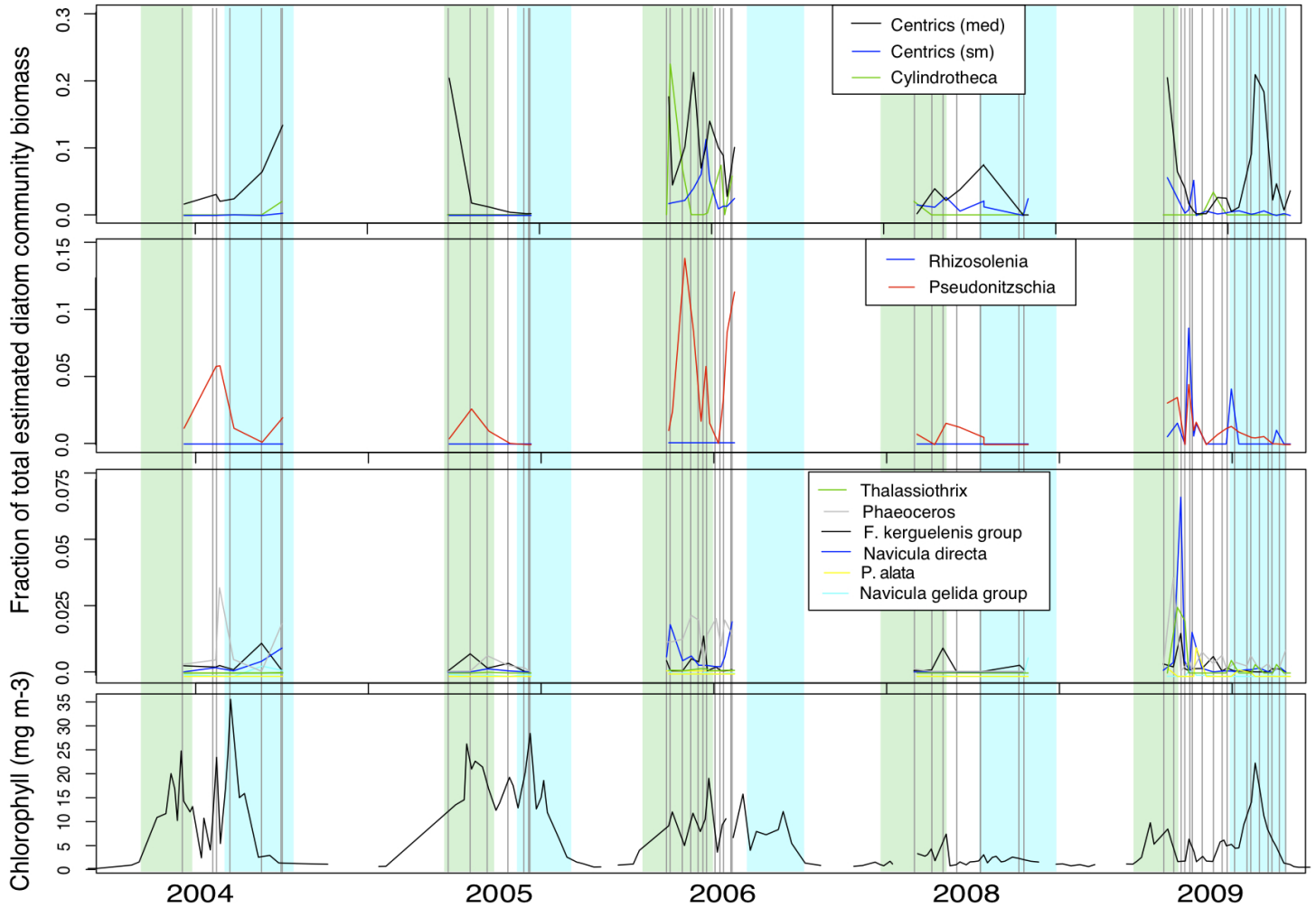

Figure 4.5b: Fractional contribution of each species to total estimated diatom community biomass. Green shading denotes early season, blue denotes late season, vertical lines show dates of diatom community analysis. Also shown for comparison is [chl] (bottom panel).

4.4.5 Intraspecific changes

4.4.5.1 Cell sizes

The high proportion of *Corethron pennatum* biomass in the very low-chl summer of 2008 prompted a closer examination of this species. The relative proportion of biomass from this species appeared to vary in tandem with Si:C ratios in particulate matter (Fig. 4.6). In order to investigate the role of cell size in setting surface area to volume ratios and if this may in turn be a cause of the trends in Si:C, all *C. pennatum* cells were measured whenever possible, using the software available during LM analysis. Commonly, the diameters measured at opposite ends of the cells were not equal, and the larger of the two is reported here. On average, the difference between the two diameters was 14 ± 9 %. Cell volumes were calculated based on the volume of a truncated cone, to account for the different apical diameters.

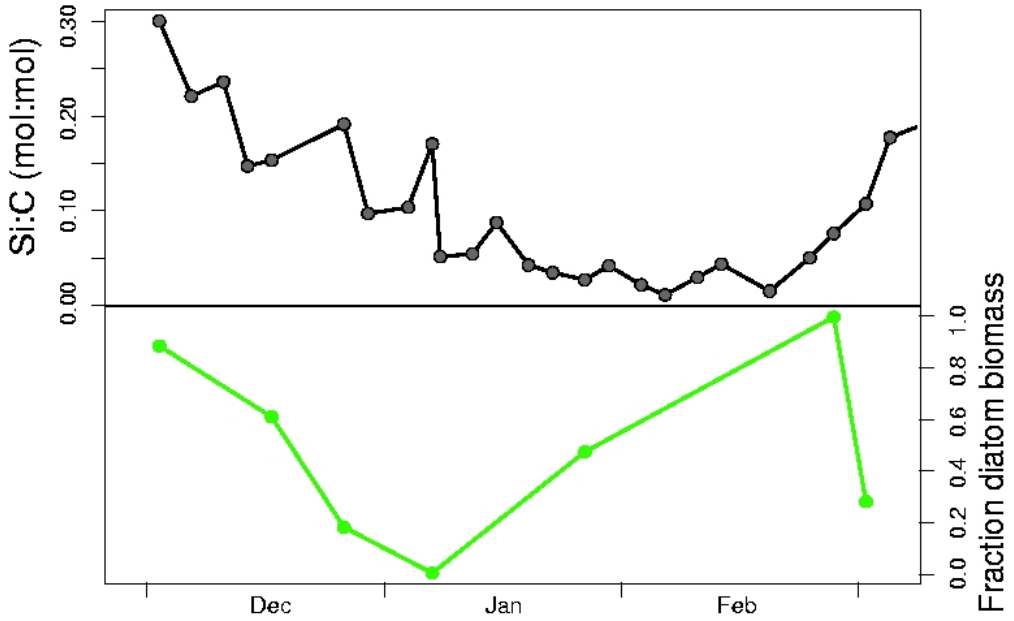

Figure 4.6: Time series trends of Si:C ratios in particulate matter (top) and fractional contribution of *Corethron pennatum* to total estimated diatom biomass (bottom), showing high values of both in early and late season.

The relationship between cell length and cell diameter is shown in Figure 4.7 (a). The correlation between length and diameter is very weak ($r^2 = 0.134$). Despite this, there is a very robust correlation between cell diameter and surface area to

volume ratios (Figure 4.7b; $r^2 = 0.976$). Although this relationship is not linear, this is to be expected, as surface area increases proportional to the square of diameter, while volume increases proportional to its cube; thus, the ratio declines as cells get larger. Both cell diameter and surface area to volume (SA:V) ratios show strong relationships with estimated cellular carbon (Figure 4.7 c and d).

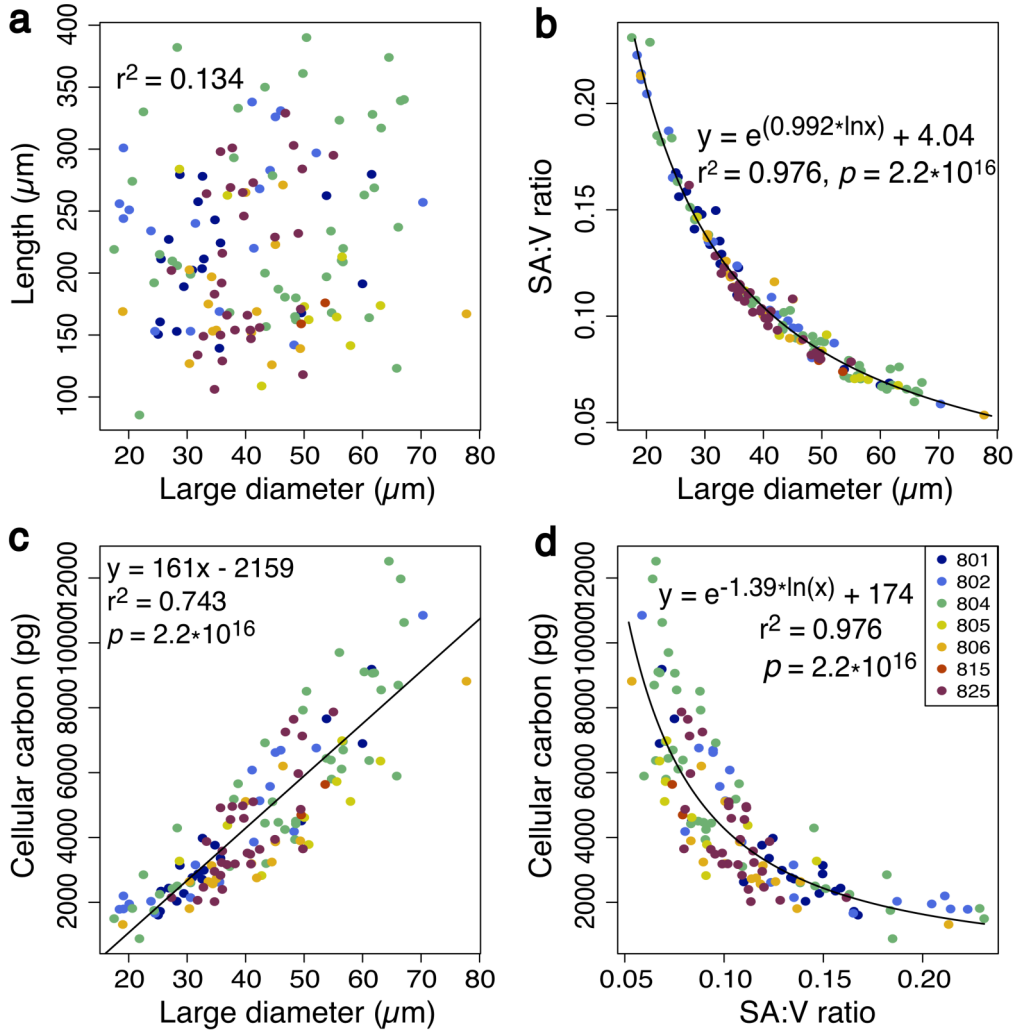

Figure 4.7: Relationships between cell dimensions, SA:V ratios and cellular carbon of *Corethron pennatum*: large diameter (see text) and length (a), SA:V versus diameter (b), cellular carbon estimate versus diameter and SA:V (c and d, respectively. Measurements were taken from seven samples during austral summer 2008, each identified as per the legend in (d); dates given in A2.1.

The measured cell sizes of *Corethron pennatum* across a single season display considerable variability (Fig 4.7a), and result in cellular biovolume and

carbon estimates spanning a 6-fold range (Fig 4.7c). Especially in the case of large or dominant diatoms, such a range in cell sizes may influence trends in species-specific or total diatom biomass if a single average biomass value is used to convert abundances to biomass, as in the case here and in many studies. As *C. pennatum* is both large and a dominant source of estimated diatom biomass during the 2008 season, this species was used here to assess the importance of using sample-specific cell sizes to estimate diatom biomass.

Biomass concentrations using average cellular C estimates (as described in section 4.3.3.3) were thus compared to those calculated using the size distributions assessed for 2008 samples (*i.e.* cell measurements presented in Fig. 4.7). The results of this comparison are given in Figure 4.8, and show a relatively high degree of agreement in most cases. Notable offsets occur only in the earliest sample (7 Dec 2008), where detailed analysis of *C. pennatum* cell sizes leads to lower *C. pennatum* biomass estimates than use of an average cell biomass value. As this species represents the majority of diatom biomass in this sample, this consequently affects the total diatom biomass estimate, which is lower using the sample-specific biomass values. The sample-specific *C. pennatum* cellular biomass results in estimates of *C. pennatum* and total diatom biomass which are ~30% lower than estimates based on average cell biomass. In other samples, for example 26 Jan 2009, the discrepancy between the two methods was much lower, 6% for *C. pennatum* biomass estimates and only 3% for total diatom biomass estimates.

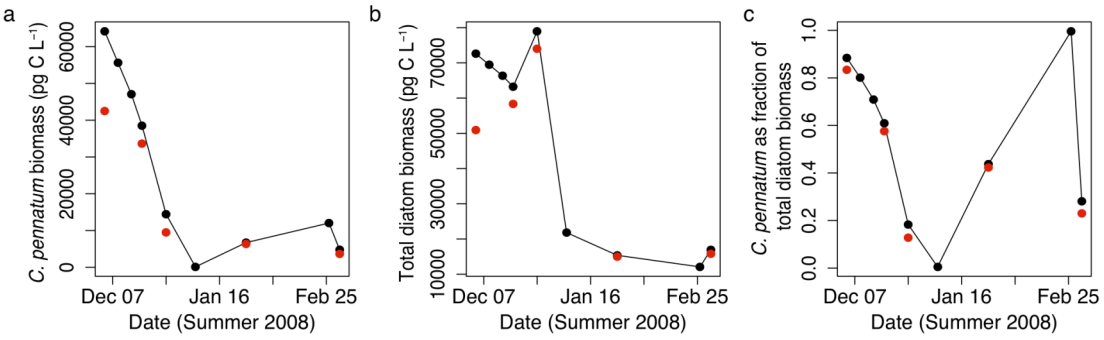

Figure 4.8: Comparison of *Corethron pennatum* biomass (a), total diatom biomass (b) and fractional contribution of *C. pennatum* to total biomass (c) when assessed using a single average cellular biomass value (black symbols and line) versus sample-specific cellular biomass (red symbols).

Results indicate little impact on fractional biomass estimates from two methods. The relative proportion of total diatom biomass attributed to *Corethron pennatum* remains very consistent regardless of the cellular biomass used (average versus sample-specific; Fig 4.8c). Overall, the impact of sample-specific sizes was reasonably small, with relative biomass estimates being very consistent, and only one of five samples showing considerable differences between absolute biomass estimates. The large range of observed cell sizes (~4-fold range in both cell diameter and length) in *C. pennatum* is an extreme case, with other diatom species showing much narrower size ranges. Additionally, the large size of this species and its high relative biomass during the 2008 season gives the size variation of *C. pennatum* a greater potential to impact diatom community biomass estimates than is the case for smaller or less prevalent species. In the extreme case of *C. pennatum*, only one sample is strongly affected by incorporating sample-specific cell sizes, and this difference does not impact any of the conclusions drawn from the results. Consequently all results presented and discussed here are calculated using average cellular biomass.

4.4.5.2 Chain-forming species

For the six groups of chain-forming diatoms studied, several showed relatively little change in the proportions of cells present in chains versus as solitary cells. There was considerable variability, making it difficult to identify any conclusive trends (Fig. 4.9). For example, >90% of *Chaetoceros* (*Hyalochaeta*) cells were found in chains in all seasons. The average length of these chains ranged from 5–8 cells, with high proportions found as chains of 2 and the longest chains exceeding 30 cells, thus the standard deviations are ≥4 cells per chain in all cases.

Large centric species (predominantly *Thalassiosira antarctica*) and small centric species (primarily *Thalassiosira gravida* and *Thalassiosira gracilis*) showed no clear correlation with chl stocks, with considerable differences between even the two high-chl years of 2004 and 2005 (especially in the case of the small centrics). Likewise, chains of *Odontella weissflogii* also had no obvious trend. While most chains were 2 or 3 cells in length, there was one sample in the 2004 season and two

in 2009 where chains over 8 cells long were observed: 21 Jan 2005, and 28 Dec 2009 to 16 Jan 2010.

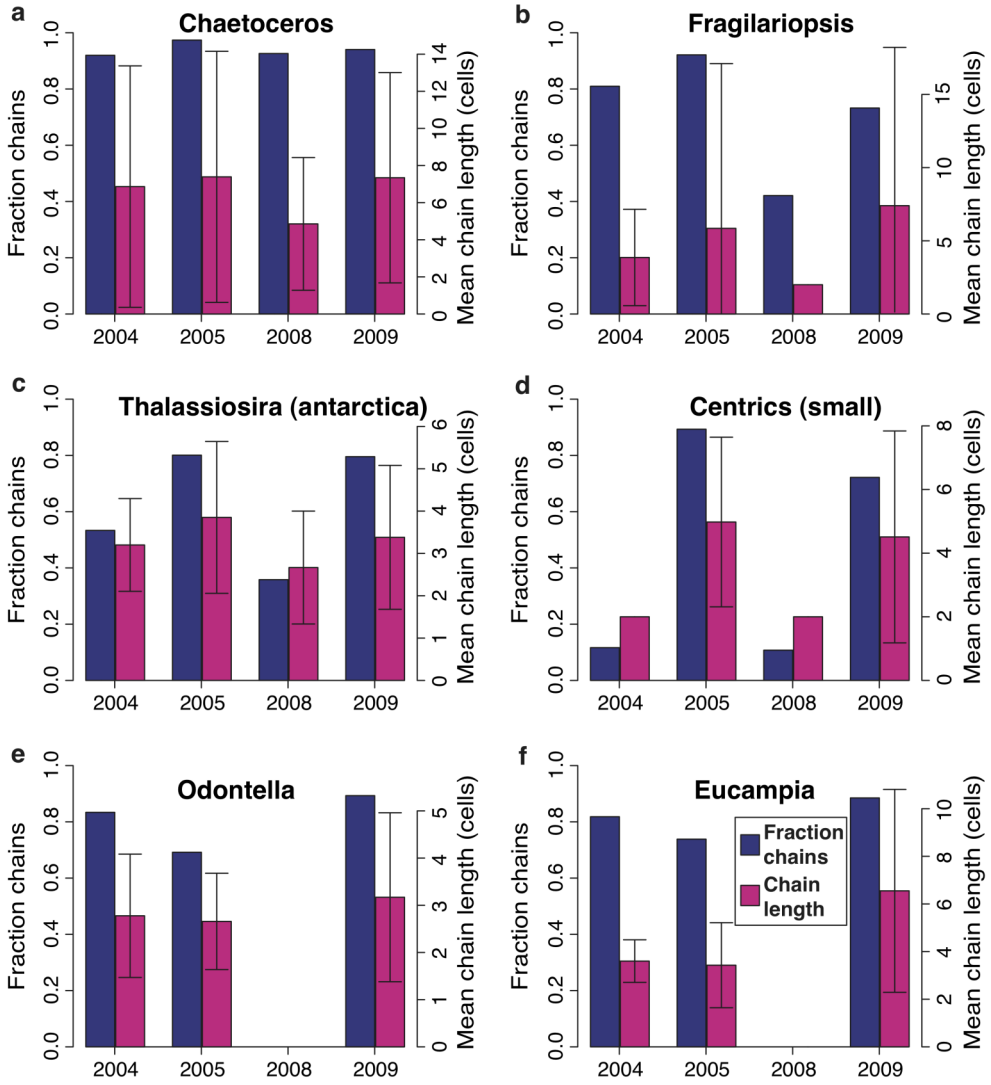

Figure 4.9: Characteristics of chains in populations of *Chaetoceros* (*Hyalochaeta* subgenus), *Fragilariopsis curta*, *Thalassiosira antarctica*, small centrics (see text), *Odontella weissflogii*, and *Eucampia antarctica* (a through f, respectively). Dark bars are fractions present as chains, lighter bars are the average number of cells in each chain. For both, values shown are for all cells analysed in that season. Error bars represent 1 standard deviation.

There seems to be a pattern of higher proportions of *Eucampia antarctica* chains in high-chl seasons (Figure 4.9f), although this trend is relatively weak and no cells were present in 2008 so the difference is based on only one value for the 2008-2009 period. However, this is found concurrently with a relatively large change in

the average number of cells in each chain, with considerably longer chains found in the 2009 samples (>6 cells versus <4 cells in 2004 and 2005).

Chain length in *Fragilariopsis curta* was also highly variable, showing no obvious trend between earlier and later seasons. In contrast, *F. curta* seemed to have lower proportions (<75%) present in chains during the final two years of the study, compared to >80% in the earlier, high-chl years. The lowest proportion of *F. curta* chains was found in the low-chl season of 2008 (Fig 4.10), although it can be seen that many samples from 2009 also had low proportions, with the higher seasonal mean (Fig. 4.9b) stemming from the high abundances of long chains in the first 2009 sample.

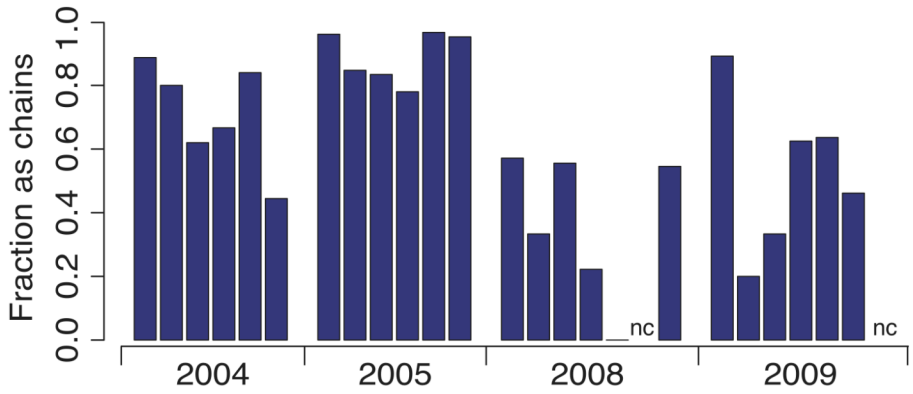

Figure 4.10: Fraction of *Fragilariopsis curta* group (excluding *F. cylindrus*) cells found in chains in each sample of the four seasons analysed. The sample where no chains were observed has a bar at 0, whereas samples where none of these cells were observed (either solitary or in chains) are denoted as no cells ("nc").

4.5 Discussion

As the key link between environmental variability and the fixation and trophic transfer of organic carbon, changes in diatom communities have broad-reaching potential impacts. Here the diatom assemblages found in the different chl regimes are discussed, in terms of broad to specific characteristics. At the most general level, diatom richness and diversity are examined. Assemblages and ratios characterising high- and low-chl seasons are identified with regard to applications for modern and sedimentary studies. Next, species succession at the seasonal level is compared to previous studies, to investigate any differences within the study period,

and consider the mechanisms which may underlie such changes. Finally, within-species variability (such as chain length and cell size) is considered as an effect of environmental conditions, and discussed in the context of using diatom fossils in sediment records to interpret past climate.

4.5.1 Diatom-level aspects of seasonal step-changes in productivity

4.5.1.1 Richness and diversity

The similar values of diversity in high- and low- chlorophyll seasons suggests that in both cases these seasons are dominated by a few species which are particularly suited to seasonal conditions. Meanwhile the higher diversity in intermediate years reflects conditions which species cannot exploit as effectively, perhaps indicating more changeable conditions in which a single species cannot outcompete others over a prolonged period.

The species richness seen in the low-chl summer of 2008 is considerably lower than in all other years. This reflects fewer species or groups being present, and lends support to a bottom-up limitation on production, in that conditions were outside the range favourable to a subset of species which subsequently were not able to grow during this season. Top-down effects, such as grazing, are highly unlikely to be so selective as to remove all individuals of a preferred prey species and result in this pattern of species richness.

While at a phytoplankton community level the increases in non-diatom taxa (*see* Chapter 3) may to some extent compensate for lower diatom species richness, the results presented here indicate a significant decrease in richness within the diatom community in low-chl conditions. Within the context of regional shifts along the WAP to reduced phytoplankton standing stocks, these results suggest that this may also be accompanied by a loss of some species over longer time scales. As geographic displacement has been seen in higher trophic levels (*e.g.* southward movement of Adelie penguins and replacement by chinstrap penguins; Ducklow *et al*. 2007), it is possible that diatom communities may also undergo such a shift, which would be expected to occur over much longer time scales than that

investigated here. Given the single low-chl year sampled here we cannot conclude that richness and overall productivity are correlated, as evaluated richness can be influenced by sample size (Warwick & Clarke 1995), and thus may be impacted by the lower overall abundances of diatom cells during the low-chl season. As the impacts of species richness and diversity can have strong ecosystem-level consequences, more work is needed to establish the strength of any relationship between diatom richness and overall production.

4.5.1.2 Community composition

Changes in species abundances allow us to characterise high and low chl assemblages. For example, higher amounts of very small centrics or *Corethron pennatum* cells suggest low-chl periods. Higher *Eucampia antarctica* is associated with intermediate-chl years, and high *Fragilariopsis* with high-chl seasons. While interseasonal diatom community records from other locations for comparison are relatively sparse, some indicate similar trends. Moline & Prézelin (1996) report that *Corethron criophilum* (= *C. pennatum*) was dominant in the waters around Palmer station in a low sea-ice, low productivity year. Additional observations by Schloss & Ferreyra (2002) noted more abundant *C. criophilum* during turbulent periods, consistent with the low-chl conditions found here. Clarke & Leakey (1996) also observed this species in low-chl waters near Signy station. Thus this species appears strongly linked with deeply-mixed, low-chl surface waters.

Comparing species with contrasting abundance patterns can exploit the differences between seasons, which may add information to interpretation of sedimentary records. During the study period here, some species ratios differentiate high from low from intermediate seasons (Fig. 4.11). *Corethron pennatum*: *Fragilariopsis* (*kerguelensis* group), *Fragilariopsis* (*curta* group:*kerguelensis* group), and *Navicula* (*gelida* group):*Eucampia antarctica* all displayed markedly higher ratios in the low-chl season than in any other seasons. In the case of *C. pennatum*:*F. kerguelensis* group, this ratio reflects the prevalence of *C. pennatum* in low-chl conditions compared to the *F. kerguelensis* group, which is comparatively consistent across seasons. The increased ratio of the *F. curta* group:*kerguelensis* group is surprising as the *F. curta* group is typically associated with high sea-ice, and

2008 was a low sea-ice year in Ryder Bay. However, regional sea-ice was high and thus this ratio may reflect regional, rather than local processes. The increase in the *N.* (*gelida* group) relative to *E. antarctica* may reflect the deeper mixing in the low-chl season, as *N. gelida* is commonly found in the benthos, and may be mixed into the water column during periods of deep MLD.

The intermediate-chl years were characterised by high ratios of *F.* (*kerguelensis* group):Large centrics and *Eucampia antarctica*:*F. kerguelensis* group, as well as the inverse of two of the low-chl year ratios, *F.* (*kerguelensis* group:*curta* group) and *Eucampia antarctica*:*Navicula* (*gelida* group). In the case of ratios with *E. antarctica*, these reflect the higher abundances of this species during the intermediate-chl years. While the ecological reasons for higher *E. antarctica* abundances in these conditions are not clear, this species is considered an autumn species (Fryxell 1989, Leventer *et al*. 2002), and thus may reflect conditions of weak stratification, similar to autumn conditions, but not so severe or long-lived as seen here in the low-chl season.

High-chl season diatom species ratios were more variable, such that only the ratio of *F.* (*kerguelensis* group):Small centrics was higher in both high-chl years than in any of the other study seasons. As the *F. kerguelensis* group was one of the few groups with comparatively consistent abundances across seasons, the trends in this ratio here reflect the lower prevalence of small centric species during the high-chl years. Again an ecological explanation for this distribution pattern remains unclear, but perhaps may reflect lower nutrient or light availability during periods of high productivity, which would result from near-complete nutrient use or self-shading, respectively.

By using multiple ratios together it may be possible to differentiate between high- and low-chl seasons even if sedimentation rates are not consistent across years. Given the relatively high species variation between all years, it is uncertain if these patterns are robust over longer time scales. However, the ratios presented here strongly reflect the three chl conditions found in this study, although they are based on only five seasons. Ratios of the species identified here may be helpful in characterising seasonal productivity in samples of limited temporal scale such as ship-based records where spatial coverage is extensive but cannot capture full

seasonal productivity. Especially where ratios may be compared across samples from multiple locations and for multiple species pairs, changes in these ratios may identify locations likely to exhibit high- or low-chl at the seasonal level.

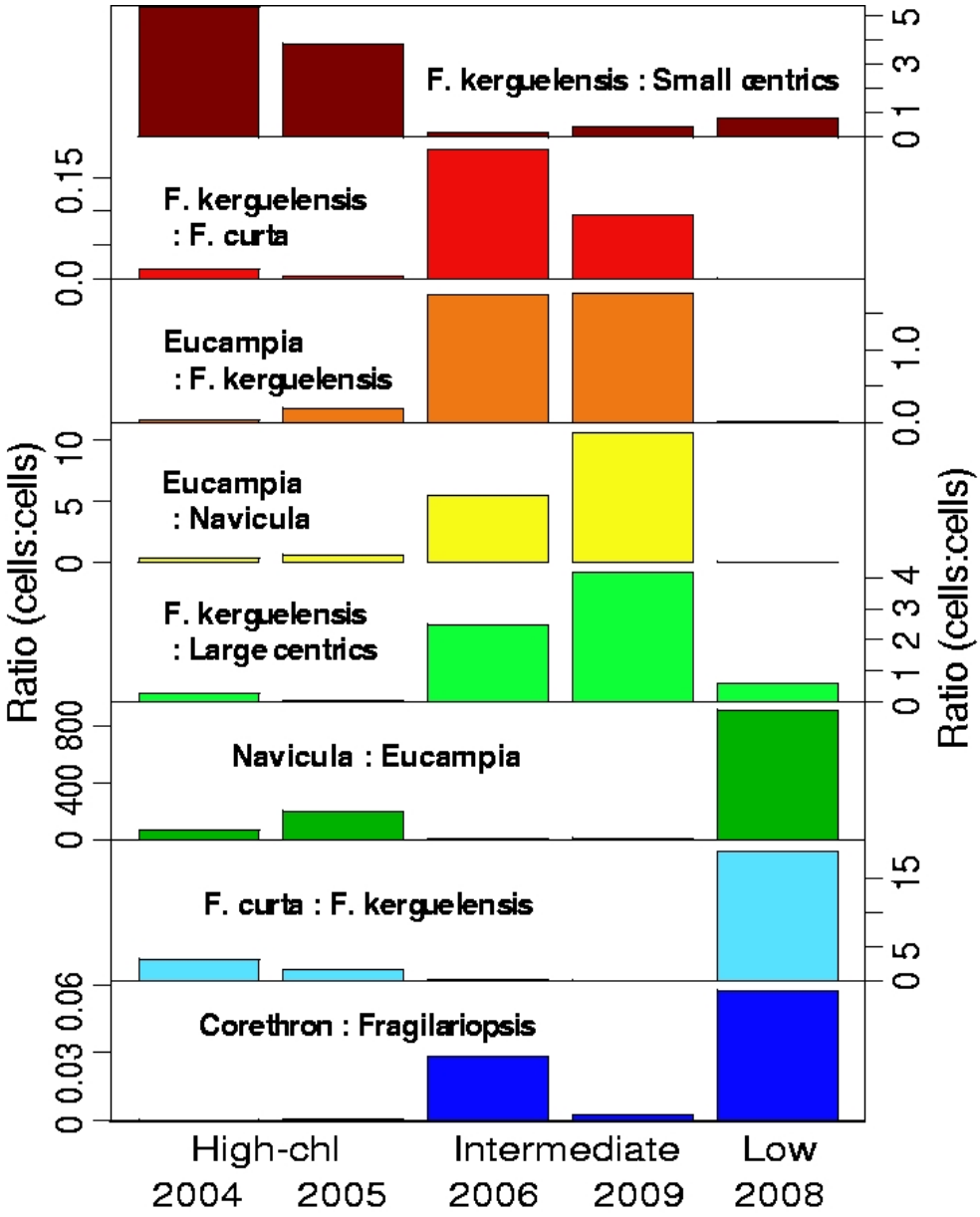

Figure 4.11: Selected species ratios that varied with overall productivity. Ratios are presented as cells:cells rather than in terms of biomass, in order to be more easily applicable to counts from water or sediment samples. Seasons are shown from high-chl to low-chl (left to right), and years are specified on the x-axis.

Additionally, the ratios of species noted here can be applied to sediment records, although additional care must be taken in order to interpret such data. The

numerical values found here are likely to change in sediments, as thinly silicified species are more prone to dissolution than those with thicker frustules. However, we postulate that increases or decreases of these ratios within a given sediment record will reflect changes in the overlying waters, and thus trends to higher or lower chl concentrations. If evaluated relative to other ratios within the same core, these ratios should indicate broad-scale changes similar to the large differences in seasonal chl seen here. Additionally, it can be noted that the ratios chosen here showed sharp changes between the different chl conditions. Sharp changes, especially if seen in several species pairs, are therefore a strong indication of changes in productivity

4.5.1.3 Changes in community size structure

A primary characteristic of the changes seen in [chl] trends (which includes non-diatom taxa) is the shift towards greater contributions of the small size fractions, especially those <5 µm. Such a shift is not clearly seen in diatom records. Small diatoms (here where all axes are <20 µm, or one is much less than 20 µm and could be expected to pass through a 20 µm filter, *e.g*. *Pseudonitzschia*), show high variability within each season, thus differences between years are difficult to detect. This is exemplified by the 2005 season, in which small diatom biomass is initially >60% of the total, but quickly declines to less than 10%. The range for this season is larger than other seasons, even though the majority of samples examined during this season display low values. It can be seen in Figure 4.12 that there is some indication of higher ratios of small:large diatom biomass in the low-chl season, as might be expected from similar shifts in chl measurements, but further data are required to confirm the presence and extent of any trend, as ratios are within the range recorded in previous seasons.

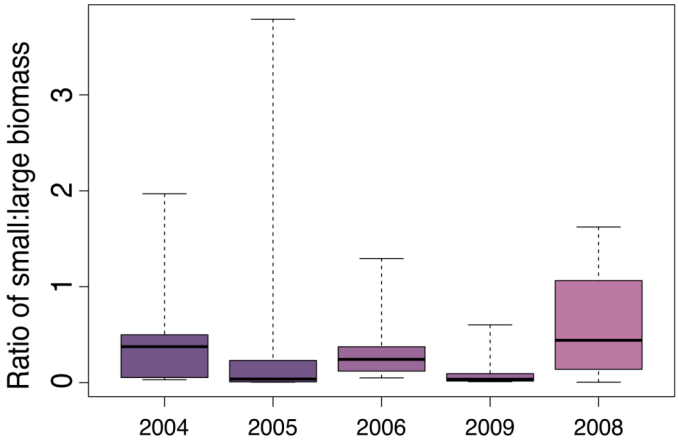

Figure 4.12: Ratios of small to large diatom biomass in high- (left), intermediate- and low- (right) chl seasons. Thick bars represent mean values, shaded boxes span second and third quartiles, and whiskers show the full range of values.

4.5.2 Intraseasonal progression of diatom species

Previous work in Ryder Bay has identified several species which were found to be associated with seasonal progression (Annett *et al*. 2010). Some of these species are also associated with specific conditions such as nutrient supply or stratification, both at this study site as well as within the greater WAP region. *Minidiscus chilensis* was identified as an early-season species, and was often accompanied by *Fragilariopsis curta* group and *Chaetoceros neglectus* and *socialis* (both in the *Hyalochaeta* group), although the *Chaetoceros* species were associated primarily with nutrient injection events (Annett *et al*. 2010). *Minidiscus chilensis* has been observed at high abundances in mid-January in Bransfield Straight (Kang *et al*. 2003). Previous work in Ryder Bay has found *M. chilensis* to be an early-season diatom in this area (Annett *et al*. 2010). In the two additional seasons studied here, there were no early peaks in the abundance of *M. chilensis*, although it was previously noted that this species is not present in the early part of every season. Interestingly, some *M. chilensis* were observed in late January through March of the 2008 season, considerably after the first and only chl peak. Oxygen isotopes from seawater indicate a pulse of sea-ice melt water from 1 Jan through 18 Jan 2010 (BAS data; not shown). As this species has been previous observed within sea-ice at this location (Table 4.1; Annett 2008), these data could indicate a release of diatoms via sea-ice melt, which could seed a small bloom of *M. chilensis*.

The *Hyalochaeta* subgroup was seen in the later two years of the study during the early part of the season, consistent with previous observations along the WAP (Varela *et al*. 2002, Garibotti *et al*. 2005, Annett *et al*. 2010). Where this group is present later in the season, it has been previously noted to coincide with nutrient injection events (Annett *et al*. 2010). The first sample from 2009 showed elevated *Hyalochaeta* group biomass, at the beginning of the season when nutrient levels would have been high. The peak in *Hyalochaeta* biomass in 2008 occurred on 27 December, and nutrient data from BAS indicate an increase in nitrate concentrations from 8 µM on 15 December to 12 µM on 27 December, continuing to a peak of 18 µM in early January. Thus the pulse of *Hyalochaeta* is in agreement with an ability to increase growth rates over those of other species in response to increasing nutrient levels.

Table 4.1: Common diatom species in Ryder Bay sea-ice samples. From samples collected in early spring of the 2004, 2005 and 2006 seasons. Data from Annett (2008).

Species/Group	Peak sea-ice brine biomass (µg C L^{-1})
Fragilariopsis curta and *cylindrus*	32
Proboscia inermis	0.5
Minidiscus chilensis	6.4
Banquisia group	16
Chaetoceros (*Hyalochaeta*)	50
Navicula gelida and *N. glaciei*	1.5
Centrics (>20 µm)	2.5
Centrics (<20 µm)	4.5

Fragilariopsis species have also been identified as early-season diatoms, in particular the *F. curta* group. Members of this group (especially *F. curta* and *F. cylindrus*) are strongly associated with sea-ice (Gersonde & Zielinski 2000, Ligowski *et al*. 1992, Riaux-Gobin *et al*. 2003), and are used extensively in sediment records to infer areas with high seasonal ice cover (Armand *et al*. 2005). As shown in Table 4.1, these species have previously been found in samples of sea-ice in Ryder Bay. *Fragiliariopsis kerguelensis*, in contrast, is associated with predominantly open-

ocean conditions (Crosta *et al*. 2005), although often several species from both groups will be present in differing amounts at any one location. Other species of *Fragilariopsis* were grouped with *F. kerguelensis* due to their low occurrence or absence from Ryder Bay sea-ice samples. Several species of *Fragilariopsis* have been observed in Ryder Bay, with *F. curta* and *F. cylindrus* being more abundant early in the season (Fig from 3.4.3). In the 2009 season, however, this group showed a significant peak late in the season (15 March 2010). While two other seasons (2005 and 2006) also showed increases of the *F. curta* group in the final samples (to ~4200 pg C L^{-1}), the peak in late 2009 was to biomass ~3 times higher (15000 pg C L^{-1}). Reasons for this late peak in 2009 could include a release of sea-ice diatoms. Similar to the case of *M. chilensis*, there is a marked increase in the contribution of sea-ice melt to surface waters over the period 1 to 10 March (BAS data; not shown). As the *F. curta* group is strongly associated with sea-ice, including in previous Ryder Bay sea-ice samples (Table 4.1; Annett 2008), melting ice could seed a population of these diatoms into the water column, resulting in a peak in their biomass uncharacteristically late in the season.

Odontella weissflogii has previously been identified as a mid-season Ryder Bay diatom (Annett *et al*. 2010), and is common along the WAP (Theriot & Fryxell 1985, Froneman *et al*. 1997, Varela *et al*. 2002, Garibotti *et al*. 2005). This species is associated with both sea-ice (Palmisano & Garrison 1993) and periods of significant stratification (Gomi *et al*. 2005, Annett *et al*. 2010). Just preceding and coincident with the second chl peak in summer 2009, *O. weissflogii* biomass peaked at ~100000 pg C L^{-1}, accounting for 18–26% of the estimated diatom community C. Over this period, the MLD was very shallow, and had been less than 5 m for nearly one month. Thus the link previously observed between high *O. weissflogii* biomass and very stable surface mixed layers is likely to explain the dynamics of this species in 2009, as illustrated in Figure 4.13. This association appears applicable to previous study years as well, with the highest *O. weissflogii* biomass recorded in summer 2004, concurrent with a period of a very stable, shallow MLD in January 2005. The decrease in *O. weissflogii* biomass in this season occurs at the same time as the deepening of the mixed layer to depths of >20 m. In contrast, the more variable January MLD in 2005 (although still relatively shallow at <10 m) was accompanied

by much lower amounts of this species. However, *O. weissflogii* was not abundant during the sampling period in 2006 despite periods of stratification, thus stratification does not guarantee high abundance of this species, and there must be additional factors which also act to encourage or limit its growth.

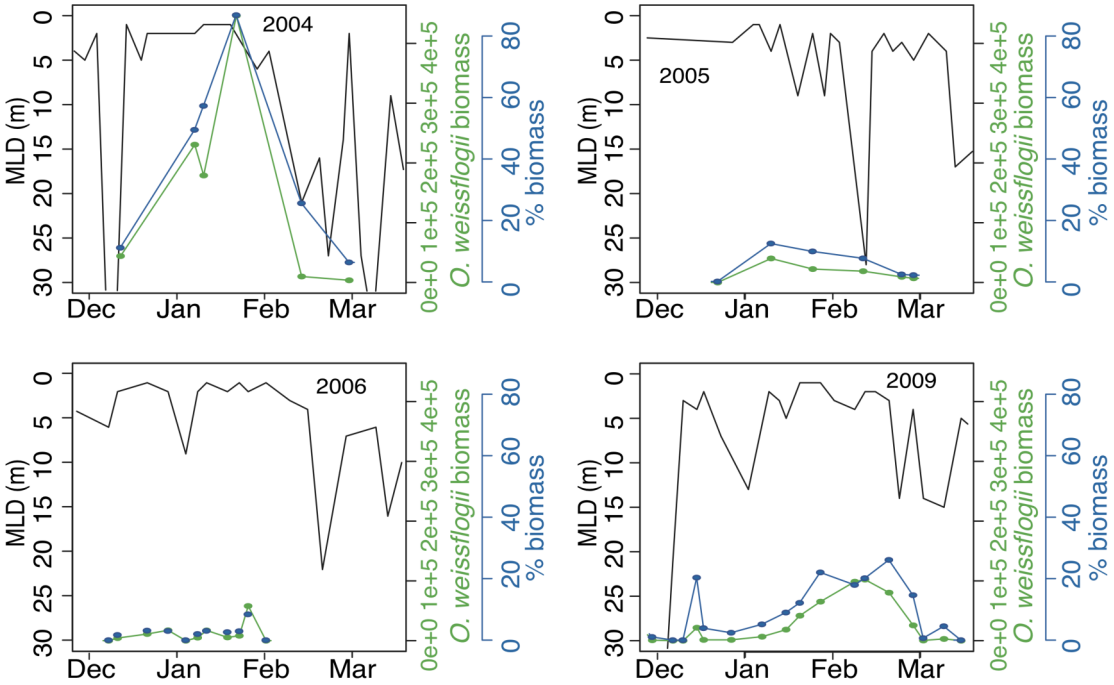

Figure 4.13: Time-series plot of mixed layer depth and *Odontella weissflogii* biomass (absolute in green; percent of total, in blue) across the four seasons where this species was present. The increase in biomass is preceded by a very stable shallow mixed layer.

Proboscia inermis is a large, rhizosolenoid species which has previously been shown to form large blooms and dominate community biomass to a very large extent in Ryder Bay (Annett *et al*. 2010). During a previous bloom event in 2005, biomass began to increase early in the season, and continued such that by the end of the season ~95% of estimated diatom C was due to this species. An increase in *P. inermis* biomass also occurred in the summer of 2009, accounting for a maximum 77% of the community biomass by early January 2010. However, in contrast to the earlier season, in 2009 the biomass of other species began to increase coincident with a decline in *P. inermis* biomass, leading to the second chl peak being dominated by large centrics, *Eucampia antarctica* and *O. weissflogii*. In shallow waters (<10 m),

there was very strong nutrient depletion at the same time as the peak in *P. inermis* biomass. Nitrate concentrations fell to <1 μM (Henley, 2012), and abundances of *P. inermis* declined sharply. This was not the case in summer 2005, when nitrate remained >3 μM throughout the summer (Carson 2008) and *P. inermis* maintained high biomass. Thus, *P. inermis* may be sensitive to nutrient depletion at a threshold ~3 μM. Many diatom species declined in biomass following the extremely low nitrate concentrations in summer 2009, but some maintained or increased their biomass despite the low nutrient availability, which may relate to an ability of these species to rely on intracellular nutrient stores during short periods of severe nutrient depletion. *Odontella weissflogii* and large centric species were the two groups that exhibited the strongest growth across the nitrate depletion event. The differences between the seasons with early increases in *P. inermis* demonstrate that diatom speciation is very fluid and responds rapidly to changing conditions.

Recent work investigating *P. inermis* dynamics has shown that presence of this species can greatly affect the geochemical signatures of particulate matter. Carbon isotopic values of particulate organic carbon (POC) in Ryder Bay were shown to display strong negative excursions during periods of high *Proboscia* biomass in the 2004 and 2005 seasons (Henley *et al*. 2012). Subsequent analysis from the three additional seasons studied here confirms and strengthens the relationship between *Proboscia* biomass and carbon isotopes (see full discussion in Henley, 2012). Thus in addition to providing information regarding physical conditions when species-specific environmental preferences are known, species records can also aid in interpretation of geochemical proxies where species-specific effects impact the formation or preservation of geochemical signals.

4.5.3 Intraspecific changes within species

4.5.3.1 Cell sizes

There is a strong relationship between the Si:C ratio in particulate matter and the biomass of *Corethron pennatum*, a very large diatom commonly associated with sea-ice zones. This species has been previously observed at high abundances in low-chl conditions (Clarke & Leakey 1996; Moline & Prézelin 1996; Schloss & Ferreyra

2002). The size structure of the *C. pennatum* population was investigated here to establish any link between size and variation in Si:C ratios, with the aim of highlighting possible interference of diatom speciation on trends in opal accumulation in sedimentary records.

The four-season average Si:C ratio is 0.152 mol:mol, which is equivalent to a C:Si ratio of 6.6:1, exactly the Redfield ratio. Periods when Si:C ratios are <0.15 (Fig. 3.8) are explained by lower contributions of diatoms compared to non-diatom phytoplankton. This occurs in the data here on two occasions, most of summer 2008 and early-mid summer 2009, the time periods where non-diatoms (*Phaeocystis antarctica*) were inferred to be most abundant (Chapter 3). Increases in the Si:C ratio are less straightforward to explain. Higher Si:C suggests that the diatom community is more heavily silicified; this may reflect changes in species where species with thicker frustules are more abundant, or may occur within all or some species if heavier silicification is triggered. The latter has been associated with Fe-limited diatoms, where higher Si:N ratios in response to Fe-limitation is well documented. There is still some uncertainty whether this reflects decreasing cell sizes resulting in increased SA:V (where Si is linked to surface area and N to cell volume), or formation of thicker frustules (*for a review, see* Marchetti & Cassar 2009). Increasing SA:V ratios are well supported by multiple studies, although frustules up to 3-fold thicker have been documented in response to limitation by light, N and P, factors which may be more likely in the present study than Fe limitation (Claquin *et al*. 2002).

Figure 4.14 shows time-series data of the seasonal changes in Si:C ratios, which start at ~0.30 mol:mol when *C. pennatum* biomass is high, decrease to a mid-season minimum value, and increase again in late summer, concurrent with a second period of high *C. pennatum* biomass. Early in the season, *C. pennatum* cells are relatively small, and decline again at the end of the season, such that smaller sizes (and higher SA:V) ratios are correlated with high particulate Si:C ratios. This relationship is emphasised in Figure 4.15, where a strong and statistically significant regression is shown between Si:C and both diatom size variables.

Sizes of *C. pennatum* have been previously shown to reflect the stage of the sexual reproductive cycle of a population (Crawford 1995), and reproductive events

can lead to mass sedimentation of this species. Small diameter cells (~25 µm) will form gametangia, while at the upper range of the size distribution, auxospores are ~70 µm diameter (Crawford 1995). Sedimentary studies (*e.g*. Leventer *et al*. 2002) have considered *C. pennatum* cell size as an indicator of sexual events leading to mass sedimentation, but found that large sedimentary fluxes were not solely linked to gametangia and auxospore formation. Thus there are multiple reasons for high sedimentary fluxes of *C. pennatum* (Leventer *et al*. 2002).

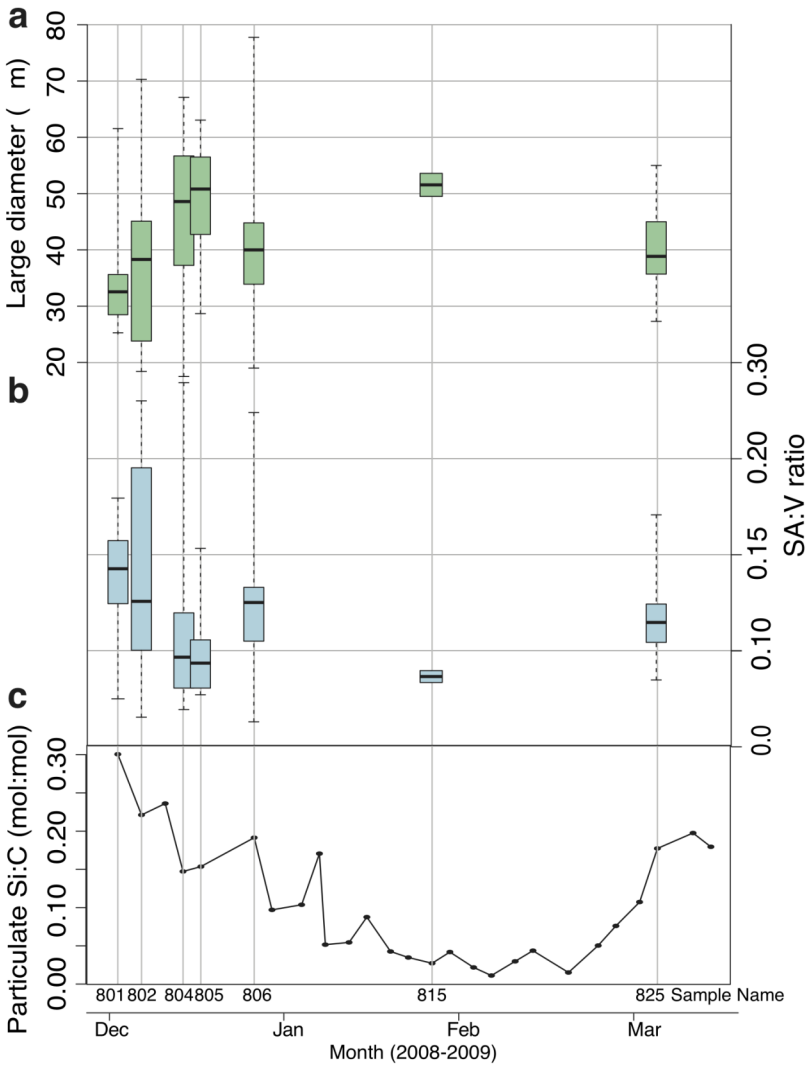

Figure 4.14: Whisker-plots of the distribution of diameter (a) and SA:V ratios (b) in Corethron pennatum during austral summer 2008. The thick black band shows the mean, the shaded boxes the limits of the upper and lower quartiles, and bars the full range of the parameter for each sample event. Also shown are the Si:C ratios in particulate matter from filter samples (c). Vertical lines denote diatom asseblage analysis dates for ease of comparison.

Here, the size ranges of *C. pennatum* are consistent with gametangia formation in samples from December 2008. Cells from later samples (January - March 2009) were not as small. Very large diameter cells (66–70 μm) spanning auxospore range were present in several of the December 2008 samples, and indeed auxospores within parent cells were observed in LM analysis. It is possible that the presence of different reproductive states influences Si:C ratios of C. pennatum, as vegetative cells of other diatom species are generally the least silicified form (*i.e.* vegetative forms of *Eucampia antarctica*, *Thalssiosira antarctica* and *Chaetoceros* compared to more heavily silicified winter forms or resting spores). As cell sizes and reproductive stages vary in tandem, we are unable to distinguish Si:C effects based purely on cell size versus reproductive state. The high Si:C seen at the end of the season would suggest that cell size (and hence SA:V ratios) may play a more prominent role, as our data do not indicate the presence of gametangia or auxospores at this time, although the sampling coverage is lower than during the early stage of the season. Silicification in response to limitation (for example by light, as found for *Thalassiosira pseudonana;* Claquin *et al*. 2002) could also contribute to the variation in Si:C seen here outside of size-related changes, although the strong correlation between SA:V and Si:C suggests that any effect from this process is likely to be of secondary importance.

The timing of peaks in *C. pennatum* abundance seen here is in agreement with the findings of Crawford (1995) who documented a sexual event leading to mass sedimentation in spring, and with the analysis of Leventer *et al*. (2002), who observed an autumnal flux of *C. pennatum* that was not associated with a reproductive event. We suggest therefore that the spring and autumn fluxes of this species are likely driven by different factors: reproductive state in the case of spring, and breakdown of summer stratification in the autumn.

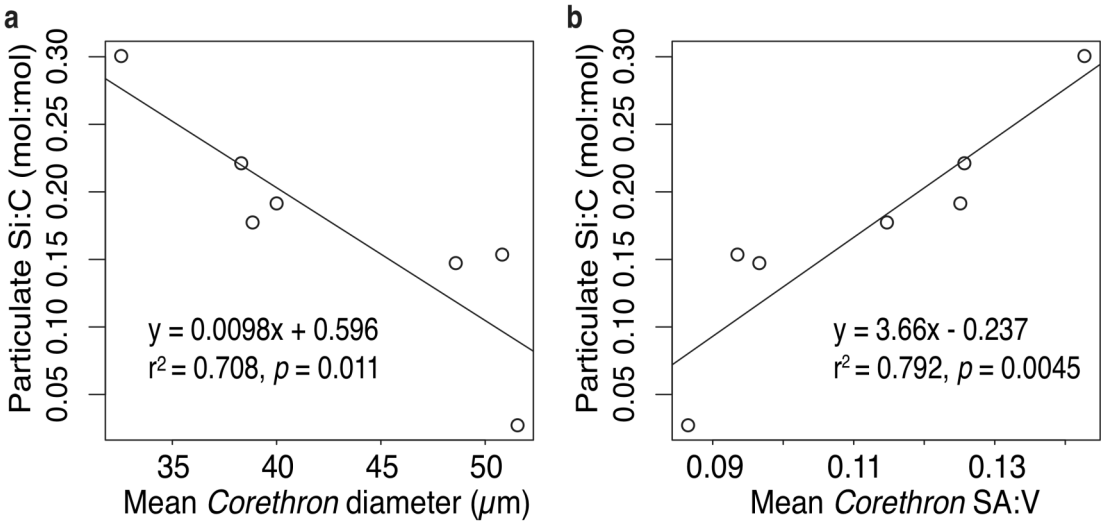

Figure 4.15: Regression of particulate Si:C ratios versus mean diameter (a) and SA:V ratios (b) in *Corethron pennatum* for summer 2008. *p* refers to *p*-value, and in both cases regressions are statistically significant at the 95% level.

4.5.3.2 Chain forming diatoms

Longer chains of *Eucampia antarctica* were seen in the intermediate-chl season of 2009. An index linked to chain length of this species has previously been used in sediment records to infer periods of higher diatom production related to winter sea-ice cover (Kaczmarska *et al*. 1993, Leventer *et al*. 2002, Whitehead *et al*. 2005). Chains of *E*. *antarctica* can be present as a spring form, as is seen here, or as a more highly silicified winter form, which are well preserved in the sediment record (Fryxell 1991, Kaczmarska *et al*. 1993). The valves at the free ends of chains are pointed in the winter form, whereas intercalary valves have flat ends so that adjacent cells can attach to each other. Chain length is thus reflected in the Eucampia index, the ratio of terminal to intercalary valves, where a high ratio indicates shorter chains. It has been noted that the more northerly form of this species (*E*. *antarctica* var. *antarctica*) forms longer chains than the southerly form, *E*. *antarctica* var. *recta*, possibly because more cell divisions are possible after the winter form is triggered (longer ice-free summer period; Fryxell & Prasad 1990, Fryxell 1991). Thus lower values of the Eucampia index have been taken to reflect higher abundances of the more northerly form where productivity is traditionally higher than in heavily ice-covered areas associated with higher abundances of the southerly form (Leventer *et*

al. 2002). *E*. *antarctica* var. *antarctica* have Eucampia index values of up to 1:120, while values for E. *antarctica* var. *recta* from Prydz Bay have been reported as 1:2 (Kaczmarska *et al*. 1993).

Here we report chain lengths of the spring form of *Eucampia antarctica* var. *recta*, as no cells of the winter form were observed (Fig. 4.16). Although our observed chain lengths are much more in keeping with those reported for the winter form of *E*. *antarctica* var. *recta* than the more northerly form, showing that spring and winter chain lengths are of a similar magnitude, we do not know if longer spring form chains will impact the winter form as this is thought to be determined by the time between triggering the winter form and cell division halting. The longer chains in the spring form occur even early in the 2009 season, indicating that a longer amount of time for chains to elongate is not likely to fully explain the variation.

A faster growth rate would account for longer chains even early in the season. Several mechanisms can be suggested that would lead to faster growth rates. For example, light levels were higher in 2009 due to the lower suspended particulate matter associated with below average chl levels. Even though the MLD is deeper in this season, greater light penetration results in higher light availability (Venables *et al*. 2012), visible in Figure 4.16 as deeper net photosynthetic irradiance (NPI) depth. The NPI is noticeably deeper in the early part of summer 2009, coinciding with the majority of samples with long *E*. *antarctica* chains. Additionally, biological reactions are temperature sensitive, thus higher temperatures could also result in faster growth in the 2009 season. Maximum summer water temperatures were higher in 2009 than in the earlier years with shorter *E*. *antarctica* chains, by >1.0 °C. However, the large increase in temperature seen in 2009 occurs primarily in January 2010, with early December temperatures being ~ -1.2 to -0.6 in all years (2004, 2005, and 2009). Therefore, temperature cannot account for the longer chains seen even in the earliest samples, but may contribute to the maximum chain lengths seen late in January. This analysis suggests that higher light levels are the most plausible explanation for high rates of cell division of *E*. *antarctica* in 2009. While we cannot link summer chain length directly to chain length of the winter form, summer chain length in this study was highly responsive to environmental conditions. If this signal is tranferred to winter chain length and thus the Eucampia index, this index (for *Eucampia*

antarctica var. *recta*) could be a very sensitive parameter with which to investigate stratification and light levels from sediment records.

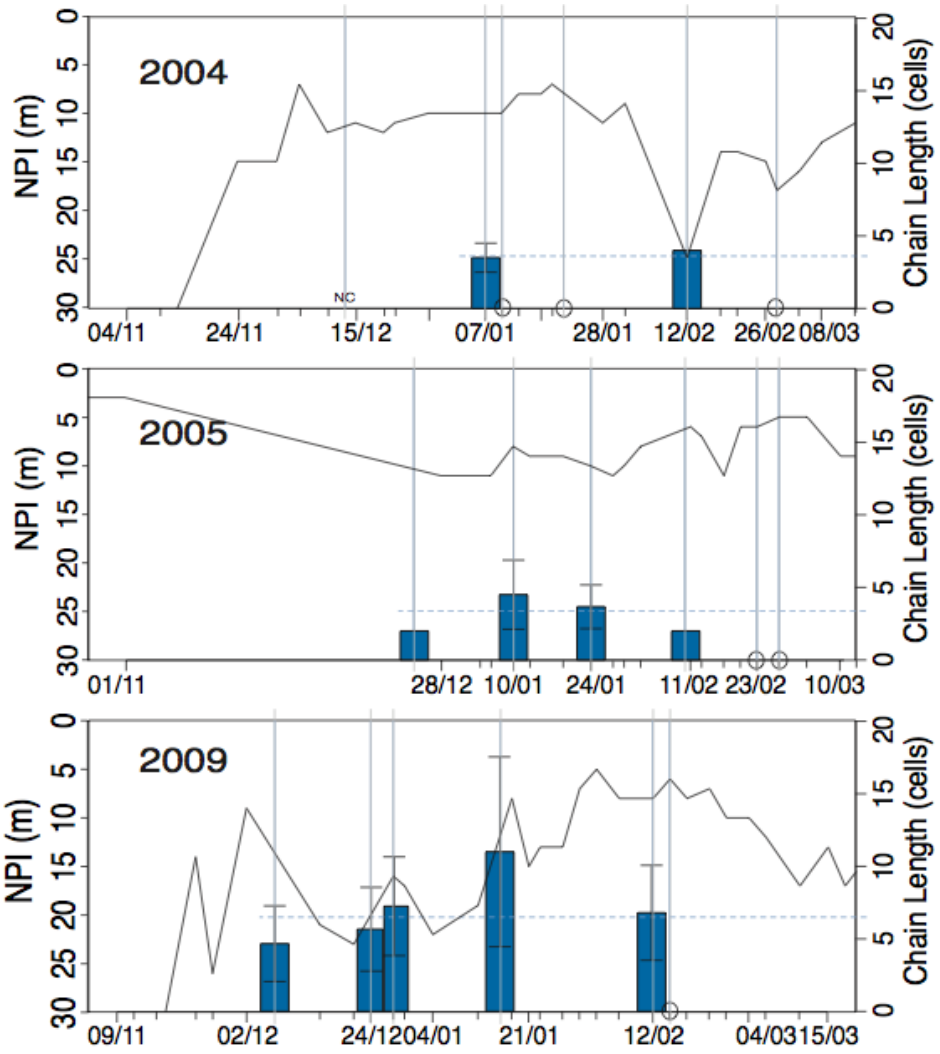

Figure 4.16: Net photosynthetic irradience (NPI) depth and chain lengths of *Eucampia antarctica* var. *recta* for all seasons where this species was present (2004, 2005 and 2009, top to bottom), for early November to mid March (x-axes are not aligned). Solid black curves are NPI. Dotted lines show the seasonal mean chain length of *E. antarctica*. All y axes are consistent between plots. Vertical lines denote sampling dates – where no *E. antarctica* cells were observed "nc" is shown, while samples with only solitary cells are indicated by an open circle at length = 0.

4.6 Conclusions

In this chapter, new records of diatom speciation at the RaTS site are presented in high resolution, adding to existing data and extending coverage to five summer growing seasons. These data are considered in the context of recent changes

in seasonal chl and ongoing climate change. Interannual variations are characterised by different proportions of very similar species assemblages, no community-level shifts were observed. However, the low-chl season shows lower average species richness, suggesting potential loss of species with continued trends to lower chl conditions.

This analysis has identified several species abundance ratios corresponding to different chl regimes. These may be useful in characterising modern surface waters, and relating changes in the sediment record to changes in environmental conditions. Some indication of greater proportions of small diatoms was seen in the low-chl season, although this was within the variability previously observed in high-chl seasons.

The observations here strengthen and refine the association of *Odontella weissflogii* and *Proboscia inermis* with stratified waters, and suggest that *P. inermis* is more sensitive to N depletion (<3 μM) than other species.

Finally, this analysis has identified surface water changes which have implications for interpreting sedimentary records. Micropaleontologically, chain length index of *Eucampia antarctica* (var. *recta*) may be highly sensitive to light availability. *Proboscia* species are associated with very low organic carbon isotope signatures. Additionally, high abundances of *Corethron pennatum* may affect Si:C ratios.

4.7 References

ANNETT, A.L. 2008. *Seasonal and interannual variations in phytoplankton assemblages in a near-shore Antarctic sea-ice environment*. MSc Thesis: University of Edinburgh.

ANNETT, A.L., CARSON, D.S., CROSTA, X., CLARKE, A. & GANESHRAM, R.S. 2010. Seasonal progression of diatom assemblages in surface waters of Ryder Bay, Antarctica. *Polar biology*, **33**, 13–29, 10.1007/s00300-009-0681-7.

ARMAND, L.K., CROSTA, X., ROMERO, O. & PICHON, J.-J. 2005. The biogeography of major diatom taxa in Southern Ocean sediments. *Palaeogeography, Palaeoclimatology, Palaeoecology*, **223**, 93–126, 10.1016/j.palaeo.2005.02.015.

ATKINSON, A., SIEGEL, V., PAKHOMOV, E. & ROTHERY, P. 2004. Long-term decline in krill stock and increase in salps within the Southern Ocean. *Nature*, **432**, 100–103.

CARSON, D.S. 2008. *Biogeochemical Dontrols on Productivity and Particle Flux in the Coastal Antarctic Sea Ice Environment*. PhD Thesis: University of Edinburgh.

CLAQUIN, P., MARTIN-JÉZÉQUEL, V., KROMKAMP, J.C., VELDHUIS, M.J.M. & KRAAY, G.W. 2002. Uncoupling of silicon compared with car- bon and nitrogen metabolism and the role of the cell cycle in continuous cultures of *Thalassiosira Pseudonana* (Bacillariophyceae) under light, nitrogen and phosphorus control. *Journal of Phycology*, **38**, 922–930.

CLARKE, A., MEREDITH, M.P., WALLACE, M.I., BRANDON, M.A. & THOMAS, D.N. 2008. Seasonal and interannual variability in temperature, chlorophyll and macronutrients in northern Marguerite Bay, Antarctica. *Deep Sea Research Part II: Topical Studies in Oceanography*, **55**, 1988–2006, 10.1016/j.dsr2.2008.04.035.

COOK, A.J., FOX, A.J., VAUGHAN, D.G. & FERRIGNO, J.G. 2005. Retreating Glacier Fronts on the Antarctic Peninsula over the Past Half-Century. *Science*, **308**, 541–544, 10.1126/science.1109164.

CRAWFORD, R.M. 1995. The role of sex in the sedimentation of a marine diatom bloom. *Limnology and Oceanography*, **40**, 200–204.

CROSTA, X., ROMERO, O., ARMAND, L.K. & PICHON, J.-J. 2005. The biogeography of major diatom taxa in Southern Ocean sediments: 2. Open ocean related species. *Palaeogeography, Palaeoclimatology, Palaeoecology*, **223**, 66–92, 10.1016/j.palaeo.2005.03.028.

DENIS, D., CROSTA, X., ZARAGOSI, S., MARTIN, B. & MAS, V. 2006. Seasonal and sub-seasonal climate changes recorded in laminated diatom ooze sediments, Adelie Land, East Antarctica. *The Holocene*, **16**, 1143-1153.

DOUCETTE, G.J. & FRYXELL, G.A. 1985. Thalassiosira antarctica (Bacillariophyceae): Vegetative and Resting Stage Ultrastructure of an Ice-Related Marine Diatom. *Polar Biology,* **4**,107-112.

DUCKLOW, H.W., BAKER, K., MARTINSON, D.G., QUETIN, L.B., ROSS, R.M., SMITH, R.C., STAMMERJOHN, S.E., VERNET, M. & FRASER, W. 2007. Marine pelagic ecosystems: the West Antarctic Peninsula. *Philosophical Transactions of the Royal Society B: Biological Sciences*, **362**, 67–94, 10.1098/rstb.2006.1955.

EPPLEY, R.W., REID, F.M.H. & STRICKLAND, J.D.H. 1970. The ecology of the plankton off La Jolla, California, in the period April through September, 1967. III. Estimates of phytoplankton crop, size, growth rate and primary production. *Bulletin of the Scripps Institute of Oceanography,* **17**, 33-42

FRONEMAN, P.W., PAKHOMOV, E.A. & LAUBSCHER, R.K. 1997. Microphytoplankton assemblages in the waters surrounding South Georgia, Antarctica during austral summer 1994. *Polar biology*, **17**, 515–522.

FRYXELL, G.A., & PRASAD A. K. S. K. 1990. *Eucampia antarctica* var. *recta* [Mangin] stat. nov.

[Biddulphiaceae, Bacillariophyceae]: Life stages at the Weddell Sea ice edge. *Phycologica*, **29**, 27-83.

FRYXELL, G.A. 1991. Comparison of winter and summer growth stages of the diatom *Eucampia antarctica* from the Kerguelen Plateau and south of the Antarctic convergence zone. *Proceedings of the Ocean Drilling Program, Scientific Results*, **119**, 675–685.

GARIBOTTI, I.A., VERNET, M. & FERRARIO, M.E. 2005. Annually recurrent phytoplanktonic assemblages during summer in the seasonal ice zone west of the Antarctic Peninsula (Southern Ocean). *Deep Sea Research Part I: Oceanographic Research Papers*, **52**, 1823–1841, 10.1016/j.dsr.2005.05.003.

GERSONDE, R. & ZIELINSKI, U. 2000. The reconstruction of late Quaternary Antarctic sea-ice distribution - the use of diatoms as a proxy for sea-ice. *Palaeogeography, Palaeoclimatology, Palaeoecology*, **162**, 263–286.

GOMI, Y., UMEDA, H., FUKUCHI, M. & TANIGUCHI, A. 2005. Diatom assemblages in the surface water of the Indian Sector of the Antarctic Surface Water in summer of 1999/2000. *Polar biology*, **18**, 1–15.

HABERMAN, K.L., QUENTIN, L.B. & ROSS, R.M. 2003. Diet of the Antarctic Krill (*Euphausia superba* Dana): I. Comparisons of grazing on *Phaeocystis antarctica* (Karsten) and *Thalassiosira antarctica* (Comber). *Journal of Experimental Marine Biology and Ecology*, **283**, 79–95.

HASLE, G.R. & SYVERTSEN, E.E. 1997. Marine diatoms. *In Identifying marine phytoplankton*, p 5-385.

HENLEY, S.F. 2012. *Climate-induced changes in carbon and nitrogen cycling in the rapidly warming Antarctic coastal ocean*. PhD Thesis: University of Edinburgh.

HENLEY, S.F., ANNETT, A.L., GANESHRAM, R.S., CARSON, D.S., WESTON, K., CROSTA, X., TAIT, A., DOUGANS, J., FALLICK, A.E. & CLARKE, A. 2012. Factors influencing the stable carbon isotopic composition of suspended and sinking organic matter in the coastal Antarctic sea ice environment. *Biogeosciences*, **9**, 1137–1157, 10.5194/bg-9-1137-2012.

HILLEBRAND, H., DURSELEN, C.-D., KIRSCHTEL, D., POLLINGHER, U. & ZOHARY, T. 1999. Biovolume calculation for pelagic and benthic macroalgae. *Journal of Phycology*, **35**, 403–424.

HORNER, R.A. 1985. Ecology of sea-ice biota. *In* Horner, R.A. *eds*. *Sea-Ice Biota*. Boca Raton, Fl: CRC Press, 83-104.

JOHANSEN, J.R. & FRYXELL, G.A. 1985 The genus Thalassiosira (Bacillariophyceae): studies on species occurring south of the Antarctic Convergence Zone. *Phycologia,* **24**,155-179.

JORDAN, R.W., LIGOWSKI, R., NOTHIG, E.M. & PRIDDLE, J. 1991. The diatom genus Proboscia in Antarctic Waters. *Diatom Research,* **6**, 63-78

KACZMARSKA, I., BARBRICK, N.E., EHRMAN, J.M. & CANT, G.P. 1993. Eucampia Index as an indicator of the Late Pleistocene oscillations of the winter sea-ice extent at the ODP Leg 119 Site 745B at the Kerguelen Plateau. *Hydrobiologia*, **269/270**, 103–112.

KANG, J.-S., KANG, S.-H., KIM, D. & KIM, D.-Y. 2003. Planktonic centric diatom Minidiscus chilensis dominated sediment trap material in eastern Bransfield Strait, Antarctica. *Marine Ecology Progress Series*, **255**, 93–99.

LEVENTER, A., DOMACK, E., BARKOUKIS, A., MCANDREWS, B. & MURRAY, J. 2002. Laminations from the Palmer Deep: A diatom-based interpretation. *Paleoceanography*, **17**, 8002, 10.1029/2001PA000624.

LIGOWSKI, R., GODLEWSKI, M. & LUKOWSKI, A. 1992 Sea ice diatoms and ice edge planktonic diatoms at the northern limit of the Weddell Sea pack ice. *Proc NIPR Symp Polar Biol,* **5**, 9-20.

LOEB, V., SIEGEL, V., HOLM-HANSEN, O., HEWITT, R., FRASER, W., TRIVELPIECE, W. & TRIVELPIECE, S. 1997. Effects of sea-ice extent and krill or salp dominance on the

Antarctic food web. *Nature*, **387**.

MADDISON, E.J., PIKE, J., LEVENTER, A., DUNBAR, R., BRACHFELD, S., DOMACK, E.W., MANLEY, P. & MCCLENNEN, C. 2006. Post-glacial seasonal diatom record of the Mertz Glacier Polynya, East Antarctica. *Marine Micropaleontology*, **60**, 66–88, 10.1016/j.marmicro.2006.03.001.

MARCHETTI, A. & CASSAR, N. 2009. Diatom elemental and morphological changes in response to iron limitation: a brief review with potential paleoceanographic applications. *Geobiology*, **7**, 419–431, 10.1111/j.1472-4669.2009.00207.x.

MASHALL, G.J, ORR, A., VAN LIPSIZ, N. & KING, J. 2006. The impact of a changing southern hemisphere annular mode on Antarctic Peninsula summer temperatures. *Journal of Climate*, **19**, 5388–5404.

MARTINSON, D.G., STAMMERJOHN, S.E., IANNUZZI, R.A., SMITH, R.C. & VERNET, M. 2008. Western Antarctic Peninsula physical oceanography and spatio-temporal variability. *Deep-Sea Research II*, **55**, 1964–1987, 10.1016/j.dsr2.2008.04.038.

MEREDITH, M.P. & KING, J.C. 2005. Rapid climate change in the ocean west of the Antarctic Peninsula during the second half of the 20th century. *Geophysical Research Letters*, **32**, 10.1029/2005GL024042.

MOLINE, M.A. & PREZELIN, B.B. 1996. Long-term monitoring and analyses of physical factors regulating variability in coastal Antarctic phytoplankton biomass, *in situ* productivity and taxonomic composition over subseasonal, seasonal and interannual time scales. *Marine Ecology Progress Series*, **145**, 143–160.

MONTES-HUGO, M., DONEY, S.C., DUCKLOW, H.W., FRASER, W., MARTINSON, D., STAMMERJOHN, S.E. & SCHOFIELD, O. 2009. Recent Changes in Phytoplankton Communities Associated with Rapid Regional Climate Change Along the Western Antarctic Peninsula. *Science*, **323**, 1470–1473, 10.1126/science.1164533.

PALMISANO, A.C. & GARRISON, D.L. 1993. Microorganisms in Antarctic Sea Ice. *In* Friedmann, E.I. *ed Antarctic Microbiology*. New York: Wiley-Liss, 167-218.

PERISSINOTTO, R. & PAKHOMOV, E.A. 1998a. Contribution of salps to carbon flux of marginal ice zone of the Lazarev Sea, Southern Ocean. *Marine Biology*, **131**, 25–32, 10.1007/s002270050292.

PERISSINOTTO, R. & PAKHOMOV, E.A. 1998b. The trophic role of the tunicate Salpa thompsoni in the Antarctic marine ecosystem. *Journal of Marine Systems*, **17**, 361–374.

PRITCHARD, H.D. & VAUGHAN, D.G. 2007. Widespread acceleration of tidewater glaciers on the Antarctic Peninsula. *Journal of Geophysical Research*, **112**, 10.1029/2006JF000597.

QUENTIN, L.B. & ROSS, R.M. 1985. Feeding by Antarctic Krill, *Euphausia superba*: does size matter? *In* Siegfried, W.R., Condy, P.R. & Laws, R.M., *eds. Antarctic Nutrient Cycles and Food Webs*. Berlin: Springer-Verlag, 372–377.

QUENTIN, L.B., ROSS, R.M., FRAZER, T.K. & HABERMAN, K.L. 1996. Factors affecting distribution and abundance of zooplankton, with an emphasis on Antarctic krill, *Euphausia superba*. *In* Ross, R.M., Hofmann, E.E. & Quentin, L.B., *eds. Foundations for ecological research west of the Antarctic Peninsula*. Washington, DC: American Geophysical Union, 357–371.

QUENTIN, L.G. & ROSS, R.M. 2003. Episodic recruitment in Antartic krill *Euphausia superba* in Palmer LTER study region. *Marine Ecology Progress Series*, **259**, 185–200.

RIAUX-GOBIN, C., POULIN, M., PRODON, R. & TREGILIER, P. 2003 Land-fast ice microalgal and phytoplanktonic communities (Adelie Land, Antarctica) in relation to environmental factors during ice break-up. *Antarctic Science* **15**:353-364

SCHLOSS, I.R., FERREYRA, G.A. & RUIZ-PINO, D. 2002. Phytoplankton biomass in Antarctic shelf zones: a conceptual model based on Potter Cove, King George Island. *Journal of*

Marine Ecosystems, **36**, 129–143.

SCOTT, F.J. & THOMAS, D.P. 2005 DIATOMS. *In:* Scott FJ, Marchant HJ *eds Antarctic Marine Protists*. Canberra: Australian Biological Resources Study, 13-201.

SMAYDA, T.J. 1978. From phytoplankters to biomass. *In* Sournia, A., *ed. Monographs on oceanographic methodology*. Paris: UNESCO, 273–279.

STAMMERJOHN, S.E., MARTINSON, D.G., SMITH, R.C. & IANNUZZI, R.A. 2008. Sea ice in the western Antarctic Peninsula region: Spatio-temporal variability from ecological and climate change perspectives. *Deep Sea Research Part II: Topical Studies in Oceanography*, **55**, 2041–2058, 10.1016/j.dsr2.2008.04.026.

STICKLEY, C.E., PIKE, J., LEVENTER, A., DUNBAR, R., DOMACK, E.W., BRACHFELD, S., MANLEY, P. & MCCLENNAN, C. 2005. Deglacial ocean and climate seasonality in laminated diatom sediments, Mac.Robertson Shelf, Antarctica. *Palaeogeography, Palaeoclimatology, Palaeoecology*, **227**, 290–310, 10.1016/j.palaeo.2005.05.021.

THERIOT, E. & FRYXELL, G.A. 1985 Multivariate Statistical Analysis of Net Diatom Species Distributions in the Southwestern Atlantic and Indian Ocean. *Polar Biology* **5**:23-30

TURNER, J., COLWELL, S.R. & HARANGOZO, S. 1997. Variability of precipitation over the coastal western Antarctic Peninsula from synoptic observations. *Journal of Geophysical Research*, **102**, 13999–14007.

VARELA, M., FERNANDEZ, E. & SERRET, P. 2002. Size-fractionated phytoplankton biomass and primary production in the Gerlache and south Bransfield Straits (Antarctic Peninsula) in Austral summer 1995-1996. *Deep-Sea Research II*, **49**, 749–768.

VAUGHAN, D.G., MARSHALL, G.J., CONNOLLEY, W.M., PARKINSON, C., MULVANEY, R., HODGSON, D.A., KING, J.C., PUDSEY, C.J. & TURNER, J. 2003. Recent rapid regional climate warming on the Antarctic Peninsula. *Climatic Change*, **60**, 243–274.

VAUGHAN, D.G. 2006. Recent Trends in Melting Conditions on the Antarctic Peninsula and Their Implications for Ice-sheet Mass Balance and Sea Level. *Arctic, Antarctic, and Alpine Research*, **38**, 147–152.

VENABLES, H.J., CLARKE, A. & MEREDITH, M.P. *In press*. Wintertime controls on summer stratification and productivity at the western Antarctic Peninsula. *Limnology and Oceanography*, 1–30.

WARWICK, R.M. & CLARKE, K.R. 1995. New 'biodiversity' measures reveal a decrease in taxonomic distinctness with increasing stress. *Marine Ecology Progress Series*, **129**, 301-305.

WHITEHEAD, J.M., WOTHERSPOON, S. & BOHATY, S.M. 2005. Minimal Antarctic sea ice during the Pliocene. *Geology*, **33**, 137–140, 10.1130/G21013.1.

Chapter 5: Silicon and silicon isotopes in Ryder Bay

5.1 Abstract

Diatoms are the dominant component of microalgal assemblages along the WAP, and have an absolute requirement for Si to produce their cell walls. Recent changes in chl concentrations in this region are suggested to be primarily a result of changes in diatom abundances, which is therefore likely to affect Si cycling as well. In this chapter, records of dissolved and particulate Si are presented from the austral summers of 2008 and 2009, to investigate Si use by diatoms at the RaTS site. Biogenic Si closely follows total chl, consistent with diatom-dominated productivity along the WAP. Thus, chl is a robust proxy for diatom biomass in this region. Samples for dissolved Si were also analysed for Si isotopic signature, to investigate biological Si fractionation in this environment, and a potential impact from species composition is suggested from coupled records of diatom assemblages. Finally, physical data and Si measurements are used to derive a seasonal budget of new Si production. Seasonal Si use is expected to vary with overall production along the WAP, such that this region may export unused Si to the wider Southern Ocean with contined chl decline.

5.2 Introduction

Diatoms require Si to produce their cell walls, or frustules, and hence dominate the biogeochemical cycling of Si in the ocean. Each atom of weathered Si from land entering the ocean is recycled through the diatoms an average of 40 times before being buried in marine sediments (Tréguer *et al*. 1995). In the Southern Ocean, diatoms are the dominant phytoplankton group, accounting for up to 75% of production (Nelson *et al*. 1995). Thus, this area is of crucial significance to the marine Si cycle.

The Southern Ocean, as a result of weak stratification and high productivity, plays a major role the biological pump of carbon, by affecting the air-sea balance of

CO_2 and the export of organic C to deep waters (Sarmiento & Toggweiler 1984, Sarmiento *et al*. 2004, 2007). The high productivity, abundant Si availability and robust diatom communities leads to extensive silicious sediment deposits between the Antarctic Polar Front (APF) and the marginal sea-ice zone to the south. North of the APF, however, availability of Si is very low and likely limits diatom (and hence Si) production throughout most or all of the growing season (Nelson *et al*. 2001). As a result of iron limitation, which leads to increased Si:N ratios in iron-limited diatoms (*reviewed in* Marchetti & Cassar 2009), Si is preferentially depleted with respect to N and P as surface waters move northward across the APF. This separates the supply of the macronutrients, and the preferential depletion of Si is significant, as these polar front waters redistribute nutrients to much of the world's surface oceans (via Sub-Antarctic Mode Water formation and meridional circulation; Rintoul *et al*. 2001, Brzezinski *et al*. 2002, Sarmiento *et al*. 2004, 2007). The reduced supply of Si relative to other nutrients limits diatoms to a relatively minor role in most other oceanic provinces (Yool & Tyrrell 2003). Changes in the export of Si from the Southern Ocean and resulting increases in diatoms at low latitudes have been proposed as a mechanism to alter atmospheric CO_2 at glacial-interglacial time scales (Matsumoto *et al*. 2002). Thus understanding Si supply to the Southern Ocean and diatom use thereof is important in constraining both current oceanic productivity as well as reconstructing past nutrient use from sediment records.

The WAP region is one where high-nutrient UCDW intrudes onto the shelf and to the surface (Martinson *et al*. 2008). The lack of a shelf-break front along the peninsula (Jacobs 1991, Whitworth *et al*. 1998) means that WAP waters can feed back into the surrounding ACC, making the WAP a source region supplying nutrients to the surface Southern Ocean. As discussed in Chapter 3, production along the WAP is dominated by diatom biomass, and hence productivity has a strong impact on Si cycling in this region. As such, changes along the WAP have the potential to affect Si supply and use on a large spatial scale. In light of the current changes in physical conditions and biological processes in the WAP (*see Chapters 1-3*), this chapter will investigate Si supply and use in Ryder Bay during two seasons of contrasting low- and intermediate-chl conditions, to better understand the extent to which Si dynamics track overall phytoplankton productivity and standing stock.

Further, a seasonal Si budget is derived for Ryder Bay, to assess variations in Si-use in the context of current climate change.

Silicon is present in the dissolved phase primarily as silicic acid ($Si(OH)_4$, 97%). The remaining 3% is $Si(OH)_3O^-$, and together both forms are referred to as "dissolved Si" (Si_d). This Si_d occurs naturally as three isotopes, ^{28}Si, ^{29}Si and ^{30}Si, the lightest being the most prevalent (92.2%). Biological uptake discriminates against the heavier isotopes, leaving the remaining reactant pool and product progressively enriched in ^{29}Si and ^{30}Si as drawdown progresses. In diatoms, Si_d is actively transported into the cell to meet cellular requirements for biogenic silica (SiO_2; hereafter "BSi"; Hildebrand 2008). Thus, the isotopic signature associated with diatom Si use has shown considerable potential as a proxy for both current Si cycling (Varela *et al*. 2004, Cardinal *et al*. 2007, Beucher *et al*. 2011, Fripiat *et al*. 2011) and paleoceanographic Si processes (De La Rocha *et al*. 1998, Beucher *et al*. 2007, Pichevin *et al*. 2009, Ellwood *et al*. 2010, Pichevin *et al*. 2012). This is especially important in the Southern Ocean, where calcareous organisms are scarce and thus the widely-used proxies based on calcareous sediments are less robust than in low-latitude regions.

However, outstanding questions remain in our understanding of the processes controlling Si fractionation. Chief among these are the effects of temperature and diatom speciation on Si fractionation in oceanographically relevant conditions. Increasing incorporation of Si concentrations and isotopic data in modelling studies (Gnanadesikan & Toggweiler 1999, Wischmeyer *et al*. 2003, Reynolds 2009) requires an understanding of the fractionation associated with biological uptake throughout the world, but especially at the low temperatures typical of the Southern Ocean, where Si availability is high and polar diatom species dominate. This chapter also reports the Si isotopic composition of the Si_d pool, and is the first to couple such *in-situ* time-series measurements with high-resolution diatom species data. These complementary records are used to investigate the effects of changing diatom speciation on Si isotopic signatures in the field.

5.3 Methods

5.3.1 Study Site

Samples for surface water Si_d and BSi were collected from RaTS sites 1 and 2 in Ryder Bay, Adelaide Island, Antarctica (Figure 2.1). The primary sampling site is situated ~4 km from shore over a local maximum water depth of 520 m. When weather or brash ice prevented access to site 1, site 2 (~400 m depth) was used as both sites have been associated with the same water mass (Clarke *et al*. 2008). Previous work at the RaTS Site has shown the primary water source to be open exchange with water masses from northern Marguerite Bay, with some modification from glacial melt and local topography (Clarke *et al*. 2008). Marguerite Bay in turn has been shown to display water mass characteristics similar to the WAP region as a whole (Meredith *et al*. 2004).

As part of the ongoing oceanographic monitoring of the RaTS programme, a suite of additional data from the same sampling events is available from the British Antarctic Survey (Cambridge, UK). This data includes hydrographic conditions (temperature, salinity, etc.) and biological activity (*i.e.* chlorophyll and nutrient concentration). Detailed methodology used by this programme for CTD data collection and chlorophyll/nutrient analysis can be found in Clarke *et al*. (2008).

5.3.2 Sample Collection

Bi-weekly sampling was done at a depth of 15 m, which Clarke *et al*. (2008) have shown to be the long-term average depth of the chl *a* maximum. Once a week, as weather permitted, additional samples were collected from 0, 5, 10 and 25 m depth. Deeper waters (50, 100 and 500 m) were sampled approximately monthly for other parameters (C isotopes, *in* Henley 2012), and small volumes (~125 mL) were collected for Si_d concentration and isotopic analysis whenever possible. Deep water was collected using a 5 L Niskin bottle and surface water (≤25 m) was collected using a submersible Whale pump attached to 32 mm diameter Tygon tubing and powered by a portable 13 V battery. Tubing was cleaned with 10% v/v HCl (reagent grade) and ultra-pure water (Milli-Q: 18MΩ, Millipore® systems) in the lab, and ~25 L of *in situ* seawater at each depth before sample collection. The flow rate of the

pump was kept at 5–8 L min^{-1} to prevent settling of particles during collection. Samples were transported back to the lab in the dark in 20 L carbuoys or 125 mL bottles.

Particulate samples for bulk BSi ([BSi]) were collected by filtration onto acid-cleaned (10% v/v HCl, Aristar grade) 47 mm polycarbonate membrane filters (0.6 μm). Volumes filtered were 1 L for [BSi]. Filters were dried overnight at ~40 °C in PetriSlides and kept at room temperature until analysis. Duplicate samples of filtrate (10 mL) were collected into centrifuge tubes for both concentration and isotopic signature of dissolved silicic acid ([Si_d] and $\delta^{30}Si_d$, respectively). Dissolved samples were acidified with 1 mL L^{-1} of 50% v/v HCl (Aristar grade) to prevent bacterial activity and stored at room temperature. All plastic ware for sample collection, filtration and storage was acid-cleaned (10% v/v HCl, Aristar grade) for at least 24 h and rinsed thoroughly with Milli-Q before use.

5.3.3 Sample Analysis

5.3.3.1 Dissolved Si concentration

Concentration of dissolved Si ([Si_d]) was determined spectrophotometrically using HACH® reagents (Silica Reagent Set, Ultra Low Range, Bulk Solution), following the manufacturer's directions. The first of these reagents contains molybdenum, which forms silicomolybdic acid in the presence of $Si(OH)_4$. After reacting for 3 minutes, Citric Acid F Solution is then added, followed by Amino Acid F Reagent after ~1 minute to produce molybdenum-blue, proportional to the original [Si_d]. All reagent additions were 100 μL per 3 mL diluted sample volume (see below). Solutions were left to sit for 10 minutes to allow for colour development, and the absorbance of 812 nm light was then measured with a spectrophotometer (1 cm path length) and converted to [Si_d], with a detection limit of <1 μM Si. Standards were prepared ranging from 0 to 90 μM Si, and l mL samples were diluted with 2 mL Milli-Q to prevent interference from the saltwater matrix, which was shown to be <5% at this dilution level (results not shown). As this method requires only 1 mL of sample for spectrophotometric Si_d determination, for three events each duplicate 10 mL filtrate aliquot was analysed in triplicate. Triplicate

samples were within 5%, and variation between duplicate aliquots was better than 10%. Thereafter only two 1 mL samples were analysed from one duplicate from each sampling event. If these varied by >10% the second aliquot was also analysed and in all cases the additional measurements agreed with one of the previous measurements, indicating that the variation in the outlier was due to handling error during the preparation for spectrophotometric analysis. Thus, the one outlier was rejected and the remaining ≥ 3 [Si_d] measurements were averaged.

5.3.3.2 Dissolved Si isotopic composition

Silicon isotopic composition ($\delta^{30}Si$) is calculated by the difference between the ratios (R) of heavy (in this case ^{30}Si) to light (^{28}Si) isotope in a sample versus a standard reference material (quartz standard NBS28):

$$\delta^{30}Si_{sample} = \frac{(R_{sample} - R_{std})}{R_{std}} \times 1000 \quad (1)$$

As the differences between isotopic ratios are very small, they are multiplied by 1000 (as in Eqn. 1), and expressed in permil (‰) notation, referring to parts per thousand.

Isotopic composition of dissolved Si ($\delta^{30}Si_d$) was analysed following the method of Reynolds *et al*. (2006) using pre-concentration and purification steps prior to analysis by High-Resolution Multi-Collector Inductively-Coupled-Plasma (HR-MC-ICP) mass spectrometry. Briefly, acidified samples were first neutralised with sodium hydroxide (NaOH, semiconductor grade), and Si was pre-concentrated by adding 110 µm of 1M NaOH. Samples were agitated for 1 h, and left to settle for 24 h; the addition of NaOH will form brucite ($Mg(OH)_2$) crystals in suspension (Beucher *et al*. 2008), and Si will co-precipitate with brucite. Samples were then centrifuged, and a second addition of NaOH was made to ensure complete precipitation of any remaining Si. Again the samples were agitated, left to settle and centrifuged. The supernatant was then carefully removed with a pipette. As fractionation can occur during precipitation, complete recovery of Si is essential to preventing any effects on the $\delta^{30}Si_d$ signature (Cardinal *et al*. 2005, Reynolds *et al*. 2006). The removed supernatant solutions were checked for any residual Si (using the same HACH® reagents and methods described in section 5.3.3.1) and samples with less than 98% recovery were not analysed for isotopic composition.

The precipitate was redissolved in small volumes of 6M HCl. As secondary precipitates that will not redissolve can be formed at concentrations >50 ppm Si, care was taken not to exceed this limit. Samples were adjusted with Milli-Q to final concentrations of 5 ppm. These concentrated samples were then purified on columns with a resin that removes cations to reduce interference from sodium and magnesium during mass spectroscopy. The resin used was Bio-RAD AG-50W-X8 resin which can absorb 1.6 milli-equivalents (meq) of cations. Less than 0.16 meq of solution (predominantly Mg^{2+} from brucite) was loaded per resin column (0.75 mL resin) to stay well below this threshold. The resin was pre-cleaned with ultra-pure acids (Aristar HCl and HNO_3, distilled in Teflon vessels by sub-boiling) prior to use following the sequence shown in Table 5.1. The resin was re-cleaned after the first use, and discarded after the second.

Table 5.1: Sequence of chemical and wash steps used to pre-clean resin. This was done in a large volume column (15 ml total volume, initially loaded with 10 ml of resin). MQe refers to Milli-Q element, ultrapure 18 MΩ water.

Chemical	Concentration	Volume
HCl	3 M	5 ml
HCl	6 M	5 ml
HCl	9.2 M	5 ml
HF	30 M	1-2 ml
HNO3	7.2 M	1-2 ml
HCl	9.2 M	2-3 ml
HCl	6 M	5 ml
HCl	3 M	5 ml
MQe	-	5 ml
MQe	-	5 ml

Before loading each sample on pre-cleaned resin, the resin and column were rinsed with ultra-pure acids. One mL of each concentrated sample was passed through the column and eluted with 4 mL Milli-Q to give a final volume of 5 mL and Si_d of 1 ppm. The cleaning, sample loading and elution sequences are shown in Table 5.2.

Purified Si samples were analysed for $^{30}Si/^{28}Si$ and $^{29}Si/^{28}Si$ ratios on a Nu1700 HR-MC-ICP mass spectrometer at ETH-Zürich, with a Nu Instruments DSN desolvator and a PFA nebuliser. Standards used were NBS28 and Diatomite reference material. Measurements were made using standard-sample-standard bracketing, with 5–9 replicate measurements for each sample, giving 95% confidence limits of <0.1 ‰ (2 standard deviations <0.2 ‰). Full details of the mass spectrometry methods are given in Georg *et al*. (2006).

Table 5.2: Sequence of chemical and wash (Milli-Q element, ultrapure 18 MΩ water) steps used on pre-cleaned resin.

Chemical	Concentration	Volume (ml)	Purpose
HCl	3 M	1 ml	Clean
HCl	6 M	1 ml	Clean
HCl	3 M	1 ml	Clean
MQe	-	2 ml	Clean
MQe	-	1 ml	Prepare
Sample	5 ppm Si	1 ml	Sample
MQe	-	4 ml	Elute

5.3.3.3 Biogenic silica concentration

Concentration of particulate biogenic Si (BSi) was determined using an adaptation of the double wet-alkaline digestion method as outlined in Ragueneau *et al*. (2005). Full details of the extraction conditions, sample analysis and processing are given in Appendix A5.1.

5.4 Results

5.4.1 Oceanographic context

Physical conditions within the water column at the RaTS site are presented in Figure 5.1, showing temperature, salinity, density and mixed layer depth (MLD) during the austral summers 2008 and 2009. Ryder Bay conditions are generally typical of a seasonal sea-ice zone, where warming and freshening due to insolation and freshwater inputs create an increasingly stratified upper water column during the

course of the summer. This uppermost layer is AASW. Below this can be found the remnant of the cold, more saline WW mass produced from deep winter mixing. The deep source for WW is CDW, which intrudes onto the Antarctic Peninsula shelf in relatively unmodified form (Klinck 1998).

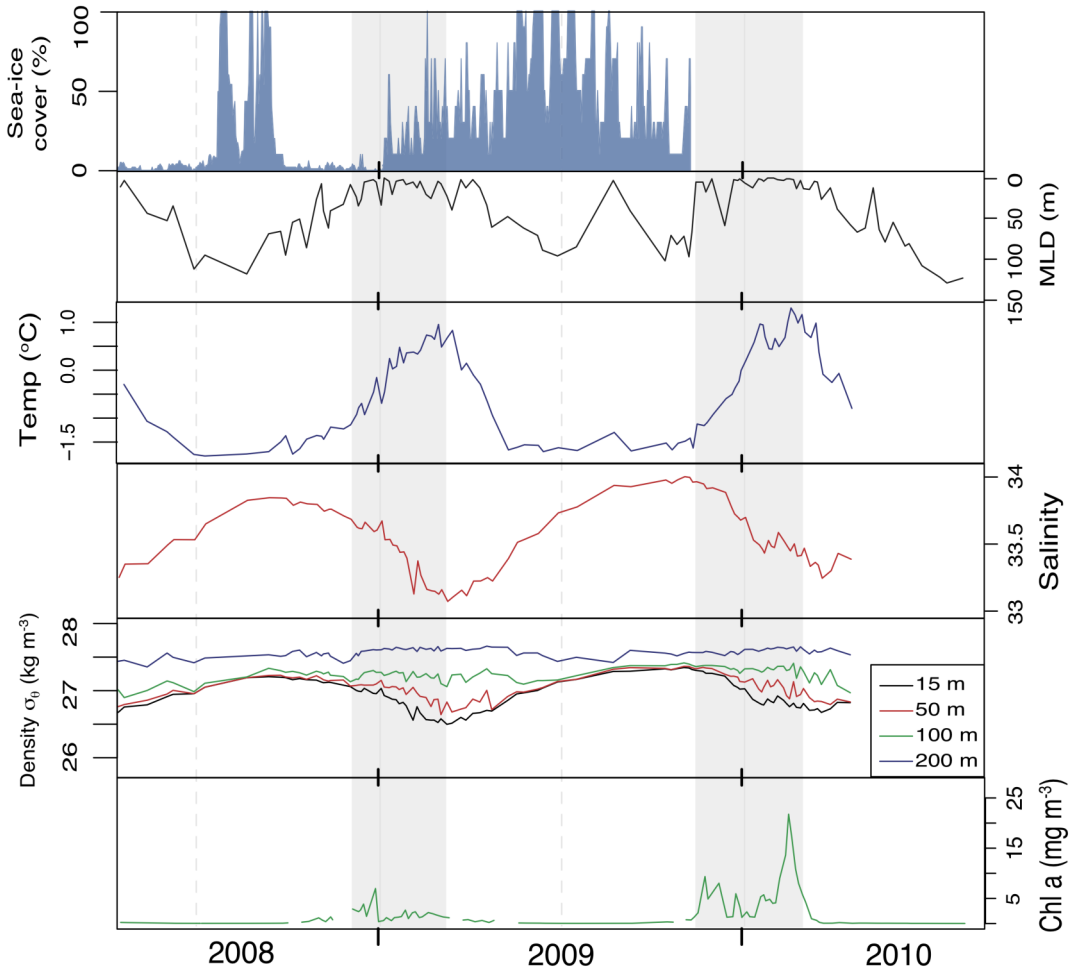

Figure 5.1: Environmental and water column conditions at the RaTS site during the study period. Sea-ice cover was assessed visually on a ~daily basis. MLD is as defined in Chapter 2. Temperature, sailinity, density anomaly (σ_θ) from CTD and chl *a* concentrations from Niskin samples are from 15 m depth, except where specified. All data courtesy of BAS.

This seasonal shallowing of the MLD is clearly seen in both seasons at the RaTS site, with 2009 showing a greater extent of stratification than 2008 (mean 12 vs. 8 m; *see discussion in* section 2.4.1). Input events of meteoric (glacial and snow) water are inferred from oxygen isotope data (not shown) and dips in salinity (*e.g.* 12 Jan, 5 and 12 Feb, 11 Mar in summer 2008; 21 Jan, 1 Mar in summer 2009), while

upwelling events may be associated with changes in salinity and oxygen isotopes seen on (*e.g.* 7 Jan, 9 Feb in summer 2008; 6 Feb, 1 Mar in summer 2009).

Chlorophyll concentrations from RaTS monitoring at 15 m water depth (Figure 5.1) show much lower biological activity than is typical for this site (*for full discussion see Chapter 2*). Peak [chl] were 6 and 20 mg m^{-3} in 2008 and 2009, respectively, with average concentrations during the summer growing period (see section 2.4.2) of 1.9 ± 1.3 and 6.3 ± 5.0 mg m^{-3}. Compared to high-chl seasons (*e.g.* summer 2004 and 2005), where average [chl] is 10 to 15 mg m^{-3} and peaks above 24 mg m^{-3}, the two seasons studied here are both considered low-chl years relative to more typical conditions at this site, although 2009 records indicate a partial recovery of chl concentrations in the later part of the season.

5.4.2 Dissolved Si concentration

As part of the RaTS programme, [Si_d] is monitored at 15 m in Ryder Bay throughout the year. These records and methods (courtesy of BAS, Cambridge UK) are detailed in Appendix A5.2, and display considerable sample-to-sample variability on top of a typical pattern of seasonal drawdown during austral summer. While longer-term records are provided in the appendix for context (2004-2010), this discussion focuses on detailed analysis of the 2008 and 2009 seasons only, when additional records are available for comparison.

For this study, samples were collected alongside the RaTS samples and processed according to the methods in 5.3.3.1. This data set is presented in Figure 5.2, covering the summers of 2008 and 2009. In 2008, [Si_d] shows a trend of gradual decrease over the season, from initial concentrations of ~65 µM to ~50 µM in March. For this season, Si yields for isotopic analysis were sometimes higher (up to 30%) than concentrations determined by spectrophotometry. This suggests that some samples may have been affected by precipitation due to freezing (*see* Appendix A5.2). There was no apparent pattern in the samples affected, and where considerable mismatch was apparent the results are not shown or included in the results or analyses here. However, some of the remaining results may also have been affected to a lesser degree, and thus care must be taken with any interpretations based on 2008 data. As a result, interpretation focuses primarily on the 2009 data.

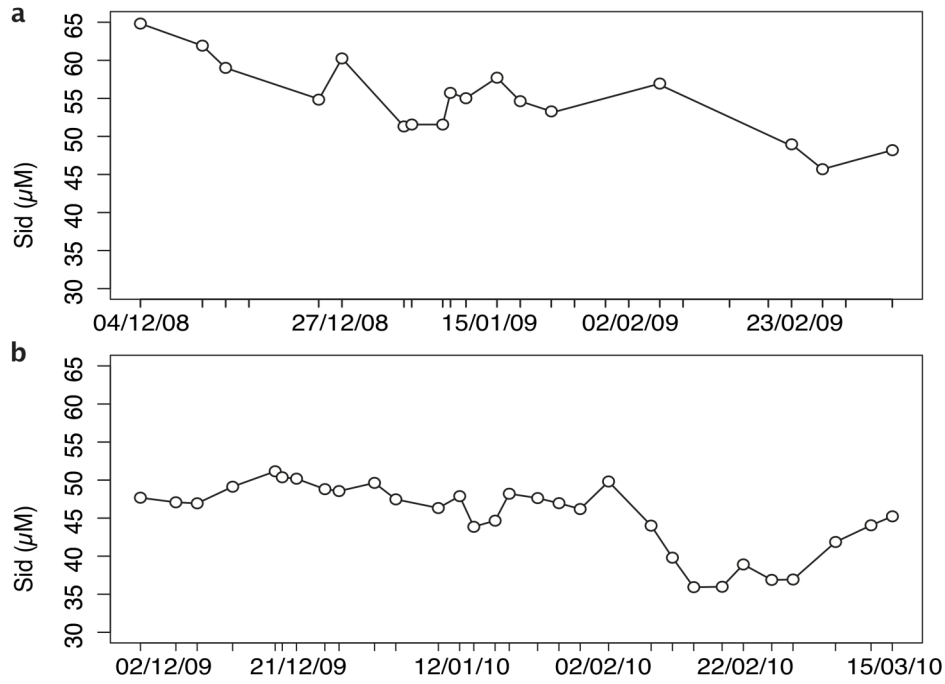

Figure 5.2: Dissolved Si concentrations measured in this study during (a) 2008 and (b) 2009. Y-axes are the same in both plots, showing the higher initial and minimum concentrations during austral summer 2008.

In 2009, the trend of moderate drawdown is very similar to that of the BAS data (average drawdown ~0.112 vs 0.118 μM d^{-1}), although with much less intersample variability and therefore a much higher correlation (r^2 = 0.454 vs 0.089; this study vs BAS data, respectively). The average summer [Si_d] (45.2 μM) was also very similar to the BAS value (46.0 μM).

In addition to time-series sampling at 15 m depth, weekly samples were collected from additional depths in the top 25 m of the water column, and deeper samples (down to 500 m) were collected when feasible, to better understand the cycling of Si through the water column within Ryder Bay. Changes in surface water [Si_d] with depth over both growing seasons are shown in Figure 5.3. Variability is noticeably less in the second summer, where concentrations are more consistent with depth. In the first season, a short-lived increase at all depths can be seen in early January, followed by depletion at 5 m and an increase at 25 m. This is followed by another depletion event greatest at the surface (0–10 m). In 2009, [Si_d] is initially considerably lower than in 2008, but increases throughout the profile by ~5 μM at

the end of December. Gradual depletion then occurs throughout the water column until early March, when concentrations show a slight increase as winter mixing begins.

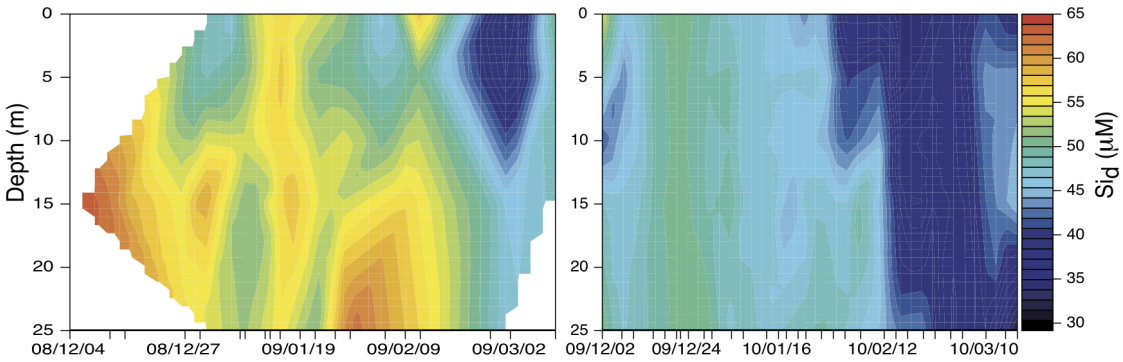

Figure 5.3: Dissolved Si in the top 25m of the water column for the summers of 2008 and 2009.

Deep waters are significantly enriched in Si_d relative to surface waters, with maximum concentrations >80 µM, seen in Figure 5.4. Deep waters were sampled only once in the 2008 season, but multiple deep samples in 2009 show changes at depth over time. A gradual increase in [Si_d] in deep water can be seen over the course of the season at depths ~200 m.

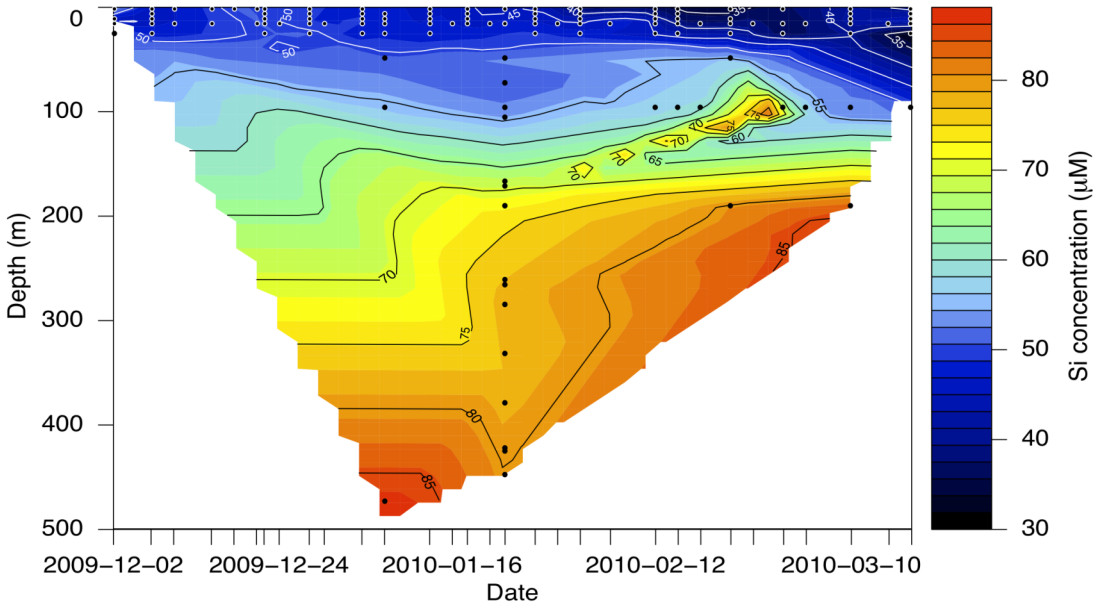

Figure 5.4: Time-series contour plot of [Si_d] with depth at the RaTS site during summer 2009, sampling events are shown as dots. Much higher [Si_d] can been seen in deeper waters.

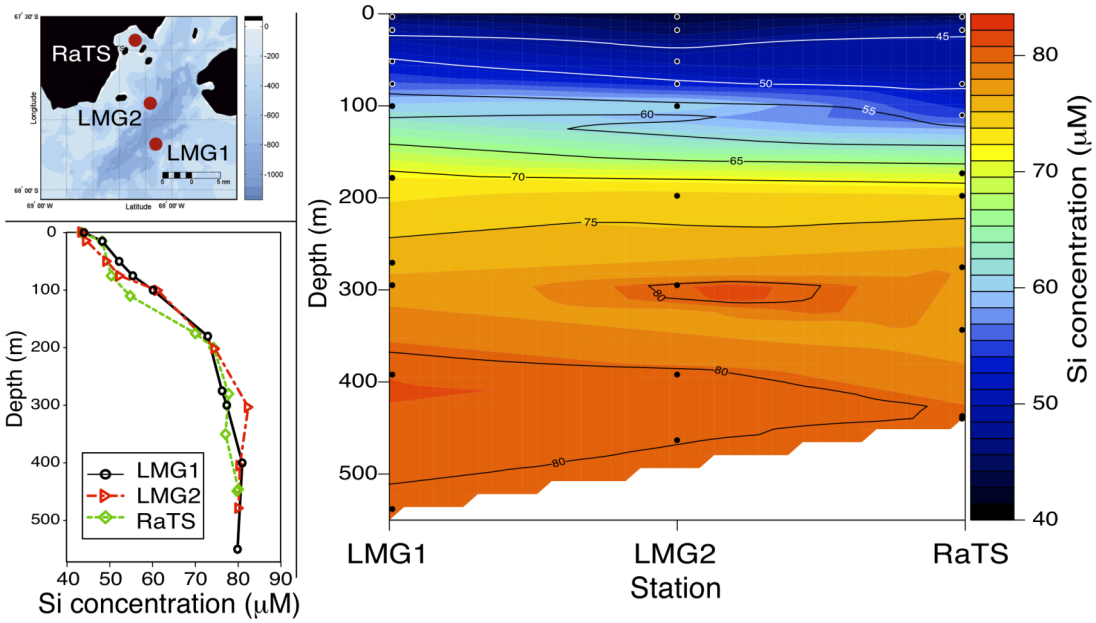

Figure 5.5: Sampling locations, depth profiles and contour plot of [Si_d] at three stations including the RaTS site, collected during a cruise aboard the *R.V. Lawrence M. Gould* on 23 January 2010. Coordinates for stations LMG1 and LMG2 are -67° 52.44 S, -68° 05.69 E and -67° 44.70 S, -68° 08.33 E, respectively. From the very close agreement at all sites it can be seen that concentrations in Ryder Bay are largely representative of Si_d in northern Marguerite Bay.

One sampling event allowed collection of depth profile samples from the RaTS site, and two locations in Marguerite Bay. Shown in Figure 5.5, these data show that [Si_d] are very consistent at the three locations, in agreement with previous studies that indicate surface waters of Ryder Bay to be highly representative of conditions in Marguerite Bay. The increase in [Si_d] with depth to a maximum concentration of ~80 μM seen in the Ryder Bay samples, is also seen into Marguerite Bay despite deeper water at station LMG1 (620 m water depth).

5.4.3 Particulate Si concentrations

Time-series data from particulate samples show that the majority of Si is from biogenic sources in the particulate phase, although the absolute value of lithogenic Si (LSi) contribution varies from sample to sample, and was generally lower in the first season (Figure 5.6). Clear differences are apparent in BSi records from the two seasons, with the most striking difference being the extended period of

very low BSi concentrations in summer 2008. Initial concentrations ranged from 2–5 µM during December 2008, largely at the upper end of this range, but dropped to <1 µM for January and February, with a slight late-season increase to ~2 µM in early March. While initially high concentrations that dropped off into January were also seen in 2009 (to ~7 µM), the low BSi was short-lived in summer 2009, with concentrations building from mid-January to ~9 µM in mid-February.

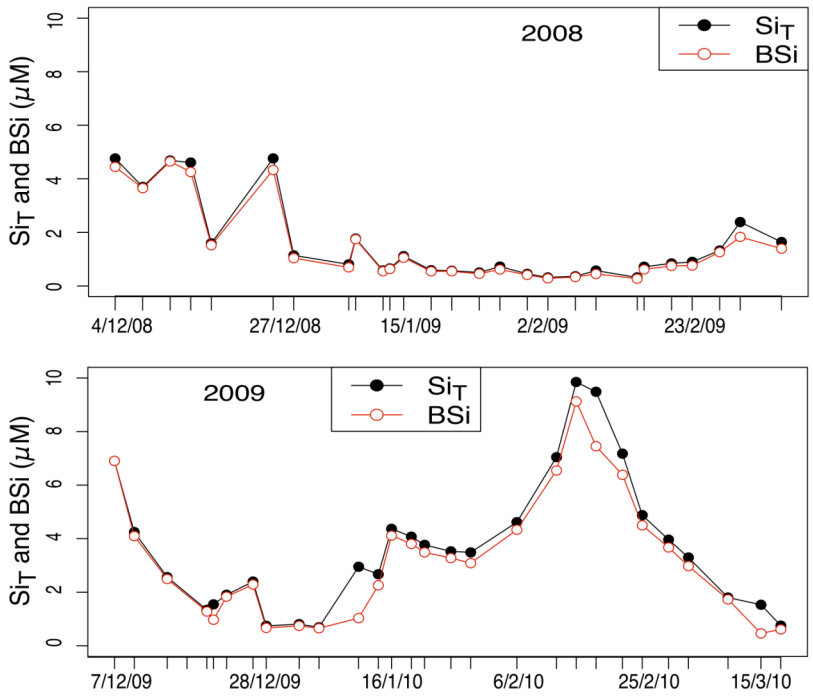

Figure 5.6: Time-series data of BSi and total particulate Si (Si_T) concentrations at 15 m depth.

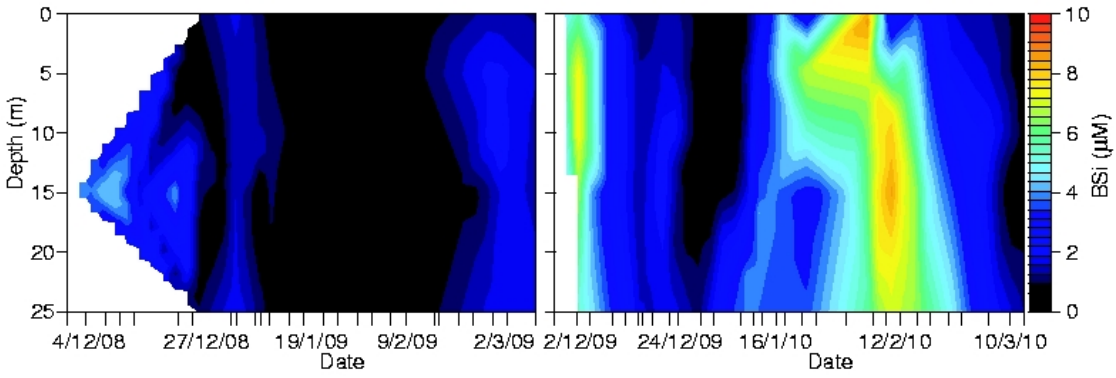

Figure 5.7: Interpolated BSi concentrations from all samples collected in the uppermost 25 m at the RaTS site during both summer growing seasons.

As for dissolved samples, BSi was also measured in the top 25 m of the water column throughout both sampling seasons. Trends from 15m water samples were found to be largely representative of the surface waters as a whole, with slightly higher BSi found at 0–10 m on two occasions in 2009 (Figure 5.7).

For comparison to previous seasons with different environmental conditions, data is also presented from particulate samples collected at 15 m in the summers of 2004 and 2005. These samples were analysed previously by X-Ray Fluorescence (XRF; of unprocessed particulate matter collected on filters, *full details in* Carson 2008). This earlier data is total particulate Si (Si_T), and as such is compared to Si_T data for the 2008 and 2009 seasons (Fig. 5.8), but as noted above, BSi is the dominant source of particulate Si at the RaTS site and will primarily reflect BSi.

A striking difference is apparent between the data from this study and Si_T records from previous years, with the earlier seasons displaying much higher particulate Si. In the two earlier years, total particulate Si is >5 μM for the majority of the season, whereas in the later two years this threshold is only exceeded for two brief periods in 2009. Variability in chl is clearly reflected in particulate Si records, with trends being broadly consistent between both parameters. This is in keeping with diatom production being the dominant phytoplankton contribution to total chl.

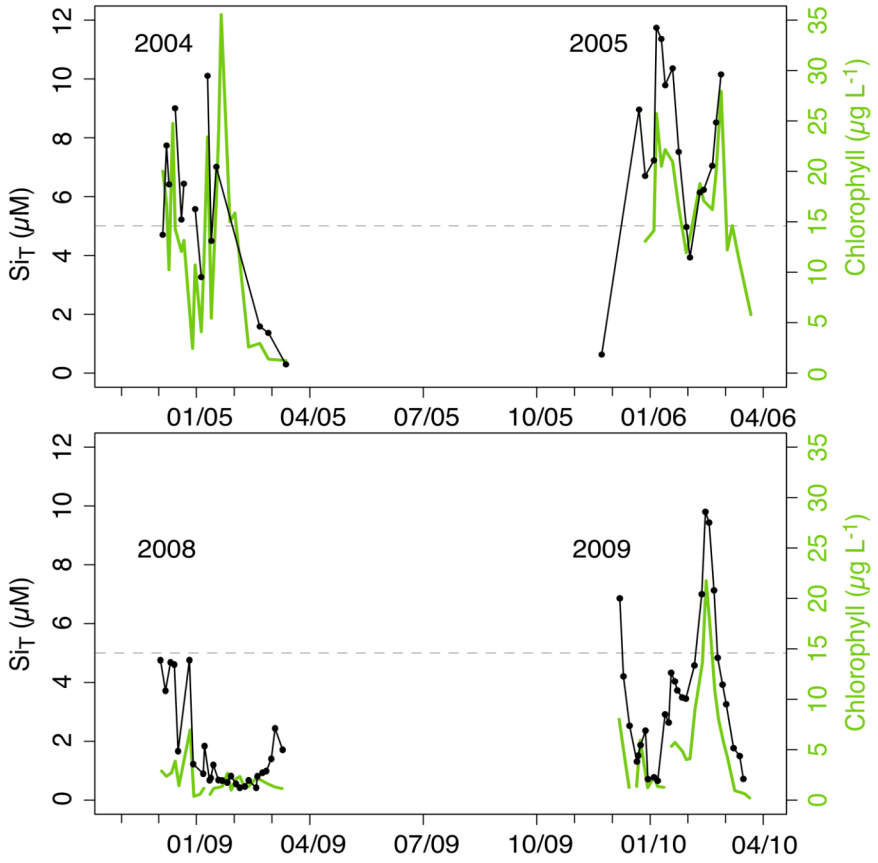

Figure 5.8: Comparison of Si_T across four seasons. All samples from 15 m. Note that these are not corrected for lithogenic Si, although this has been shown to be very low. Bottom plot shows BSi from this study for 2008 and 2009. Green lines (right hand y-axes) are chl records, for comparison. Horizontal lines are drawn at 5 µM to highlight differences between the earlier and later years. Data from 2008 are from Carson (2008), where extracted Al data were combined with Si:Al ratios from XRF analysis to calculate total Si. This requires a homogeneous distribution of particulate matter on filters. Reliability of this approach was assessed based on Si:Al ratios. Although this ratio will vary during the season, the change should be gradual. Where this ratio showed a single event anomaly that was >2-fold different from the preceding and subsequent data points, that event was assumed to be affected by non-uniform distribution of material. This could be caused by clumping of diatoms due to a high proportion of chain-forming species, species with setae, filter clogging, rapid or slow filtration, etc. Only 6 points in total displayed anomalous Si:Al ratios, all from the 2004-2005 season, and are excluded from further analysis.

5.4.4 Isotopic composition of dissolved Si

Isotopic composition of Si_d was analysed in a subset of samples from each season, focusing primarily on changes in surface waters. Figure 5.9 shows that in the 2008 data, relatively little variation is seen in $\delta^{30}Si_d$, with most samples around 1.62 ‰. Only a few samples have values above this, with the most significant

enrichment (1.98 ‰), seen on 27 Dec 2008. Deep waters (100 m) were sampled on one occasion, and were found to be lighter, ~1.2 ‰.

In keeping with the clearer trend of drawdown in summer 2009, there is a gradual enrichment in $\delta^{30}Si_d$ over the course of this season (Figure 5.9). Early season samples were ~1.6 ‰, similar to the 2008 average, but increased to ~2.0 ‰ by March 2010. More deep (100 m) samples were collected for summer 2009, and these again showed lighter isotopic signatures. In deep waters as well, an increase towards heavier values was seen at the end of the season, which may be a reflection of surface water being mixed downwards as stratification breaks down in austral fall.

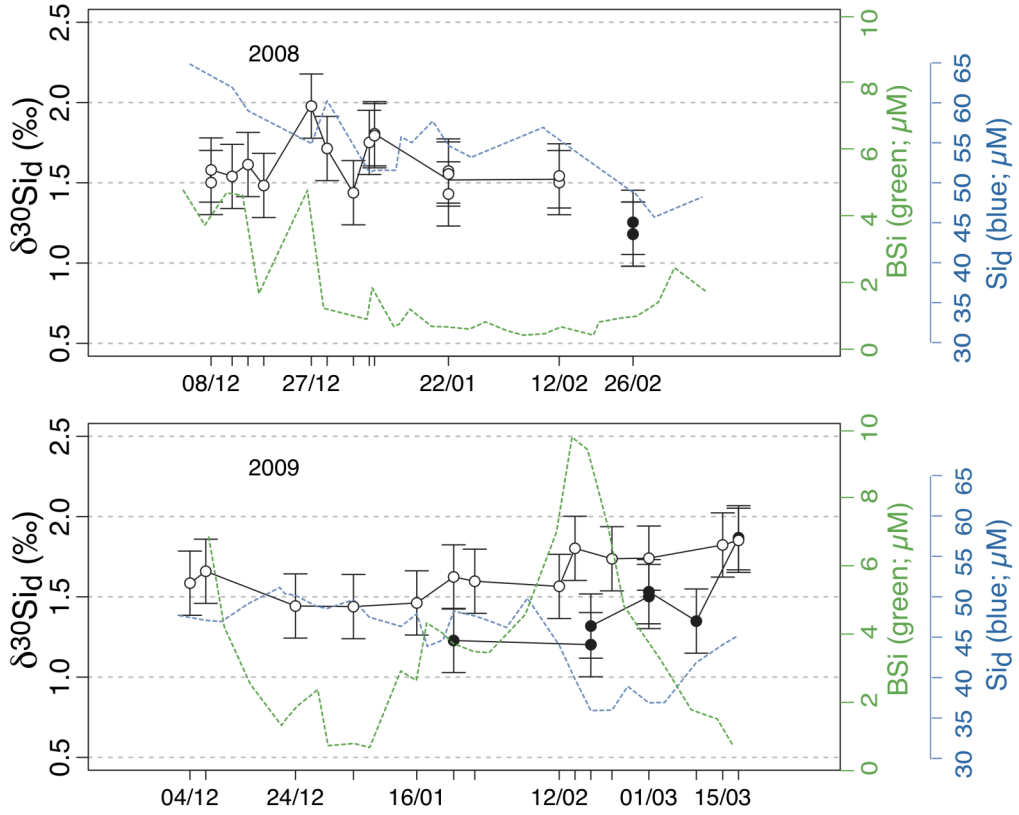

Figure 5.9: Isotopic signature of Si_d for 2008 (top) and 2009 (bottom). In both cases trends are shown for shallow samples (<25 m) as open symbols. Deep waters (>100 m) are denoted by filled symbols. For context, Si_d concentration (blue) and BSi (green) are also shown as dotted lines.

Five samples were collected from deeper waters on 23 Jan 2010, in order to investigate isotopic signatures below the winter water layer. These were collected from 200, 280, 350, 446 and 496 m, where bottom depth was ~500 m. These samples

gave values ranging from 0.8 to 1 ‰, with the lightest value at the deepest depth. A composite depth profile including most of the samples from the season (excluding the late-season, 100 m samples displaying very enriched $\delta^{30}Si_d$) is shown in Figure 5.10. From this profile the trend towards heavier surface values is evident, consistent with preferential biological uptake of lighter isotopes in the euphotic zone.

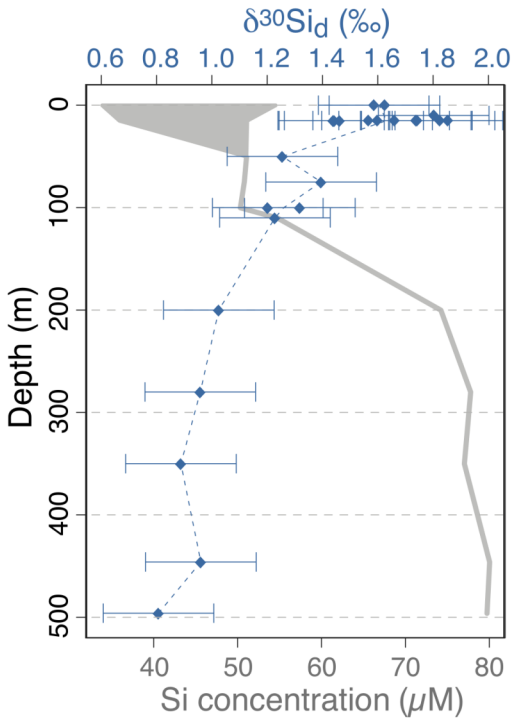

Figure 5.10: Isotopic composition of Si_d with depth at the RaTS Site, in blue. Grey shading/line shows the range of Si_d concentrations in the same samples – variability in [Si_d] is greatest above 50 m where more samples were analysed. Samples from 100 m on the two final sampling events (where increased vertical mixing is suggested to have occurred) are not shown.

5.5 Discussion

5.5.1 Dissolved and particulate silicon concentrations

Like most of the Southern Ocean, [Si_d] in Ryder Bay surface waters is relatively high, ranging from 35–60 μM. Long-term average trends from BAS data show a seasonal cycle of winter concentrations of ~65 μM gradually decreasing throughout the summer to a minimum of 50 μM in March (Clarke *et al*. 2008). The data from this study show the same trend of slow decline through the summer season. While these trends are consistent, there are discrepancies between the data from this

study and those from BAS records during the two seasons. The reasons for this mismatch are discussed in Appendix A5.2. Here the long-term BAS trends are considered robust, but the data from this work more reliable at the resolution of individual sampling events. The data from this study suggest that winter replenishment was lower prior to summer 2009 than for 2008, although sampling missed the initial increase in chl and BSi, thus the early season [Si_d] is likely to have been higher than the first samples collected here. Records from BAS indicate winter [Si_d] of almost 80 μM in early November, which gives a seasonal drawdown of ~55%, compared to only ~30% in summer 2008.

The concentration of BSi shows a bi-modal seasonal pattern, typical of [chl] in this area (Clarke *et al*. 2008). Periods of higher BSi are coincident with lower [Si_d], reflecting uptake of Si into the particulate phase as a result of biological production. This is in agreement with current understanding of biological processes in Ryder Bay, where phytoplankton biomass is generally dominated by diatoms, as other Si-containing microorganisms (*i.e*. silicoflagellates) are comparatively rare (Annett *et al*. 2010). Further, the minimal drawdown suggested here for 2008 and the greater extent of Si drawdown in 2009 are consistent with chl and N-use data in 2009 presented in Chapter 3. Both Si- and N-use indicate greater drawdown in 2009, the intermediate-chl season, than in 2008 when chl was very low.

5.5.2 Particulate silica and chlorophyll

As can be seen by the comparison of summers 2008 and 2009 with earlier particulate Si data (Fig. 5.8), the BSi accumulation during this study period was low. This can be explained primarily by lower overall biological production, as records show uncommonly low [chl] in these summers. A secondary cause may be the shift to lower relative contributions from diatoms (*see Chapters 2, 3*). The differences in BSi during 2008 and 2009 agree well with trends in Si_d, as well as phytoplankton/diatom and N-use data, reflecting the low- and intermediate-chl conditions in 2008 and 2009, respectively.

Biogenic Si and chl time-series data are very similar. As Figure 5.8 shows, the timing and relative magnitude of most changes in chl are closely mirrored by BSi. When plotted relative to each other, there is a strong relationship between the

two variables (Fig 5.11). This is not surprising, as it is well established that diatoms dominate phytoplankton communities along the WAP. This strong (r^2 = 0.85) quantitative relationship is significant as it implies that BSi concentrations can be predicted based on [chl], according to the equation:

$$BSi = (0.38 \pm 0.018)*[chl] + 0.96 \quad (2)$$

To our knowledge, this is the first study to derive a quantitative link between BSi and chl in WAP waters.

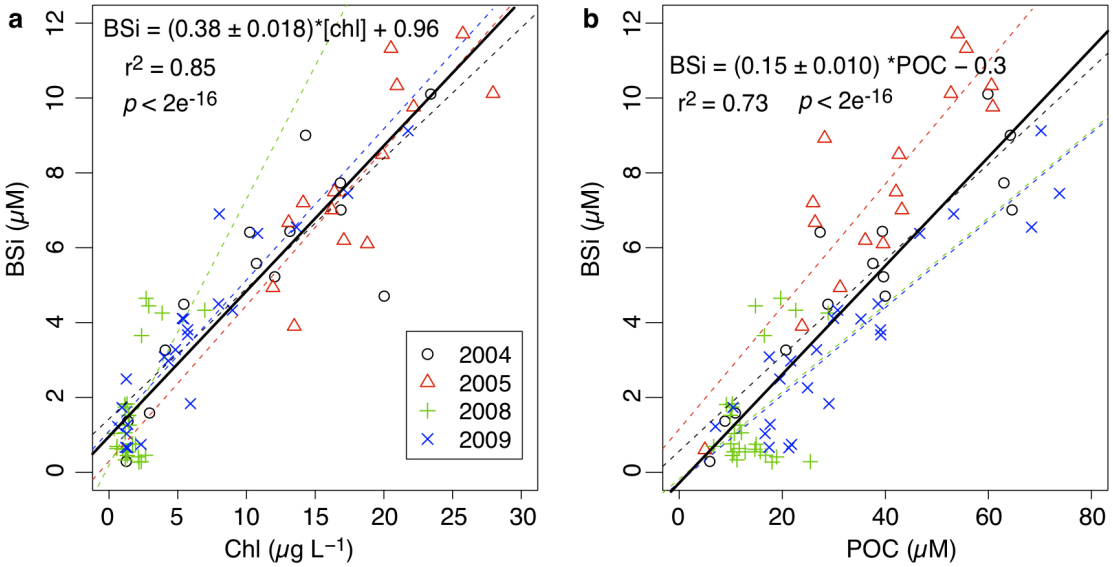

Figure 5.11: Particulate Si versus (a) chl and (b) POC for 4 seasons at the RaTS site. Data from the first two seasons are total particulate Si, 2008 and 2009 are BSi. A strong overall correlation (solid line) is shown for both relationships. Seasonal data (dashed lines) show very similar relationships in all cases, with some offset for the 2008 data (see text). All regressions are highly statistically significant (p < 0.001). All samples from 15 m.

Interestingly, the slope of BSi versus [chl] in the low-chl year (2008) is greater than for the other seasons and the overall regression. Based on the lower proportions of non-diatom taxa in this season, which do not have absolute Si requirements, a lower BSi:[chl] would have been expected. The greater slope value reflects the high Si which is hypothesised to result from *Corethron pennatum* populations (*see* Chapter 4), as well as the much smaller range of values such that outliers have a strong impact on the slope. As can be seen from the very good agreement of the slope of the total dataset and the high- and intermediate-chl seasons individually (Fig. 5.11a), the 2008 data do not affect the overall relationship, and

indeed the r^2 value for 2008 only is weak (0.39). Thus while the relative uncertainty for BSi estimates based on [chl] may be somewhat greater in low-chl conditions, this only affects values at the low end of the [chl] range, and will have very little impact on comparisons of interannual BSi dynamics.

There is also a highly significant ($p < 2 \times 10^{-16}$) and similarly robust ($r^2 = 0.73$) relationship between BSi and POC. As chl is measured more often than POC, and can be estimated from satellite data, the BSi versus chl regression is likely to be more useful in estimating standing stocks of BSi. However, the strong BSi:POC relationship indicates that estimates of WAP productivity and fluxes in terms of C can be also be expressed in terms of Si, and vice-versa.

The Si:C relationship found here is 0.15 (Fig 5.11b), exactly in line with the classical Redfield ratio. Given the differences in Si requirements between phytoplankton groups, this is strong evidence that productivity in this region is diatom-based, with non-siliceous groups having negligible impact on productivity over the productive summer bloom period. This understanding of the WAP as diatom-dominated during both high- and low-productivity conditions contrasts with conditions in the Ross Sea, where productivity is similar between communities dominated by either diatoms or prymnesiophytes (Ducklow *et al*. 2006). In the case of the WAP, low chl is accompanied by low BSi and low Si_d drawdown, which are both consistent with the trends seen in Si isotopes.

5.5.3 Isotopic fractionation

5.5.3.1 Interseasonal trends

The very good agreement between summer 2009 trends in Si_d, BSi and $\delta^{30}Si_d$ suggests that the data from this season are a reliable and accurate reflection of Si dynamics in the water column. These data indicate Si use of ~55%, along with an enrichment in $\delta^{30}Si_d$ values in surface waters of ~0.4 ‰. While there is some uncertainty regarding individual sample measurements of [Si_d] in summer 2008 (*see Appendix A5.2*), the reported trends in 2008 [Si_d] where datasets agree and the very limited range of $\delta^{30}Si_d$ values in 2008 are both consistent with very low seasonal productivity in this year. Thus the overall phytoplankton standing stocks and

production based on chl, diatom counts and nitrate concentrations described in Chapter 3 are strongly supported by dissolved and particulate Si concentrations and Si isotopes.

5.5.3.2 Seasonal trends

Given the very low range of isotopic data from 2008, the following interpretations are based only on 2009 data. Two important trends are evident in the time-series and depth profile values of $\delta^{30}Si_d$. Firstly, the seasonal decrease in $[Si_d]$ is accompanied by isotopic enrichment. Compared to surface waters in other regions, this enrichment and drawdown is relatively minor (minimum ~30 μM and ~1.8 ‰ here, compared to *e.g.* <1 μM and >3 ‰ in the North Pacific, Reynolds *et al*. 2006). Biological utilisation preferentially incorporates lighter isotopes into biogenic material, as lighter isotopes have lower bond energy and therefore react to form biological products marginally faster than their heavier counterparts. This is true of many elements, including Si. As biological activity continues, more and more of the lighter isotopes preferentially accumulate in the particulate (biogenic) phase, leaving the dissolved reactant pool enriched in the heavier isotopes. Thus with increasing extent of Si utilisation over the course of the growing season, it would be expected that $\delta^{30}Si_d$ increases. Therefore the moderate enrichment (from ~1.6 to 2.0 ‰) seen during the 2009 season is consistent with the moderate extent (from ~50 to 35 μM, or 30%) of Si use.

Secondly, deep waters have much higher concentrations of Si_d (up to 80 μM), and display much lighter $\delta^{30}Si_d$ values. This is consistent with deep waters being the source of Si to surface waters. The very light values also suggest that deep water in this region has experienced very little utilisation. The 0.81 ‰ values at depth are the lowest reported from the Southern Ocean, and in line with the estimate made for AABW based on very deep North Pacific water (0.8 ‰; Reynolds *et al*. 2006). The high $[Si_d]$ may reflect some extent of remineralisation, and this process would contribute to light isotopic signatures, because remineralisation preferentially releases the light isotopes that have been incorporated into sinking particles (with a fractionation factor of ~0.55 ‰; Demarest *et al*. 2009).

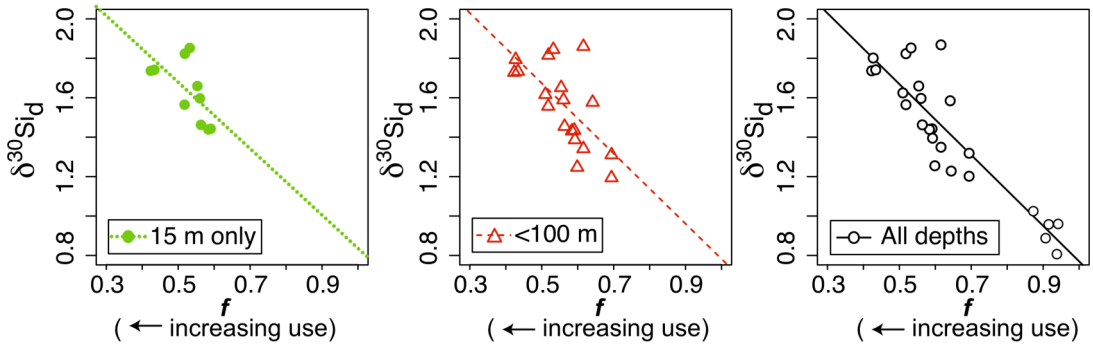

Figure 5.12: $\delta^{30}Si$ vs. *f* (fraction remaining) for shallow stations (left) and all depths (right). For the shallow waters only, the correlation is weak and the error of the slope is greater – which would be expected due to the smaller range of values.

Table 5.3: Results of regression analysis for subsets of $\delta^{30}Si_d$ data versus fraction remaining (*f*), shown in Figure 5.12.

Data	r^2	*p*-value	slope	intercept
15 m only (n = 10)	0.317	0.0524	-1.68 ± 0.74	2.52 ± 0.39
100 m and above (n = 19)	0.424	0.00150	-1.78 ± 0.47	2.56 ± 0.27
All samples (n = 25)	0.798	1.12×10^{-9}	-1.80 ± 0.18	2.57 ± 0.12

The different values of $[Si_d]$ and $\delta^{30}Si_d$ in deep waters compared to those at the surface contribute significantly to the overall range of values assessed in this study. Isotopic signatures of shallow water samples (<15 m depth) versus fraction remaining (*f*, a commonly used index of use where $f = [Si_d]_{obs}/[Si_d]_{max}$, subscripts referring to observed and maximum, respectively, and taking a maximum value of 85 μM) are shown in Figure 5.12. The correlation between the two variables for surface water samples is weak ($r^2 = 0.317$) and not statistically significant (Table 5.3). However, including the samples from deeper waters extends this relationship: the equation of the regression is very similar in all cases, indicating that the inclusion of these samples does not force the trend seen in surface water, but over the greater range of values the correlation is much stronger and highly significant. This is strong evidence that trends in the surface water isotopic measurements reflect fractionation associated with biological uptake, and is consistent with deeper waters being the primary Si source.

5.5.3.3 Open versus closed system dynamics

There are two different sets of conditions under which isotopic fractionation can be modelled. The first is Rayleigh or closed fractionation, which assumes a closed system where reactant (R) is converted to product according to a fractionation factor "ε", and the product builds up in the system. Thus the product considered can either be instantaneously formed product (P_{inst}), or accumulated (P_{acc}). The second is open fractionation, which assumes an open system where the reactant pool can be continually replenished from an outside source, and is converted to product according to the same ε, with the product leaving the system such that only P_{inst} is present.

There is considerable debate as to whether oceanographic systems are better represented by closed- or open-system dynamics, and may depend largely on physical conditions. For example, a strongly stratified water column might be physically isolated from resupply of nutrients and may be best approximated by a closed system. In contrast, highly productive systems with continual upwelling are often thought to function as open systems, where particulate material sinks out of the surface waters and the underlying sediments therefore represent P_{inst}.

Several studies have investigated surface water isotope dynamics with a view to determining if open or closed systems are more appropriate, for Si (*e.g.* Varela *et al*. 2004) and also with N (*e.g.* Karsh *et al.* 2003). The equations describing the evolution of $\delta^{30}Si_d$ in the reactant pool as drawdown progresses differ based on the system assumption. For a closed system, $\delta^{30}Si_d$ can be described as:

$$^{30}Si_d = \delta^{30}Si_{d\text{-initial}} + \varepsilon \ln(f) \quad (3)$$

where $\delta^{30}Si_{d\text{-initial}}$ is the isotopic signature of the original reactant pool, and ε is the fractionation factor associated with biological uptake (Varela et al. 2004). For an open system, the equation describing $\delta^{30}Si_d$ is:

$$\delta^{30}Si_d = \delta^{30}Si_{d\text{-initial}} - \varepsilon (1-f) \quad (4)$$

(Varela *et al*. 2004). Taking a literature value of -1.1 ‰ for ε (De La Rocha *et al.* 2000), 85 μM for $[Si_d]_{max}$, and 0.8 ‰ for $\delta^{30}Si_{d\text{-initial}}$, the modelled evolution of $\delta^{30}Si_d$ under both scenarios is shown in Figure 5.13.

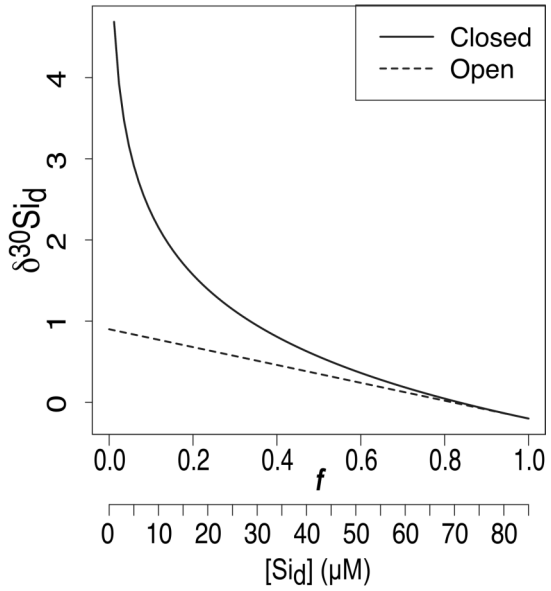

Figure 5.13: Theoretical evolution of $\delta^{30}Si_d$ for both closed- (solid) and open- (dashed) system dynamics. Values for maximum $[Si_d]$, initial $\delta^{30}Si_d$ and ε are 85 μM, 0.8 ‰, and -1.1 ‰, respectively.

Plotting the data from this study against $\ln[Si_d]$ or *f* should give a linear relation in the case of closed or open system dynamics, respectively. As shown in Figure 5.14, there is a very strong linear regression for each case. Because of the relatively moderate extent of drawdown (maximum 30%), the two theoretical trends are very similar to each other over this range of *f* values, and therefore both models give a reasonable fit to the data presented here (Fig. 5.14). It is interesting to note that the closed system dynamics display a slightly better fit when late-season 100 m samples are excluded. These autumn samples may be affected by the breakdown of stratification and thus reflect more open conditions. This is consistent with the majority of seasonal samples reflecting predominantly closed dynamics, indicated by relatively stable MLDs. When all samples are taken into account, possibly representing the inclusion of more open conditions late in the season, the open system shows a better fit to the data. However, the differences in correlations are very slight, and while we suggest that most of the season may be dominated by closed-system dynamics, it is highly likely that the true conditions represent a mix of the two, with more open conditions towards the end of the season, and possibly during occasional mixing events such as (6 Feb, 10 Mar 2009). Data from N isotopes, which show a greater extent of drawdown owing to lower maximum

concentrations, indicate that open system dynamics are more applicable to N cycling over the course of the season (Henley 2012). Therefore it is likely that under conditions of periodic mixing events as seen in summer 2009, open-system dynamics are more valid at seasonal time scales.

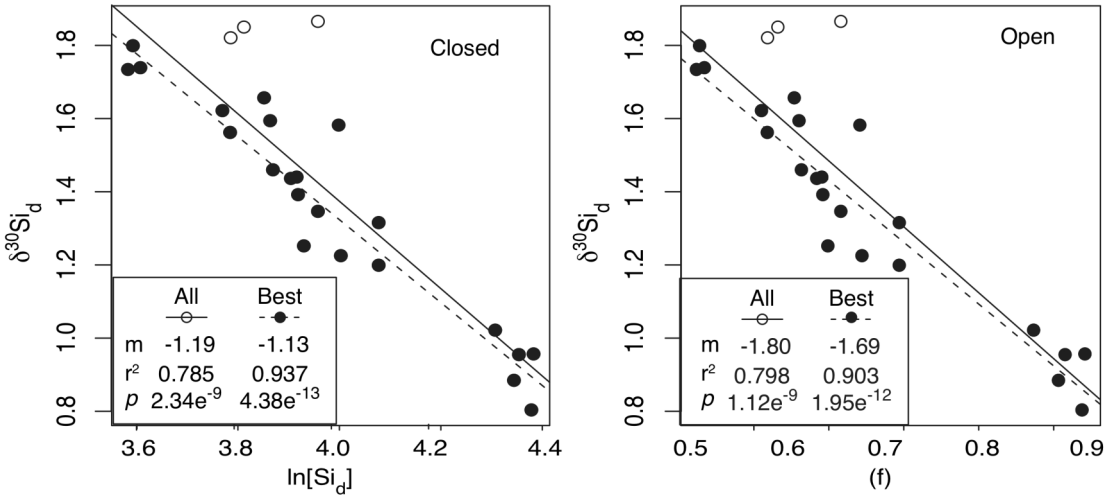

Figure 5.14: Closed (left) versus open (right) fractionation. Over this range the two systems are virtually indistinguishable. Open symbols are from late-season samples (15, 18 March 2010) and are not included in the "best" estimate fits (see text).

5.5.3.4 Estimating fractionation factors

Of special significance in the analyses above are the slope values, as plotting $\delta^{30}Si_d$ against $\ln[Si_d]$ and f rearranges equations (3) and (4) such that the slope represents ε in both cases. The relevant equations are:

$$\delta^{30}Si_d = Y_c + \varepsilon \times \ln[Si_d] \quad (5)$$

for closed systems, where Y_c is the y-intercept and is set equal to $\delta^{30}Si_{d\text{-initial}} - (\varepsilon \times \ln[Si_d]_{initial})$; and

$$\delta^{30}Si_d = Y_o + \varepsilon \times f \quad (6)$$

for open systems, where the y-intercept is Y_o, equal to $\delta^{30}Si_{d\text{-initial}} - \varepsilon$.

The values for ε estimated here are -1.13 to -1.19 ‰ (closed) and -1.69 to -1.80 ‰ (open), which are in very good agreement with those found in laboratory and other field studies (*i.e.* De La Rocha *et al*. 1997, Varela *et al*. 2004). One of the first studies to investigate open/closed system dynamics and ε values in the field was done by Varela *et al.* (2004), in Southern Ocean waters north of the Ross Sea.

Results from that study are compared to those presented here in Figure 5.15. Here, 85 μM was used as a maximum initial concentration (section 5.5.3.3), while Varela *et al*. (2004) used 65 μM, based on their applicable study conditions. Both studies estimate greater ε based on open system dynamics, and are encouragingly consistent.

The good agreement between studies is evidence not only that the $\delta^{30}Si$ reported here are robust, but also that Si cycling in Ryder Bay is subject to the same dominant (biological) control as elsewhere in the Southern Ocean. As it was considered unlikely that physical conditions were consistent with a closed system throughout the study, Varela *et al*. (2004) suggest that the higher, open-system estimates may be more accurate. If this is the case, it follows that Southern Ocean diatoms may fractionate Si to a greater degree than those found in more temperate waters or used in laboratory studies, which have consistently shown -1.1 ‰ fractionation (Varela *et al*. 2004).

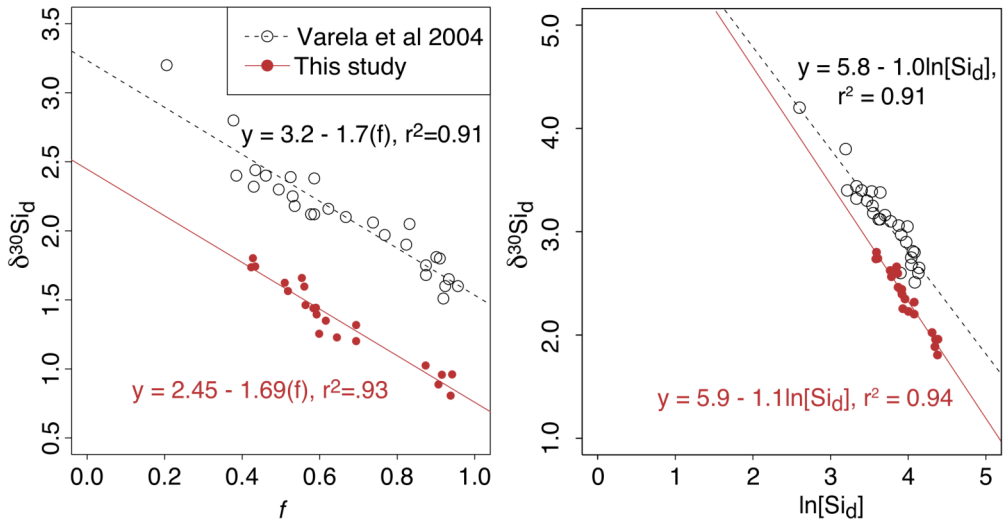

Figure 5.15: Isotopic signature versus ln(Si concentration) for (a) this study, and (b) this study in comparison to data from Varela *et al*. (2004). Here, we used 85 μM as a maximum initial concentration, while Varela *et al*. (2004) used 65 μM, based on their applicable study conditions. The concentrations taken as initial conditions determine the intercept, and thus the two data sets are not expected to overlap completely. The similarity in slope values (*i.e*. estimate of ε) is more important here.

5.5.3.5 Factors affecting biological fractionation of Si

5.5.3.5.1 Diatom speciation

Several studies have speculated on the impacts of species-specific effects on Si fractionation. There is no published evidence for species effects on Si fractionation; while there is some evidence for fractionation being similar between species (De La Rocha *et al*. 1997), to date only three species have been examined, and only in the laboratory. Diatom species-specific effects have been observed in the fractionation of other elements (*e.g*. C, N; Wong & Sackett 1978, Popp *et al*. 1999, Waser *et al*. 1998, Needoba *et al*. 2003). For C, this effect is related to the uptake of C. Differences in C transport across the cell membrane, for example use of different C concentration mechanisms, fractionates the C during the transport step. This results in an intracellular C pool with a depleted (lighter) isotopic signature relative to ambient seawater. Processes affecting the rate of C uptake such as cell size, shape, and growth rate, have thus all been shown to impact C fractionation (Popp *et al*. 1998). This effect is not isolated to surface water communities; sediment records have revealed a good correlation of C isotopic signatures with ratios of small:large diatoms (Crosta *et al*. 2005).

Uptake of Si offers a theoretical basis for species differences in fractionation of Si. Many studies have investigated Si uptake and frustule formation in diatoms (*reviewed in* Martin-Jézéquel *et al*. 2000, Hildebrand 2008), although such studies have not been coupled with studies of fractionation. It is well established that diatoms concentrate Si in silica deposition vesicles (SDVs), where [Si_d] can exceed saturation (2 mM) and is hypothesised to be kept in solution by complexation with organic molecules (Martin-Jézéquel *et al*. 2000, *and references therein*).

The mechanisms of diatom Si uptake remain only partially characterised. This is partly due to the unique Si uptake by diatoms, for which genetic analyses have found no homologous sequences in any other organism (Hildebrand 2008). Several different proteins mediate active transport of silicic acid across the cell membrane and into SDVs (Hildebrand 2008). Active transport responds to changes in Si requirements during different stages of the cell cycle, and is tightly regulated by

the cell. However, different species have been shown to accumulate very large internal Si pools, while others maintain small pools by actively taking in Si only during frustule synthesis (Chisholm *et al*. 1978). For one species, active transport occurs only at [Si_d] below 30 μM, with diffusion supplying Si above this threshold (Reuter & Morel 1981). These differences in Si uptake mechanisms between species could easily explain differences in fractionation, analogous to that seen for C and N. Additionally, use of different transport proteins could fractionate Si differently during the transport step. Genetic analyses have identified 97 transport-associated sequences in 45 species of a single genus, indicating a high degree of variability within transporter genes. In theory, Si polymerisation in SDVs and efflux could also affect the $\delta^{30}Si$ of the internal Si pool, but experimental work by Milligan *et al*. (2004) indicates that fractionation is associated with the uptake step.

As with C, cell size may also affect Si fractionation. Size effects have been observed in the oxygen isotopes of BSi, and a species-specific effect was inferred although not conclusively shown (Swann *et al*. 2007). While these findings clearly demonstrate that SiO_2 synthesis is affected by size (and potentially species composition), no investigation of the fractionation of Si was made, with the authors highlighting the need for further study of size- and species-coupled records to resolve potential problems with interpretation of sediment records (Swann *et al*. 2007).

Figure 5.14 shows a very strong relationship between Si use and $\delta^{30}Si_d$. However, there are some values that fall away from the line, which are highlighted in Figure 5.16. Looking at these points individually, some are associated with deeper waters (especially in the case of the unexpectedly light values, where preferential remineralisation of light BSi may contribute to the light signatures), but others occur in surface waters. Due to the negligible diatom uptake at depth and the confounding effect of Si dissolution and mixing with water of different Si utilisation, we do not consider the deep water values further. Several factors can affect isotopic fractionation, including temperature, sea-ice material, mixing, or species effects. Temperature is very unlikely to have a significant effect, owing to the relatively small temperature range here (~2 °C; and section 5.5.3.4.2). Sea-ice material is also an unlikely explanation, as little to no sea-ice was present in Ryder Bay during summer 2009. A negative excursion from the expected relationship can be explained

by mixing with lighter source water, as in the case of 50 – 100 m samples, but the positive excursions imply a greater degree of fractionation and cannot be explained by mixing. Therefore, this section explores the potential for diatom species composition to affect $\delta^{30}Si_d$ signatures.

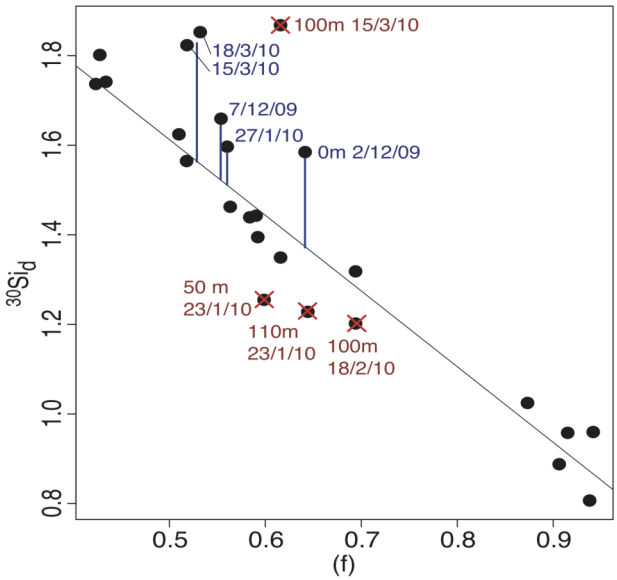

Figure 5.16: Isotopic signature of dissolved Si versus fraction remaining (f), and the regression based on open system dynamics. Points with dates highlight samples that fall away from the expected trend, and the extent of the offset is denoted by blue lines. Points in red (crosses) are deep waters and not considered further due to potential interference from remineralisation and mixing with partially used sources. Points labelled in blue are from 15 m depth, except where noted.

Of the surface samples, 5 are identified as having anomalously high $\delta^{30}Si_d$ relative to the expected relationship. The earliest and latest samples (December 2–7 2009 and March 15-18 2010, respectively) show the greatest difference from the expected trend, and another mid-season sample (Jan 27 2010) also has slightly heavy $\delta^{30}Si_d$. The difference between measured $\delta^{30}Si_d$ and expected $\delta^{30}Si_d$ ("residual") is shown versus time in Figure 5.17, and is compared to diatom assemblages to evaluate the likelihood of species-specific effects in enhancing the residual value.

Overall, the diatom community composition is relatively diverse, although the greatest residual $\delta^{30}Si_d$ values occur at the end of the season, when there is the greatest degree of dominance by a single diatom species (*Coscinodiscus*). High residual values are also found at the beginning of the sampling regime, when

Chaetoceros (Hyalochaeta subgenus) contributed a large proportion of diatom biomass. Factors potentially influencing ε pointed out by De La Rocha (2006) and linked to *Chaetoceros* spp. include the timing of productivity through the season, and variable life history strategies, such as resting spore formation. Cells of the subgenus *Hyalochaeta* are known to form *Chaetoceros* resting spores (CRS) early in the growing season in Antarctic waters, in response to low nutrient availability following high productivity (Leventer *et al*. 2002). These spores are heavily silicified (Garrison 1984), and it is possible that higher values of ε are associated with resting spore formation. In the samples collected here, early season abundances of CRS were over 3-fold higher on 7 Dec 2009 than in any other sample. While a full investigation of potential mechanisms is beyond the scope of this study, differences in ε between species could be related to changes in Si uptake during different stages of the cell cycle, interspecific differences in Si transporters, or contrasting uptake strategies.

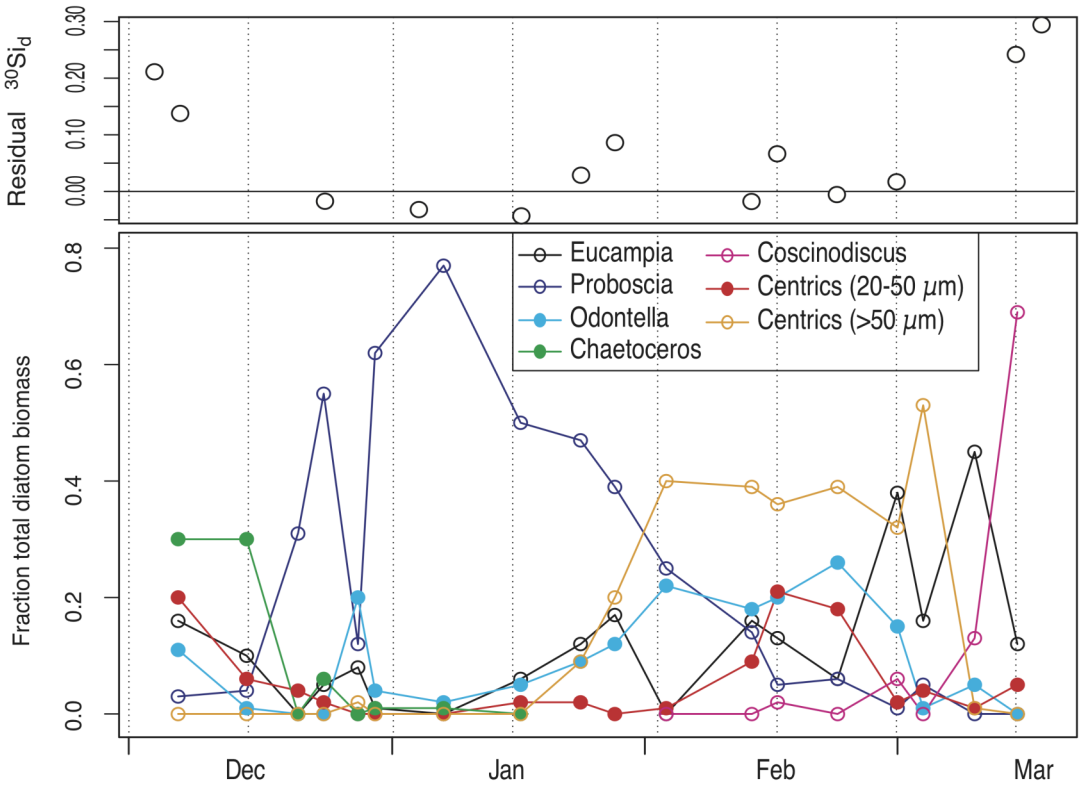

Figure 5.17: Time-series plot of residual $\delta^{30}Si_d$ (difference between measured and expected values) and key diatom species as fraction of total diatom biomass. Species shown are *Eucampia antarctica*, *Proboscia inermis*, *Odontella weissflogii*, *Chaetoceros* (*Hyalochaeta* subgenus), *Coscinodiscus* spp., and medium (20-50 μm) and large (>50 μm) discoid centric species.

Several other groups account for a moderate amount of biomass in all the anomalous samples, including *Proboscia inermis*, *Eucampia antarctica*, *Odontella weissflogii*, and medium to large (20 to >50 μm) centric species (see Chapter 4 for a full list of species included in this grouping). While we cannot rule out influences from these species, given that they are present at similar levels in samples where the residual is very small, it is unlikely that these species have any consistent or significant effect on community ε. Unfortunately, there are not many data points available with which to identify recurrent patterns of isotopic excursion. Thus, we can identify species that are candidates for having anomalous fractionation factors, but more investigation is needed to determine what those ε vales may be, and if speciation is indeed a main factor decoupling $\delta^{30}Si_d$ from Si use. Recent culture work suggests that one of the relationships suggested here - higher ε in *Chaetoceros* - is indeed the case, with preliminary laboratory results indicating that the fractionation factor is ~ -2.09 ‰ for *Chaetoceros brevis* (Sutton *et al*. *submitted*). This greater ε compared to average (-1.1 ‰) laboratory values would result in particulate matter isotopically lighter than expected, thus leaving the remaining Si_d more enriched (*i.e*. a heavier, or positive, residual) as seen here.

It should also be noted that while individual samples show small variations, the overall correlation seen here is extremely robust (Fig. 5.14). This initially suggests that in natural systems a species effect would be unlikely to be seen at the resolution typically available in sedimentary records. However, differential dissolution and preservation of diatom species may influence the overall relationship. *Chaetoceros* species, one of the groups suggested here (and in laboratory studies; Sutton *et al*. *submitted*) to have a greater ε than other species, is often dominant in Southern Ocean sediment cores (as CRS), particularly in coastal areas. In sediment traps from Ryder Bay, CRS accounted for 52% of diatom valves during the 2004 and 2005 summers, compared to an average 12% of surface water diatoms (by abundance; data from Carson 2008, Annett *et al*. 2010). Thus, disproportionate preservation of this species could bias sediment records. Higher proportions of CRS, with a lighter particulate $\delta^{30}Si$ signal than other species, might be interpreted as reflecting lower Si use if a species-specific ε is not considered. In agreement, model

results of Sutton *et al*. (*submitted*) suggest that diatom species variation can explain up to 67% of $\delta^{30}Si$ variation in core records.

Therefore we highlight here the need for more work to assess the impact of species variability on $\delta^{30}Si$ signatures in both water column and core samples, and the relationship between them. The results presented here are consistent with data from Sutton *et al.* (*submitted*) indicating that *Chaetoceros* spp. have higher ε values. This study also suggests that *Coscinodiscus* spp. may have high ε values, although at present no laboratory studies exist to test this hypothesis or suggest a physiological mechanism for higher fractionation of Si in this species.

5.5.3.5.2 Temperature:

While temperature was suggested as a potential factor affecting ε very early in the development of $\delta^{30}Si$ as a proxy, only one study has directly investigated this effect. De La Rocha *et al*. (1997) cultured three diatom species for ε assessment, at temperatures of 12, 15 and 22 °C. When consistent ε values (-1.1 to -1.5 ‰) were determined from a field study in Monterey Bay (De La Rocha *et al*. 2000) and further confirmed by similar values from a Southern Ocean study (-1.7 to -1.1 ‰; Varela *et al*. 2004), ε values were widely regarded as in agreement, and a mean value of -1.1 ‰ considered applicable to all ocean basins (De La Rocha *et al*. 2006). A Southern Ocean study by Cardinal *et al*. (2007) concluded that while temperature needed more careful investigation, other factors (primarily $[Si_d]$) explained more of the variation in $\delta^{30}Si_d$.

The estimated ε values found in this study are compared to those from other studies in Figure 5.18. It can be seen that in several Southern Ocean studies where temperatures are very low, highly negative values have been found for ε. In contrast, at temperatures >5 °C, ε is consistently > -1.1 ‰. This is unlikely to be an effect purely of temperature, as at oceanic temperatures, equilibrium fractionation of heavy stable isotopes is small, with kinetic (=biological, in this case) fractionation having a much greater effect on isotopic signatures (Schauble 2004). However, temperature could act on proteins involved in Si uptake, potentially affecting the fractionation associated with transport of Si across the cell membrane. As Cardinal *et al*. (2007)

point out, temperature gradients in field data are accompanied by gradients in many other parameters, making determination of causative relationships difficult or impossible. For example, changes in species assemblage composition or growth rates would likely vary along a temperature gradient, and could strongly affect ε.

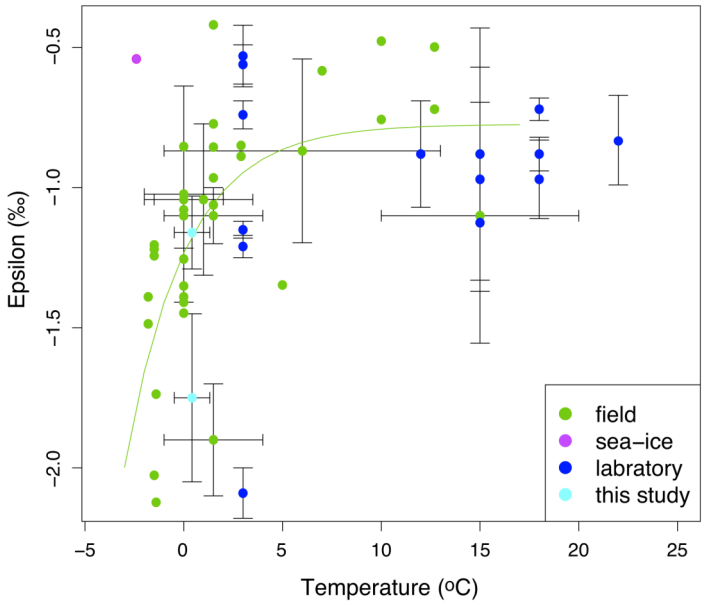

Figure 5.18: Estimated fractionation factors versus temperature for field (green; this study in aqua) and laboratory (blue) studies. Where both open and closed dynamics were used to estimate ε, both are shown. Data from Fripiat *et al*. (2011) measured in sea-ice brine is shown in purple. The curve is fitted using only field data (including this study). Data sources are: De La Rocha *et al*. (1997 and 2000); Varela *et al*. (2004), Cardinal *et al*. (2005 and 2007), Cavagna *et al*. (2011), Sutton *et al*. (submitted) and this study. Temperatures are for the surface mixed layer where available (shown as a range), for surface where depth profiles are available, or shown as a range where epsilon was calculated for a transect. Cardinal *et al*. (2007) estimated ε under conditions of both deep and shallow winter mixed layers, both estimates are shown here. Values from Cavagna *et al*. (2011) are not strictly ε, but rather the difference between the BSi isotopic value minus that of the dissolved phase, a parameter referred to as "$^{30}\Delta$Si". However, as the authors of the study note, this should give a value highly representative of ε under the assumption of synchronous processes, which they assess to be valid for the study area.

This review reveals a clear difference in the ranges of ε values above and below ~5 °C, with the largest range of estimated ε values found at the lower end of the oceanic temperature range. As the use of $\delta^{30}Si_d$ as a paleoproxy is most applicable in low-temperature, Southern Ocean waters due to high BSi production,

this suggests that further investigation is needed to constrain the influences on ε which may be significant in this area.

5.5.4 Silicon budgets in Ryder Bay estimated from isotopic data

Silicon isotopic measurements can also facilitate estimates of seasonal scale Si budgets based on overturning of the upper water column. Fripiat *et al*. (2011) used this approach near the Kerguelen Plateau to derive seasonal export values of 4.0 ± 0.7 mol Si m^{-2} y^{-1}. This approach assumes a one-dimensional model of homogenous WW that results from mixing of two end-members: Si-deplete surface waters following the summer bloom, and Si-rich deep water (UCDW in the case of Fripiat *et al*. 2011). The same model is employed here, using late-season (March) surface waters (depleted source) and deep Ryder Bay water (>200 m, below the WW layer; Si-rich source) as end members. A schematic illustrating the boxes used for Ryder Bay is shown in Fig. 5.19. Assuming that these water masses mix vertically (with negligible horizontal variation at the regional scale), the depletion experienced at the surface during the summer bloom will be balanced by resupply from depth at annual scales. Given the highly consistent [Si_d] observed from Ryder Bay into Marguerite Bay, this should be a valid approach for Ryder Bay. If steady state conditions apply at the annual scale (*i.e.* export equals supply), then this vertical supply should be equal to the annual production of BSi.

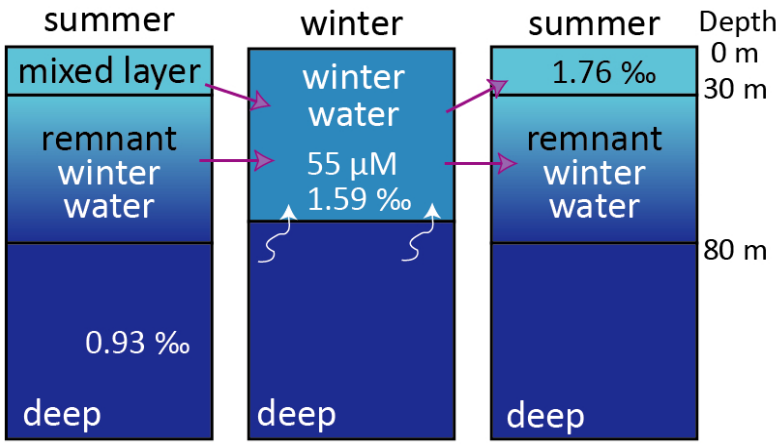

Figure 5.19: Schematic showing mixing of the water masses in the one-dimensional model used here to estimate seasonal Si demand. Values used in the model are indicated on each water mass: isotopic composition for all, and [Si_d] for WW.

For this one-dimensional model, average deep water values of 0.93 ‰ were used for the high-Si end-member. The first sample collected from the 2009 season was used as a best approximation of WW conditions (55 μM, 1.585 ‰), although there is evidence that there had been some BSi production (and hence Si_d drawdown) already, thus this should result in a low estimate of total BSi production. Samples from the period between 15 Feb and 1 March spanned the seasonal minimum in Si_d and were relatively consistent, thus $\delta^{30}Si_d$ from these samples were averaged to obtain values for the most deplete end-member (1.76 ‰). The fractional contribution of deep Si-rich waters to the WW layer (f_{DEEP}) was calculated following the equation in Fripiat *et al*. (2011):

$$f_{DEEP} = \frac{\delta^{30}Si_d^{WW} - \delta^{30}Si_d^{SML}}{\delta^{30}Si_d^{DW} - \delta^{30}Si_d^{SML}} \quad (7)$$

where superscripts refer to winter water (WW), summer mixed layer (SML) and deep waters (DW). The values for 2009 and equation (6) give an f_{DEEP} of 0.21. However, as noted this is likely to be a low estimate as some drawdown had already occurred prior to sampling, thus the true $\delta^{30}Si_d$ of WW is likely to be lower which would give a higher f_{DEEP}.

The depth of the winter mixed layer towards the end of winter was 80 m. Integrating $[Si_d]$ over the depth of this layer and multiplying by the proportion supplied from deeper waters gives a total Si contribution (from deep water to winter water) of 930 mmol Si m^{-2}. In the summer, depletion of Si occurred in the surface waters in mid-February, with low concentrations throughout the top 25 m that were sampled. CTD casts of temperature and density indicate that a pynocline was present at ~30 m, thus we consider the depth of the surface mixed layer subject to summer Si drawdown to be 30 m. Thus the proportion of WW entrained into the surface layer was 0.38 (= 30 m ÷ 80 m), or 350 mmol Si m^{-2}. Assuming that production of new BSi in the surface is equal to this supply term on an annual scale, BSi production for summer 2009 was ~350 mmol Si m^{-2}. However, as some accumulation of BSi had occurred prior to the onset of sampling, this figure will be an underestimate. Initial values of BSi were ~8 μM, somewhat less than the February peak of 10 μM. As the early productivity event was smaller in magnitude, it should represent less

production than during the February maximum. Thus, doubling the value of 350 mmol Si m^{-2} y^{-1} is a reasonable upper limit, and the true value is highly likely to fall within the resulting range of 350 – 700 mmol Si m^{-2} y^{-1}.

In order to contrast this intermediate-chl situation with more typical, high-chl seasons, the average Si_d drawdown based on long-term BAS data was taken from Clarke *et al*. (2008), where WW [Si_d] is ~65 μM, and summer minima occur in March, averaging 50 μM. These were converted to expected isotopic signatures, based on the regression of $\delta^{30}Si_d$ versus [Si_d] from 2009 data. These values, -1.13 and -1.43 ‰, respectively, were combined with the deep water values (assumed not to change annually) and give an f_{DEEP} value of 0.59. The average maximum winter MLD is 60 m for pre-2006 conditions (Clarke *et al*. 2008), giving an integrated WW Si content of 2300 mmol Si m^{-2}. As for 2009, temperature and density profiles were evaluated for March of 2005–2007 (summers 2004–2006) and the average depth of the pycnocline, above which [Si_d] is likely to be consistent, is 30 m (range 20 – 40 m). These values suggest that in typical high-chl years, supply of Si (and therefore new BSi production) is approximately 1200 mmol Si m^{-2} y^{-1}.

Thus the estimate of BSi production in the low-chl conditions of summer 2009 (350–700 mmol Si m^{-2} y^{-1}) represents a 40–70% reduction compared to the estimate for typical high-chl seasons (1200 mmol Si m^{-2} y^{-1}). This is very much in keeping with the estimated reductions in average [chl] (where summer 2009 was 45% lower than the 2004-2006 average) and integrated seasonal chl (50–55% lower in 2009 than high-chl years; Chapter 2). The estimated reduction in BSi is also consistent with the 40% lower C drawdown reported for 2009 compared to 2004 (Henley 2012). The overlapping ranges of reductions in both BSi and [chl] are highly consistent with the strong BSi:chl and BSi:POC relationship determined above (section 5.5.2) As recent studies have indicated a climate-induced shift towards lower chl conditions progressing southward along the WAP, this is expected to strongly impact Si cycling. The potential implications of changing Si use with productivity decline are explored in detail in Chapter 8.

5.6 Conclusions

The RaTS programme has shown that chl patterns in Ryder Bay are typical of coastal polar regions, with a period of elevated summer production relative to low winter levels. The data presented here show that these trends are also reflected in Si drawdown and BSi production. Importantly, a very tight relationship exists between interannual variability in [chl], POC and BSi concentrations (Fig. 5.11), highly consistent with diatom production being the primary determinant of overall productivity along the WAP. This relationship is robust between years, despite significantly higher relative contributions of non-diatom phytoplankton. Higher proportions of non-diatoms, including small absolute increases in biomass, occur during low-chl conditions, thus the absolute contributions from these phytoplankton is small and does not strongly impact the diatom-chl relationship. This finding is highly significant as it allows characterisation of diatom production and BSi dynamics based on chl or C data, in addition to highlighting the central role of diatoms in the WAP ecosystem.

Isotopic data reflect gradual, slight drawdown of Si, as seen in the enrichment of $\delta^{30}Si_d$ during the 2009 season. Lighter signatures are found at depth, consistent with lower utilisation and potentially some release of Si from remineralisation. Estimated biological fractionation factors are -1.16 ‰ and -1.75 ‰ for closed and open systems, respectively. Given the small range of values here we are unable to discriminate between the two systems, but both estimates are highly consistent with those found for a previous Southern Ocean study (Varela *et al*. 2004).

Diatom speciation can potentially affect ε, and the data presented here suggest that *Chaetoceros* species, especially their resting spores, and *Coscinodiscus* species may have ε values higher than the bulk community average. Within our ability to resolve Si isotopes, these effects are relatively minor relative to seasonal trends in surface waters. However, *Chaetoceros* species are often a significant component of sedimentary diatoms, such that complementary diatom assemblage data must be taken into account when interpreting sedimentary $\delta^{30}Si$ as a proxy for Si drawdown.

Combining Si concentrations and isotopic signatures with mixed layer depths, an annual Si budget of 350-700 mmol Si m^{-2} y^{-1} was derived for Ryder Bay for 2009. This is considerably lower (40–70% lower) than the estimate for conditions typical of high-chl years. The implications of a continued shift to a warmer climate resulting in low-chl conditions would be reduced BSi production, and thus reduced drawdown of Si_d in surface waters along the WAP.

5.7 References

ANNETT, A.L., CARSON, D.S., CROSTA, X., CLARKE, A. & GANESHRAM, R.S. 2010. Seasonal progression of diatom assemblages in surface waters of Ryder Bay, Antarctica. *Polar biology*, **33**, 13–29, 10.1007/s00300-009-0681-7.

BEUCHER, C.P. & AL, E. 2008. Sources and biological fractionation of Silicon isotopes in the Eastern Equatorial Pacific. *Geochimica et Cosmochimica Acta*, **72**, 3063–3073, 10.1016/j.gca.2008.04.021.

BEUCHER, C.P., BRZEZINSKI, M.A. & CROSTA, X. 2007. Silicic acid dynamics in the glacial sub-Antarctic: Implications for the silicic acid leakage hypothesis. *Global Geochemical Cycles*, **21**, 1–13, 10.1029/2006GB002746.

BEUCHER, C.P., BRZEZINSKI, M.A. & JONES, J.L. 2011. Mechanisms controlling silicon isotope distribution in the Eastern Equatorial Pacific. *Geochimica et Cosmochimica Acta*, **75**, 4286–4294, 10.1016/j.gca.2011.05.024.

BRZEZINSKI, M.A., PRIDE, C.J., FRANCK, V.M., SIGMAN, D.M., SARMIENTO, J.L. & MATSUMOTO, K. 2002. A switch from $Si(OH)_4$ to NO_3 depletion in the glacial Southern Ocean. *Geophysical Research Letters*, **29**, 10.1029/2001GL014349.

CARDINAL, D., ALLEMAN, L.Y., DEHAIRS, F., SAVOYE, N., TRULL, T.W. & ANDRÉ, L. 2005. Relevance of silicon isotopes to Si-nutrient utilization and Si-source assessment in Antarctic waters. *Global Biogeochemical Cycles*, **19**, 1–13, 10.1029/2004GB002364.

CARDINAL, D., SAVOYE, N., TRULL, T.W., DEHAIRS, F., KOPCZYNSKA, E.E., FRIPIAT, F., TISON, J.-L. & ANDRÉ, L. 2007. Silicon isotopes in spring Southern Ocean diatoms: Large zonal changes despite homogeneity among size fractions. *Marine Chemistry*, **106**, 46–62, 10.1016/j.marchem.2006.04.006.

CARSON, D.S. 2008. *Biogeochemical Dontrols on Productivity and Particle Flux in the Coastal Antarctic Sea Ice Environment*. PhD Thesis: University of Edinburgh.

CAVAGNA, A.J., FRIPIAT, F., DEHAIRS, F., WOLF-GLADROW, D., CISEWSKI, B., SAVOYE, N., ANDRÉ, L. & CARDINAL, D. 2011. Silicon uptake and supply during a Southern Ocean iron fertilization experiment (EIFEX) tracked by Si isotopes. *Limnology and Oceanography*, **56**, 147–160, 10.4319/lo.2011.56.1.0147.

CHISHOLM, S.W., AZAM, F. & EPPLEY, R.W. 1978. Silicic acid incorporation in the marine diatoms on light:dark cycles: use as an essay for phased cell division. *Limnology and Oceanography*, **23**, 518–529.

CLARKE, A., MEREDITH, M.P., WALLACE, M.I., BRANDON, M.A. & THOMAS, D.N. 2008. Seasonal and interannual variability in temperature, chlorophyll and macronutrients in northern Marguerite Bay, Antarctica. *Deep Sea Research Part II: Topical Studies in Oceanography*, **55**, 1988–2006, 10.1016/j.dsr2.2008.04.035.

CROSTA, X., CRESPIN, J., BILLY, I. & THER, O. 2005. Major factors controlling Holocene $\delta^{13}C$ orgchanges in a seasonal sea-ice environment, Adélie Land, East Antarctica. *Global Biogeochemical Cycles*, **19**, 10.1029/2004GB002426.

DEMAREST, M.S., BRZEZINSKI, M.A. & BEUCHER, C.P. 2009. Fractionation of silicon isotopes during biogenic silica dissolution. *Geochimica et Cosmochimica Acta*, **73**, 5572–5583, 10.1016/j.gca.2009.06.019.

DUCKLOW, H.W., FRASER, W., KARL, D.M., QUETIN, L.B., ROSS, R.M., SMITH, R.C., STAMMERJOHN, S.E., VERNET, M. & DANIELS, R.M. 2006. Water-column processes in the West Antarctic Peninsula and the Ross Sea: Interannual variations and foodweb structure. *Deep Sea Research Part II: Topical Studies in Oceanography*, **53**, 834–852, 10.1016/j.dsr2.2006.02.009.

ELLWOOD, M.J., WILLE, M. & MAHER, W. 2010. Glacial silicic acid concentrations in the Southern Ocean. *Science*, **330**, 1088–1091, 10.1126/science.1194614.

FRIPIAT, F., CAVAGNA, A.-J., SAVOYE, N., DEHAIRS, F., ANDRÉ, L. & CARDINAL, D. 2011. Isotopic constraints on the Si-biogeochemical cycle of the Antarctic Zone in the Kerguelen area (KEOPS). *Marine Chemistry*, **123**, 11–22, 10.1016/j.marchem.2010.08.005.

GARRISON, D.L. 1984. Planktonic diatoms. *In* Steindinger, K.A., *ed. Marine Plankton Life Cycle Strategies*. Boca Raton: CRC Press Inc., 1–17.

GEORG, R.B., REYNOLDS, B.C., FRANK, M. & HALLIDAY, A.N. 2006. New sample preparation techniques for the determination of Si isotopic compositions using MC-ICPMS. *Chemical Geology*, **235**, 95–104, 10.1016/j.chemgeo.2006.06.006.

GNANADESIKAN, A. & TOGGWEILER, J.R. 1999. Constraints placed by silicon cycling on vertical exchange in general circulation models. *Geophysical Research Letters*, **26**, 1865–1868.

HENLEY, S.F. 2012. *Climate-induced changes in carbon and nitrogen cycling in the rapidly warming Antarctic coastal ocean*. PhD Thesis: University of Edinburgh.

HILDEBRAND, M. 2008. Diatoms, Biomineralization Processes, and Genomics. *Chemical Reviews*, **108**, 4855–4874, 10.1021/cr078253z.

JACOBS, S.S. 1991. On the nature and significance of the Antarctic Slope Front. *Marine Chemistry*, **35**, 9–24, 10.1016/S0304-4203(09)90005-6.

KARSH, K.L., TRULL, T.W., LOUREY, M.J. & SIGMAN, D.M. 2003. Relationship of nitrogen isotope fraction to phytoplankton size and iron availability during the Southern Ocean Iron Release Experiment (SOIREE). *Limnology and Oceanography*, **48**, 1058–1068.

KLINCK, J.M. 1998. Heat and salt changes on the continental shelf west of the Antarctic Peninsula between January 1994 and January 1994. *Journal of Geophysical Research*, **103**, 7617–7636.

LA ROCHA, DE, C.L. 2006. Opal-based isotopic proxies of paleoenvironmental conditions. *Global Biogeochemical Cycles*, **20**, 10.1029/2005GB002664.

LA ROCHA, DE, C.L., BRZEZINSKI, M.A. & DENIRO, M.J. 2000. A first look at the distribution of the stable isotopes of silicon in natural waters. *Geochimica et Cosmochimica Acta*, **64**, 2467–2477.

LA ROCHA, DE, C.L., BRZEZINSKI, M.A. & DENIRO, M.J. 1997. Fractionation of silicon isotopes by marine diatoms during biogenic silica formation. *Geochimica et Cosmochimica Acta*, **61**, 5051–5056.

LA ROCHA, DE, C.L., BRZEZINSKI, M.A., DENIRO, M.J. & SHEMESH, A. 1998. Silicon-isotope composition of diatoms as an indicator of past oceanic change. *Nature*, **395**, 680–683.

LEVENTER, A., DOMACK, E., BARKOUKIS, A., MCANDREWS, B. & MURRAY, J. 2002. Laminations from the Palmer Deep: A diatom-based interpretation. *Paleoceanography*, **17**, 8002, 10.1029/2001PA000624.

MARCHETTI, A. & CASSAR, N. 2009. Diatom elemental and morphological changes in response to iron limitation: a brief review with potential paleoceanographic applications. *Geobiology*, **7**, 419–431, 10.1111/j.1472-4669.2009.00207.

MARTIN-JÉZÉQUEL, V., HILDEBRAND, M. & BRZEZINSKI, M.A. 2000. Silicon metabolism in diatoms: Implications for growth. *Journal of Phycology*, **36**, 821.

MARTINSON, D.G., STAMMERJOHN, S.E., IANNUZZI, R.A., SMITH, R.C. & VERNET, M. 2008. Western Antarctic Peninsula physical oceanography and spatio-temporal variability. *Deep-Sea Research II*, **55**, 1964–1987, 10.1016/j.dsr2.2008.04.038.

MATSUMOTO, K., SARMIENTO, J.L. & BRZEZINSKI, M.A. 2002. Silicic acid leakage from the Southern Ocean: A possible explanation for glacial atmospheric pCO_2. *Global Biogeochemical Cycles*, **16**, 1–23, 10.1029/2001GB001442.

MEREDITH, M.P., RENFREW, I.A., CLARKE, A., KING, J.C. & BRANDON, M.A. 2004. Impact of the 1997/98 ENSO on upper ocean characteristics in Marguerite Bay, western Antarctic Peninsula. *Journal of Geophysical Research*, **109**, 10.1029/2003JC001784.

MILLIGAN, A.J., VARELA, D.E., BRZEZINSKI, M.A. & MOREL, F.M.M. 2004. Dynamics of silicon metabolism and silicon discrimination in a marine diatom as a function of pCO_2. *Limnology and Oceanography*, **49**, 322–329.

NEEDOBA, J.A., WASER, N.A., HARRISON, P.J. & CALVERT, S.E. 2003. Nitrogen isotope fractionation in 12 species of marine phytoplankton during growth on nitrate. *Marine Ecology Progress Series*, **255**, 81–91.

NELSON, D.M., BRZEZINSKI, M.A., SIGMAN, D.E. & FRANCK, V.M. 2001. A seasonal progression of Si limitation in the Pacific sector of the Southern Ocean. *Deep-Sea Research II*, **48**, 3973–3995.

NELSON, D.M., TRÉGUER, P., BRZEZINSKI, M.A., LEYNAERT, A. & QUÉGUINER, B. 1995. Production and dissolution of biogenic silica in the ocean: Revised global estimates, comparison with regional data and relationship to biogenic sedimentation. *Global Biogeochemical Cycles*, **9**, 359–372.

PICHEVIN, L., GANESHRAM, R.S., BEN C REYNOLDS, PRAHL, F., PEDERSEN, T.F., THUNELL, R. & MCCLYMONT, E.L. 2012. Silicic acid biogeochemistry in the Gulf of California: Insights from sedimentary Si isotopes. *Paleoceanography*, **27**, 1–14, 10.1029/2011PA002237.

PICHEVIN, L.E., REYNOLDS, B.C., GANESHRAM, R.S., CACHO, I., PENA, L., KEEFE, K. & ELLAM, R.M. 2009. Enhanced carbon pump inferred from relaxation of nutrient limitation in the glacial ocean. *Nature*, **459**, 1114–1117, 10.1038/nature08101.

POPP, B.N., LAWS, E.A., BIDIGARE, R.R., DORE, J.E., HANSON, K.L. & WAKEHAM, S.G. 1998. Effect of phytoplankton cell geometry on carbon isotopic fractionation. *Geochimica et Cosmochimica Acta*, **62**, 69–77.

POPP, B.N., TRULL, T., KENIG, F., WAKEHAM, S.G., RUST, T.M., TILBROOK, B., GRIFFITHS, F.B., et al. 1999. Controls on the carbon isotopic composition of Southern Ocean phytoplankton. *Global Biogeochemical Cycles*, **13**, 827–843.

RAGUENEAU, O., SAVOYE, N., DEL AMO, Y., COTTEN, J., TARDIVEAU, B. & LEYNAERT, A. 2005. A new method for the measurement of biogenic silica in suspended matter of coastal waters: using Si:Al ratios to correct for the mineral interference. *Continental Shelf Research*, **25**, 697–710, 10.1016/j.csr.2004.09.017.

REYNOLDS, B.C. 2009. Modeling the modern marine $\delta^{30}Si$ distribution. *Global Biogeochemical Cycles*, **23**, 10.1029/2008GB003266.

REYNOLDS, B.C., FRANK, M. & HALLIDAY, A.N. 2006. Silicon isotope fractionation during nutrient utilization in the North Pacific. *Earth and Planetary Science Letters*, **244**, 431–443, 10.1016/j.epsl.2006.02.002.

RINTOUL, S.R. & TRULL, T.W. 2001. Seasonal evolution of the mixed layer in the Subantarctic Zone south of Australia. *Journal of Geophysical Research*, **106**, 31447–31462.

RUETER, J.G., Jr & MOREL, F.M.M. 1981. The interaction between zinc deficiency and copper toxicity as it affects the silicic acid uptake mechanisms in *Thalassiosira pseudonana*. *Limnology and Oceanography*, **26**, 67–73.

SARMIENTO, J.L. & TOGGWEILER, J.R. 1984. A new model for the role of the oceans in determining atmospheric pCO_2. *Nature*, **308**, 621–624.

SARMIENTO, J.L., GRUBER, N., BRZEZINSKI, M.A. & DUNNE, J.P. 2004. High-latitude controls of thermocline nutrients and low latitude biological productivity. *Nature*, **427**, 56–60.

SARMIENTO, J.L., SIMEON, J., GNANADESIKAN, A., GRUBER, N., KEY, R.M. & SCHLITZER, R. 2007a. Deep ocean biogeochemistry of silicic acid and nitrate. *Global Biogeochemical Cycles*, **21**, 10.1029/%5D2006GB002720.

SARMIENTO, J.L., SIMEON, J., GNANADESIKAN, A., GRUBER, N., KEY, R.M. & SCHLITZER, R. 2007b. Deep ocean biogeochemistry of silicic acid and nitrate. *Global Biogeochemical Cycles*, **21**, 10.1029/2006GB002720.

SCHAUBLE, E.A. 2004. Applying Stable Isotope Fractionation Theory to New Systems.

Reviews in Mineralogy and Geochemistry, **55**, 65–111.

SUTTON, J.N., VARELA, D.E., BRZEZINSKI, M.A. & BEUCHER, C.P. *In review*. Species-dependent silicon isotope fractionation by polar and sub-polar marine diatoms. *Geochimica et Cosmochimica Acta*.

SWANN, G.E.A., LENG, M.J., SLOANE, H.J., MASLIN, M.A. & ONODERA, J. 2007. Diatom oxygen isotopes: Evidence of a species effect in the sediment record. *Geochemistry Geophysics Geosystems*, **8**, 10.1029/2006GC001535.

TRÉGUER, P., NELSON, D.M., VAN BENNEKOM, A.J., DEMASTER, D.J., LEYNAERT, A. & QUÉGUINER, B. 1995. The silica balance in the world ocean: A reestimate. *Science*, **268**, 375–379.

VARELA, D.E., PRIDE, C.J. & BRZEZINSKI, M.A. 2004. Biological fractionation of silicon isotopes in Southern Ocean surface waters. *Global Biogeochemical Cycles*, **18**, 10.1029/2003GB002140.

WASER, N.A., YIN, K., YU, Z., TADA, K., HARRISON, P.J., TURPIN, D.H. & CALVERT, S.E. 1998. Nitrogen isotope fractionation during nitrate, ammonium and urea uptake by marine diatoms and coccolithophores under various conditions of N availability. *Marine Ecology Progress Series*, **169**, 29–41.

WHITWORTH, T.I., ORSI, A.H., KIM, S.-J. & NOWLIN, W.D. 1998. Water masses and mixing near the Antarctic slope front. *Antarctic Research Series*, **75**, 1–27.

WISCHMEYER, A.G., LA ROCHA, DE, C.L., MAIER-REIMER, E. & WOLF-GLADROW, D.A. 2003. Control mechanisms for the oceanic distribution of silicon isotopes. *Global Biogeochemical Cycles*, **17**, 1–12, 10.1029/2002GB002022.

WONG, W.W. & SACKETT, W.M. 1978. Fractionation of stable carbon isotopes by marine phytoplankton. *Geochimica et Cosmochimica Acta*, **42**, 1809–1815.

YOOL, A. & TYRELL, T. 2003. Role of diatoms in regulating the ocean's silicon cycle. *Global Biogeochemical Cycles*, **17**, 10.1029/2002GB002018.

Chapter 6: Radium isotopes as tracers of sediment inputs and mixing rates

6.1 Abstract

In the western Antarctic Peninsula region, micronutrient injection facilitates strong plankton blooms that support productive food webs, unlike large areas of the low-productivity Southern Ocean. Naturally-occurring radioisotopes of radium were used to constrain rates of chemical fluxes into Ryder Bay, and hence to evaluate possible sources of sediment-derived micronutrients and estimate sediment-ocean mixing rates. We present the first coupled, short-lived radium isotope (^{223}Ra and ^{224}Ra) measurements from Antarctic waters, both present at very low activities (mean 0.155 and 3.21 dpm m^{-3}, respectively), indicating much lower radium inputs than in other coastal environments. Longer-lived ^{228}Ra activity was also lower than existing near-shore values, but higher than open ocean waters, indicating some degree of coastal radium input on timescales exceeding the week-to-month range reflected by ^{223}Ra and ^{224}Ra. Using a simple diffusion model along a shore to mid-bay transect, "effective" horizontal eddy diffusivity was 0.22 and 0.83 m^2 s^{-1} from ^{223}Ra and ^{224}Ra, respectively, much lower than already-low mixing estimates for the Southern Ocean. Significant radium enrichment and much faster mixing (18 m^2 s^{-1}) was found near a marine-terminating glacier and consequently any sediment-derived micronutrient inputs in this location are more likely dominated by glacial processes than groundwater, land runoff, or marine sediment sources.

The results and discussion presented in this chapter have been published as an original article in the journal Antarctic Science. The manuscript is provided in Appendix A6.1.

6.2 Introduction

The WAP, a region of high phytoplankton production supporting a large and productive food web, is currently undergoing the most pronounced recent rapid

regional warming in the southern hemisphere (Vaughan e*t al*. 2003). Average air temperature on the WAP has increased at a rate of 3.6 ± 1.4 °C per century, several times the global average (Vaughan *et al.* 2003). The majority of glaciers in the region are retreating, and the rate of this retreat is accelerating (Cook *et al*. 2005). At sea, an increase of >1 °C has been recorded in the surface waters in summer, decreasing to near zero at 100 m depth (Meredith & King 2005). There has also been a significant reduction in sea-ice duration, with trends of later advance and earlier retreat in the Marguerite Bay area (Stammerjohn *et al*. 2008).

Unique in its proximity to the Antarctic Circumpolar Current (ACC), the WAP is subject to frequent incursions of circumpolar deep water (CDW), which transports heat, salt and nutrients (Klinck 1998) onto the shelf, thereby influencing water mass properties and productivity along the WAP. Martinson *et al*. (2008) have shown increasing trends in ocean heat content over the shelf, consistent with an increase in frequency of CDW incursions, believed to be at least partially driven by changes in atmospheric circulation (Martinson *et al*. 2008, Meredith *et al*. 2010). The observed changes in glacial retreat are also consistent with warmer waters, as it has been shown that the temperature of marine waters can significantly impact the melt rates of marine-terminating glaciers (Shepherd *et al*. 2004; Pritchard *et al.* 2012).

From a biological perspective, a key influence on primary productivity along the WAP is stratification, as a more stable water column provides higher average light levels to cells in near-surface waters, thus encouraging phytoplankton growth (Garibotti *et al*. 2003, Vernet *et al*. 2008, Venables et al. 2012). Changes in freshwater inputs, heat content, and the associated changes in sea-ice cover can affect stratification, and therefore productivity in this region. Indeed, phytoplankton dynamics already show changes linked to sea-ice cover and stratification in both the northern and southern regions of the WAP (Montes-Hugo *et al*. 2009). In addition to light, growth of phytoplankton in Southern Ocean waters can be further limited by availability of micronutrients, primarily iron (Hoffmann *et al.* 2008; Gall *et al.* 2001). Freshwater inputs (surface run-off, glacial meltwater and groundwater) are clearly important to biological production due to their role in stratification, but are also a potential source of micronutrients such as iron (Edwards & Sedwick 2001,

Raiswell 2011), an element known to limit phytoplankton productivity in large regions of the Southern Ocean (for a review, *see* Boyd & Ellwood 2010).

To address these topics, this study measured radium (Ra) in seawater at a coastal Antarctic site at the WAP. Radium is produced continuously in both continental and deep sea sediments by the decay of the particle reactive element thorium (Th). Radium occurs naturally in seawater as four radioisotopes: the short-lived isotopes ^{223}Ra and ^{224}Ra (half-life ($t_{1/2}$) = 11.435 days and $t_{1/2}$ = 3.66 days, respectively), and the long-lived ^{226}Ra and ^{228}Ra ($t_{1/2}$ = 1600 years and $t_{1/2}$ = 5.75 years, respectively). The ability to measure short-lived ^{223}Ra and ^{224}Ra has been made viable by the development of the Radium Delayed Coincidence Counter (RaDeCC), a radon (Rn) detection system pioneered by Giffin *et al.* (1963) and adapted for Ra isotopes by Moore & Arnold (1996). This sensitive and transportable technique allows measurement of ^{223}Ra and ^{224}Ra in the field, as well as activity of progenitor radionuclides (actinium (^{227}Ac) and ^{224}Ra$_{supported}$ (^{228}Th) respectively) following the decay of the short-lived isotopes.

The information obtained by RaDeCC analysis covers isotopes of different half-lives, as well as of different sources. The concentration of Ra isotopes is highest at sediment margins due to the Th source, and decreases away from these margins due to dilution and radioactive decay. In the case of ^{227}Ac, the dominant source is deep water, open ocean sediments, where low sediment accumulation rates and deep overlying water columns lead to higher accumulation of the parent isotope than in shallow shelf settings (Geibert *et al.* 2002). The different sources and decay rates can be exploited to detect and differentiate multiple inputs (*e.g.* for different groundwater reservoirs) as well as to estimate rates of the processes affecting these inputs on different time scales. In the last two decades, the short-lived isotopes of Ra have been used in the Southern Ocean to investigate coastal mixing rates and eddy diffusivity coefficients (Charette *et al.* 2007), water mass pathways (van Beek *et al.* 2008), iron inputs (Dulaiova *et al.* 2009) and terrigenous material from icebergs (Shaw *et al.* 2011).

The aim of this study was to use Ra isotopes to further constrain the sources of surface water in Ryder Bay and the extent to which they interact with sediments, while establishing a baseline against which any future change in Ra distributions

may be interpreted. These Ra radioisotopic data are the most southerly reported to date (67°34.02'S). The relative importance of surface water sources, marine and glacial sediment interaction, and the timescales on which mixing processes occur will aid in understanding not only oceanographic processes and local circulation patterns, but also trace metal availability in a region of very rapid change (Wallace *et al.* 2008, Meredith *et al.* 2010).

6.3 Radium and Radium Delayed Coincidence Counter (RaDeCC) principles

The RaDeCC system exploits the different half-lives of the decay products of ^{223}Ra and ^{224}Ra. Radium from seawater samples is collected on manganese-coated fibre, and the Rn (both ^{219}Rn and ^{220}Rn) produced via Ra decay is swept into a zinc-sulfide coated scintillation tube by a circulating flow of helium (He). A photomultiplier tube attached to the scintillation cell detects emission of alpha particles as ^{219}Rn decays to ^{215}Po and ^{220}Rn decays to ^{216}Po. The two Po isotopes also emit alpha particles, and have different half lives (^{215}Po: $t_{1/2}$ = 1.8 ms and ^{216}Po: $t_{1/2}$ = 150 ms), such that the detection of two decay events within 5.6 ms can be attributed to ^{219}Rn/^{215}Po, while two events separated by an interval of 25 – 600 ms can be attributed to ^{220}Rn/^{216}Po. Thus each "pair" of decay events is counted in either the 219 or 220 channel based on the time lapse between them (Moore & Arnold 1996). Corrections are made for chance coincidences (Giffin *et al.* 1963), cross-talk between channels, and the small fraction (~2.55%) of ^{216}Po decay events which can occur during the time period counted as ^{215}Po decay (Moore & Arnold 1996). Corrected ^{219}Rn and ^{220}Rn counts can then be converted to ^{223}Ra and ^{224}Ra activities by accounting for background counts (typically 0.001 - 0.007 and 0.03 - 0.07 counts per minute for 219 and 220, respectively; Garcia-Solsona *et al.* 2008) and the efficiency of the RaDeCC system, which is monitored by frequent measurement of standards, interferences and decay.

In addition to being sufficiently portable to use in the field, the RaDeCC system has the advantage of measuring activities of the parent nuclides (^{227}Ac for ^{223}Ra; ^{228}Ra and ^{228}Th for ^{224}Ra) after sufficient decay of the short-lived daughters. This allows calculation of unsupported or "excess" (^{223}Ra$_{ex}$ and ^{224}Ra$_{ex}$) activity at

the time of sampling, in addition to the activity supported by the parents (^{227}Ac and ^{228}Th), thus resolving a quartet of isotopic measurements on a single sample.

6.4 Methods

6.4.1 Sample collection

Samples for RaDeCC analysis were collected from a small boat using a 12 V impeller pump attached to acid-clean (10% HCl) silicon tubing. The tubing was rinsed with at least 25 L of seawater before collecting an appropriate volume (110 – 180 L) of seawater from 10 m depth into clean 20 L containers. Five samples were collected on 13 and 14 February 2010, along a transect from shore to the RaTS site, which is located approximately 2 km from shore in Ryder Bay (station 5; Fig. 6.1). Mixing rates derived from RaDeCC measurements along this line were used to assess the potential of sediment-derived nutrient sources for near-surface productivity at this site. Following this transect, four additional samples were collected on 25 February 2010, in order to investigate potential input signals from nearby islands and Sheldon Glacier. Sampling transects are shown in Fig. 6.1.

6.4.2 Sample processing

Radium radioisotopes were concentrated from seawater by slowly (~200 mL min^{-1}; van Beek *et al*. 2007) passing the samples through a column filled with ~20 g loosely-packed MnO_2-impregnated acrylic fibre (~20 g dry; Mn-fibre), which quantitatively adsorbs Ra from seawater (97% extraction for samples up to 400 L; Moore 2008). The Mn-fibre was then rinsed with Milli-Q water (Millipore systems) to remove salts and particles. Excess water was removed by squeezing, and samples were weighed to ensure correct moisture content. Moisture can trap Rn on the fibre and prevent accurate detection of decay events, therefore a moisture to fibre ratio of 0.3 – 1 g_{H2O}: g_{fibre} was maintained in order to maximize movement of Rn from the columns to the counting chambers (Sun & Torgersen 1998).

6.4.3 Sample analysis

Columns were then introduced into the RaDeCC system, which had been purged with air for ~30 min and He for >2 min. Helium was circulated through the

column and scintillation counter for a further 2 min at a flow rate of ~6 L min^{-1}, then the circuit was closed and allowed to equilibrate for 10 min. The short-lived ^{219}Rn ($t_{1/2}$ = 4 s), produced from decay of ^{223}Ra, is carried from the Mn-fibre into the scintillation chambers where the majority of it decays during the 24.6 s residence time of gas in the 1.1 L chamber (Garcia-Solsona *et al.* 2008). The 10 min delay before counting begins allows uniform distribution of the longer-lived ^{220}Rn (product of ^{224}Ra decay, $t_{1/2}$ = 55 s) throughout the system. Counting was performed for as long as possible whilst still allowing all samples from a single sampling event to be analyzed within a 2-day period. Counting time averaged 1000 min per sample, and in all cases exceeded 400 min.

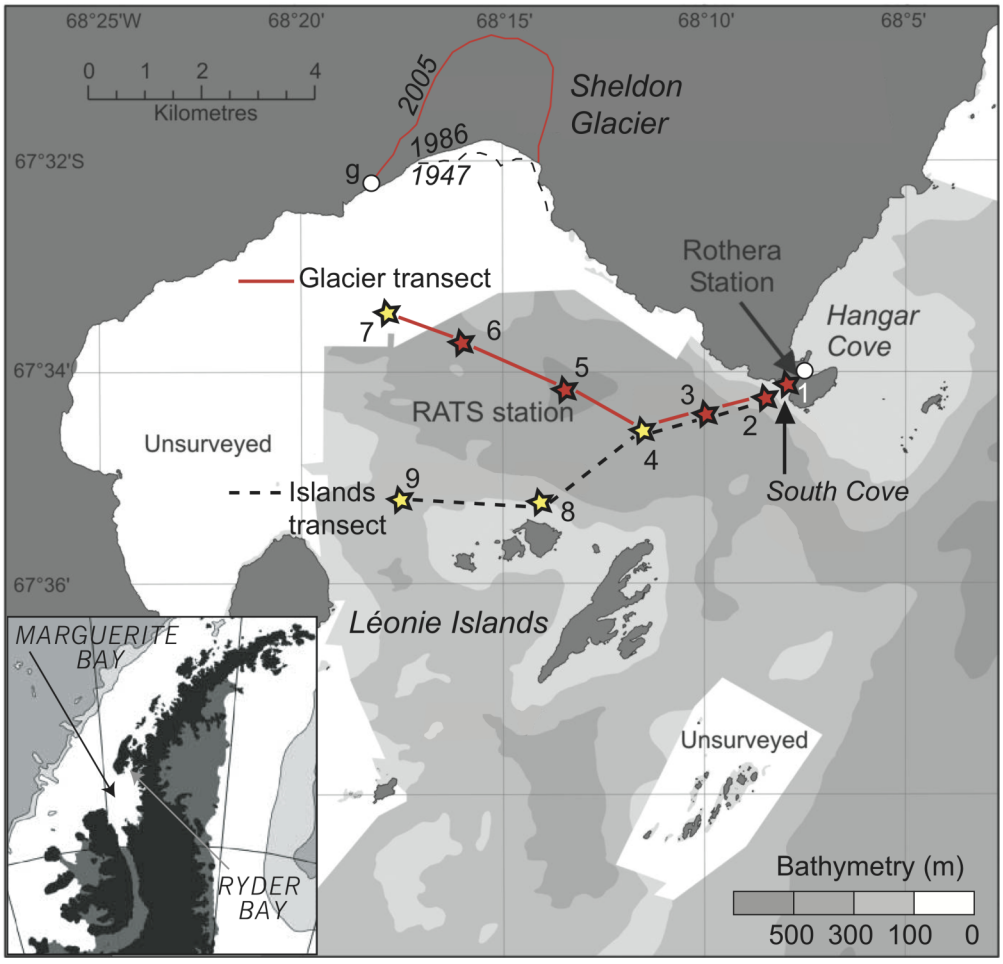

Figure 6.1: Station numbers and locations in Ryder Bay. Red stations sampled Feb 13/14, yellow stations sampled Feb 25. Maximum depth is 520m, (at station 5, which is also the RaTS monitoring site). Station 1 is within South Cove, and is adjacent to the British Antarctic Survey's Rothera Research Station (labelled). Also shown is the edge of Sheldon Glacier, and the point used for glacially-derived mixing rates (denoted by "g").

6.4.4 Detector efficiency and standards

The final 219 and 220 counts were corrected as described above and converted to ^{223}Ra and ^{224}Ra activities in decays per minute (dpm) using the efficiencies measured for each scintillation chamber (~ 0.35 and 0.60, respectively). Detector efficiency was monitored using standards obtained from the International Atomic Energy Agency (Monte Carlo, Monaco) and prepared at LEGOS, OMP (Toulouse, France). For ^{223}Ra, a standard solution of the parent isotope ^{227}Ac was adsorbed to Mn-fibre with a final activity of 10.49 dpm. A second standard of ^{232}Th (in equilibrium with ^{228}Ra) was prepared with a final activity of 12.20 dpm. Both standards were prepared using Ra-free seawater (Dimova *et al.* 2008; Moore 2008; Scholten *et al*. 2010) and were allowed to adsorb to the Mn-fibre overnight. After removal of the fibre into columns, the remaining solutions were acidified (HCl) to solubilize any Ac or Th adsorbed to the container walls. Solutions were neutralized using ammonia and immediately passed over the Mn-fibre three times to ensure complete transfer of Ac and Th from solution to the fibre.

Standards were measured several times throughout the duration of the study to monitor detector efficiency. Problems have been reported with decay of ^{227}Ac standards (≤ 12%; Scholten *et al*. 2010) in the first ~50 days after preparation, although we were unable to assess this for our standards due to the timing of preparation and measurement. As this would affect only absolute (not relative) activities and are within the error reported here, this effect is not considered further.

All samples were measured at least 4 times in order to correct for interference from longer-lived Ra isotopes. Initial counting was done as soon after collection as possible, and samples were re-counted after 8, 21, and >90 days to correct for interference from ^{224}Ra, ^{224}Ra supported by ^{228}Th, and ^{227}Ac, respectively.

6.4.5 Error calculation

Estimation of error followed the equations of Garcia-Solsona *et al.* (2008), with minor changes to the error propagation in correcting for long-lived isotopes. In our case, the third and fourth counts were used to estimate ^{228}Th and ^{277}Ac, respectively. Interference from these sources was assumed to be constant and

therefore not corrected for time since sample collection. Ingrowth of ^{228}Th from ^{228}Ra was not accounted for, as this contributed < 1% of ^{228}Th in all cases. These long-lived interferences were subtracted from the time-corrected first counts according to the formula:

$$A_{ex} = A_1 \cdot e^{-\lambda t} - A_{3/4} \quad (1)$$

where A_{ex} is the excess activity (at the time of collection), A_1 is the activity measured in the first count, $A_{3/4}$ is the activity measured during the third or fourth count, λ is the decay constant of ^{223}Ra or ^{224}Ra, and t is the time between collection and the first count. Error combination followed the standard formula

$$\Delta A_{ex}^2 = (\Delta A_1 \cdot e^{-\lambda t})^2 + \Delta A_{3/4}^2 \quad (2)$$

where Δ denotes the absolute error of each term. Note that reported ^{227}Ac has not been corrected for activity supported by ^{231}Pa; assuming ^{231}Pa to be ~0.1 dpm m^{-3} (determined by Geibert *et al.* (2002) for surface waters south of the Antarctic Polar Front), the corrected ^{227}Ac$_{ex}$ would be 0.1 dpm m^{-3} less than the numbers shown here.

6.4.6 Gamma counting

Once the analyses using RaDeCC were performed, the Mn-fibers were ashed (16 h at 820°C) and transferred into sealed vials for gamma counting, following Charette *et al*. (2001). Radium isotopes adsorbed on MnO_2 ash were analyzed using low-background gamma-ray spectrometry at the underground laboratory of Ferrières (LAFARA, for LAboratoire de mesure des FAibles RAdioactivités) located in the French Pyrénées, 100 km from Toulouse (van Beek *et al*. 2010; van Beek *et al*. *in press*). Radium-228 activities were determined using the 338, 911 and 969 keV peaks of ^{228}Ac. Uncertainties reported for ^{228}Ra activities are errors due to counting statistics (one standard deviation).

6.5 Results

6.5.1 Oceanographic context

Seasonal records of water column conditions are available for station 5 (the RaTS Site) as part of the RaTS monitoring program (British Antarctic Survey,

Cambridge, UK). Upper layer temperature and salinity data indicate a typical seasonal progression from well-mixed wintertime waters in November (with temperatures less than 0 °C and comparatively high salinity) to more stratified summer conditions characterized by warmer surface waters (>1 °C) and significant freshening due to meltwater input (salinity as low as ~33.1; Fig. 6.2). Beneath the summertime surface layer, the WW layer is apparent as a temperature minimum at ~100 m depth, with properties largely dictated by those of the winter mixed layer.

From these temperature and salinity records, it can be seen that physical conditions between the two sampling events were very similar, implying that no significant upwelling or mixing events occurred (such as might be expected during *e.g.* strong weather events; Wallace *et al.* 2008), and that any lateral advection occurred within a relatively uniform water mass. We therefore interpret stations from both transects on the assumption that differences chiefly reflect steady-state diffusive and advective processes.

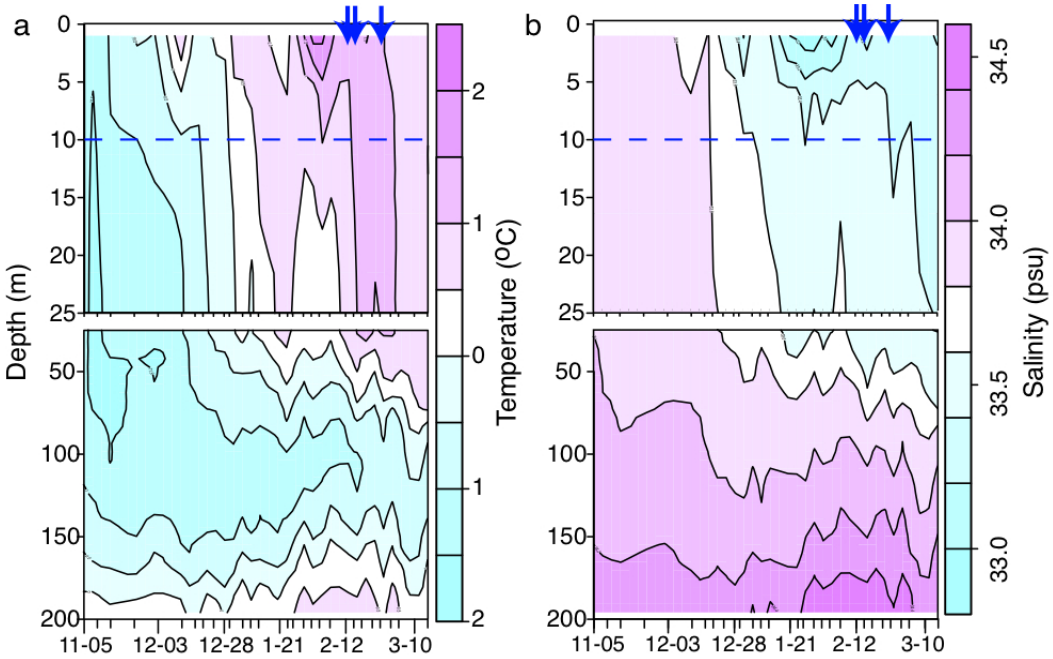

Figure 6.2: Temperature (a) and salinity (b) at Station 5. The top 25 m is expanded in the top plot. Arrows show dates of sampling, and dashed line marks sampling depth (10 m). Data courtesy of BAS.

6.5.2 Activities of radium isotopes

Activities of the short-lived isotopes of Ra and their progenitors are low compared to many coastal areas (Table 6.1). Few studies have examined Ra isotopes

Table 6.1: Mean (range) activities for short-lived Ra isotopes ($^{223}Ra_{ex}$ and $^{224}Ra_{ex}$) and their parent isotopes (^{227}Ac and $^{228}Th/^{228}Ra$). Ranges of activities reported from similar environments are also given for comparison. All activities are given in dpm m^{-3}, "bdl" denotes below detection limit.

Source	Location	$^{223}Ra_{ex}$	$^{224}Ra_{ex}$	^{227}Ac	^{228}Th	^{228}Ra
This study	Ryder Bay	0.155 (bdl – 0.649)	3.21 (0.066 – 14.6)	0.335 (0.052 – 0.897)	1.68 (bdl – 3.40)	19.8 (13.0 – 39.5)
Dulaiova *et al*. 2009	Surface, coastal Antarctic Peninsula		(8 – 17)			(10-20)
Charette *et al.* 2007	Inshore (to 12.5 km), Crozet Islands	(0.02 – 5.2)	(1.4 – 47)			(8.9 – 41)
Van Beek *et al*. 2008	Surface, offshore of Kerguelen Islands					(0.4 – 3.9)
Geibert *et al.* 2002	Surface waters, UCDW			(0.1 – 0.5)		
Shaw & Moore, 2002	Surface, offshore South Shetland Islands			0.20		
Hanfland 2002	Surface, shelf waters Antarctic Peninsula and Weddell Sea					(2 – 20)
Moore 2000a[a]; Moore & Arnold 1996[b]	Typical coastal values	22.4[a] (4.6 – 300)[b]	144[a] (4.9 – 660)[b]			

[a]From the South Atlantic Bight
[b]From the Mississippi and Atchafalaya River mixing zones, and Tampa Bay, Florida (for samples with salinity > 27 parts per thousand)

Table 6.2: Station details and short-lived radium activities from RaDeCC analysis. As sample collection occurred on two occasions, station superscript “b” denotes samples from the second sampling event. Distances given are to the nearest shore line for each individual station. For glacial stations, distances are given to a point on the edge of Sheldon Glacier (denoted in the table by (*), location shown on Fig. 6.1).

Station	Latitude	Longitude	Water column depth (m)	Distance (km)	Sample volume (L)	$^{223}Ra_{ex}$ (dpm m^{-3})	$^{224}Ra_{ex}$ (dpm m^{-3})
1	-67.569	-68.133	15	0.01	163.7	0.643 ± 0.35	14.6 ± 0.84
2	-67.570	-68.137	100	0.28	153.7	0.248 ± 0.23	2.95 ± 0.43
3	-67.573	-68.167	400	0.90	168.6	0.039 ± 0.14	1.12 ± 0.22
4^b	-67.575	-68.190	450	1.70	109.7	bdl	0.762 ± 0.26
5	-67.567	-68.234	520	2.00	125.1	0.006 ± 0.16	0.463 ± 0.19
6	-67.562	-68.267	320	*5.55	177.0	bdl	4.48 ± 0.58
7^b	-67.557	-68.297	300	*4.25	113.4	0.277 ± 0.25	2.13 ± 0.44
8^b	-67.589	-68.258	150	5.50	107.0	0.209 ± 0.31	2.33 ± 0.55
9^b	-67.583	-68.300	160	1.80	114.1	0.204 ± 0.16	0.066 ± 0.223

in Southern Ocean locations, but the scarce data suggest that as a whole the Southern Ocean displays low Ra activity, except for ^{226}Ra (Ku & Lin 1976, Hanfland 2002). Reported activities for ^{223}Ra and ^{224}Ra in coastal areas of the Antarctic Peninsula (Dulaiova *et al.* 2009) and Crozet Island (Charette *et al.* 2007), as well as waters offshore of Kerguelen Island (van Beek *et al.* 2008) are higher on average than those reported here, but the ranges overlap in all cases.

6.5.3 Short-lived isotopes

Activity of $^{223}Ra_{ex}$ (below detection limit ("bdl")-0.649 dpm m^{-3}) is considerably lower than that of $^{224}Ra_{ex}$ (0.066–14.6 dpm m^{-3}), although both isotopes show very similar trends (Table 6.2). Very low activities were found in the central, deep area of Ryder Bay (stations 3, 4 and 5; depth > 300 m; hereafter "mid-bay"), on average 0.023 and 0.076 dpm m^{-3} for $^{223}Ra_{ex}$ and $^{224}Ra_{ex}$, respectively. The most pronounced enrichment is seen at station 1, nearest the shore (in South Cove, alongside Rothera station) and in shallowest water depth (<30 m). This high activity decreases with distance from the shore, through stations 1 to 5. An enrichment is also seen in the sample nearest the Léonie Islands group (station 8), which is sustained in $^{223}Ra_{ex}$ at station 9, but not in $^{224}Ra_{ex}$. The two samples taken from nearer to Sheldon Glacier (stations 6 and 7) exhibit higher activities of $^{224}Ra_{ex}$ relative to mid-bay samples. This enrichment is also seen in $^{223}Ra_{ex}$ for station 7, although station 6 $^{223}Ra_{ex}$ was below detection limits.

Many of the values reported here, especially those from central Ryder Bay, are below the detection limits estimated by Moore (2008) for RaDeCC analysis (0.2 and 0.5 total collected dpm for ^{223}Ra and ^{224}Ra, respectively). However, the background activity measured with our RaDeCC system was much lower than all samples analyzed (mean 3% and 9% of raw counts for 219 and 220 channels, respectively) and reproducibility was good (~20% standard deviation for 3 consecutive readings). Furthermore, samples from similar areas display much less variation than the error of individual samples (*see Discussion*). Therefore we consider our results above the detection limit of RaDeCC analysis, except in the three cases noted in Table 6.2.

For coastal waters, the activities of short-lived Ra isotopes reported here are extremely low. Studies from the Crozet and South Shetland Islands (Charette *et al.* 2007, Dulaiova *et al.* 2009) report similar, very low ranges compared to locations outwith the Southern Ocean. The South Atlantic Bight, for example, displays inshore Ra activities of 22.4 and 144 dpm m^{-3} ($^{223}Ra_{ex}$ and $^{224}Ra_{ex}$, respectively; Moore 2000a) – up to four orders of magnitude higher than those in Ryder Bay. However, even other Southern Ocean samples, when compared by distance from shore (Charette *et al.* 2007, Dulaiova *et al.* 2009), have high activity compared to Ryder Bay. As such, the $^{223}Ra_{ex}$ and $^{224}Ra_{ex}$ activities in Ryder Bay are among the lowest reported for an inshore (<5 km) setting, although they are in keeping with low, offshore Southern Ocean measurements.

6.5.4 Parent isotopes

The average activity of ^{227}Ac is lower than that of ^{228}Th (^{227}Ac: 0.052–0.897 dpm m^{-3}; ^{228}Th: bdl–3.40 dpm m^{-3}; Table 6.3), in keeping with the relationship between the daughter nuclides ($^{223}Ra_{ex} < ^{224}Ra_{ex}$). The spatial distribution of ^{228}Th is similar to that of $^{223}Ra_{ex}$ and $^{224}Ra_{ex}$, with marked enrichment near Rothera station (South Cove, stations 1 and 2) and nearest the Islands (station 8). As with $^{224}Ra_{ex}$, the increase in ^{228}Th near station 8 is not seen at station 9, slightly further from land and in deeper water.

The distribution of ^{227}Ac shows very different trends from the short-lived Ra isotopes. The highest activity reported (0.897 ± 0.217 dpm m^{-3}) is at station 7, nearest Sheldon Glacier, with all other stations displaying less than half of this value. Excluding station 7, the trends of ^{227}Ac are roughly opposite to those of the Ra suite, with mid-bay stations displaying high values (0.37 ± 0.02 dpm m^{-3}), and near-shore stations (1, 2, 8, 9) having slightly lower activities of 0.29 ± 0.17 dpm m^{-3}, although these are not statistically different to mid-bay waters.

6.5.5 Long-lived Ra isotopes

The long-lived Ra isotope ^{228}Ra shows slightly different trends from the short-lived isotopes (Table 6.3). Station 1 again shows enrichment, although this is minor compared with the enrichment seen in $^{223}Ra_{ex}$, $^{224}Ra_{ex}$ and ^{228}Th. Stations 3-5

show relatively consistent values (~17.5 dpm m^{-3}), but in contrast to other Ra isotopes, station 2 displays lower activity than the mid-bay stations. The highest ^{228}Ra activity was measured at station 6, coincident with a peak (although not to maximum activity) of ^{228}Th.

Due to the different sources of each radioisotope, ratios such as ^{228}Ra:^{227}Ac can be helpful in distinguishing between different sources waters. Station 6 shows a peak in the ratio of ^{228}Ra:^{227}Ac (Table 6.3). A second peak is seen at station 9, and a minimum at station 7, although these latter variations are driven by the activity of ^{227}Ac, and within error these ratios are not significantly different from the average for other stations.

6.6 Discussion

6.6.1 Radium sources to Ryder Bay

From the activities of $^{223}Ra_{ex}$ and $^{224}Ra_{ex}$ along both transects, we identify sources near South Cove, the Léonie Islands, and Sheldon Glacier. Station 1, with the shallowest water depth and short distance from shore, would be expected to exhibit the greatest activity, and indeed shows strong enrichment in $^{223}Ra_{ex}$, $^{224}Ra_{ex}$ and ^{228}Th.

Radium-223, in excess of that supported by decay of dissolved ^{227}Ac, is produced from the decay of ^{227}Th which is strongly bound to sediments. Thus $^{223}Ra_{ex}$ displays a strong source along any interface (land-water or sediment-water). A clear enrichment in $^{223}Ra_{ex}$ is evident at station 1 (Table 6.2), to values of 0.65 dpm m^{-3}. To our knowledge, these are the first coupled short-lived Ra isotope activities reported for Antarctic waters. The only published $^{223}Ra_{ex}$ activities from coastal Southern Ocean waters are 0.42 to 5.2 dpm m^{-3}, from waters within 2.6 km of the sub-Antarctic Crozet Islands (Charette *et al.* 2007), generally higher than the range for this study (bdl to 0.65 dpm m^{-3}) but in keeping with activity in our South Cove sample. Further offshore from Crozet Islands, however, $^{223}Ra_{ex}$ dropped to 0.02 – 0.19 dpm m^{-3} (~12 km from shore; Charette *et al.* 2007), in close agreement with the values reported here for distances of 0.5 – 2 km.

As with $^{223}Ra_{ex}$, $^{224}Ra_{ex}$ shows a strong signal of enrichment from sediments due to its Th progenitor. The decay of ^{228}Ra, present mainly in the dissolved phase, produces ^{228}Ac which quickly decays ($t_{1/2}$ = 6.15 h) to ^{228}Th. This ^{228}Th is rapidly scavenged and slowly releases ^{224}Ra from sediments. In coastal areas, ^{228}Th may also be sourced from the surrounding rock in addition to its production within the water column, and indeed this terrigenous source is much greater than the marine source. Published values for $^{224}Ra_{ex}$ range from 3.1–47 dpm m^{-3} (Crozet Islands; Charette *et al.* 2007) and 8–17 dpm m^{-3} (coastal Antarctic Peninsula surface waters; Dulaiova *et al.* 2009). Only station 1 of the Ryder Bay samples falls within this range (14.6 dpm m^{-3}), although other near-shore samples clearly show this land-interface signal.

This shore-derived signal is transported offshore, and stations 2 and 8, both at similar distances from the shore line (South Cove and Leonie Islands, respectively) and at similar depths, display very similar activities of all nuclides measured here (Table 6.2). Station 9 also shows some enrichment in $^{223}Ra_{ex}$ relative to mid-bay samples, which does not appear in the other isotopes. This could be explained by slow mixing such that ^{224}Ra, with its shorter half-life, would decay more quickly than ^{223}Ra during a given period of mixing. Additionally, the difference in signal between these two isotopes may be small, as the errors on $^{223}Ra_{ex}$ are relatively large, due to the much lower activity of this isotope and sampling constraints preventing the collection of larger volume samples. This signal of higher activities in the near-shore sampling locations is consistent with a Ra source from surrounding rocks, and/or production of Ra in shallow marine sediments.

Notably, there are also enrichment signals towards Sheldon Glacier, which in the case of $^{224}Ra_{ex}$, ^{228}Th and ^{228}Ra are very high given the distance from land at these stations. Glacial flour, sub-glacial and/or surface meltwater flows, or sediment/sea water interaction beneath the ice shelf could all potentially act as a source for Ra enrichment near Sheldon Glacier. While we are unable to discriminate here between these processes, it is likely that the signal is at least partly derived from the glacier (and entrained terrigenous material) itself. Shaw *et al.* (2011) report $^{224}Ra_{ex}$ activities of ~1.2–9.4 dpm m^{-3} in surface waters near free-drifting icebergs (Weddell gyre), showing that glacial material alone can account for a highly significant $^{224}Ra_{ex}$ enrichment in the absence of any bottom sediments.

There is some variability between the activities at stations 6 and 7, although records of $\delta^{18}O$ (Meredith et al. 2012) in water samples at the RaTS site indicate similar proportions of meteoric (glacial/snow) water in the water column on both sampling days. Thus we infer that glacial sources of Ra are highly variable, as might be expected given the potential for different processes (ice melt versus sub-glacial sediment-water mixing) to contribute terrigenous material, in addition to potential differences in the composition of that material. Additionally, small scale flow filaments could contribute to different Ra activity being collected from these two stations, even if sediment composition were invariant. Despite this variability, the average activities at stations nearest Sheldon Glacier show a clear signal of all four Ra nuclides (Fig. 6.3). "Glacier" stations exhibit statistically higher $^{224}Ra_{ex}$ and ^{228}Th than mid-bay samples (3.30 dpm m^{-3} *vs.* 0.78 dpm m^{-3}, *p*-value = 0.0344; 0.24 *vs.* 0.027, *p*-value = 0.050; respectively, 2-sample *t*-tests). The two glacier stations show very different $^{223}Ra_{ex}$ activities, consistent with high variability of glacial sources. One sample is below the detection limit, but activity nearest the glacier (0.277 dpm m^{-3}, station 7) is an order of magnitude higher than the mid-bay average of 0.023 dpm m^{-3}, indicating an intermittent but significant glacial source of $^{223}Ra_{ex}$, as with ^{224}Ra.

Trends in ^{228}Ra are also consistent with a glacial source, as station 6 displays pronounced enrichment to an activity ~2-fold higher than at station 1 (Table 6.2). While variable, average ^{228}Ra was 28.3 dpm m^{-3} near the glacier, compared to 18.9 dpm m^{-3} in mid-bay stations, although this difference was not statistically significant (*p*-value = 0.236). The highly significant enrichment at station 6 leads to elevated ^{228}Ra:^{227}Ac ratios (Table 6.3) compared to all other stations, suggestive of a distinct water source which is enriched in ^{228}Ra. This enrichment, coupled with the very low ^{227}Ac activity (produced in deep ocean sediments – see below) indicate a terrestrial source, consistent with glacial meltwater. In keeping with its much longer half life ($t_{1/2}$ = 5.75 y), the distribution of ^{228}Ra shows less variability between the different location types than the shorter-lived isotopes. Due to its long half-life, variations in ^{228}Ra activity within Ryder Bay must reflect dilutive processes, rather than decay during advection which is seen in the shorter-lived isotopes. The increase in ^{228}Ra activity near the glacier is consistent with an input of enriched water to the surface,

as by a thin lens of glacial meltwater. Even a modest extent of mixing with the underlying water column would then dilute this signal due to the very small relative volume of a thin meltwater lens, in accordance with the lower values of ^{228}Ra in mid-bay stations.

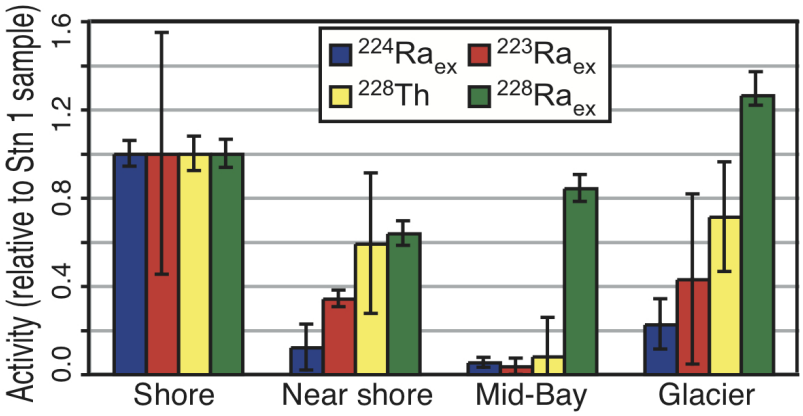

Figure 6.3: Radium activities grouped by location type, and relative to the highest measured activity (in all cases at station 1 (shore), error bars show sample uncertainty). Near shore stations: 2, 8 and 9. Mid-bay stations: 3, 4 and 5. Glacier stations: 6 and 7. Error bars on near-shore, mid-bay and glacier stations represent 1 standard deviation, except in the case of $^{223}Ra_{ex}$ at the glacier station where sample error is shown because only one sample was above the detection limit.

6.6.2 Deep water renewal

In general, the values reported here are low compared with other Southern Ocean studies (Table 6.1). This is especially true in the case of mid-Ryder Bay samples, where mean $^{223}Ra_{ex}$ was 0.023 dpm m^{-3}, and that of $^{224}Ra_{ex}$ was 0.76 dpm m^{-3}. Activity of $^{223}Ra_{ex}$ offshore from Crozet Islands is reported as 0.02 - 0.19 dpm m^{-3} (~12 km from shore; Charette *et al.* 2007), and the Ryder Bay values are in keeping with the lower limit of this range despite being significantly closer to shore. Low values of $^{224}Ra_{ex}$ were also observed in Southern Ocean surface waters: Dulaiova *et al.* (2009) report $^{224}Ra_{ex}$ activities of 2–4 dpm m^{-3} above the continental shelf, while Drake Passage/ACC waters were found to contain no $^{224}Ra_{ex}$. The activities measured here for mid-Ryder Bay samples are in keeping with offshore waters, suggesting limited input from sediment-water interaction, coastal runoff or submarine groundwater discharge. Taken together, the activities of both short-lived Ra isotopes in central Ryder Bay suggest an open ocean source for surface waters,

with slow diffusion of Ra enrichment derived from interfaces (sediment-water and land-water).

Table 6.3: Progenitor isotope activities from RaDeCC analysis (^{228}Th and ^{227}Ac) and gamma spectroscopy (^{228}Ra). Also shown are ratios of ^{228}Ra:^{227}Ac. As in Table 6.2, station superscript "b"denotes samples from the second sampling event. All activities are given in dpm m^{-3}.

Station	^{228}Th	^{227}Ac	^{228}Ra	^{228}Ra:^{227}Ac
1	3.40 ± 0.26	0.271 ± 0.14	22.4 ± 1.4	82 ± 47
2	2.69 ± 0.25	0.400 ± 0.14	13.0 ± 0.95	33 ± 14
3	bdl	0.338 ± 0.12	19.2 ± 1.3	57 ± 24
4^{b}	0.430 0.12	0.378 ± 0.19	17.5 ± 1.3	46 ± 27
5	0.776 ± 0.14	0.383 ± 0.15	19.8 ± 1.5	52 ± 24
6	3.02 ± 0.28	0.052 ± 0.072	39.5 ± 2.1	760 ± 1090
7^{b}	1.83 ± 0.26	0.897 ± 0.22	17.1 ± 1.3	19 ± 6
8^{b}	2.59 ± 0.28	0.437 ± 0.20	16.8 ± 1.6	38 ± 21
9^{b}	0.764 ± 0.14	0.059 ± 0.10	13.0 ± 1.2	220 ± 400

The distribution of ^{227}Ac is very different from that of short-lived Ra species. Actinium-227 is produced from decay of ^{231}Pa, which itself is produced from ^{235}U, an isotope with a near-uniform distribution throughout the global ocean. Upon production, ^{231}Pa is rapidly scavenged, and builds up in slowly-accumulating deep sea sediments (Geibert *et al.* 2002). Thus the deep sea is a major source for the more soluble ^{227}Ac which diffuses out of the sediment into the overlying bottom water. Geibert *et al.* (2002) have shown that UCDW and LCDW can be distinguished based on their ^{227}Ac activities, with the deeper LCDW having higher activity. However, Shaw & Moore (2002) show that in surface waters of the Southern Ocean, enrichment of ^{227}Ac can also be seen in shelf and coastal regions due to decay of terrigenous ^{235}U in shelf sediments, and a global dataset of ^{227}Ac by delayed coincidence counting has demonstrated that ^{227}Ac is supplied to some extent by coastal environments (Geibert & Vöge 2008).

The ^{227}Ac reported here, with the exception of station 7, show highest activities in mid-bay samples (0.37 ± 0.02 dpm m^{-3}). The higher activity at station 7 may be due to a glacial source with extremely high spatial and temporal variability, as is indicated by the Ra isotopes. However, since there is no definitive single explanation for the higher values at station 7, we restrict discussion of ^{227}Ac data to mid-bay stations. Most sites along the Islands transect are within error of the mid-bay samples, and significant variations in ^{227}Ac activity would not be expected, as the very long half-life of ^{227}Ac (21.77 years) vastly exceeds the time scale relevant to circulation in Ryder Bay.

The mean mid-bay ^{227}Ac activity of 0.37 dpm m^{-3} is somewhat higher than those reported by Shaw & Moore (2002) for open Drake Passage surface waters (0.13–0.23 dpm m^{-3}), and even for on-shelf sites (around the South Shetland Islands and South America; 0.20-0.27 dpm m^{-3}). The greater activity may either reflect interaction with the continental shelf or slope, or ^{227}Ac-rich source waters. Geibert *et al.* (2002) studied ^{227}Ac with depth in the Weddell Gyre and Drake Passage, finding that UCDW was characterized by ^{227}Ac$_{ex}$ activities of 0.2–0.4 dpm m^{-3} (equivalent to ^{227}Ac ~0.43–0.75 dpm m^{-3}). Waters in the Drake Passage were found to have slightly lower activities, with surface water reported at 0.10–0.27 dpm m^{-3} (Shaw & Moore 2002) and UCDW (~500 m) ^{227}Ac activity measured as 0.37 dpm m^{-3} (supplemental data from Geibert *et al.* (2002); we compare ^{227}Ac activities rather than ^{227}Ac$_{ex}$ to avoid introducing any uncertainty arising from an estimation of the ^{231}Pa correction for our data). The values measured in Ryder Bay, especially the mid-bay stations, are in better agreement with the ^{227}Ac of sub-surface (500 m) Drake Passage waters than surface waters. Current understanding of regional circulation is that Marguerite Bay is subject to frequent but irregular incursions of UCDW at depth via Marguerite Trough (Martinson *et al*. 2008, Moffat *et al*. 2009), with CDW being the ultimate source of waters in Marguerite Bay and Ryder Bay. This water mixes up into the WW and AASW layers, with mixing occurring primarily in coastal and shallow regions expected (Howard *et al*. 2004, Wallace *et al*. 2008). Additionally, δ^{18}O data at station 5 indicates that > 96% of the water at 15 m comes from CDW during the sampling period (Meredith et al. 2012). The lack of enrichment in Ryder Bay ^{227}Ac relative to UCDW values indicates very little shelf input of ^{227}Ac.

However, ^{228}Ra is higher than expected for open-ocean UCDW, indicating a certain extent of recent interaction of the water mass with sediments, which also has the potential to contribute some ^{227}Ac. Activity of ^{228}Ra reported for Antarctic Polar Front and ACC waters have been reported as 0.25–2 dpm m^{-3} ((Kaufman *et al*. 1973*;* Charette *et al.* 2007). Our measurements are an order of magnitude higher than these open water values, but consistent with surface waters near the Crozet Islands (8.9–41 dpm m^{-3}; Charette *et al.* 2007) and in the Weddell Gyre (21–32 dpm m^{-3}; Rutgers van der Loeff 1994). Despite being higher than more oceanic regions, the activities measured here are still much lower than temperate coastal areas (*e.g*. 75–246 dpm m^{-3} in the South Atlantic Bight; Moore 2000a), suggesting relatively minor ^{228}Ra inputs relative to river-influenced locations.

We therefore consider the combination of the UCDW source water and modest interaction with the continental shelf or shelf-break likely to explain the elevated ^{227}Ac and ^{228}Ra activities in Ryder Bay. Indeed, the path of UCDW from the ACC onto the WAP shelf is consistent with a shelf-break or margin source, which has been proposed as a major contributor to oceanic micronutrient budgets (*e.g*. Jeandel *et al*. 2011). While ^{228}Ra indicates some shelf interaction, there is no observed enrichment in ^{227}Ac relative to offshore UCDW, which is as expected for a shelf setting. Relatively shallow depths (~500 m) allow for limited ^{231}Pa production, and a high rate of sediment accumulation on the shelf will dilute ^{231}Pa in sediments, leading to low ^{227}Ac release therefrom. The ^{227}Ac activities also suggest negligible inputs from coastal or land sources although without depth profile samples it is not possible here to quantify ^{227}Ac from terrigenous sources versus UCDW. We suggest that future work assessing ^{227}Ac activities in deeper waters could aid in constraining the extent of UCDW incursions integrated over several years

6.6.3 Mixing rates within Ryder Bay

Short-lived Ra isotopes have previously been used to estimate horizontal eddy diffusivity in other Southern Ocean waters (Charette *et al.* 2007). If the distribution of Ra can be described by diffusion, as opposed to advection, then a one-dimensional diffusion model can be used to calculate eddy diffusion coefficients (k_h) along an onshore-offshore transect, according to the equation

$$A_x = A_o \cdot e^{-x\sqrt{\lambda/k_h}} \quad (3)$$

where A_x and A_o are the activities at distance x (from shore) and at the source ($x = 0$), respectively, and λ is the decay constant.

Based on this model, k_h is estimated by plotting ln(Ra activity) versus distance (x), where k_h is determined based on the slope (m), according to the equation:

$$k_h = \lambda / m^2 \quad (4)$$

This estimate of eddy diffusivity does not solely reflect eddy diffusion, and significant advection will result in a non-linear relationship, either concave (onshore advection) or convex (offshore; Dulaiova *et al.* 2009). Thus, provided the data display a reasonably linear fit, the k_h can be considered an "effective" horizontal eddy diffusion coefficient giving an estimate of offshore mixing (Charette *et al.* 2007). For transects from South Cove into central Ryder Bay, the k_h values determined for this study are 1.0 m^2 s^{-1} for $^{224}Ra_{ex}$ (0.64 m^2 s^{-1} if island stations are included) and 0.13 m^2 s^{-1} for $^{223}Ra_{ex}$ (0.31 m^2 s^{-1} if island stations are included; Fig. 6.4).

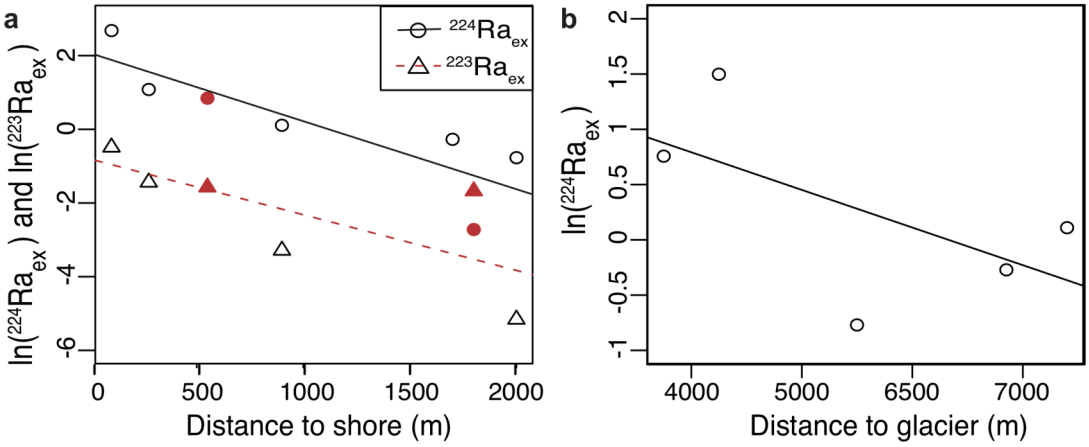

Figure 6.4: (a) Determination of effective eddy diffusivity coefficients (k_h) based on activity of $^{223}Ra_{ex}$ and $^{224}Ra_{ex}$ versus distance for the Islands transect. Due to the semi-enclosed nature of Ryder Bay, distance was measured to nearest land (including the islands), to better reflect a source of Ra in sediments which would be present along the entire shoreline, rather than solely at a fixed point such as South Cove. Shown are all stations along the Islands transect as well as station 5 (the RaTS site). Filled symbols are those stations nearest the Léonie Islands group (stations 8 and 9); stations 1 through 5 are shown as open symbols. (b) Effective eddy diffusivity coefficients (k_h) from $^{224}Ra_{ex}$ for the Glacier transect. Glacier transect distances are relative to a point on the edge of Sheldon Glacier (indicated in Fig. 6.1), included are stations 3 through 7.

There is some offset between the two $^{224}Ra_{ex}$ estimates (mean = 0.83 $m^2 s^{-1}$), and the two $^{223}Ra_{ex}$ estimates (mean = 0.22 $m^2 s^{-1}$), although previous studies have reported k_h values for these two isotopes as different as 6.6 and 39 for $^{223}Ra_{ex}$ and $^{224}Ra_{ex}$ respectively (Charette *et al.* 2007) - a 6-fold difference versus 4-fold for Ryder Bay. It was shown by Okubo (1971) that the longer half-life of ^{223}Ra can yield k_h values ~3 fold higher than those of $^{224}Ra_{ex}$, due to the greater distance over which the signal is dispersed. However, the k_h values determined here are actually lower for $^{223}Ra_{ex}$ than for $^{224}Ra_{ex}$, a feature present all short-lived Ra analyses of mixing (Stachelhaus & Moran 2012). This discrepancy has been ascribed to use of a non-shore perpendicular transect and uncertainties in mixing behaviour (Charette *et al*. 2007), spatial or temporal variations in mixing (Moore 2000), and in some cases can be reconciled by accounting for differential diffusion (Stachelhaus & Moran 2012).

As Ryder Bay is enclosed on three sides, a simple diffusion model may be inadequate to represent the pattern of circulation in Ryder Bay, and the data here are unlikely to fulfill the assumption that activity decreases to zero at some distance. However, while there are significant potential caveats in the determination of k_h here, the semi-enclosed nature of Ryder Bay should contribute to higher Ra activities in mid-bay stations than if the only Ra source was a point source (*i.e.* station 1), which would result in the calculated mixing rates being overestimates. Nevertheless, the k_h employed here is an "effective" eddy diffusivity and should to some extent reflect advective processes as well. As a result, the overall magnitude of mixing suggested here ($\leq$1.0 $m^2 s^{-1}$) is worthy of note.

This range of eddy coefficients from the Islands transect (0.13 to 1.0 $m^2 s^{-1}$) is much lower than the 6.6-39 $m^2 s^{-1}$ range estimated by Charette *et al*. (2007). Both of these k_h estimates are extremely low in comparison to those estimated for other coastal regions (*e.g*. 360–420 $m^2 s^{-1}$ for the South Atlantic Bight; Moore 2000a) including the northern Antarctic Peninsula (596–63000 $m^2 s^{-1}$; Dulaiova *et al*. 2009). This strongly supports very slow diffusion from the margins to the centre of the bay, implying that mid-bay waters are sourced predominantly from more open ocean or deep waters, with very little influence from land-water exchange. Any sedimentary source of micronutrients (iron, for instance), would thus be expected to be very low

in central Ryder Bay, and likely Marguerite Bay as well, and to occur via sediment-water interaction before the modified UCDW enters Ryder Bay. However, as noted above, ^{228}Ra is higher than in open ocean surface waters, and the $t_{1/2}$ gives an indication of the time-scale of the inferred sediment interaction. This interaction is likely on the order of several months to several years before the water enters Ryder Bay, while the very low short-lived Ra isotope activities reflect little or no input on the scale of one week to one month.

In addition to mixing rates, short-lived Ra measurements can also be used to estimate the length of time a water parcel has been isolated from the Ra source. Ratios of $^{224}Ra_{ex}$:^{228}Ra were used to estimate ages in mid-bay samples, following Moore (2000b) and Dulaiova *et al*. (2009). Taking the activity ratio at station 1 as the source end-member, stations 3–5 display Ra ages of 13, 14 and 18 days, respectively. The very low rates of horizontal transport determined above are consistent with these age estimates, as studies in other regions have found younger ages for water much farther offshore (*e.g*. Ra age of ~7 days up to 150 km offshore; Dulaiova *et al*. 2009).

Similar evaluation of k_h was performed for the Glacier transect. As Sheldon Glacier terminates over a large area at the northern end of Ryder Bay, distances were measured from an arbitrarily chosen point on the nearest ice edge (shown in Fig. 6.1). As the calculation for k_h depends on the slope of the plot versus *x*, only relative distances are taken into account, such that the absolute distance between source and sample does not affect the estimated k_h. Due to the two values bdl for $^{223}Ra_{ex}$, only $^{224}Ra_{ex}$ activity was used to assess k_h, giving an estimate of 18 m^2 s^{-1} for mixing between the area around Sheldon Glacier and mid-Ryder Bay (Fig. 6.4). In agreement, ages derived using station 7 ratios as a source (0.5 and 8 days, for stations 6 and 5, respectively), are considerably lower than those calculated for sediment sources. That the k_h estimate for glacial mixing is an order of magnitude greater than the estimates for the Islands transect may reflect the nature of the underlying dispersive processes. If the enrichment signal derives from glacial meltwater as postulated, this would be present in a shallow freshwater lens at the surface. This water could be differentially affected by processes that induce horizontal mixing at the surface (potentially atmospherically-forced; *i.e.* wind, inertial currents etc), in addition to overall horizontal mixing occurring in the water column. This may

potentially account for the faster effective horizontal diffusivity of a glacier-derived signal compared to that from sediments.

Previous studies have combined estimates of k_h with ^{228}Ra gradients to estimate offshore fluxes of ^{228}Ra (*see* Dulaiova *et al*. 2009). Following this approach, we used the Islands transect stations, plus the RaTS site, to assess the gradient of ^{228}Ra away from shore in Ryder Bay, which gave a slope of 0.61 ± 2.0 dpm m^{-3} km^{-1}. There was considerable scatter in the data and the r^2 value for the regression (^{228}Ra versus distance to nearest land) was very low (0.18). Thus there is a high degree of uncertainty in this calculation, reflected in the standard error of the slope, but the magnitude of the resulting ^{228}Ra flux estimate is worthy of note. To obtain an upper estimate for ^{228}Ra flux, we used an upper limit of the ^{228}Ra-gradient slope plus error (2.6 dpm m^{-3} km^{-1}) multiplied by the highest value estimated for k_h (1.0 m^{-2} s^{-1}; from $^{224}Ra_{ex}$ data along this transect) which gives a ^{228}Ra flux of 230 dpm m^{-2} d^{-1}. Compared to other Southern Ocean locations this flux is relatively low. For example, the ^{228}Ra flux calculated for the study by Charette *et al*. (2007) around the Crozet Islands is 1630-9660 dpm m^{-2} d^{-1}. The estimate for Livingston Island (South Shetland Islands) is 31900 dpm m^{-2} d^{-1}, although the estimate for Elephant Island (South Shetland Islands) is very low (15.8 dpm m^{-2} d^{-1}, Dulaiova *et al*. 2009). We suggest that location plays a large role in determining fluxes: low values are found in Ryder Bay (coastal Antarctic), high values near the Crozet Islands (Subantarctic islands), and the large range of the Dulaiova study at the northern tip of the western Antarctic Peninsula may include regions with both Antarctic and Subantarctic characteristics. Our analysis shows that land-ocean inputs are low in the Antarctic environment, and as such ice-ocean fluxes may dominate in these regions.

Analysis by Cochran & Krishnaswami (1980) determined that bioturbation is by far the most significant process contributing to sedimentary ^{228}Ra flux, and as such our very low upper estimate of ^{228}Ra flux may indicate a relatively low amount of bioturbation in Ryder Bay and/or the sediments underlying the path of water entering Ryder Bay. Marine surveys around Rothera Research Station report high abundances of benthic organisms and largely bare rock substrates (Bowden 2005) thus it is more likely that the low Ryder Bay fluxes reflect comparatively low amounts of sediments in shallow (mixed-layer) waters, as opposed to scarcity of

bioturbating organisms. Frequent scouring by icebergs, as is the case in shallow waters of Ryder Bay (Smale *et al*. 2008), or the very steep sides of the bay, may also contribute to low amounts of sediment.

6.7 Conclusions

Here we present short-lived Ra isotope activities in a shallow embayment on the western Antarctic Peninsula, the most southerly to date, and the activities of their progenitor isotopes. The activities of both $^{223}Ra_{ex}$ and $^{224}Ra_{ex}$ were low compared to other coastal Southern Ocean locations, and extremely low compared to those reported for low-latitude regions.

Waters near Sheldon Glacier show a clear enrichment signal in $^{223}Ra_{ex}$, $^{224}Ra_{ex}$, and ^{228}Ra. Although seawater-sediment interaction underneath the ice is also a potential source for this enrichment, material entrained within the ice itself is a more likely source, as other studies have found (Shaw *et al*. 2011).

The mid-bay activities resemble relatively open water, indicating very little interaction with sediment-water or land-water interfaces, although elevated ^{228}Ra indicates some continental shelf influence over timescales on the order of several months to years. The high activities of ^{227}Ac reflect that the ultimate source for Ryder Bay surface waters is UCDW, which is known to intrude onto the WAP shelf aperiodically (Martinson *et al*. 2008, Moffat *et al*. 2009).

Horizontal mixing rates between mid-bay and shore waters are significantly slower than those reported for other coastal areas, consistent with relatively high Ra ages for such an environment. Given the slow mixing rates and extremely low short-lived Ra activities for a relatively shallow coastal environment, sediment interaction and coastal runoff are therefore not likely to be a major source of micronutrients to Ryder Bay. The mixing rate estimate for glacial to mid-bay waters, however, is more than an order of magnitude greater than those for non-glacial samples, indicating that glacially influenced waters represent a more dispersive source of terrestrial material (and any associated micronutrients) in coastal areas.

6.8 References

BOWDEN, D.A. 2005. Quantitative characterization of shallow marine benthic assemblages at Ryder Bay, Adelaide Island, Antarctica. *Marine Biology*, **146**, 1235–1249, 10.1007/s00227-004-1526-0.

BOYD, P.W. & ELLWOOD, M.J. 2010. The biogeochemical cycle of iron in the ocean. *Nature Publishing Group*, **3**, 675–682, 10.1038/ngeo964.

CHARETTE, M.A., BUESSELER, K.O. & ANDREWS, J.E., 2001. Radium isotopes for evaluating the input and transport of groundwater-derived nitrogen to a Cape Cod estuary, *Limnology and Oceanography* 46 (2), 465–470.

CHARETTE, M.A., GONNEEA, M.E., MORRIS, P.J., STATHAM, P., FONES, G., PLANQUETTE, H., SALTER, I. & GARABATO, A.N. 2007. Radium isotopes as tracers of iron sources fueling a Southern Ocean phytoplankton bloom. *Deep Sea Research Part II: Topical Studies in Oceanography*, **54**, 1989–1998, 10.1016/j.dsr2.2007.06.003.

CLARKE, A., MEREDITH, M.P., WALLACE, M.I., BRANDON, M.A. & THOMAS, D.N. 2008. Seasonal and interannual variability in temperature, chlorophyll and macronutrients in northern Marguerite Bay, Antarctica. *Deep Sea Research Part II: Topical Studies in Oceanography*, **55**, 1988–2006, 10.1016/j.dsr2.2008.04.035.

COCHRAN, J.K. & KRISHNASWAMI, S. 1980. Radium, Thorium, Uranium and 210Pb in deep-sea sediments and sediment pore waters from the North Equatorial Pacific. *American Journal of Science*, **280**, 849–889.

COOK, A.J., FOX, A.J., VAUGHAN, D.G. & FERRIGNO, J.G. 2005. Retreating Glacier Fronts on the Antarctic Peninsula over the Past Half-Century. *Science*, **308**, 541–544, 10.1126/science.1109164.

DIMOVA, N., DULAIOVA, H., KIM, G. & BURNETT, W.C. 2008. Uncertainties in the preparation of ^{224}Ra Mn fiber standards. *Marine Chemistry*, **109**, 220–225, 10.1016/j.marchem.2007.06.016.

DUCKLOW, H.W., BAKER, K., MARTINSON, D.G., QUETIN, L.B., ROSS, R.M., SMITH, R.C., STAMMERJOHN, S.E., VERNET, M. & FRASER, W. 2007. Marine pelagic ecosystems: the West Antarctic Peninsula. *Philosophical Transactions of the Royal Society B: Biological Sciences*, **362**, 67–94, 10.1098/rstb.2006.1955.

DULAIOVA, H., ARDELAN, M.V., HENDERSON, P.B. & CHARETTE, M.A. 2009. Shelf-derived iron inputs drive biological productivity in the southern Drake Passage. *Global Biogeochemical Cycles*, **23**, 10.1029/2008GB003406.

DULAIOVA, H. & BURNETT, W.C. 2008. Evaluation of the flushing rates of Apalachicola Bay, Florida via natural geochemical tracers. *Marine Chemistry*, **109**, 395-408.

EDWARDS, R. & SEDWICK, P. 2001. Iron in East Antarctic snow: Implications for atmospheric iron deposition and algal production in Antarctic waters. *Geophysical Research Letters*, **28**, 3907–3910, 10.1029/2001GL012867.

GALL, M.P., STRZEPEK, R., MALDONADO, M. & BOYD, P.W. 2001. Phytoplankton processes. Part 2: Rates of primary production and factors controlling algal growth during the Southern Ocean Iron RElease Experiment (SOIREE). *Deep Sea Research Part II: Topical Studies in Oceanography*, **48**, 2571–2590.

GARCIA-SOLSONA, E., GARCIA-ORELLANA, J., MASQUÉ, P. & DULAIOVA, H. 2008. Uncertainties associated with ^{223}Ra and ^{224}Ra measurements in water via a Delayed Coincidence Counter (RaDeCC). *Marine Chemistry*, **109**, 198–219, 10.1016/j.marchem.2007.11.006.

GARIBOTTI, I.A., VERNET, M., FERRARIO, M.E., SMITH, R.C., ROSS, R.M. & QUENTIN, L.B. 2003. Phytoplankton spatial distribution patterns along the western Antarctic Peninsula (Southern Ocean). *Marine Ecology Progress Series*, **261**, 21–39.

GEIBERT, W. & VÖGE, I. 2008. Progress in the determination of ^{227}Ac in sea water. *Marine Chemistry*, **109**, 238–249, 10.1016/j.marchem.2007.07.012.

GEIBERT, W., RUTGERS VAN DER LOEFF, M.M., HANFLAND, C. & DAUELSBERG, H.-J. 2002. Actinium-227 as a deep-sea tracer: sources, distribution and applications. *Earth and Planetary Science Letters*, **198**, 147–165.

GIFFIN, C., KAUFMAN, A. & BROECKER, W. 1963. Delayed Coincidence Counter for the Assay of Actinon and Thoron. *Journal of Geophysical Research*, **68**, 1749–1757.

HANFLAND, C. *Radium-226 and radium-228 in the Antlantic sector of the Southern Ocean, Berichte zur Polar und Meeresforschung*. PhD Thesis: Alfred Wegener Institute.

HOFFMANN, L.J., PEEKEN, I. & LOCHTE, K. 2008. Iron, silicate, and light co-limitation of three Southern Ocean diatom species. *Polar biology*, **31**, 1067–1080, 10.1007/s00300-008-0448-6.

HOFMANN, E.E., KLINCK, J.M., LASCARA, C.M. & SMITH, D.A. 1996. Water mass distribution and circulation west of the Antarctic Peninsula and including Bransfield Strait. *In* Ross, R.M., *ed. Foundations for Ecological Research West of the Antarctic Peninsula*. American Geophysical Union, 61–80.

HOWARD, S.L., HYATT, J. & PADMAN, L. 2004. Mixing in the pycnocline over the western Antarctic Peninsula shelf during Southern Ocean GLOBEC. *Deep-Sea Research II*, **51**, 1965-1979.

JEANDEL C., PEUCKER-EHRENBRINK, B., JONES, M.T., PEARCE, C.R., OELKERS, E.H., GODDERIS, Y., LACAN, F., AUMONT, O. & ARSOUZE, T. 2011. Ocean Margins: The Missing Term in Oceanic Element Budgets? *Eos Trans. AGU*, **92**(26), 217-224. 10.1029/2011EO260001.

KAUFMAN, A., TRIER, R.M., BROECKER, W.S. & FEELY, H.W. 1973. Distribution of Ra-228 in the world ocean. *Journal of Geophysical Research*, **78**, 8827–8849.

KLINCK, J. 1998. Heat and salt changes on the continental shelf west of the Antarctic Peninsula between January 1993 and January 1994. *Journal of Geophysical Research*, **103**, 7617–7636.

KU, T.-L. & LIN, M.-C. 1976. ^{226}Ra distribution in the Antarctic Ocean. *Earth and Planetary Science Letters*, **32**, 236–248.

MARTINSON, D.G., STAMMERJOHN, S.E., IANNUZZI, R.A., SMITH, R.C. & VERNET, M. 2008. Western Antarctic Peninsula physical oceanography and spatio-temporal variability. *Deep-Sea Research II*, **55**, 1964–1987, 10.1016/j.dsr2.2008.04.038.

MEREDITH, M.P. & KING, J.C. 2005. Rapid climate change in the ocean west of the Antarctic Peninsula during the second half of the 20th century. *Geophysical Research Letters*, **32**, 10.1029/2005GL024042.

MEREDITH, M.P., BRANDON, M.A., WALLACE, M.I., CLARKE, A., LENG, M.J., RENFREW, I.A., VAN LIPZIG, N.P.M. & KING, J.C. 2008. Variability in the freshwater balance of northern Marguerite Bay, Antarctic Peninsula: Results from δ^{18}O. *Deep Sea Research Part II: Topical Studies in Oceanography*, **55**, 309–322, 10.1016/j.dsr2.2007.11.005.

MEREDITH, M.P., WALLACE, M.I., STAMMERJOHN, S.E., RENFREW, I.A., CLARKE, A., VENABLES, H.J., SHOOSMITH, D.R., SOUSTER, T. & LENG, M.J. 2010. Changes in the freshwater composition of the upper ocean west of the Antarctic Peninsula during the first decade of the 21st century. *Progress In Oceanography*, **87**, 127–143, 10.1016/j.pocean.2010.09.019.

MEREDITH, M.P., VENABLES, H.J., CLARKE, A., DUCKLOW, H.J., ERICKSON, M., LENG, M.J., LENAERTS, J.T.M., & VAN DEN BROEKE, M.R. *In press*. The freshwater system west of the Antarctic Peninsula: spatial and temporal changes. Journal of Climate.

MOFFAT, C., BEARDSLEY, R.C., OWENS, B. & VAN LIPZIG, N. 2008. A first description of the Antarctic Peninsula Coastal Current. *Deep-Sea Research Part II*, **55**, 277–293,

10.1016/j.dsr2.2007.10.003.

MOFFAT, C., OWENS, B. & BEARDSLEY, R.C. 2009. On the characteristics of Circumpolar Deep Water intrusions to the west Antarctic Peninsula Continental Shelf. *Journal of Geophysical Research*, **114**, 10.1029/2008JC004955.

MONTES-HUGO, M., DONEY, S.C., DUCKLOW, H.W., FRASER, W., MARTINSON, D., STAMMERJOHN, S.E. & SCHOFIELD, O. 2009. Recent Changes in Phytoplankton Communities Associated with Rapid Regional Climate Change Along the Western Antarctic Peninsula. *Science*, **323**, 1470–1473, 10.1126/science.1164533.

MOORE, W.S. 1976. Sampling ^{226}Ra in the deep ocean. *Deep Sea Research*, **23**, 647–651.

MOORE, W.S. 1996. Large groundwater inputs to coastal waters revealed by ^{226}Ra enrichments. *Nature*, **380**, 612–614.

MOORE, W.S. 2000. Determining coastal mixing rates using radium isotopes. *Continental Shelf Research*, **20**, 1993–2007.

MOORE, W.S. 2000b. Ages of continental shelf waters determined from ^{223}Ra and ^{224}Ra. *Journal of Geophysical Research*. **105**, 22,117-22,122.

MOORE, W.S. 2003. Sources and fluxes of submarine groundwater discharge delineated by radium isotopes. *Biogeochemistry*, **66**, 75–93.

MOORE, W.S. 2008. Fifteen years experience in measuring ^{224}Ra and ^{223}Ra by delayed-coincidence counting. *Marine Chemistry*, **109**, 188–197, 10.1016/j.marchem.2007.06.015.

MOORE, W.S. & ARNOLD, R. 1996. Measurement of ^{223}Ra and ^{224}Ra in coastal waters using a delayed coincidence counter. *Journal of Geophysical Research*, **101**, 1321–1329.

MOORE, W.S., ASTWOOD, H. & LINDSTROM, C. 1995. Radium isotopes in coastal waters on the Amazon shelf. *Geochimica et Cosmochimica Acta*, **59**, 4285–4298.

OKUBO, A. 1971. Oceanic diffusion diagrams. *Deep Sea Research and Oceanographic Abstracts*, **18**, 789–802.

PRITCHARD, H.D., LIGTENBERG, S.R.M., FRICKER, H.A., VAUGHAN, D.G., VAN DEN BROEKE, M.R. & PADMAN, L. 2012. Antarctic ice-sheet loss driven by basal melting of ice shelves. *Nature*, **484**, 502-505. 10.1038/nature10968.

RAISWELL, R. 2011. Iceberg-hosted nanoparticulate Fe in the Southern Ocean Mineralogy, origin, dissolution kinetics and source of bioavailable Fe. *Deep-Sea Research Part II*, **58**, 1364–1375, 10.1016/j.dsr2.2010.11.011.

RUTGERS VAN DER LOEFF, M.M. 1994. ^{228}Ra and ^{228}Th in the Weddell Sea. *In* Johannessen, O.M., Muench, R.D. & Overland, J.E., *eds. The Polar Oceans and their Role in Shaping the Global Environment: The Nansen Centennial Volume- Geophysical Monograph*. Washington, DC, USA: American Geophysical Union, 177–186.

SCHOLTEN, J.C., PHAM, M.K., BLINOVA, O., CHARETTE, M.A., DULAIOVA, H. & ERIKSSON, M. 2010. Preparation of Mn-fiber standards for the efficiency calibration of the delayed coincidence counting system (RaDeCC). *Marine Chemistry*, **121**, 206-214, 10.1016/j.marchem.2010.04.009.

SHAW, T.J. & MOORE, W.S. 2002. Analysis of ^{227}Ac in seawater by delayed coincidence counting. *Marine Chemistry*, **78**, 197–203.

SHAW, T.J., RAISWELL, R., HEXEL, C.R., VU, H.P., MOORE, W.S., DUDGEON, R. & SMITH, K.L. 2011. Input, composition, and potential impact of terrigenous material from free-drifting icebergs in the Weddell Sea. *Deep-Sea Research Part II*, **58**, 1376–1383, 10.1016/j.dsr2.2010.11.012.

SHEPHERD, A., WINGHAM, D. & RIGNOT, E. 2004. Warm ocean is eroding West Antarctic Ice Sheet. *Geophysical Research Letters*, **31**, 10.1029/2004GL021106.

SMALE, D.A., BARNES, D.K.A., FRASER, K.P.P., PECK, L.S. 2008. Benthic community response to iceberg scouring at an intensely disturbed shallow water site at Adelaide

Island, Antarctica. *Marine Ecology Progress Series*, **355**, 85-94, 10.3354/meps07311.

STACHELHAUS, S.L. & MORAN, S.B. 2012. A simple differential diffusion model to account for the discrepancy between ^{223}Ra- and ^{224}Ra-based eddy diffusivities. *Journal of Geophysical Research*, **117**, 10.1029/2011JC007500.

STAMMERJOHN, S.E., MARTINSON, D.G., SMITH, R.C., YUAN, X. & RIND, D. 2008. Trends in Antarctic annual sea ice retreat and advance and their relation to El Niño–Southern Oscillation and Southern Annular Mode variability. *Journal of Geophysical Research*, **113**, 10.1029/2007JC004269.

SUN, Y. & TORGERSEN, T. 1998. The effects of water content and Mn-fiber surface conditions on ^{224}Ra measurement by ^{220}Rn emanation. *Marine Chemistry*, **62**, 299–306.

VAN BEEK, P., BOURQUIN, M., REYSS, J-.L., SOUHAUT, M., CHARETTE, M.A. & JEANDEL, C. 2008. Radium isotopes to investigate the water mass pathways on the Kerguelen Plateau (Southern Ocean). *Deep Sea Research Part II: Topical Studies in Oceanography*, **55**, 622–637, 10.1016/j.dsr2.2007.12.025.

VAN BEEK P., SOUHAUT M. & REYSS J.-L., 2010. Measuring the radium quartet (^{226}Ra, ^{228}Ra, ^{224}Ra, ^{223}Ra) in water samples using gamma spectrometry, *Journal of Environmental Radioactivity*, 101, 521-529.

VAN BEEK P., SOUHAUT M., LANSARD B., BOURQUIN M., REYSS J-L., JEAN P. & VON BALLMOOS P., LAFARA : A new underground laboratory in the French Pyrénées for ultra low-level gamma-ray spectrometry, *Journal of Environmental Radioactivity*, in press.

VAUGHAN, D.G., MARSHALL, G.J., CONNOLLEY, W.M., PARKINSON, C., MULVANEY, R., HODGSON, D.A., KING, J.C., PUDSEY, C.J. & TURNER, J. 2003. Recent rapid regional climate warming on the Antarctic Peninsula. *Climatic Change*, **60**, 243–274.

VENABLES, H.J., CLARKE, A., & MEREDITH, M.P. *In press*. Wintertime controls on summer stratification and productivity at the western Antarctic Peninsula. *Limnology and Oceanography*.

VERNET, M., MARTINSON, D., IANNUZZI, R., STAMMERJOHN, S., KOZLOWSKI, W., SINES, K., SMITH, R. & GARIBOTTI, I. 2008. Primary production within the sea-ice zone west of the Antarctic Peninsula: I—Sea ice, summer mixed layer, and irradiance. *Deep Sea Research Part II: Topical Studies in Oceanography*, **55**, 2068–2085, 10.1016/j.dsr2.2008.05.021.

WALLACE, M.I., MEREDITH, M.P., BRANDON, M.A., SHERWIN, T.J., DALE, A. & CLARKE, A. 2008. On the characteristics of internal tides and coastal upwelling behaviour in Marguerite Bay, west Antarctic Peninsula. *Deep Sea Research Part II: Topical Studies in Oceanography*, **55**, 2023–2040, 10.1016/j.dsr2.2008.04.033.

Chapter 7: Iron and aluminium in Ryder Bay

7.1 Abstract

Coastal areas are generally considered to not be subject to Fe limitation, although it has been demonstrated that Fe is unevenly distributed in these regions and significant Fe limitation can occur during periods of high productivity. Coastal Antarctic sources of Fe include melting sea-ice, upwelling of deeper waters, and glacial inputs. Along the continental WAP, very few Fe measurements have been undertaken. The only data from West Antarctica south of 65°S come from a recent study at Pine Island Bay, in the nearby Amundsen Sea. Thus the relative importance of different Fe sources is very poorly constrained in the WAP region. In this highly productive area, little is known of the potential for Fe limitation, or how Fe dynamics may respond to environmental warming. This chapter presents dissolved and total dissolvable Fe data from a coastal site on the WAP, spanning the peak of summer productivity in 2009. A significant glacial source of Fe is identified, and annual Fe flux associated with Sheldon Glacier (northern Ryder Bay) is estimated ranging from 80 μmol Fe m^{-2} y^{-1} to 246 μmol m^{-2} d^{-1} using two independent methods. This supply is very high compared to assessed biological demand, and Fe concentrations remain high even during peak productivity. Depth profile data also indicate a significant supply from WAP shelf sediments, making Fe limitation highly unlikely in the overlying waters. Measurements of dissolved and total dissolvable Al are also presented, highlighting the decoupling of Fe and Al sources, with very shallow sediments possibly influenced by sea-ice brines representing a greater source of Al than either glacial processes or shelf sediments.

7.2 Introduction

The biological role of dissolved Fe is of particular importance in the Southern Ocean. As the largest HNLC region in the world, the Southern Ocean holds the largest inventory of unused nutrients in surface waters. Iron is the primary factor

limiting productivity in this region, as determined by several mesoscale, *in-situ* Fe-enrichment experiments (Boyd *et al.* 2007). Low availability of light and silicate can also negatively affect phytoplankton growth, with co-limitation by Fe and light and/or Si being widespread (Boyd *et al*. 1999, Franck *et al*. 2000, Nelson *et al*. 2001). Further, this role is not limited to the modern ocean: variable Fe supply to the Southern Ocean over glacial-interglacial time scales has a disproportionate role on global climate (*e.g*. Martin 1990, Martinez-Garcia *et al*. 2011).

There are many pathways supplying Fe to the ocean, including coastal inputs, shelf/slope sediment resuspension, hydrothermal vent activity, glacial runoff, iceberg melt and atmospheric deposition (*reviewed in* Boyd *et al*. 2012). The role of Southern Ocean Fe supply to global climate has lead to increased understanding of the relative importance of Fe sources and the effects of Fe limitation on phytoplankton (Boyd & Ellwood 2010, Strzepek *et al*. 2012, Boyd *et al*. 2012, etc.). Recent studies (Boyd *et al*. 2012) suggest that the balance of Fe supply and use may change with global warming. However this same study highlights the need for more detailed and regional data, especially with regard to interannual variability.

In this regard, the WAP region deserves individual attention for several reasons. In addition to being one of the most productive regions of the Southern Ocean, the WAP shelf has been identified as a source region of Fe to the Atlantic sector (De Baar et al. 1995, Holeton *et al*. 2005, de Jong *et al*. 2012). High Fe concentrations near shore result in a horizontal Fe gradient observed at distances up to 3500 km (de Jong *et al*. 2012). Inputs from incursions of CDW (Moffat *et al*. 2009) and meltwater (Meredith *et al*. 2012) are balanced by export of shelf waters, some of which feed back into the ACC; in the north via Bransfield and Gerlache Straits (Hofmann *et al*. 1996, Zhou *et al*. 2002), and where topography or cyclonic gyres direct the flow offshore (*e.g*. Beardsley *et al*. 2004, Klinck *et al*. 2004). Thus the WAP is a key source of Fe to the productive Atlantic sector of the southern Ocean, but is also the fastest warming region in the southern hemisphere (King 1994, Vaughan *et al*. 2003). Continued warming can alter sediment Fe inputs (via increased deep water incursions) and glacial Fe sources (via greater melt and retreat).

There are relatively few Fe measurements from coastal areas of the WAP. Much of the research into Fe cycling has targeted offshore regions, (*e.g*. Martin *et al*.

1990, Löscher *et al*. 1997) or the northern WAP and nearby islands (<64 °S; *e.g*. Dulaiova *et al*. 2009, Ardelan *et al*. 2010). A very recent study in the Amundsen sea found a strong source of Fe from glacial melt (Gerringa *et al*. 2012), but the relative importance of glacial Fe remains poorly constrained (de Jong *et al*. 2012).

In this chapter, dissolved Fe concentrations ([dFe]) and total dissolvable Fe concentrations ([TDFe]) are presented from the austral summer of 2009 at a coastal site on the WAP. The TDFe fraction is Fe from both dissolved and particulate phases which is solubilised by a mild acid (1% HCl) leach, giving and indication of the readily labile fraction of total Fe. Time-series and depth profile data are examined to better constrain the relative importance of different Fe supply mechanisms in this region. These data are complemented by particulate elemental analyses, silicon isotopic measurements and naturally-occurring radiotracers to investigate supply versus biological demand, with the aim of better understanding how this balance may change with continued climate warming.

7.3 Methods

7.3.1 Sample collection

Samples for dissolved Fe concentrations ([dFe]) and total dissolvable Fe concentrations ([TDFe]) were collected from RaTS site 1 in Ryder Bay, Adelaide Island, Antarctica (Figure 2.1) from December 2009 to March 2010. The sampling site is situated ~4 km from shore over a local maximum water depth of 520 m. Previous work at the RaTS Site has shown the primary water source to be open exchange with water masses from northern Marguerite Bay, although surface waters can be modified by glacial melt and local topography (Clarke *et al*. 2008, Meredith *et al*. 2010). Marguerite Bay in turn has been shown to display water mass characteristics similar to the WAP region as a whole (Meredith *et al*. 2004).

Bi-weekly samples were collected from a depth of 15 m. Deeper waters (50-200 m) were sampled ~monthly. Water samples were collected using a 1.7 L Niskin-style bottle (Ocean Technical Equipment (OTE), Florida). All metal parts on the outside of the bottle were coated with paint and were inspected and recoated at regular intervals to prevent any rust from forming. The OTE bottle was soaked for

>24 h in 10% v/v HCl (Aristar grade) before each use. The original spigot was removed and replaced with one made of teflon, which was also acid-washed before each use. The bottle and spigot were rinsed with Milli-Q water before sampling. The OTE bottle was lowered on a Kevlar line and triggered with an acid-washed plastic messenger. On recovery of the OTE bottle, the water samples for [TDFe] were immediately collected in acid-clean and Milli-Q-rinsed 125mL LDPE bottles (Nalgene; cleaning details below). These LDPE bottles were rinsed with sample 3 times before being filled. Samples for [dFe] were collected in 4 L acid-washed (10% v/v HCl, >24 h) HDPE bottles that were also rinsed with seawater before filling. Samples for [dFe] were then kept in the dark until processing in the lab. The LDPE sample bottles were pre-washed by soaking in 50% v/v HNO_3 (Reagent grade) for 1 week, 50% v/v HCl (Reagent grade) for 1 week, and rinsed thoroughly with Milli-Q water. The bottles were then stored with Milli-Q and 1mL L^{-1} UpA-grade concentrated HCl (Romil, UK).

7.3.2 Aqueous sample processing

Samples for [TDFe] were acidified with 1 mL L^{-1} of concentrated UpA-grade HCl and stored in the dark at room temperature. Samples for [dFe] were filtered through a polycarbonate membrane filter (0.2 μm) in a polysulfone filter tower. All filtration equipment was washed in 10% v/v HCl (Aristar grade) at least overnight and thoroughly rinsed with Milli-Q prior to each use. The filtrate container and fresh 125 mL LDPE sample bottle were rinsed with filtrate three times before filling, then the [dFe] sample was acidified and stored as for [TDFe] samples. To minimise contamination, all manipulations were performed in a laminar flow hood. Samples for both [dFe] and [TDFe] were stored for at least 10 months prior to analysis, and were processed identically for Fe determination.

7.3.3 Determination of dissolved and total dissolvable iron concentrations

Dissolved Fe concentrations were measured using flow-injection analysis with 8-hydroxyquinoline (8-HQ) immobilized resin for pre-concentration and *N*,*N*-dimethyl-*p*-phenylenediamine di-hydrochloride (DPD, Sigma-Aldrich) (FIA-DPD-

NTA) after Measures *et al*. (1995). This method is based on the catalytic oxidation of DPD by H_2O_2 in the presence of Fe to create a bright pink-coloured semi-quinone derivative. Dissolved Fe in the sample is pre-concentrated on an 8-HQ chelating resin before being eluted into the reagent stream: the products of the reaction can be monitored using a spectrophotometer at 514 nm. The signal detection in this study was based on measured voltage, a proxy to measure the signal for transmission which can be converted to absorbance. This gives a quantitative measure of the reaction, which is converted to concentration by comparison with absorbance values of standards of known concentration. LabVIEW 7.1 software was used for instrument control and data collection, and a separate LabVIEW 6.1 programme for data processing. For lower Fe concentrations (<10 nM), peak heights were used; for higher [Fe] (>10 nM), peak areas were used as these gave a more linear calibration. The blank for reagents and colour developing stage is accounted for by measuring sample peak heights and areas relative to the baseline, or background, absorbance.

Certified reference materials were analysed to ensure accuracy of [Fe] measurements. The determined concentrations are listed in Table 7.1. Overall precision (based on duplicate measurements) was determined as ±3.4%, although this is somewhat higher at low concentrations. Precision at ~30 nM was better than 2%, and was 5–10% for concentrations below 10 nM. The detection limit, based on the lowest value for precision, is estimated at 0.75 nM, ~4-fold lower than the lowest [dFe] reported here. All analyses were performed by P. J. Statham and Marta Skiba at the NOC, Southampton, UK.

Table 7.1: Concentrations and results of certified reference material analyses. Standards used were Nearshore Seawater Reference Material for Trace Metals (CASS-5) and Seawater Reference Material for Trace Metals (NASS-6; both from NRC, Canada)

Reference material	Fe Concentration	Measured
CASS-5	25.78 ± 1.97	24.81
CASS-5	25.78 ± 1.97	26.81
NASS-6	8.86 ± 0.82	8.66
NASS-6	8.86 ± 0.82	9.95

Samples for TDFe were processed as for dFe, after gently decanting the solution into an acid-clean container such that any particulate material would not be transferred. After >10 months of storage, any readily-leachable Fe will be maintained in solution by the 1% HCl conditions.

7.3.4 Determination of dissolved aluminium concentrations

Concentrations of dissolved and total dissolvable Al were determined following the Lumogallion method of Hydes & Liss (1976). Lumogallion (3-(2,4-dihydroxyphenylazo)-2-hydroxy-5-chlorobenzenesulphonic acid) reacts with Al to form a fluorescent complex. The fluorescence of samples can thus be compared to standards to determine [Al]. Measurements of Al were performed on the same samples collected for Fe analysis, and all analyses were performed by P. J. Statham at the NOC, Southampton, UK. A standard solutions of Al was prepared from analytical grade aluminium potassium sulphate ×12 H_2O (1.758 g per 100 mL) to give a 1000 mg L^{-1} standard). This primary standard was diluted as needed to provide the standards used in the analyses.

As no certified reference materials exist for the determination of dissolved Al, measurement quality was assessed by relatively consistent fluorescence readings for standard solutions (within ~10%) between analyses, and the agreement of data acquired here with published values for comparable marine settings. Both of these aspects indicate reliable data quality.

7.3.5 Particulate sample processing

Particulates for were collected on acid-washed, 0.8 μm filters (to correspond with the filter pore size used for C and N analysis; 47 mm, polycarbonate membrane) under gentle vacuum (~50 mbar) using the same filtration device as for [dFe]. Filters were dried in a laminar flow hood and stored in acid-washed PetriSlides at room temperature.

Extractions were done by wet-alkali digestion methods, primarily to measure biogenic Si. Full methodology and details of the extraction conditions and trace metal determinations are given in Appendix A5.1. For Al, the values reported here are the total amounts of metal extracted during two sequential digestions, per L of

seawater. As the second extraction of this method focuses on the lithogenic fraction for corrections of lithogenic silica, the numbers presented here will reflect both biological and lithogenic Al, although this will underestimate the lithogenic fraction as full digestion was not possible due to filter degradation after long extraction times. Under the alkali and subsequent neutralised conditions used here, extracted Fe can precipitate as Fe (oxyhydr)oxides, therefore only particulate Al (PAl) data are reported.

7.4 Results

7.4.1 Aqueous metal concentrations

7.4.1.1 Concentration range in comparison to other studies

The ranges of dissolved metals were 3.3–9.7 nM for dFe, and 2–26 nM for dAl. Dissolvable metals (TDFe and TDAl) were much higher: 56–237 nM and 15.5–358 nM, respectively. A comparison is given in Table 7.2 between the concentrations found here and those from a range of other Southern Ocean locations including both nearshore and offshore. Concentrations of both dFe and dAl were high in Ryder Bay compared to many areas of the ocean, but consistent with other coastal Antarctic studies. Offshore surface water concentrations are generally very low (often <1 nM for both Fe and Al), with significant enrichment in coastal areas. The very good agreement of dFe concentrations from this study and values reported for the Gerlache Straight (Martin *et al*. 1990), northern WAP (Sanudo-Wilhelmy *et al*. 2002) and near the Kerguelen Islands (Bucciarelli *et al*. 2001), in addition to good values for reference materials, indicate that we have accurately measured dFe in Ryder Bay. The range for dAl agrees very well with recent data for Ryder Bay surface waters (Hendry *et al*. 2010), indicating that dAl measurements are also in line with other studies.

Table 7.2: Comparison of dissolved and total dissolvable Fe and Al in Southern Ocean waters in the vicinity of the WAP. Where available, results are given as a range, or (mean ± standard deviation).

Study	Location	dFe (nM)	TDFe (nM)	dAl (nM)	TDFe (nM)
Martin et al. 1990	Drake Passage, surface	0.16			
	– Gerlache Straight, surface	7.4			
Westerlund & Ohman 1991	Weddell Sea	0.44 – 13			
de Baar 1995	Antarctic Circumpolar Current	0.4 – 1.3			
	Polar Front	1.5 – 2.5			
	Drake Passage	<0.25			
Löscher et al. 1997	UCDW	0.6 – 1.1	0.9 – 2.3		
Bucciarelli et al. 2001	Kerguelen Islands – offshore	0.46 – 0.71			
	– near shore (2 km), near surface	5.3 – 12.6			
	– near shore, near bottom	18.4 – 22.6			
Planquette et al. 2007	Crozet Islands	0.086 – 2.48			
Hewes 2008	Weddell-Scotia confluence	0.35 – 3.05			
Planquette et al. 2009	Crozet Islands		0.15 – 13.2*		0.11 – 25.5*
Ardelan et al. 2010	Northern WAP – coastal	1 – 3	8 - 140		
	– offshore	0.1 – 3			

Table 7.2 (continued):

Study	Location	dFe (nM)	TDFe (nM)	dAl (nM)	TDFe (nM)
Measures and Edmond 1990	UCDW			(3)	
	– brine			70 - 300	
Moran et al. 1992	Weddell Sea			1 - 5	
Préndez et al. 1996 (*in* Préndez & Carrusco 2003)	KGI, superficial waters			3040 - 10200	
Sañudo-Wilhelmy et al. 2002	Weddell Sea, surface waters	(1.7 ± 0.46)		(3.17 ± 1.33)	
	Northern WAP, coastal	4.5 - 31		56 - 660	
Préndez and Carrasco 2003	King George Island (KGI), lagoons			< 3.7 – 1100 (163)	37 – 1100
Middag et al. 2011	Weddell Sea, surface waters			(0.7 ± 0.43)	
	– sub-surface minimum			0.33	
Hendry et al. 2010	Ryder Bay surface water			2 – 27	
	– sea-ice			17.3 – 41.7	
This study	Ryder Bay – 15m time-series	3.5 – 9.4	57 – 237	3.6 – 17	15.7 – 357
	– all depths	3.3 – 9.7	56 – 237	2.0 – 26	15.5 – 358

*Total metal concentrations of the particulate (>53 μm) fraction, the labile portion of which would be included in TDFe analysis.

7.4.1.2 Trends in dissolved and dissolvable iron concentrations

Concentrations of dFe and TDFe are shown in Figure 7.1. Sampling was most frequent at 15 m, the long-term average depth of the chl maximum (Clarke *et al*. 2008). At this depth, dFe ranged from 3.5 to 9.4 nM. The main features of dFe at 15 m were the sharp increase in late December (followed by a steep decline), and the more gradual increase in the second half of January followed by a decrease during February. In general, concentrations at 100 m were very similar to those at 15 m, although the early sample (7 January) was ~2.5 nM higher at depth than at 15 m. Where sampling resolution at 100 m increased after mid-February, there was good agreement between samples from the two depths.

Total dissolvable Fe includes both the dissolved phase and particulate Fe that can be released by mild proton attack, and should thus reflect labile or potentially bioavailable Fe. Total dissolvable Fe was present at much higher concentrations than dFe, and again there was relatively good agreement between depths for samples where data is available at both 15 m and 100 m. Concentrations varied from ~50–230 nM, with a distinct maximum on 30 January, when a maximum was also seen in dFe.

In addition to time-series samples, water was also collected from additional depths ~monthly as time allowed. On three occasions, multiple samples (to 100 m or 200 m) were collected to investigate changes in [dFe] and [TDFe] with depth, and these are shown in Figure 7.2. These data show a subsurface minimum in [dFe] at 50m. At 200 m, dFe reached a maximum of almost 10 nM. No TDFe measurements are currently available to see if the 50 m minimum was also present in TDFe as well.

7.4.1.3 Trends in dissolved and dissolvable aluminium concentrations

The distribution of dAl near the surface (15 m) shows two distinct periods with respect to the trends in dFe (Fig. 7.1). During the first half of the season, dAl was highly variable and showed no clear relationship with dFe. In contrast, the trends in dAl were very similar to those of dFe during the second half of the season.

While there is only one early season sample available at depth (100 m), this sample had relatively high dAl compared to the later part of the season. In contrast, early dFe at depth was within the same range as samples from February-March.

From mid-February, where sampling resolution is higher, dAl and dFe at 100m exhibited very similar trends, as in surface waters.

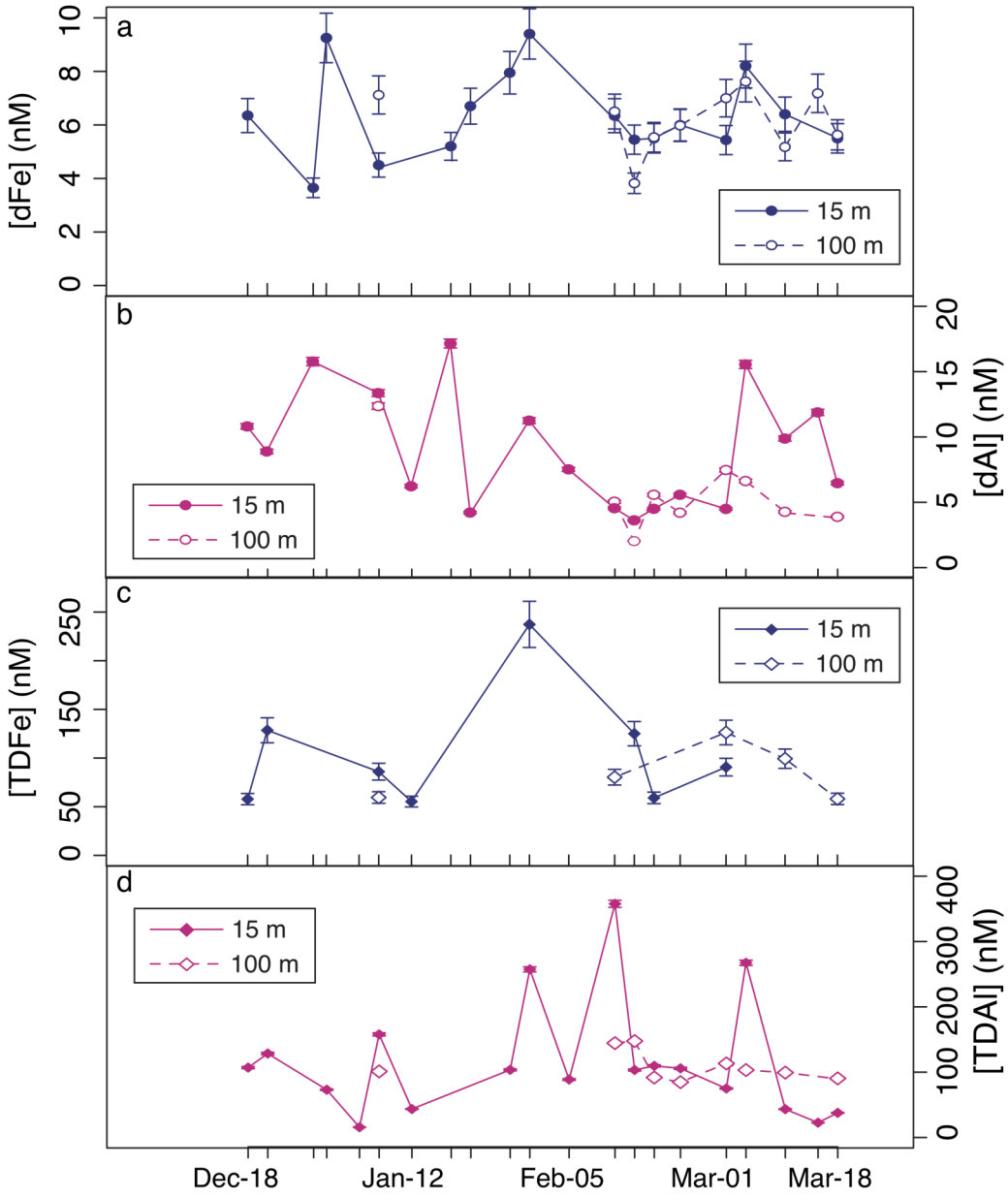

Figure 7.1: Time-series data of dissolved (a and b) and total dissolvable (c and d) metals from the 2009-2010 austral summer. Iron is given in blue, Al in pink. Samples from 15 m are filled symbols, and those from 100 m are open symbols. All error bars are shown as the precision of the method, as this is greater than the error of replicate measurements.

As with Fe, the distribution of Al with depth was also examined. Figure 7.2 shows both dAl and TDAl throughout the water column on three separate days, from

early January to late season. Trends in dAl were somewhat more variable than for dFe, with the greatest degree of enrichment near the surface (5 m) but low concentrations at 10 m depth. At 15 m there was enrichment, and lower concentrations at 50 m, similar to the dFe minimum, although for Al, the lowest concentrations were found at 5 m. Concentrations from 50-200 m were very consistent, with higher values seen in the early sample compared to the two later ones.

Total dissolvable Al showed some differences from the dissolved phase. In the early sample, concentrations in shallow waters were much higher than at 50 m, with the very low dAl at 10 m not reflected in TDAl. The later two profiles had very similar values of TDAl at 15 m and 100 m. At 50 m, there was a peak in the concentration of TDAl in the 22 February sample that again was not seen in dAl. Given the very high value of this sample, it is possible that this sample may have been contaminated, as there was no peak in dAl, dFe or TDFe on this date. The final depth profile included a sample at 200 m that indicates some enrichment of TDAl below 100 m, in contrast to dAl.

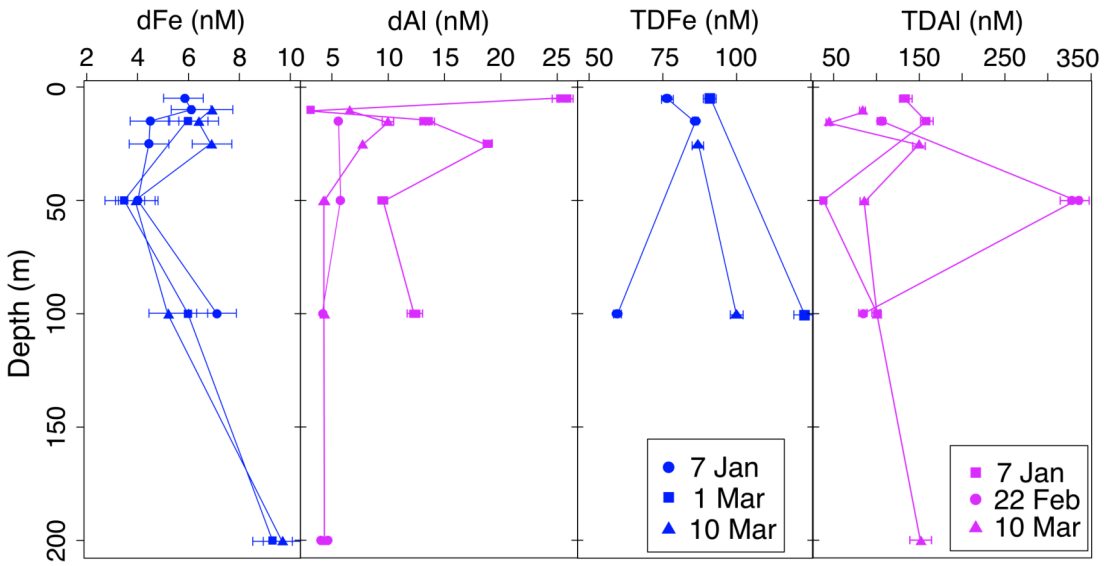

Figure 7.2: Depth profile samples for dissolved (left) and total dissolvable (right) Fe (blue) and Al (pink) concentrations. Error bars are shown as the precision of the method, as this error is greater than that for replicate analysis.

7.4.1.4 Spatial variability in metal concentrations

Three additional stations were sampled to investigate variations in metal concentrations near a glacier terminus and exposed land (Fig. 7.3). Samples were collected by hand from the boat, at 0 m water depth. The concentration of dFe was slightly lower near the glacier (5.6 ± 0.9 nM) than at the other two stations (7.7 ± 0.2 nM; Table 7.3). Dissolved and total dissolvable Al varied over a greater range, from 3.9 ± 0.2 nM near the glacier to 24.6 ± 4.3 nM at the stations near land. The ratio of dissolved Fe:Al for the glacier station (1.4) was much higher than near land (~0.3; Table 7.3).

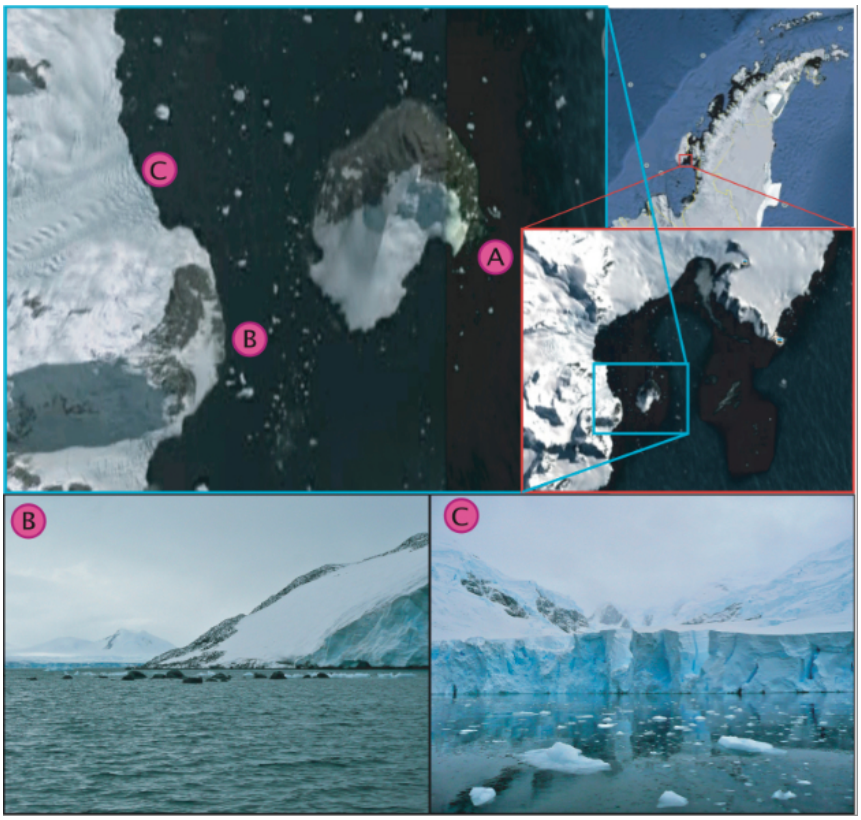

Figure 7.3: Locations of sampling near exposed land (A, B) and the edge of a glacier (C). Lower photographs show the surroundings at sites B and C.

Table 7.3: Concentrations of dissolved and total dissolvable Fe and Al at the three sampling locations shown in Fig. 7.5 ("nd" denotes no data is available.) Where repeat analyses of a sample are available, results are given as mean ± SD.

Station	dFe (nM)	TDFe (nM)	dAl (nM)	TDAl (nM)	dFe:dAl
A	7.8	nd	27.6	153	0.28
B	7.7 ± 0.2	nd	21.6	95.9	0.35
C	5.6 ± 0.9	nd	3.9 ± 0.2	39.4	1.4

7.4.2 Particulate data

Ideally, TDFe would be equal to the sum of the dissolved and particulate fractions. However, in practice the separation between the two phases and presence of non-labile minerals can often disrupt this relationship. Especially here, the use of alkali digestion for particulates to target BSi versus the TDFe/TDAl leaches using acid will target different mineral phases. While Al should be released by both acid and alkali leaches, the disagreement between TDAl and PAl plus dAl suggests that different phases and/or the incomplete dissolution of the lithogenic faction are significant factors. Nevertheless, while absolute concentrations of PAl determined here may reflect different fractions of metals and thus not be directly comparable to TDFe/TDAl data, as all particulate samples were analysed in the same manner, the timing, direction and magnitude of relative changes in this fraction still provide useful information to investigate sources and fate of these metals.

Particulate Al, which should include both biogenic and lithogenic fractions, is shown in Figure 7.4 A peak in particulate Al was seen on the same date as the maxima in dFe, dAl, and total to dissolved ratios of both metals. This occurred on 30 January, approximately 15 days before the chl peak.

There was relatively little agreement between trends in PAl and BSi. A small increase in BSi in late December was also present in PAl, but the main pulse of BSi in February was absent in the PAl record (Fig. 7.4). Thus there was no clear relationship between the variations in PAl and BSi.

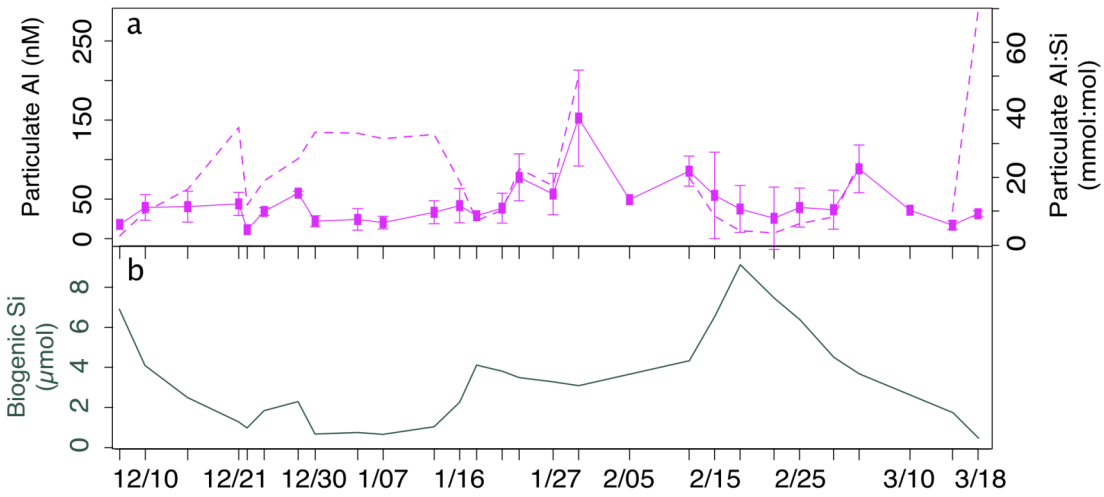

Figure 7.4: (a) Particulate Al extracted from particulate samples from 15 m depth during two 1-hour wet alkali digestions (solid line). Error bars represent standard deviations from duplicate filters. Particulate Al:BSi from the same analysis is also shown (dashed line). Error bars are not displayed, but due to the very low metal concentrations range from 10% to 90% of the sample mean. (b) Trends in BSi per L at 15 m are shown for comparison.

Particulate Al data showed considerable variability with water column depth (Figure 7.5). Shallower waters had higher PAl than deeper waters, in general. Variation between depths was greatest during the first half of the season. One sample is available for 100 m, in which PAl was low, but PAl:BSi was within the range of surface sample variation.

Particulate Al is also available from austral summer 2008 for comparison (Fig 7.5). Summer 2008 was a low-chl year (see Chapter 2): [chl], POC and BSi were low throughout December, and very low thereafter. The range of PAl was similar to 2009, and averages at 15 m were 43 and 49 nM in 2008 and 2009, respectively. Again, the surface waters (0 m) tended towards higher PAl than deeper samples. Due to the low BSi, ratios of PAl:BSi were noticeably higher in 2008 (mean 47 mmol:mol at 15 m, versus 20 in 2009).

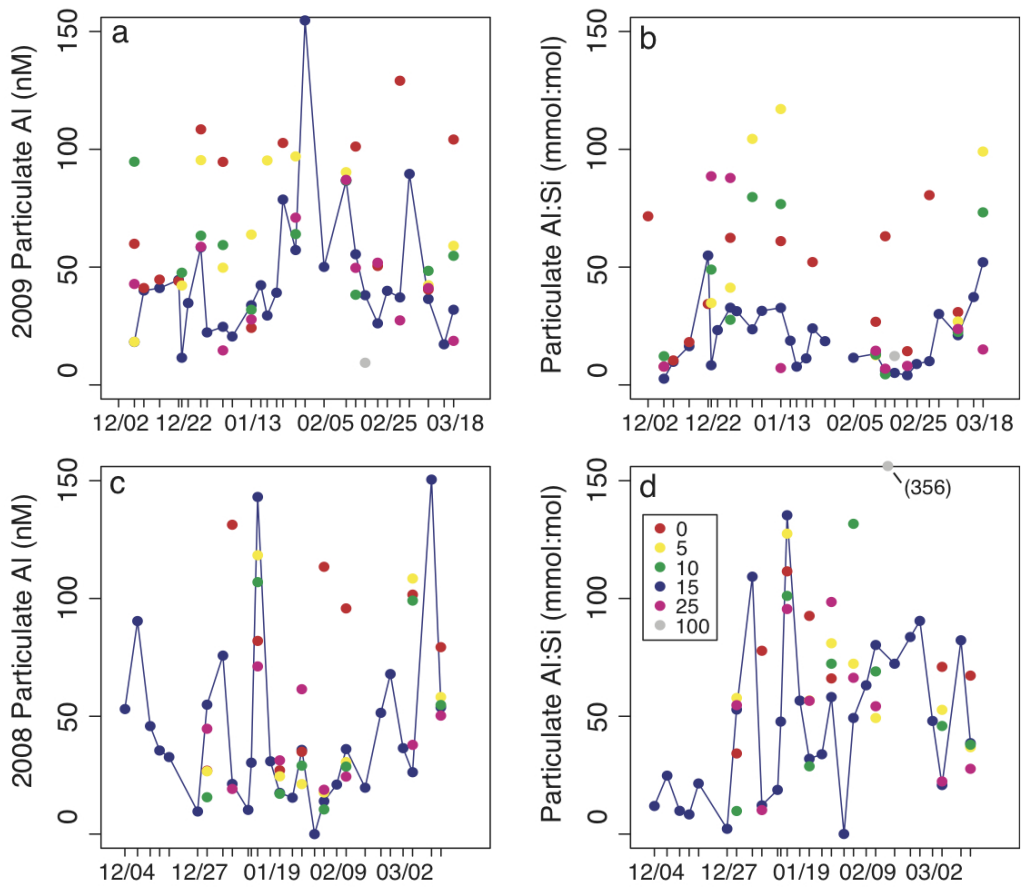

Figure 7.5: Particulate total wet-alkali digestible Al (a) and Al:Si (b) in the top 25 m for the 2009 summer season. One sample is also available for 100 m (shown in grey). PAl (c) and Al:Si (d) from 2008 are also shown for comparison. Samples are coloured by depth, as shown in the legend.

7.4.2.1 Readily available particulate iron

Previous studies have indicated that some of the Fe in particulates may be bioavailable (*e.g.* Wells *et al.* 1995, Planquette *et al.* 2009). However, the analysis and even definition of bioavailable Fe remains problematic and unresolved. Here, an index of the readily available fraction of particulate Fe (PFe_{RA}) was calculated as the difference between TDFe and dFe. As the use of HCl to store TDFe samples will extract the more labile phases of particulate Fe, this gives an indication of the particulate Fe which may be most available to phytoplankton, similar to that presented by Planquette et al. (2009), although this cannot be considered an accurate measure of bioavailability.

The calculated PFe_{RA} are presented in Figure 7.6. As other studies have shown (De Baar & de Jong 2001, Lam *et al*. 2006, Planquette *et al*. 2009, Ardelan *et al*. 2010), the majority of Fe in surface waters is present in the particulate phase, and thus PFe_{RA} exceeds dFe by an average of 9-fold in the data from Ryder Bay. As PFe_{RA} is the dominant fraction of TDFe, the trends identified in the PFe_{RA} data are the same as those found in TDFe. In shallow waters, [PFe_{RA}] peaked on 30 January; at depth the maximum concentration was found on 1 March. As for TDFe, the range of values was largely similar at 15 m and 100 m.

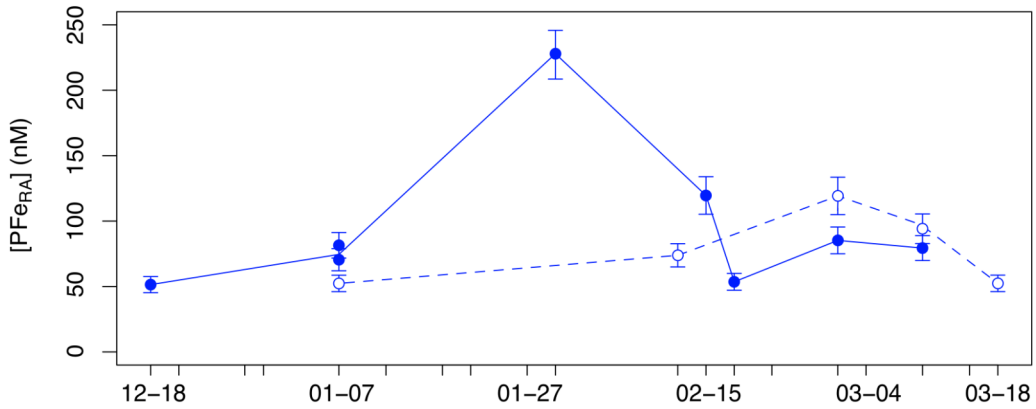

Figure 7.6: Readily available particulate Fe (PFe_{RA}) at the RaTS site. Shallow waters (15 m) are shown as solid symbols, deep waters (100 m) are denoted by open symbols.

7.5 Discussion

7.5.1 Iron supply

Iron is supplied to the oceans via several different pathways. In open-ocean regions, dust fluxes can be a significant source, with low dust fluxes largely believed to be responsible for Fe limitation in the Southern Ocean (Mahowald *et al*. 2005, Lancelot *et al*. 2009, Boyd & Ellwood 2010). Upwelling of deeper waters can bring Fe to the surface, and in coastal areas this is enhanced by Fe release from sediments due to the role of Fe in microbial respiration of POC (Froelich *et al*. 1979). For the WAP shelf region, Fe enrichment from shelf and island sources is well established (Charette *et al*. 2007, Planquette *et al*. 2007, Dulaiova *et al*. 2009, Ardelan *et al*. 2010), and de Jong *et al*. (2012) have demonstrated a significant signal of Fe in

surface waters up to 3500 km downstream of shelf sources. Terrestrial runoff and riverine fluxes are significant sources, although the solubility of Fe decreases on entry into the marine environment as salinity increases. In polar regions with low or no terrestrial runoff, sea-ice and glacial meltwater can both release Fe into surface waters. Sea-ice can acquire metals from sea water during formation, and accumulate atmospheric fluxes over the winter. These are then released during melt (Sedwick & DiTullio 1997, Sedwick *et al*. 2000, Lannuzel *et al*. 2007, 2011). Glacial ice contains terrigenous material which can release Fe (Raiswell *et al*. 2006, 2008, Statham *et al*. 2008, Raiswell 2011, Shaw *et al*. 2011), and studies indicate that iceberg presence increases local Fe concentrations (Gerringa *et al*. 2012). On a larger scale, glacial melt and subglacial flow, especially of land-terminating glaciers, can be associated with extremely high metal concentrations (up to 3 orders of magnitude greater than marine concentrations for a Greenland glacier; Charette 2012).

7.5.1.1 Deep water sources of iron to Ryder Bay

Below 50 m, dFe in Ryder Bay increased from <5 nM to ~10 nM at 200 m depth (Fig. 7.7). No deeper samples are available, but offshore concentrations of Fe in CDW, the source for subsurface WAP waters, have been measured as 0.6–1.1 nM (Löscher *et al*. 1997). The high [dFe] seen here at 200 m indicates that the water mass must acquire Fe as it moves onto the shelf from the ACC. This reflects a strong Fe source from the sediment on the WAP shelf and/or slope, consistent with observations from other studies (de Jong *et al*. 2012, Gerringa *et al*. 2012, Ardelan *et al*. 2010, Dulaiova *et al*. 2009, Korb *et al*. 2005).

Iron supply from shelf sediments reflects the redox chemistry of Fe. In areas of high POC flux, microbial respiration can deplete oxygen, resulting in anoxic conditions within the sediments. If nitrate is also depleted, oxidation of POC proceeds via the reduction of sulphate (SO_4^{2-}) and Fe^{3+} (Froelich *et al*. 1979). This microbially mediated process produces Fe^{2+}, which is soluble in seawater. Due to the strong concentration gradient, this Fe^{2+} can diffuse out of sediment pore waters and into the overlying water column, a process which can be enhanced by bioturbation

(Severmann *et al*. 2010). This high-Fe deep water can then act as a source to shallower waters via upwelling, deep mixing or diffusion.

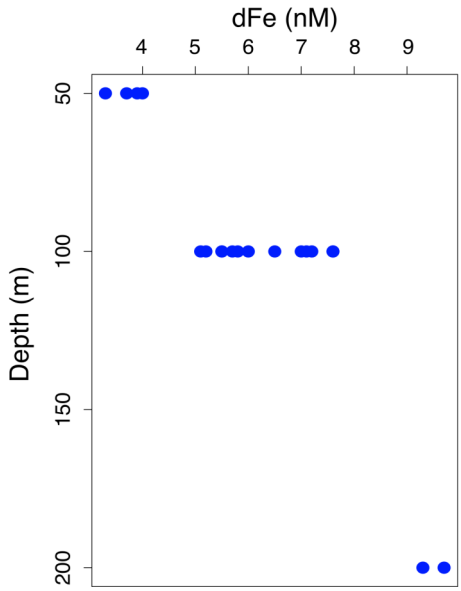

Figure 7.7: Deep (>50 m) water values of dFe. While there is some scatter, where 3 points are available for the same day, the linear regression between them has r^2 values of > 0.98 in all cases.

The magnitude of sedimentary Fe release to overlying waters depends on several factors, including the solubility of such Fe. While organic ligands can help to retain Fe in solution, they are generally considered saturated and present in low concentrations in deeper waters. Iron released from sediments by resuspension has been shown to rapidly adsorb onto particles, although this Fe is thought to be labile and readily returns to the dissolved phase (Homoky *et al*. 2012). However, offshore Fe advection is already known to occur based on previous studies (Buciarelli *et al*. 2001, Planquette *et al*. 2007, Charette *et al*. 2007, Dulaiova *et al*. 2009, Ardelan *et al*. 2010, De Jong *et al*. 2012), indicating that solubility of sedimentary Fe is sufficient to allow signficant transport by advection.

7.5.1.2 Potential for iron limitation

Iron limitation is a significant problem in many of the world's oceans, creating vast areas of nutrient under-utilisation due to low Fe availability. In Ryder Bay, proximity to coastal Fe sources, as well as inputs from high-Fe deep waters

make Fe-limitation an unlikely scenario, although high biological demand has been demonstrated to cause sporadic Fe-limitation even in coastal waters (Hutchins *et al*. 1997). The ratios of nutrients supplied to the surface mixed layer compared to the ratio of uptake determine which nutrient will be depleted first, and therefore if Fe has the potential to limit productivity in Ryder Bay.

Macronutrient and dFe concentrations from deep water (100 m) are shown in Table 7.4. These measurements indicate that supply of nutrients from depth will have a ratio of 200–340 µmol/mol Fe:N and 2.5–4 mmol/mol Fe:P.

Table 7.4: Deep water (100 m) nutrient and Fe concentrations and ratios for dates where all three elements were measured.

Date	Fe (nM)	N (µM)	P (µM)	Fe:N (µmol/mol)	Fe:P (mmol/mol)
Jan 7	7.1	24.4	1.86	287	3.82
Feb 12	6.5	19.23	1.62	338	4.01
Feb 22	6.0	30.11	2.4	199	2.50
Mar 10	5.15	22.58	2.05	228	2.51
Range				200 - 340	2.5 - 4
Fe:C*				30 - 52	24 – 38

*Converted to Fe:C ratio based on the Redfield ratio (106:16:1 for C:N:P)

Literature values for Fe-replete phytoplankton in the field are ~40 µmol Fe:mol C (Twining *et al*. 2004), and culture work indicates that diatoms are unlikely to suffer Fe stress at ratios above 10 µmol Fe: mol C (Sunda & Huntsman 1995, Maldonado &Price 1996). Using Redfield ratios (C:N:P of 106:16:1), for Fe-replete cells, these ratios would be ~260 µmol:mol for Fe:N, and 4.2 mmol:mol for Fe:P. Thus the supply from Ryder Bay deep water can be compared to Fe nutrition: deep water Fe supply is comparatively high relative to N, although Fe:P supply is lower than the theoretical demand for Fe-replete cells. For Fe-stress to occur, however, ratios would have to fall below 66 µmol:mol Fe:N and 1.1 mmol:mol Fe:P, which in both cases are at least 2-fold lower than the supply here, indicating that the supply of Fe from below is sufficient to preclude Fe-limitation in Ryder Bay.

The slopes of nutrient concentration in deeper waters (50–200 m for Fe; 15-100 m for N, P; data not shown) reflect the ratios of nutrient depletion relative to depth. The ratios of nutrient use from this analysis are 140–460 (mean = 280) μmol:mol Fe:N, and 2.1–5.0 (mean = 3.8) mmol:mol Fe:P, both in very good agreement for the theoretical values of Fe-replete phytoplankton. Ratios of Fe:N and Fe:P were lowest in samples near the peak of productivity (Feb 22nd), indicating that Fe acquisition slowed relative to macronutrients, and in the case of Fe:P was below the supply (deep water) ratio. However, even these lowest Fe:P ratios (and Fe:N) are still well above the ratios for Fe-stressed cells. Again, this indicates Fe-limitation would not occur in Ryder Bay, based on upward nutrient fluxes (Table 7.4).

7.5.1.3 Seasonal sources of iron to Ryder Bay

Any upward flux of Fe during summer must largely be a diffusive process, as water mass properties through the season show predominantly downward movement due to the development of a low-density, meltwater-rich layer at the surface that depresses the other water masses (Fig. 7.8). The movement of these water masses (and meltwater rich surface layer development) is clearly seen in dFe concentrations (Fig. 7.9). In the modified CDW that intrudes onto the shelf, concentrations of dFe are ~9.5 nM in Ryder Bay. Samples from 100 m are near the centre of the WW layer, and decrease from 7.1 nM to 6.0 nM from January to February. The lowest value at this depth (5.2 nM) is from the March sample which is predominantly AASW. Concentrations further decrease into the AASW layer (~50 m), where dFe is ~4 nM. Above this, AASW mixes with melt water, and this surface meltwater has high dFe concentrations.

The robust association of [dFe] with Ryder Bay water masses, especially the strong and sustained [dFe] minimum in the AASW layer, has important implications for Fe supply in this location. The Fe-replete deep waters can act as a source of Fe to WW, and replenish Fe that is removed by biological production. However, given the strong gradients restricting vertical mixing during summer this is unlikely to occur during the summer bloom period, and even diffusion-driven supply must be small. Over winter, deep mixing and homogenisation of the upper water column will make deep water supply of Fe a significant source, redistributing Fe throughout the WW

layer. This is linked to very strong mixing during unstratified winter conditions (*e.g.* winter/spring storms), as even in March when stratification begins to break down, the MLD remains well above the depth of the [dFe] minimum. Over the shorter time periods relevant to [dFe] fluctuations at 15 m during summer, there must be additional Fe sources to explain the high [dFe] seen in shallow waters.

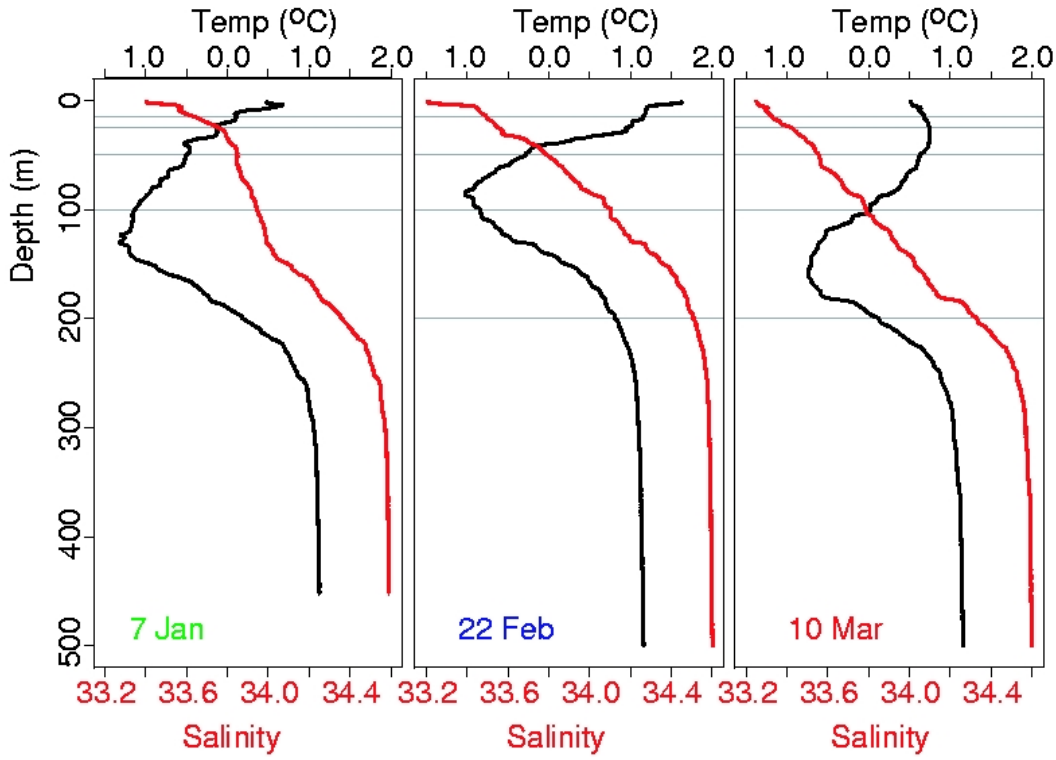

Figure 7.8: Depth-profile temperature and salinity for the three Fe depth profile sampling events. Presence of WW is clearly seen in a temperature minimum, and initially shallows slightly (22 Feb; although the first two samples at 100 m are definitely within this WW layer). However the last sample at 100 m is above the centre of the WW layer, and the 200 m sample includes a much greater proportion of WW. Fe sample depths are shown by the grey lines. Differentiation of water masses (especially above 50 m) is aided by T-S plots).

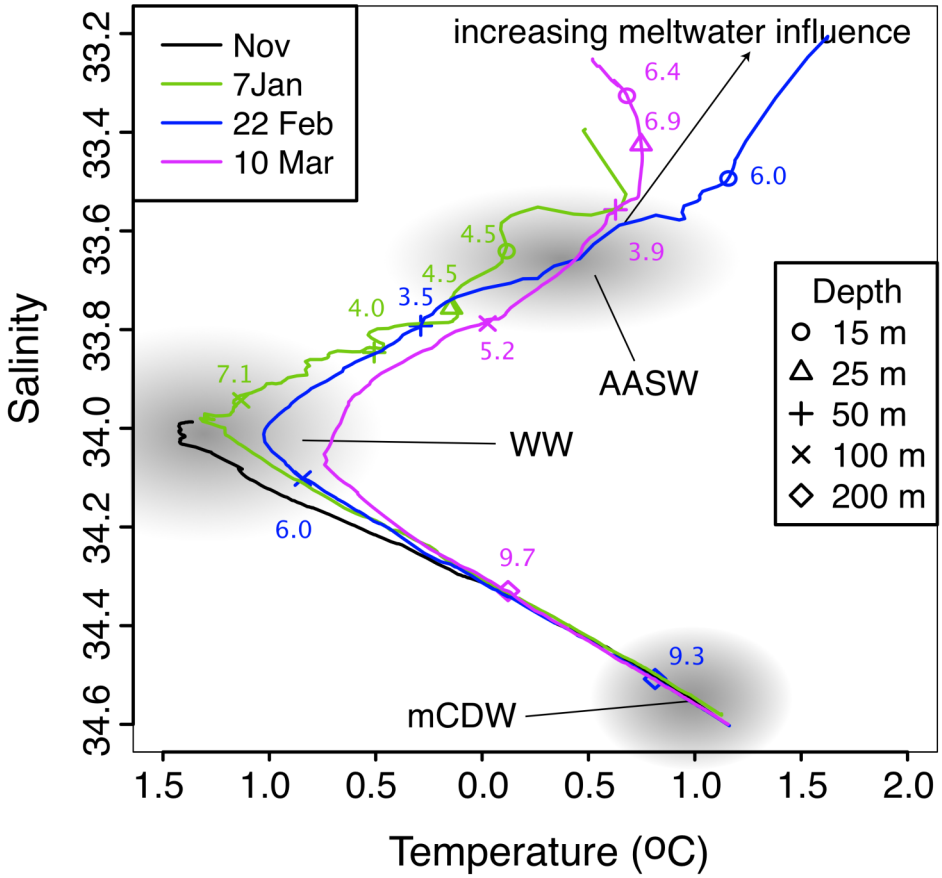

Figure 7.9: Temperature-salinity plot showing water column properties from four sampling events. Depths are indicated by symbols as shown in the legend. Symbols are accompanied by dFe concentrations (in nM). The shaded regions correspond to properties of mCDW, WW, AASW and melt water influenced AASW, and are labelled on the diagram.

7.5.2 Summertime sources of iron to Ryder Bay surface waters

7.5.2.1 Dominant surface inputs

Despite the high concentrations of dFe at depth, deeper waters are unlikely to be a significant source of Fe to surface waters during the summer bloom period. The high [dFe] in surface waters (0–25 m) reflect inputs at the surface. Such sources could be glacial melt (direct and via land run-off), sea-ice melt, sea water interaction with shallow sediments, or atmospheric inputs.

Over the day-to-week scale of Fe enrichment seen here, atmospheric deposition in a low-dust environment is very unlikely to account for the significant surface signal seen in Ryder Bay. Iron can be released from shallow sediments, but

this process is expected to be limited within the season, as activities, mixing rates and water ages derived from radium isotopes all imply very low fluxes from the coast into central Ryder Bay (see Chapter 6). Consequently, this section examines melt water as a source of summer Fe inputs.

7.5.2.2 Meltwater from glacial versus sea-ice sources

Both sea-ice and glacial melt water have been shown to supply Fe to polar surface waters. Sedwick & DiTullio (1997) observed high [dFe] near sea-ice, alleviating Fe-limitation in the Ross Sea. Lannuzel *et al*. (2007) measured sea-ice Fe concentrations up to an order of magnitude higher than those in underlying waters, and estimate that melting sea-ice may supply up to 70% of daily Fe inputs during the melt period. Similarly, icebergs have been observed in small-scale bloom areas (Smith *et al*. 2007) and were postulated to stimulate productivity via Fe release. Indeed, glacial ice releases significant amounts of terrigenous material and Fe into sea water (Raiswell *et al*. 2006, 2008, Statham *et al*. 2008, Shaw & Moore 2011, Raiswell 2011). There are three episodes of increasing surface dFe concentrations during the study period, and this section examines these more closely to elucidate the relative importance of different Fe inputs at the surface.

There is a sharp increase in [dFe] from 3.65 nM on 28 December to 9.25 nM on 30 December 2009, where salinity also changes abruptly (Figure 7.10), indicating an influx of low-salinity melt water. Salinity averaged over the top 15 m of the water column shows an even greater decrease in salinity, thus the melt water would have been present primarily above 15 m, consistent with a surface meltwater source. While meltwater can potentially come from sea-ice, the very low preceding winter sea-ice cover in the region and absence of sea-ice in Ryder Bay just prior to this date points to a meteoric source (glacial ice and snow) instead.

There is a steady increase in [dFe] from 7–30 January. During this period, salinity at 15 m, and average salinity over the top 15 m, both decrease. This suggests an extended period of meltwater influx, which as discussed above, is highly likely to come from meteoric sources rather than sea-ice. Based on these two periods of

increases in dFe, it can be concluded that meteoric runoff is a significant source of Fe to Ryder Bay during summer.

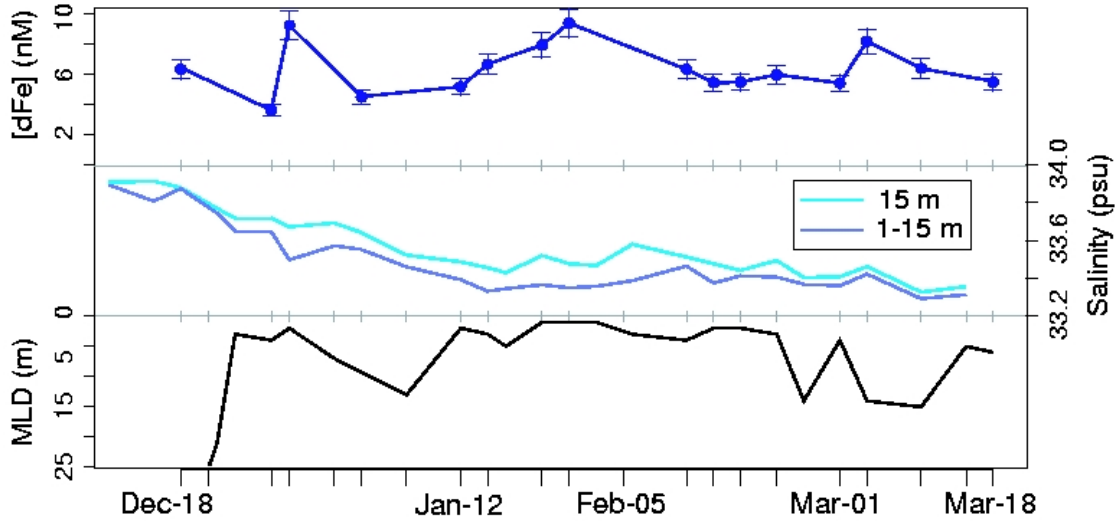

Figure 7.10: Time-series data of [dFe] (top plot), compared to water column physical properties: (middle) average salinity in the top 15 m and salinity at 15 m (light and dark lines, respectively); and (bottom) mixed layer depth.

However, the late-season (4 March) increase in dFe does not show such a straightforward relationship to salinity. The increase in dFe (of ~2.7 nM) occurs where salinity increases very slightly. This suggests that meltwater inputs are not the only source of [dFe] variability in Ryder Bay surface waters. Records at the RaTS site show rapid changes in the MLD over this period, with the higher [dFe] associated with deeper MLD (although still above the sampling depth of 15 m). We postulate that the increase in [dFe] at this time is due to redistribution of Fe in the upper water column driven by physical mixing. In support of this, all samples from 25 m and above from the depth profile on 10 March displayed the same [dFe] (within error; mean 6.8 nM; Fig. 7.1). There is an increase in the concentration of both dissolved metals on this date, and this is discussed further in section 7.5.4.2.

In addition to the close agreement of [dFe] trends with glacial inputs, changes in PFe_{RA} also suggest a glacial rather than sea-ice source. Particulate data reflects TDFe rather than BSi, indicating that the majority of the readily available metals in particulate phase is lithogenic. A strong lithogenic component suggests a glacial source carrying entrained terrigenous material.

Sea-ice is also a potential source for Fe in Ryder Bay, as several studies have observed high Fe concentrations in sea-ice (*i.e.* Sedwick & DiTullio 1997, Sedwick *et al*. 2000, Lannuzel *et al*. 2007, Lannuzel *et al*. 2011). However, Lannuzel *et al*. (2007) show that [dFe] is greatest in winter ice, and much lower in the more porous, spring ice found before and during sea ice melt. Due to the very low preceding winter sea-ice coverage here, we were unable to systematically sample sea-ice. One small piece was recovered during a sampling event in early January; the ice was very porous and left to drain during transport back to the lab where it melted and was filtered. Iron in the filtrate was measured at 1.9 nM, which is very low, but consistent with porous, Fe-poor sea-ice. This suggests that melting sea-ice is not a source of Fe to underlying waters in Ryder Bay, especially when considered with the scarcity of sea-ice in Ryder Bay preceding this study. This is also consistent with the evidence for predominantly lithogenic PFe, as accumulation of lithogenic material in sea-ice is expected to be much lower than for glacial ice and glacial melt processes.

7.5.2.3 Glacial iron input estimates

Glacial sources have already been shown to contribute significantly to Southern Ocean Fe supply, thus it is not surprising that they are also highly significant in Ryder Bay. This section uses two separate methods to estimate the magnitude of seasonal Fe inputs from glacial sources to Ryder Bay, based on salinity and radium.

The contribution of meteoric water to the water column can be calculated based on salinity and $\delta^{18}O$ data (Meredith *et al*. 2008). The maximum difference between % meteoric water contributions at 15 m for the summer of 2009-2010 is 2.58% (= 4.21% in March 2010 minus 1.62% in October 2009; Meredith *et al*. 2012). Assuming this contribution is constant within the top 15 m (which will lead to a minimum glacial contribution), and using published measurements of [dFe] in glacial ice (20–50 nM dFe; Raiswell *et al*. 2006) results in a minimum seasonal input of 7.5–19.5 μmol Fe m^{-2}. If melt is constant during the 130 day season, this equates to a daily flux of 58–150 nmol Fe m^{-2} d^{-1} to the top 15 m of Ryder Bay. There is more uncertainly around TDFe content in glacial ice (9–86 mM, excluding an estimated

90% that will sink out as particulates; De Baar & de Jong 2001, Raiswell *et al*. 2006), giving an estimated flux of 27–250 μmol Fe m^{-2} d^{-1} for total particle-reactive iron. As melt will not be uniform throughout the season, daily input may vary considerably beyond these range estimates.

Alternatively, analysis of Ra allows a second, independent estimate of Fe flux. An upper estimate of coastal sediment fluxes was calculated as 230 dpm ^{228}Ra m^{-2} d^{-1} (*see* Chapter 6). Using the Fe:^{228}Ra ratio measured at the northern tip of the WAP (9.5×10^{-8} mol Fe dpm^{-1}; Dulaiova *et al*. 2009), this can be converted to an Fe flux estimate of 22 μmol Fe m^{-2} d^{-1}. In comparison, the ^{228}Ra gradient between the RaTS site and Sheldon Glacier is 0.006 ± 0.004 dpm m^{-3} m^{-1}. Using the lower bound of this (0.002 dpm m^{-3} m^{-1}) and combining it with the Ra-derived mixing rate for the glacier (15 m^2 s^{-1}) results in a minimum ^{228}Ra flux estimate of 7776 dpm m^{-2} d^{-1}. The same Fe:^{228}Ra ratios used above gives a glacial Fe flux of 246 μmol m^{-2} d^{-1}, and ~2.5 mmol m^{-2} d^{-1} for TDFe. While there are very large errors on these estimates, due to the high uncertainties in the slopes used to estimate gradients and mixing rates, the order of magnitude difference between the minimum glacial estimate and the maximum coastal sediment estimate clearly demonstrates the dominance of glacial Fe inputs versus sediment sources, and that this area is well supplied with Fe.

The Ra-derived estimate is much higher than that obtained from the glacial Fe concentrations. The estimate from glacial [dFe] is almost certainly too low, and even the Ra-derived estimate may be an underestimate. The glacial [dFe] estimate does not account for the presence of any "dirty" basal ice which is frequently seen in Ryder Bay (Fig 7.11) and would be expected to carry considerably more Fe due to the greater terrigenous material content. By considering literature values for basal ice (sediment load of 40–200 kg m^{-3}; Raiswell *et al*. 2006 *and references therein*) compared to "clean" ice (sediment load of 0.5 kg m^{-3}; Raiswell *et al*. 2006), and assuming 2% of ice likely to be basal, we derive a seasonal glacial estimate of 80–200 μmol Fe m^{-2} (or 620–1500 nmol Fe m^{-2} d^{-1}), ~10 times higher than the initial estimate. Additionally, this method will underestimate inputs of meteoric water, as the contribution in the water column above 15 m will be much higher than at 15 m.

While Ra-based fluxes are calculated from a sampling event when glacial inputs appear to be relatively high, these too may underestimate Fe, as an Fe:^{228}Ra

estimate from data here is an order of magnitude higher than the literature value used above. However, the Ra method may include Ra (and Fe) associated with the presence of the glacier, but not strictly sourced from glacial melt. For example, resuspension of sediments in sea-water beneath the glacier, or terrestrial sediment in sub-glacial flow could both contribute Ra and Fe. These sources would thus be included in the Ra-derived estimate of glacial Fe flux, but missed entirely by the ice-concentration estimate.

Figure 7.11: Photograph of a basal ice iceberg in Ryder Bay on 19 February 2009.

While this analysis focuses primarily on dFe fluxes, the results presented here indicate that glacial processes deliver a much greater particulate component (92 ± 52 nM, ~ 90% of TDFe), consistent with earlier studies (Raiswell *et al*. 2006, Statham *et al*. 2008, Raiswell 2011, Gerringa *et al*. 2012). Much of this particulate material will sink out of the surface, but in the sediments this fraction may be subject to reduction to Fe^{2+} and subsequent dissolution into overlying waters. Even before reaching the sediments, particulate Fe may be available to phytoplankton use, as strongly suggested by the observations of Planquette *et al*. (2011). Although the proportion of available Fe and rate of release are still areas of active research, recent work by Thuroczy *et al*. (2012) suggests that release of glacial Fe and subsequent productivity results in undersaturation of organic ligands, which will favour the solubilisation of glacial Fe and enhance the proportion available to phytoplankton.

While glacial inputs are suggested to be both spatially and temporally variable, both estimates here indicate that Fe inputs from Sheldon Glacier are very

large. However, the magnitude of supply must be considered relative to the demand for Fe. The next section explores the biological signal in [dFe] trends and quantifies biological Fe requirements.

7.5.3 Biological influence on iron distributions

7.5.3.1 Biological signal

As iron is an essential micronutrient, it is expected that biological processes will influence its distribution via uptake and remineralisation. Given the high biological requirement for Fe compared to its relatively low availability in seawater, Fe is a metal with one of the strongest relationships with productivity. While this relationship will be stronger in Fe-limited areas, the same processes act in coastal regions and thus to some extent [dFe] should reflect chl dynamics in Ryder Bay.

As previously established, summer 2009 showed relatively low biological activity (see Chapters 1, 2). An early increase in [chl] (before the initiation of sampling here) was followed by a mid-season period of very low phytoplankton biomass. Chlorophyll concentrations in Ryder Bay, ~5 μg L^{-1} during the second half of January through 2 February, show a steep increase beginning 2 February and peak at >20 μg L^{-1} on 15 February (Figure 7.6); this relatively high but very short-lived late season chl peak was dominated by diatoms. At the same time, [dFe] fell by ~4 nM from the seasonal maximum on 30 January, to ~5.5 nM during the [chl] peak. This decrease is consistent with biological uptake of Fe during this period.

Due to the role of biological control on some of the variation in dFe, it would be expected that other nutrients also show the influence of biological processes during the same period. The decrease in dFe during the first half of February is accompanied by reduction in concentrations of Si, N and P (Fig. 7.12). Interestingly, when [chl] stops increasing, drawdown of Fe stops, but macronutrients continue to decrease for a further 3 days (to the next sampling event). Availability of Fe remains high, well above the levels associated with Fe limitation and higher even than in samples from earlier in the season. To our knowledge, this is the first study from the WAP region which spans the full period of peak chl, and indicates that Fe does not limit production even during peak productivity. Although we cannot fully explain the

continued depletion of macronutrients, a potential cause might be light levels (PAR), which drop from >400 (15 µE m^{-2} s^{-1}) at 15 m to ~100 µE m^{-2} s^{-1} on 15 February. This could be a factor in reduced Fe uptake, as Fe is used primarily for photosynthesis and chl synthesis (Raven 1990, Raven *et al*. 1999), requirements which would be reduced under lower light conditions.

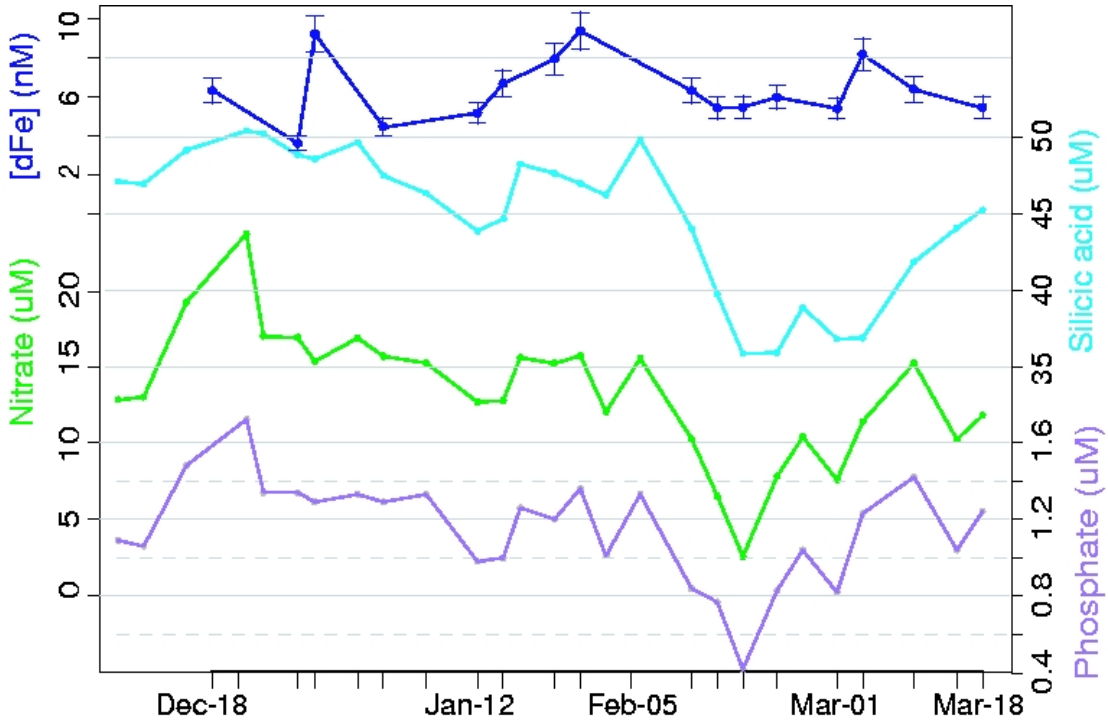

Figure 7.12: Concentrations of dFe and macronutrients (Si, N and PO_4) in 15 m samples at the RaTS site. Macronutrient data courtesy of BAS.

7.5.3.2 Biological iron requirements

In order to understand seasonal Fe demand, we investigate biological iron requirements. Ratios of Fe and nutrients during a drawdown event should reflect the relative biological utilisation of these elements. From the inverse of the slopes in Fig. 7.13, we calculate dFe to N, Si and P as 360 µmol:mol, and 370 µmol:mol for N and Si, and 5.1 mmol:mol P, respectively. These values are within the ranges found for dFe:N and dFe:P based on depth profiles.

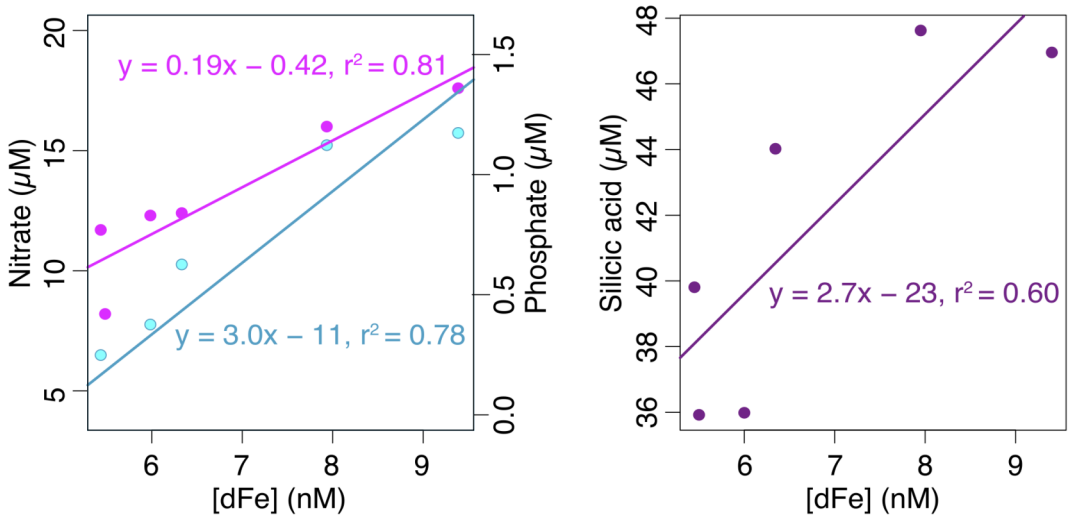

Figure 7.13: Macronutrients (N and P: a; Si: b) versus dissolved Fe in 15 m water samples. Only the period of 30 Jan to 18 Feb was used, as biological activity dominated the Fe signal during this period whereas non-biological lithogenic inputs had strong effects on dFe outwith this time period.

The value of dFe:N here is higher than those measured across the pycnocline farther north on the WAP (170 and 50 µmol:mol for Bransfield Straight and Drake Passage, respectively; Ardelan *et al*. 2010). Values for dFe:P were also lower than that found in this study (2.5 and 0.6 mmol:mol for the same northern WAP locations). This is in keeping with the 6- to 10-fold lower [dFe] in Bransfield Straight and Drake Passage (0.5-1.5 and 0.3-1.3 nM, respectively), and indicates that phytoplankton in Ryder Bay acquire considerably more cellular Fe than those further north. Converting particulate elemental ratios measured at the RaTS site for C:N and C:Si (6.4 and 11.7, respectively) and the Redfield ratio for C:P (106:1), leads to Fe:C estimates of 53, 32 and 48 µmol:mol, very similar to the ~40 µmol Fe:mol C estimated by Twining *et al*. (2004) for Fe-enriched conditions. It has been observed that coastal diatoms require more Fe than their oceanic counterparts (Brand 1991, Sunda *et al*. 1991, Sunda & Huntsman 1995, Maldonado *et al*. 2006), which is believed to result from adaptive reorganisation of photosynthetic architecture (Strzepek & Harrison 2004) and substitution of Fe-containing enzymes with non-Fe containing ones (Peers & Price 2006). However, the ratios observed here are much higher than laboratory-estimated Fe requirements, which range from ~3 to ~12 µmol Fe:mol C for oceanic and coastal diatoms respectively (Sunda *et al*. 1991, Sunda &

Huntsman 1995, Maldonado & Price 1996), again indicating that our study site is Fe-replete.

7.5.3.3 Seasonal iron budget

Seasonal budgets of Si demand associated with new production have been estimated from Si isotopic measurements, concentrations, and physical water column conditions (Chapter 5). Using the biological Fe:Si ratios determined above, the Si demand can be converted to annual requirement of Fe for new production. As this is based on Fe:Si ratios and thus only reflects diatom production, higher non-diatom production in intermediate- and low-chl years may lead to Fe demand being somewhat higher. However, the upper range of the estimated Si demand was calculated as an upper limit, and when non-diatom biomass is high the total biomass is very low, thus accounting for non-diatom phytoplankton will introduce only small uncertainty to the Fe range estimated here. Thus, considering the Fe:Si ratio for predominantly diatom communities, the Fe requirement for 2009 is estimated at 130-260 μmol Fe m^{-2} y^{-1} in 2009, compared to ~400 μmol Fe m^{-2} for a high-chl year. This amounts to a 40-70% drop in Fe demand in intermediate years relative to high-chl conditions.

The Fe inputs estimated here from glacial sources are very large in comparison. The daily Ra-derived Fe input (246 μmol m^{-2} d^{-1}) is roughly equal to the seasonal Fe demand estimated for 2009. Fluxes based on published glacial Fe concentrations are lower, but as discussed in section 7.5.2.3, this is likely to significantly underestimate true inputs due to presence of basal ice and greater meteoric water contributions above the sampling depth. Seasonally, even the lower glacial Fe estimate based on glacial [dFe] is similar to demand (80–200 μmol Fe m^{-2} y^{-1}; assuming 2% basal ice). This analysis strongly suggests that glacial Fe inputs are a very substantial source of Fe to a region which is unlikely to be Fe-deficient due to the ratios of vertical nutrient fluxes. This further indicates that there is a significant excess supply of Fe from glacial inputs. This is consistent with the WAP region being a source of Fe to the ACC, which stimulates productivity up to 3500 km downstream (de Jong *et al*. 2012). The potential for glacial Fe to be exported to the

ACC and off the WAP shelf, and the potential impacts of this mechanism to deliver Fe to the wider Southern Ocean, are further explored in Chapter 8.

7.5.4 Decoupling of iron and aluminium in Ryder Bay

Aluminium and Fe have several common sources. Like Fe, Al is supplied to open ocean areas by atmospheric dust deposition, and is used as a valuable tracer for dust flux and a proxy for aeolian Fe (Measures & Brown 1996, Measures *et al*. 2001). Significant Al is delivered to the ocean by riverine fluxes (Hydes & Liss 1977), although like Fe most of this is rapidly scavenged upon entry into more saline waters (Orians & Bruland 1986). Due to its scavenging rate, Al is relatively short-lived in surface waters, with a residence time of 3–5 years (Orians & Bruland 1986). Unlike Fe, which is released from sediments due to its redox chemistry, Al is not redox reactive and thus organic-rich marine sediments are much less of a source of Al than of Fe. Although it is present in diatom silica, Al has a small biological role (Moran & Moore 1992), with most of the Al incorporated into organic material resulting from structural incorporation of Al into the crystal structure of diatom silica after deposition (Dixit *et al*. 2001, Koning *et al*. 2007). Due to the shared and unique sources of Fe and Al, trends in Al concentrations can be used to further constrain sources and sinks of Fe, as well as of Al itself.

Similar to Hendry *et al*. (2010), this study finds a high degree of variability in dissolved Al concentrations in Ryder Bay surface waters (15 m), reflecting significant and variable sources of Al in this region. Previous work has explained these fluctuations as a combination of upwelling, and mixing with underlying waters enriched in Al due to sea-ice brine rejection (Hendry *et al*. 2010). However, in contrast to trends in dFe, there is no evidence of an Al source at depth, due to the low and consistent [dAl] found below 50 m (Fig. 7.2). While there is one sample from 25 m with higher [dAl] than at 15 m, given the lower concentrations deeper in the water column this cannot reflect a deep water source, but instead must be a product of variable surface inputs and stratification. Thus this section investigates potential surface inputs in more detail.

To assess changes in sampling across the MLD, sample collection depth is shown with density anomaly (σ_θ) in Fig. 7.14. It can be seen that the large increase in

[dAl] on January 18 was associated with slightly less dense surface waters at the sampling depth. This same isopycnal was sampled at 5 m depth on January 7, and had very high dAl (~25 nM). Thus there must be some Al source at the surface. In contrast, the large [dAl] increase on March 4 occurred when density increased, indicating the upward mixing of deeper water to the sampling depth. This suggests that the deeper, more dense water, previously present at ~30 m depth, had higher [dAl], similar to the 25 m sample on 7 January. The likely source of Al to the surface will be considered first, followed by sources to water at 25-30 m depth where some enrichment was present in both December and March.

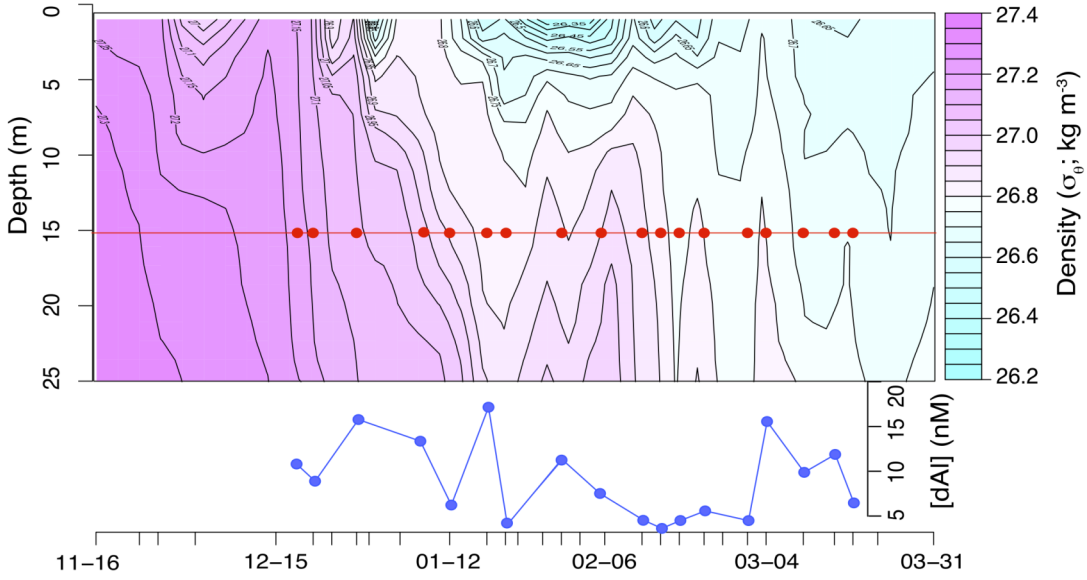

Figure 7.14: Interpolated contour plot of density anomaly (σ_θ) in the top 25 m of the water column. Sampling depth is indicated by the red line, and sample dates shown by red symbols. Bottom plot shows [dAl] in 15 m water samples.

7.5.4.1 Surface sources of aluminium

Potential sources of surface Al inputs are glacial and snow melt, sea-ice melt, atmospheric deposition and shallow-sediment Al release. Previously measured Al in glacial ice and snow (72 and 98 nM respectively; Hendry *et al*. 2010) suggest that meteoric inputs are small in relation to the water column. A glacial source cannot explain the fluctuations in dAl of greater absolute magnitude than the simultaneous

changes in dFe, as the station sampled here near a marine-terminating glacier had very low [dAl] (3.9 nM; Fig. 7.3, Table 7.3), and dAl:dFe ratios <1 mol:mol.

Sea-ice brine and interstitial waters have been shown in many studies to have high concentrations of dissolved and/or particulate Al (*e.g*. Hendry *et al*. 2010, Lannuzel *et al*. 2011). Despite elevated [dAl], Hendry *et al*. (2010) concluded that sea-ice was not a significant source of Al driving spikes in surface water concentrations, due the volume of sea-ice melt in Ryder Bay surface waters. The same approach was used here to calculate the [dAl] in sea-ice required to account for the January 18 increase in [dAl] at 15 m. Sea-ice melt increased from 0% to 0.6% of the water column (from $\delta^{18}O$), and [dAl] increased from 6 nM to 17 nM. To account for this change, melting sea-ice would have had to contain nearly 2 μM dAl, several orders of magnitude higher than literature values (20–40 nM, Hendry *et al*. 2010; 11 nM, Lannuzel *et al*. 2011). In agreement with Hendry *et al*. (2010), these results suggest a minor role for melting sea-ice in Al supply.

Atmospheric deposition could also potentially explain the increase in [dAl] seen on 18 January, as water of the same density was present at the surface ~6-14 days earlier (Fig. 7.14). However, atmospheric inputs are thought to accumulate on sea-ice, such that sea-ice melt would be a greater source of atmospheric Al than a single dust event. If even sea-ice melt is not expected to supply sufficient Al to explain the large increase in [dAl] seen on 18 January, it is very unlikely that atmospheric deposition over the short time period where this water mass may have been at the surface would be sufficient to explain the observed spike.

The remaining potential mechanism is Al release from shallow sediments, due to diffusion or resuspension, which could then be advected from the margins to central Ryder Bay. The high [dAl] found at stations A and B, both near exposed land and very shallow waters (<15 m water depth) support shallow sediments as a significant source of Al. In contrast to the respiration-driven redox release of Fe from deeper sediments, a shallow sediment source is more likely to release Al from lithogenic material by dissolution and desorption. This process would also release Fe, although the crustal content of 4.3% Fe and 8.0% Al (Fe:Al molar ratio of ~0.26; Wedepohl 1995) is consistent with this being a more significant source of Al than of Fe. As the ratio of dFe:dAl was very low at the two near-shore stations, a shallow

sediment source would explain the much greater enrichment seen in [dAl] relative to [dFe].

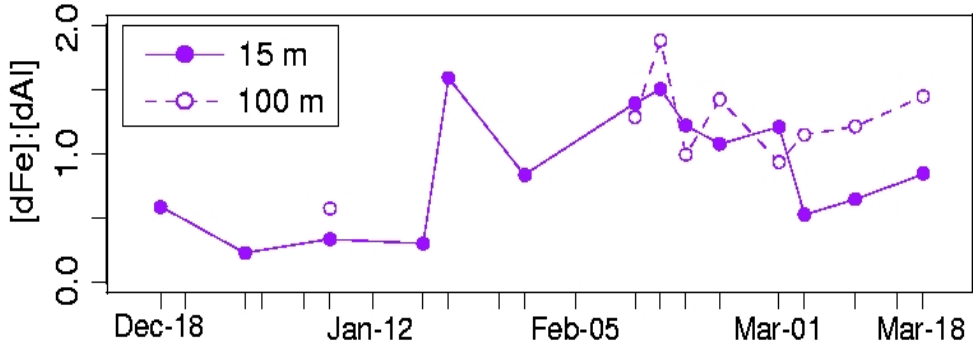

Figure 7.15: Surface (15 m) and deep (100 m) water ratios of dissolved Fe:Al concentrations at the RaTS site.

The ratios of dFe:dAl in surface and deep waters are shown in Fig. 7.15. At 15 m, the season can be divided into three periods: (1) where dFe:dAl is <1 mol:mol (to Jan 18), (2) where the ratio increases to >1 mol:mol (Jan 21 to Mar 1) and (3) where dFe:dAl decreases during autumn. During period (1), dissolved ratios in surface waters are in very good agreement with those measured at stations A and B (Fig 7.3, Table 7.3), which are likely to have a strong sediment influence. During period (2), when productivity and meteoric water contributions are highest, metal ratios increase to values very similar to those measured near the glacier. We therefore infer that during the early season, Al inputs derive primarily from sediment sources. As melting proceeds over summer, glacial (low-Al) sources dominate the inputs to surface waters, with higher-Al waters present deeper in the water column (*i.e.* 25-30 m), below the glacial melt dominated layer. Late in the season when mixing increases (period 3), intermediate dissolved metal ratios reflect an autumnal mixing of glacial-derived surface waters and sediment-influenced sub-surface waters. This is consistent with the proposed redistribution of Fe throughout surface waters as the mechanism for late-season increases in [dFe] (section 7.5.2.2).

7.5.4.2 Sub-surface sources of aluminium

High concentrations of Al (~20 nM) were found at ~25 m (and suggested to upwell to 15 m in March) in this study. This is predominantly below the MLD. During the summer, this water can therefore act as a source to the surface layer following mixing events. The high [dAl] sampled in both January and March is from water with density ≥26.8 kg m^{-3} (Fig. 7.14). This water was present at the surface during November and early December. Thus a sediment source as described above could supply Al by advection during late winter. This high-Al subsurface water does not then reflect a subsurface source of Al, but rather that high-Al surface water is displaced downwards by inputs of very low salinity meltwater during summer. This is consistent with the signal of very low coastal sediment inputs during mid-summer inferred from Ra activities in mid-Ryder Bay (*see* Chapter 6). A shallow sediment source for subsurface dAl does not necessitate the source of Al from brine rejection and cascades hypothesised by Hendry *et al*. (2010). Runoff from land and tidal/wave action can explain sediment supply, resuspension and Al release, although sea-ice related processes may act to enhance Al enrichment from shallow sediments during winter.

7.5.4.3 Importance of sediment trace-metal inputs

A significant shallow sediment source, as indicated by [dAl], could help to reconcile the difference in Ra- and [dFe]- derived estimates of seasonal glacial Fe flux, as suggested in section 7.5.2.3. Material of a terrestrial/lithogenic origin could be deposited in marine sediments beneath marine-terminating glaciers. Marine processes could enhance sediment resuspension and metal release via seawater mixing (*e.g*. tidal/inertial currents). These processes could contribute to the large fluctuations in [dAl] seen here, and would be associated with higher Ra activities. Thus an estimate of Fe flux derived from Ra would encompass all of these inputs, but may overestimate Fe due to the lower Fe:Al associated with sediment sources. In contrast, the estimate based on measured glacial [dFe] would exclude these inputs and therefore be much lower than the Ra estimate, as is the case here, and the true flux associated with the glacier. As even the lower estimate (from glacial [dFe]) was determined above to be roughly equal to biological demand, a true value for Fe

fluxes somewhere between the two estimates indicates that this region is well supplied with Fe from glacial sources during the summer growing season.

7.6 Conclusions

Concentrations of dissolved Fe and Al were successfully measured in time-series samples and depth profiles from Ryder Bay. These measurements supplement very sparse coastal WAP data for both Fe and Al, and are the first in this location for Fe. These data identify a strong source of Fe from WAP shelf sediments, leading to high dFe (~10 nM) at depth. Deep water Fe:N and Fe:P ratios are consistent with Fe-replete phytoplankton, and 2- to 4-fold above laboratory values for phytoplankton requirements. This indicates that the Fe flux from deep waters alone is sufficient to prevent Fe limitation in coastal WAP waters.

Unlike many Southern Ocean studies based from ships, this time-series spans both the chl peak and autumn decline. Uptake of Fe relative to macronutrients was high relative to open ocean regions, but was consistent with Fe-replete phytoplankton communities. By combining nutrient use ratios from time-series data and an estimate of annual Si demand (*see* Chapter 5), an annual Fe budget of 130-260 μmol Fe m^{-2} y^{-1} was estimated to support new production in 2009. This season was one of intermediate chl concentrations, and Fe demand is expected to vary with overall productivity.

Supply of Fe from deep waters is augmented in summer by significant glacially-derived Fe. The supply from glacial sources was estimated by two independent methods. These supply estimates vary considerably, and range from meeting a minimum 50% of seasonal demand, to supplying almost the entire seasonal Fe requirement in a single glacial meltwater input event.

Despite the high Fe use relative to macronutrients, the combined deep water and glacial inputs provide Fe in excess supply. As a result, the WAP region has the potential to act as a net source of Fe to the wider Southern Ocean. Projections of increasing inputs and lower Fe use suggest future increases in the WAP Fe inventory, which is explored in detail in Chapter 8.

7.7 References

ARDELAN, M.V., HOLM-HANSEN, O., HEWES, C.D., REISS, C.S., SILVA, N.S., DULAIOVA, H., STEINNES, E. & SAKSHAUG, E. 2010. Natural iron enrichment around the Antarctic Peninsula in the Southern Ocean. *Biogeosciences*, **7**, 11–25.

BEARDSLEY, R.C., LIMEBURNER, R. & OWENS, W.B. 2004. Drifter measurements of surface currents near Marguerite Bay on the western Antarctic Peninsula shelf during austral summer and fall, 2001 and 2002. *Deep-Sea Research II*, **51**, 1947–1964, 10.1016/j.dsr2.2004.07.031.

BOYD, P., LAROCHE, J., GALL, M., FREW, R. & MCKAY, R.M.L. 1999. Role of iron, light, and silicate in controlling algal biomass in subantarctic waters SE of New Zealand. *Journal of Geophysical Research*, **104**, 13395–13408.

BOYD, P.W. & ELLWOOD, M.J. 2010. The biogeochemical cycle of iron in the ocean. *Nature Publishing Group*, **3**, 675–682, 10.1038/ngeo964.

BOYD, P.W., ARRIGO, K.R., STRZEPEK, R. & VAN DIJKEN, G.L. 2012. Mapping phytoplankton iron utilization: Insights into Southern Ocean supply mechanisms. *Journal of Geophysical Research*, **117**, 1–18, 10.1029/2011JC007726.

BOYD, P.W., JICKELLS, T., LAW, C.S., BLAIN, S., BOYLE, E.A., BUESSELER, K.O., COALE, K.H., et al. 2007. Mesoscale iron enrichment experiments 1993-2005: Synthesis and future directions. *Science*, **315**, 612–617, 10.1126/science.1131669.

BRAND, L.E. 1991. Minimum iron requirements of marine phytoplankton and the implications for the biogeochemical control of new production. *Limnology and Oceanography*, **36**, 1756–1771.

BUCCIARELLI, E., BLAIN, S. & TRÉGUER, P. 2001. Iron and manganese in the wake of the Kerguelen Islands (Southern Ocean). *Marine Chemistry*, **73**, 21–36.

CHARETTE, M.A., GONNEEA, M.E., MORRIS, P.J., STATHAM, P., FONES, G., PLANQUETTE, H., SALTER, I. & GARABATO, A.N. 2007. Radium isotopes as tracers of iron sources fueling a Southern Ocean phytoplankton bloom. *Deep Sea Research Part II: Topical Studies in Oceanography*, **54**, 1989–1998, 10.1016/j.dsr2.2007.06.003.

CHARETTE, M.A., BHATIA, M.P., LINHOFF, B., HENDERSON, P., DAS, S.B., KUJAWINSKI, E.B., BUTLER, C. AND WADHAM, J.L.: Radon Tracing of Subglacial Hydrologic Processes. *Presented at*: 4th International Radium-Radon Workshop; 2012 June 3-8; Narragansett, USA.

CLARKE, A., MEREDITH, M.P., WALLACE, M.I., BRANDON, M.A. & THOMAS, D.N. 2008. Seasonal and interannual variability in temperature, chlorophyll and macronutrients in northern Marguerite Bay, Antarctica. *Deep Sea Research Part II: Topical Studies in Oceanography*, **55**, 1988–2006, 10.1016/j.dsr2.2008.04.035.

DE BAAR, H.J.W. & DE JONG, J.T.M. 2001. Distributions, sources and sinks of iron in seawater. *In* Turner, D. & Hunter, K., *eds. The biogeochemistry of iron in seawater*. Chichester: John Wiley & Sons Ltd., 123–253.

DE BAAR, H.J.W., DE JONG, J.T.M., BAKKER, D.C.E., LOSCHER, B.M., VETH, C., BATHMANN, U. & SMETACEK, V. 1995. Importance of iron for plankton blooms and carbon dioxide drawdown in the Southern Ocean. *Nature*, **373**, 412–415.

DE JONG, J., SCHOEMANN, V., LANNUZEL, D., CROOT, P., DE BAAR, H. & TISON, J.-L. 2012. Natural iron fertilization of the Atlantic sector of the Southern Ocean by continental shelf sources of the Antarctic Peninsula. *Journal of Geophysical Research*, **117**, 1–25, 10.1029/2011JG001679.

DIXIT, S., VAN CAPPELLEN, P. & VAN BENNEKOM, A.J. 2001. Processes controlling solubility of biogenic silica and pore water build-up of silicic acid in marine sediments. *Marine Chemistry*, **73**, 333–352.

DULAIOVA, H., ARDELAN, M.V., HENDERSON, P.B. & CHARETTE, M.A. 2009. Shelf-derived iron inputs drive biological productivity in the southern Drake Passage. *Global Biogeochemical Cycles*, **23**, 10.1029/2008GB003406.

FRANCK, V.M., BRZEZINSKI, M.A., COALE, K.H. & NELSON, D.M. 2000. Iron and silicic acid concentrations regulate Si uptake north and southn of the Polar Frontal Zone in the Pacific Sector of the Southern Ocean. *Deep-Sea Research II*, **47**, 3315–3338.

FROELICH, P.N., KLINKHAMMER, G.P., BENDER, M.L., LUEDTKE, N.A., HEATH, G.R., CULLEN, D., DAUPHIN, P., HAMMOND, D., HARTMAN, B. & MAYNARD, V. 1979. Early oxidation of organic matter in pelagic sediments of the eastern equatorial Atlantic: suboxic diagenesis. *Geochimica et Cosmochimica Acta*, **43**, 1075–1090.

GERRINGA, L.J.A., ALDERKAMP, A.-C., LAAN, P., THURÓCZY, C.-E., DE BAAR, H.J.W., MILLS, M.M., VAN DIJKEN, G.L., VAN HAREN, H. & ARRIGO, K.R. 2012. Iron from melting glaciers fuels the phytoplankton blooms in Amundsen Sea (Southern Ocean) Iron biogeochemistry. *Deep-Sea Research Part II*, **71-76**, 16–31, 10.1016/j.dsr2.2012.03.007.

HENDRY, K.R., MEREDITH, M.P., MEASURES, C.I., CARSON, D.S. & RICKABY, R.E.M. 2010. The role of sea ice formation in cycling of aluminium in northern Marguerite Bay, Antarctica. *Estuarine, Coastal and Shelf Science*, 1–10, 10.1016/j.ecss.2009.12.017.

HEWES, C.D., REISS, C.S., KAHRU, M., MITCHELL, B.G. & HOLM-HANSEN, O. 2008. Control of phytoplankton biomass by dilution and mixed layer depth in the western Weddell-Scotia Confluence. *Marine Ecology Progress Series*, **366**, 15–29, 10.3354/meps07515.

HOFMANN, E.E., KLINCK, J.M., LASCARA, C.M. & SMITH, D.A. 1996. Water mass distribution and circulation west of the Antarctic Peninsula and including Bransfield Strait. *In* Ross, R.M., *ed. Foundations for Ecological Research West of the Antarctic Peninsula*. American Geophysical Union, 61–80.

HOLETON, C.L., NEDELEC, F., SANDERS, R., BROWN, L., MOORE, C.M., STEVENS, D.P., HEYWOOD, K.J., STATHAM, P.J. & LUCAS, C.H. 2005. Physiological state of phytoplankton communities in the Southwest Atlantic sector of the Southern Ocean, as measured by fast repetition rate fluorometry. *Polar biology*, **29**, 44–52, 10.1007/s00300-005-0028-y.

HYDES, D.J. & LISS, P.S. 1976. Fluorimetric Method for the Determination of Low Concentrations if Dissolved Aluminium in Natural Waters. *Analyst*, **101**, 922–931, 10.1039/an9760100922.

KING, J.C. 1994. Recent climate variability in the vicinity of the Antarctic Peninsula. *Journal of Climatology*, **14**, 357–369.

KLINCK, J.M., HOFMANN, E.E., BEARDSLEY, R.C., SALIHOGLU, B. & HOWARD, S. 2004. Water-mass properties and circulation on the west Antarctic Peninsula Continental Shelf in Austral Fall and Winter 2001. *Deep Sea Research Part II: Topical Studies in Oceanography*, **51**, 1925–1946, 10.1016/j.dsr2.2004.08.001.

KONING, E., GEHLEN, M., FLANK, A.-M., CALAS, G. & EPPING, E. 2007. Rapid post-mortem incorporation of aluminum in diatom frustules: Evidence from chemical and structural analyses. *Marine Chemistry*, **106**, 208–222, 10.1016/j.marchem.2006.06.009.

KORB, R.E., WHITEHOUSE, M.J., ATKINSON, A. & THORPE, S.E. 2005. Magnitude and maintenance of the phytoplankton bloom at South Georgia: A naturally iron-replete environment. *Marine Ecology Progress Series*, **368**, 75–91.

LAM, P.J., BISHOP, J.K.B., HENNING, C.C., MARCUS, M.A., WAYCHUNAS, G.A. & FUNG, I.Y. 2006. Wintertime phytoplankton bloom in the subarctic Pacific supported by continental margin iron. *Global Biogeochemical Cycles*, **20**, 10.1029/2005GB002557.

LANCELOT, C., DE MONTETY, A., GOOSSE, H., BECQUEVORT, S., SCHOEMANN, V., PASQUER, B. & VANCOPPENOLLE, M. 2009. Spatial distribution of the iron supply to phytoplankton in the Southern Ocean: a model study. *Biogeosciences*, **6**, 2861–2878.

LANNUZEL, D., BOWIE, A.R., VAN DER MERWE, P.C., TOWNSEND, A.T. & SCHOEMANN, V. 2011. Distribution of dissolved and particulate metals in Antarctic sea ice. *Marine Chemistry*, **124**, 134–146, 10.1016/j.marchem.2011.01.004.

LANNUZEL, D., SCHOEMANN, V., DE JONG, J., TISON, J.-L. & CHOU, L. 2007. Distribution and biogeochemical behaviour of iron in the East Antarctic sea ice. *Marine Chemistry*, **106**, 18–32, 10.1016/j.marchem.2006.06.010.

LOSCHER, B.M., DE BAAR, H.J.W., DE JONG, J.T.M., VETH, C. & DEHAIRS, F. 1997. The distribution of Fe in the Antarctic Circumpolar Current. *Deep-Sea Research II*, **44**, 143–187.

MAHOWALD, N.M., BAKER, A.R., BERGAMETTI, G., BROOKS, N., DUCE, R.A., JICKELLS, T.D., KUBILAY, N., PROSPERO, J.M. & TEGEN, I. 2005. Atmospheric global dust cycle and iron inputs to the ocean. *Global Biogeochemical Cycles*, **19**, 1–17, 10.1029/2004GB002402.

MALDONADO, M., ALLEN, A.E., CHONG, J.S., LIN, K., LEUS, D., KARPENKO, N. & HARRIS, S.J. 2006. Copper-dependent iron transport in coastal and oceanic diatoms. *Limnology and Oceanography*, **51**, 1729–1743.

MALDONADO, M.T. & PRICE, N.M. 1996. Influence of N substrate on Fe requirements of marine centric diatoms. *Marine Ecology Progress Series*, **141**, 161–172.

MARTIN, J.H. 1990. Glacial-interglacial CO2 change: The iron hypothesis. *Paleoceanography*, **5**, 1–13.

MARTIN, J.H., GORDON, R.M. & FITZWATER, S.E. 1990. Iron in Antarctic waters. *Nature*, **345**, 156–158.

MARTÍNEZ-GARCIA, A., ROSELL-MELÉ, A., JACCARD, S.L., GEIBERT, W., SIGMAN, D.M. & HAUG, G.H. 2011. Southern Ocean dust-climate coupling over the past four million years. *Nature*, **476**, 312–315, 10.1038/nature10310.

MEASURES, C.I. & EDMOND, J.M. 1990. Aluminium in the South Atlantic: steady state distribution of a short residence time element. *Journal of Geophysical Research*, **95**, 5331–5340.

MEASURES, C.I., YUAN, J. & RESING, J.A. 1995. Determination of iron in seawater by flow injection analysis using in-line preconcentration and spectrophotometric detection. *Marine Chemistry*, **50**, 3–12.

MEREDITH, M.P., RENFREW, I.A., CLARKE, A., KING, J.C. & BRANDON, M.A. 2004. Impact of the 1997/98 ENSO on upper ocean characteristics in Marguerite Bay, western Antarctic Peninsula. *Journal of Geophysical Research*, **109**, 10.1029/2003JC001784.

MEREDITH, M.P., VENABLES, H.J., CLARKE, A., DUCKLOW, H., ERIKSON, M., LENG, M.J., LENAERTS, J.T.M. & VAN DEN BROEKE, M.R. 2012. The freshwater system west of the Antarctic Peninsula: spatial and temporal changes. Journal of Oceanography.

MEREDITH, M.P., WALLACE, M.I., STAMMERJOHN, S.E., RENFREW, I.A., CLARKE, A., VENABLES, H.J., SHOOSMITH, D.R., SOUSTER, T. & LENG, M.J. 2010. Changes in the freshwater composition of the upper ocean west of the Antarctic Peninsula during the first decade of the 21st century. *Progress In Oceanography*, **87**, 127–143, 10.1016/j.pocean.2010.09.019.

MIDDAG, R., VAN SLOOTEN, C., DE BAAR, H.J.W. & LAAN, P. 2011. Dissolved aluminium in the Southern Ocean. *Deep-Sea Research Part II*, **58**, 2647–2660, 10.1016/j.dsr2.2011.03.001.

MOFFAT, C., OWENS, B. & BEARDSLEY, R.C. 2009. On the characteristics of Circumpolar Deep Water intrusions to the west Antarctic Peninsula Continental Shelf. *Journal of Geophysical Research*, **114**, 10.1029/2008JC004955.

MORAN, S.B. & MOORE, R.M. 1992. Kinetics of the removal of dissolved aluminum by diatoms in seawater: A comparison with thorium. *Geochimica et Cosmochimica Acta*, **56**, 3365–3374.

MORAN, S.B., MOORE, R.M. & WESTERLUND, S. 1992. Dissolved aluminium in the Weddell Sea. *Deep Sea Research A*, **39**, 537–547.

NELSON, D.M., BRZEZINSKI, M.A., SIGMAN, D.E. & FRANCK, V.M. 2001. A seasonal progression of Si limitation in the Pacific sector of the Southern Ocean. *Deep-Sea Research II*, **48**, 3973–3995.

ORIANS, K.J. & BRULAND, K.W. 1986. The biogeochemistry of aluminium in the Pacific Ocean. *Earth and Planetary Science Letters*, **78**, 397–410.

PEERS, G. & PRICE, N.M. 2006. Copper-containing plastocyanin used for electron transport by an oceanic diatom. *Nature*, **441**, 341–343, 10.1038/nature04630.

PLANQUETTE, H., FONES, G.R., STATHAM, P.J. & MORRIS, P.J. 2009. Origin of iron and aluminium in large particles (>53 μm) in the Crozet region, Southern Ocean. *Marine Chemistry*, **115**, 31–42, 10.1016/j.marchem.2009.06.002.

PRÉNDEZ, M. & CARRASCO, M.A. 2003. Elemental composition of surface waters in the Antarctic Peninsula and interactions with the environment. *Environmental Geochemistry and Health*, **25**, 347–363.

RAISWELL, R. 2011. Iceberg-hosted nanoparticulate Fe in the Southern Ocean Mineralogy, origin, dissolution kinetics and source of bioavailable Fe. *Deep-Sea Research Part II*, **58**, 1364–1375, 10.1016/j.dsr2.2010.11.011.

RAISWELL, R., BENNING, L.G., TRANTER, M. & TULACZYK, S. 2008. Bioavailable iron in the Southern Ocean: the significance of the iceberg conveyor belt. *Geochemical Transactions*, **9**, 7, 10.1186/1467-4866-9-7.

RAISWELL, R., TRANTER, M., BENNING, L.G., SIEGERT, M., DE'ATH, R., HUYBRECHTS, P. & PAYNE, T. 2006. Contributions from glacially derived sediment to the global iron (oxyhydr)oxide cycle: Implications for iron delivery to the oceans. *Geochimica et Cosmochimica Acta*, **70**, 2765–2780, 10.1016/j.gca.2005.12.027.

SAÑUDO-WILHELMY, S.A., OLSEN, K.A., SCELFO, J.M., FOSTER, T.D. & FLEGAL, A.R. 2002. Trace metal distributions off the Antarctic Peninsula in the Weddell Sea. *Marine Chemistry*, **77**, 157–170.

SEDWICK, P.N. & DITULLIO, G. 1997. Regulation of algal blooms in Antarctic shelf waters by the release of iron from melting sea ice. *Geophysical Research Letters*, **24**, 2515–2518.

SEDWICK, P.N., DITULLIO, G. & MACKEY, D.J. 2000. Iron and manganese in the Ross Sea, Antarctica: Seasonal iron limitation in Antarctic shelf waters. *Journal of Geophysical Research*, **105**, 11321–11336.

SEVERMANN, S., MCMANUS, H., BERELSON, W.M. & HAMMOND, D.E. 2010. The continental shelf benthic iron flux and its isotopic composition. *Geochimica et Cosmochimica Acta*, **74**, 3984–4004, 10.1016/j.gca.2010.04.022.

SHAW, T.J., RAISWELL, R., HEXEL, C.R., VU, H.P., MOORE, W.S., DUDGEON, R. & SMITH, K.L. 2011. Input, composition, and potential impact of terrigenous material from free-drifting icebergs in the Weddell Sea. *Deep-Sea Research Part II*, **58**, 1376–1383, 10.1016/j.dsr2.2010.11.012.

SMITH, K.L., Jr, ROBISON, B.H., HELLY, J.J., KAUFMAN, R.S., RUHL, H.A., SHAW, T.J., TWINING, B.S. & VERNET, M. 2007. Free-drifting icebergs: hot spots of chemical and biological enrichment in the Weddell Sea. *Science*, **317**, 478–482.

STATHAM, P.J., SKIDMORE, M. & TRANTER, M. 2008. Inputs of glacially derived dissolved and colloidal iron to the coastal ocean and implications for primary productivity. *Global Biogeochemical Cycles*, **22**, 10.1029/2007GB003106.

STRZEPEK, R.F. & HARRISON, P.J. 2004. Photosynthetic architecture differs in coastal and oceanic diatoms. *Nature*, **431**, 689–692.

STRZEPEK, R.F., HUNTER, K.A., FREW, R.D., HARRISON, P.J. & BOYD, P.W. 2012. Iron-light interactions differ in Southern Ocean phytoplankton. *Limnology and Oceanography*, **57**, 1182–1200, 10.4319/lo.2012.57.4.1182.

SUNDA, W.G. & HUNTSMAN, S.A. 1995. Iron uptake and growth limitation in oceanic and coastal phytoplankton. *Marine Chemistry*, **50**, 189–206.

SUNDA, W.G., SWIFT, D. & HUNTSMAN, S.A. 1991. Low iron requirement for growth in oceanic phytoplankton. *Nature*, **351**, 55–57.

TWINING, B.S., BAINES, S.B., FISHER, N.S. & LANDRY, M.R. 2004. Cellular iron contents of plankton during the Southern Ocean Iron Experiment (SOFeX). *Deep-Sea Research I*, **51**, 1827–1850, 10.1016/j.dsr.2004.08.007.

VAUGHAN, D.G., MARSHALL, G.J., CONNOLLEY, W.M., PARKINSON, C., MULVANEY, R., HODGSON, D.A., KING, J.C., PUDSEY, C.J. & TURNER, J. 2003. Recent rapid regional climate warming on the Antarctic Peninsula. *Climatic Change*, **60**, 243–274.

WELLS, M.L. & TRICK, C.G. 2004. Controlling iron availability to phytoplankton in iron-replete coastal waters. *Marine Chemistry*, **86**, 1–13, 10.1016/j.marchem.2003.10.003.

WELLS, M.L., PRICE, N.M. & BRULAND, K.W. 1995. Iron chemistry in seawater and its relationship to phytoplankton: a workshop report. *Marine Chemistry*, **48**, 157–182.

WESTERLUND, S. & ÖHMAN, P. 1991. Iron in the water column of the Weddell Sea. *Marine Chemistry*, **35**, 199–217, 10.1016/S0304-4203(09)90018-4.

ZHOU, M., NIILER, P.P. & HU, J.-H. 2002. Surface currents in the Bransfield and Gerlache Straits, Antarctica. *Deep-Sea Research I*, **49**, 267–280.

Chapter 8: Synthesis

8.1 Introduction

Changes in the WAP ecosystem are being observed in response to the fastest warming region in the Southern Hemisphere (Vaughan *et al*. 2003). Documented environmental changes in this region include warming air and sea surface temperatures, atmospheric and marine circulation changes, accelerating glacial retreat, declining sea-ice cover, and reduced chl concentrations (*see* Chapter 1). This chapter brings together the results and discussion from Chapters 3 through 7, by considering the implications of the findings presented therein in the context of observed and projected changes of the ecosystem and climate.

8.2 Discussion

8.2.1 Impacts of low-chlorophyll, non-diatom dominated conditions

Existing models of productivity in the coastal Antarctic differ by region. In the Ross Sea, communities are dominated either by diatoms or prymnesiophytes, with production being similarly high in both cases. A key difference documented by this detailed, time-series study is that in the WAP region, production differs significantly between high-diatom and low-diatom communities. In low-chl conditions, size-fractionated chl records indicate higher absolute concentrations of the <5 μm size fraction, and a significant reduction in the relative contribution of the largest size class, which in this region are predominantly diatoms (Chapter 3). Direct observations of diatom communities (Chapter 4) support the conclusion that diatom abundances decrease significantly, indicating that overall changes in chl primarily reflect changes in the diatom community. Large seasonal differences were found in the standing stock of BSi (Chapter 5), supporting significant differences in diatoms.

Records of particulate organic matter and chl all indicate that years with reduced diatom abundances (low-chl years) are accompanied by lower productivity. The relative degree of nutrient use (Si, Chapter 5; N, Chapter 3) further supports this conclusion. Together, all of these data indicate that WAP chl is dominated by diatoms, and a decline in the diatom fraction is the main reason for observed low-chl conditions, which are accompanied by lower productivity. This is a very different ecosystem model to that of the Ross Sea. The prime importance of diatoms in this region is likely the basis for WAP-Ross Sea differences, such as the much greater role of krill grazing at the WAP (Ducklow *et al*. 2006).

The strong link between stratification and biological productivity, explored in Venables *et al*. (2012), is accompanied by a shift from diatom-dominated communities with high biomass to lower-biomass communities with greater proportions of non-diatom phytoplankton. It is hypothesised that in Ryder Bay a significant proportion of these non-diatom algae are *Phaeocystis antarctica*. Lower productivity and changes in community structure have several potential impacts, regardless of the taxonomy of the non-diatom fraction. Some impacts, *i.e.* high versus low productivity on C drawdown and sequestration, as well as N drawdown and cycling, are discussed in Henley (2012). This chapter explores the potential impacts of diatom versus non-diatom community structure on nutrient ratios and grazing, both locally and at the regional scale.

8.2.1.1 Impacts on nutrient ratios

The different levels of production associated with high- and low-diatom phytoplankton communities will affect uptake ratios and export of nutrients. Communities dominated by *Phaeocystis antarctica* have high N:P and C:P ratios (Arrigo *et al*. 2002), and low Si:C (*see section* 8.2.3), and these nutrient ratios are transported to depth (Dunbar *et al*. 1998, Arrigo *et al*. 2002). At a Ross Sea site dominated by prymnesiophytes, surface water and sediment trap samples had C:P ratios ~twice those of a site dominated by diatoms (Arrigo *et al*. 2002). Thus in this area a switch between the two dominant phytoplankton groups has the potential to sequester more C per unit P when prymnesiophytes are abundant.

However, there remains considerable uncertainty regarding the export efficiency of *P. antarctica* in comparison to diatoms (Verity *et al*. 2007). DiTullio *et al*. (2000) observed high concentrations of dimethylsulphonio-propionate (a marker for prymnesiophytes) in sediments immediately following a *P. antarctica* bloom in the Ross Sea. Additionally, very high sinking rates (>200 m d^{-1}) have been observed in that region (Asper & Smith 1999), suggesting efficient C export by this plankton group. In contrast, an evaluation of sediment trap data including both Arctic and Antarctic locations concluded that the contribution of *Phaeocystis* to particulate organic carbon is small (Reigstad & Wassmann 2007).

In contrast to Ross Sea conditions, Ryder Bay (and the WAP as a whole) does not display similar production from different algal communities, but rather exhibits high-chl conditions when diatoms are abundant versus low-chl conditions when they are not. Thus while the C:P ratio may be higher in prymnesiophytes than in diatoms, the C drawdown and export potential of *P. antarctica* in Ryder Bay (and the WAP) are likely to be moderated by the much lower overall productivity.

8.2.1.2 Impacts on grazing, trophic transfer and export

Along the WAP region as a whole, there are data to support a long-term shift in salp and krill densities (Loeb *et al*. 1997, Atkinson *et al*. 2004). As outlined in Chapter 3, analysis of nutrient use and overall [chl] indicate very close coupling of production and grazing at the RaTS site. These observations are consistent with WAP-wide increases in salp abundance and decreases in krill stocks being a response to changes in phytoplankton communities, which in turn are responding to environmental change. High [chl] along the coastal WAP is related to sun-adapted diatom assemblages, whereas areas dominated by cryptophytes and prymnesiophytes usually occur in areas of deep mixing and therefore have much lower standing stocks of phytoplankton (Walsh *et al*. 2001). An environmentally-driven shift to lower diatom abundances and lower production can thus explain the lower krill abundances. As areas of high diatom biomass are avoided by salps, a shift to lower diatom abundances results in more favourable feeding conditions for salps. If low chl is accompanied by small increases in non-diatom phytoplankton biomass, this may be an additional factor favouring increases in salp populations, although this is not

required to explain the increase in salp abundance. Thus the small change in non-diatom biomass is likely much less important to the phytoplankton-grazer dynamics that the overall decrease in productivity.

As sea-ice cover and winter mixing are key components that condition the water column prior to the summer bloom, the continued loss of sea-ice would suggest that early season stratification necessary for the spring diatom bloom (Venables *et al*. 2012) will be less common in the future. Deeper mixing resulting in lower [chl] may encourage salp grazing, thereby preventing phytoplankton stocks from forming a bloom. While summer insolation and glacial inputs may help to stratify the water column later in the season (as we observe in 2009 where a diatom bloom is seen in February), this scenario leaves a much shorter time available for krill grazing compared to a December diatom bloom. However, a late bloom of diatoms, if not grazed, may also represent an effective C export mechanism, as Ducklow *et al*. (2007) suggest that export of C by undigested phytoplankton cells is greater than C export via krill fecal pellets.

8.2.1.3 Impacts of changes in diatom community speciation

The analysis presented here identifies diatoms as a key mechanism linking physical conditions and the WAP ecosystem. Changes in water column conditions that impact diatom communities determine overall production, thereby affecting the efficiency of C transfer to higher trophic levels. Thus, diatoms are the mediator between the observed trends in chl (Montes-Hugo *et al*. 2009) and changes in grazer communities (Loeb *et al*. 1997, Atkinson *et al*. 2004). Given this key role of diatoms along the WAP, monitoring of diatom production will be increasingly important in assessing the ecosystem response to climatic change. As a result of the strong relationship between BSi and both C and chl, we suggest that both chl records from satellite and *in situ* records can be used to investigate Si in the WAP.

The balance of diatom versus non-diatom phytoplankton was predicted to strongly impact particulate Si:C ratios. However, changes within the diatom community were found to counteract these changes at a seasonal level, resulting in a very robust overall relationship between BSi, C and chl (Chapter 5). This is suggested to result from high relative biomass of *Corethron pennatum* and low Si-

free, non-diatom biomass. As *C. pennatum* has been documented by several previous studies in low-chl and/or deep MLD conditions, the association of this species with low-chl conditions may be common throughout the WAP (Chapter 4). Higher abundance of this species in low-chl seasons will work to offset the lower Si:C ratios from low proportions of diatoms. As seen in this study, the Si:C and Si:chl ratios in a very low chl year (2008) were not significantly different from other seasons or the overall mean. As such, the ratios of Si:C and Si:chl observed here were robust across all seasons (Fig. 5.11). This opposing effect results in minimal changes in BSi:C and BSi:chl compared to the larger changes in absolute nutrient use, the latter being driven by overall production rather than phytoplankton or diatom speciation.

The robust relationship between BSi and both C and chl suggests that both chl records from satellite and *in situ* records can be considered to reflect Si in the WAP region. The cycling of Si throughout this area has the potential for both local and remote impacts, which are further explored in the next section.

8.2.2 Implications of continued climate trends for seasonal Si budgets

The intense warming and strong decrease in [chl] in the northern areas of the WAP (Montes-Hugo *et al*. 2009) suggest that as warming progresses, more areas will experience a decline in phytoplankton production. As this decrease results from changes in diatom communities, a reduction in productivity will strongly impact the extent of opal production and Si cycling along the WAP. In this section, we use the study periods here compared to earlier, high-chl seasons to investigate potential impacts for Si cycling. Given the extreme latitudinal gradient along the WAP and small-scale regional differences, comparing high- and low- chl seasons at a single site should be a more robust characterisation of changes than inter-regional comparisons, where local processes can obscure or modify any climate signal.

The annual Si budget estimated here for 2009 reflects a year with relatively low [chl] levels compared to the long-term mean (*Chapter 2*). Given the even lower measured BSi and lower [chl] in 2008, 2009 is a conservative case for considering the magnitude of changes associated with a shift such as that seen in the northern WAP subregion. For example, the estimated new opal production suggests that

variations in [chl] are accompanied by changes of similar magnitude in BSi production (and export), in keeping with the strong BSi:chl relationship (Fig. 5.11). In this case, it can be suggested that BSi production in the northern WAP has already declined by up to 89% since 1978-1986 (based on the 89% decrease in [chl] calculated by Montes-Hugo *et al*. 2009). During this same period, a moderate increase in [chl] levels occurred in the southern subregion (12%; Montes-Hugo *et al*. 2009), which should offset some of the northern decrease. However, if warming and sea-ice retreat continue to progress southwards, overall WAP primary production will decline, reducing BSi production and export. This reduced biological demand is significant when considered alongside likely trends is Si sources.

Supply of Si to Ryder Bay is related to mixing from below with deeper, Si-rich waters, balanced by dilution from low-salinity meltwater inputs. Higher mixing associated with continued reductions in winter sea-ice cover would act to increase [Si_d] in surface waters. Although projected increases in glacial melt may counter this trend during summer, this effect would be relatively minor, as meteoric water contributions are <6% in WAP surface waters (Meredith *et al*. 2012). At a regional scale, the suggested increased frequency of UCDW incursions, bringing high-nutrient waters onto the WAP shelf (Martinson *et al*. 2008) would also act to increase [Si_d]. The reduced biological uptake would be a further factor acting to increase [Si_d], by lowering the removal rate.

Over long time scales, such as those relevant to the interpretation of sediment records and paleoreconstructions, greater supply and reduced drawdown would lead to Si accumulation in waters along the WAP. As the WAP region is linked to other adjacent water masses by the lack of a shelf-break front, some seaward current flow (*e.g*. above Marguerite Trench; Savidge & Amft 2009) and northward transport into the Bransfield and Gerlache Straights (Hofmann *et al*. 1996, Zhou *et al*. 2002), WAP shelf waters must gradually feed back into waters of the ACC. Based on this regional circulation, this water should ultimately be redistributed further north along the Peninsula. This Si-enriched water would eventually move into the Southern Ocean, where it is currently not fully utilised. The relative volume of WAP shelf water is low with respect to large ocean basins, but over long time scales this represents a mechanism to increase Southern Ocean Si fluxes.

Thus the excess Si from the WAP shelf would eventually be directed either to the polar front zone (PFZ), or into Antarctic Intermediate Water (AAIW). In the Southern Ocean, Fe is the primary factor limiting phytoplankton growth, but north of the PFZ diatoms can be limited by low concentrations of Si (Brzezinski *et al*. 2005). Even south of the PFZ, co-limitation of diatom production by Fe and Si has been hypothesised by Leblanc *et al*. (2005), and supported by laboratory work (Hoffmann *et al*. 2008). Increased Si in the PFZ could be used both in the south and north of this region by diatoms, or may be entrained into AAIW. While Si in AAIW would not be immediately available to phytoplankton, this is a key mechanism distributing macronutrients to low-latitude regions, and thus could eventually increase diatom production in more temperate waters (similar to the Silicic Acid Leakage Hypothesis of Brzezinksi *et al*. 2002). The scenario above, of increases in Si supply to Southern Ocean waters, could help to enhance currently limited productivity in the PFZ and eventually in low-latitude waters.

A comprehensive assessment of how much Si may be redistributed to the open ocean via this mechanism over short time scales is beyond the scope of this study. Over long time scales, however, such an estimate is not constrained by the rate of supply of Si from WAP waters back into the ACC. Under the assumption that all unutilised Si will eventually follow this pathway, we can estimate the maximum impact of this Si supply on Southern Ocean C drawdown. An estimate of average WAP productivity from Vernet *et al*. (2008) of 182 ± 107 g C m^{-2} y^{-1} can be converted to Si using the strong BSi:POC found here of 0.15 mol:mol (Fig. 5.11), giving 27.3 ± 16 g Si m^{-2} y^{-1}. From [chl] trends observed by Montes-Hugo *et al*. (2009) in the northern WAP subregion (a decline of 89%), the same decrease relative to 1978-1986 is assumed for Si production (we consider only the northern subregion as the south showed an increase). Based on the northern subregion as defined by Montes-Hugo *et al*. (2009), which accounts for ~36% of the WAP area, or ~360 km by 200 km, this is ~1.93 ± 1.1 Tg Si y^{-1}. If this "current" value represents only 11% of the 1978-1986 value, then the 89% reduction in Si amounts to 15.6 ± 9.2 Tg Si y^{-1} which is now going unused (assuming that Si supply was formerly adequate to meet demand and has not changed significantly). If all of this Si were to eventually be

distributed to open ocean waters where it could be fully used, at Redfield ratios this equates to 104 ± 61 Tg C y^{-1}.

By this estimate, the proposed mechanism could potentially stimulate an additional 2.4 ± 1.4 % of Southern Ocean primary production (relative to an estimated 4414 Tg C y^{-1}; Arrigo *et al*. 1998) over long time scales. This rough estimate has many sources of uncertainty, including the 66% increase in [chl] seen in the southern WAP subregion (Montes-Hugo *et al*. 2009) which would act to oppose this off-shelf supply of Si. However, if southward propagation of [chl] decline does occur with continued warming, this would increase the potential Si supply from the WAP, revising the estimate upwards. While such an effect would be manifest only over relatively long time scales, this is a mechanism bringing Si to the Southern Ocean, in addition to changes to circulation or overturning, which has not previously been considered.

8.2.3 Implications for iron cycling

Iron, like Si, is likely to be impacted in the future by lower use due to declining primary productivity, as well as by changes in supply rate. As the WAP shelf has been found here (Chapter 7) and in other studies (*e.g*. Holeton *et al*. 2005, Lancelot *et al*. 2009, De Jong *et al*. 2012) to release significant amounts of Fe to the overlying water column, more frequent UCDW incursions may supply Fe to WAP waters by increasing the amount of water flowing over the shelf. In this regard, LCDW incursions may be even more significant as a supply source, as this water mass will be in direct contact with shelf sediments. Although no studies have looked directly at LCDW, the increase in WAP shelf heat content (Martinson *et al*. 2008) is consistent with increasing CDW inputs, which may include both UCDW and LCDW. As such, Fe supply via LCDW processes may already be occurring, and may increase with continued changes to atmospheric circulation, as is suggested for UCDW (Martinson *et al*. 2008, Meredith *et al*. 2010).

In addition to an important sedimentary source on annual time scales, this study also identified a large glacial source of Fe. This glacial source is the dominant Fe input to surface water at the intraseasonal scale. While we are unable here to discriminate between Fe purely from glacial ice melt and Fe which may be

resuspended by seawater mixing beneath marine-terminating glaciers, all of these processes are here considered as glacially-derived Fe sources. Increased rates of glacial melt will supply more Fe to surface waters, and retreat of marine terminating glaciers could expose additional subglacial sediments, enhancing seawater driven sediment mixing and Fe release. Following substantial retreat, Fe release may decline if these glaciers become land-terminating, but even in this case terrestrial erosion may act to keep glacial Fe supply high. Thus continued climate change can be expected to enhance Fe supply to coastal surface waters.

In addition to dFe, some Fe will stay in particulate form, and indeed in surface waters the majority of Fe is present as particulates (De Baar & de Jong 2001, Planquette *et al*. 2009, Ardelan *et al*. 2010). While much of the Fe resuspended from sediments is rapidly depleted in the upper water column due to vertical settling (Boyd *et al*. 2012), particles represent an important transport mechanism by which Fe can bypass biological utilisation in the surface mixed layers (Homoky *et al*. 2012). While relatively few studies have considered transport of the particle phase, evidence suggests that transport of particulate Fe may be significant in many regions (Frew *et al*. 2006, Lam *et al*. 2006, Planquette *et al*. 2009, 2011). While constraining glacially-derived fluxes of particulate Fe and their bioavailability is outside the scope of this study, continued trends of increasing glacial melt and retreat indicate enhanced delivery of both dissolved and particulate Fe to WAP surface waters in the future.

However, changes in the supply of Fe must be considered in the context of biological demand. Importantly, this work identifies a very high ratio of Fe to macronutrient supply from deep waters. This high supply of Fe (2- to 4-fold above phytoplankton requirements) from below is significant, as it indicates that the WAP shelf will not be Fe-limited. Glacial sources of Fe (especially icebergs) have been suggested to contribute to Southern Ocean productivity by alleviating Fe limitation, but this mechanism will only function where phytoplankton production is limited by scarcity of Fe. In offshore areas (*e.g*. Shaw *et al*. 2011) or other coastal settings (*e.g*. Gerringa *et al*. 2012) glacial melt may indeed represent a crucial supply of Fe for phytoplankton, but along the WAP Fe delivered from glacial sources is likely to go predominantly unused.

Under the projected scenario of continued warming and reduced biological productivity, Fe removal due to biological utilisation is expected to decline. The Fe:Si ratios determined here from concentration changes, coupled with modelled Si production, indicate a reduction in Fe demand of 40-70% in 2009 (an intermediate-chl year) compared to the estimated average for high-chl years.

The combination of increased supply and reduced Fe drawdown suggests that the WAP shelf Fe inventory will increase into the future. Similar to the potential export of Si to ACC waters, Fe could also be transported off the WAP shelf. In contrast to the off-shelf Si fluxes estimated above, an Fe budget is complicated by additional glacial sources, the balance between glacial and deep-water inputs, and uncertainty in the magnitude and bioavailability of particulate Fe fluxes. As such, an estimate of potential Fe supply to the ACC is outside the scope of the present study. However, both greater supply and reduced demand suggest increasing Fe in WAP shelf waters, which would subsequently be advected to some extent into the ACC. This represents a pathway delivering Fe to currently Fe-limited offshore regions, where it could stimulate primary production and act as a C drawdown mechanism. In particular, offshore transport of particulate glacial Fe may represent a significant flux of Fe to the Southern Ocean.

8.3 Key findings

This study has documented interannual variability in phytoplankton communities and diatom assemblages at a coastal Antarctic location spanning five austral summers and a range of environmental conditions. This extensive data set covering full summer bloom periods at a single location allows a comparison between different climatic conditions which can account for differences in bloom timing, a factor that often complicates shorter ship-based studies. The analysis presented here identifies physical conditions, in particular light levels resulting from stratification, as the key factor driving fluctuations in diatom production and hence overall production along the WAP. Stratified conditions are associated with higher diatom biomass and greater nutrient drawdown. Conversely, deeper MLDs are concurrent with greater proportions of non-diatoms (primarily *Phaeocystis antarctica*) and a decrease in chl and productivity.

The diatom species present are similar across all seasons, although there is some indication of reduced species richness during low-chl seasons, and increases in relative proportions of small diatom species. High-resolution records allow the characterisation of indicator diatom assemblages, ratios of species which can be used to assess standing stock in modern studies or variability within the sediment record.

Trends in chl are closely mirrored by changes in BSi production. At a seasonal level, changes in chl are consistent with both dissolved (nutrient drawdown) and particulate (BSi, POC, diatom biomass) analyses indicating low primary production in low-chl years. As a result of the strong diatom component of WAP productivity, a very robust relationship was found between BSi and chl, suggesting that trends in the diatom community can be estimated from chl records. Further, an annual Si budget of 350-700 mmol Si m^{-2} y^{-1} was derived for Ryder Bay for 2009, which is considerably lower (40 – 70% lower) than the estimate for conditions typical of high-chl years, but in agreement with the change in [chl]. Continued warming resulting in low-chl conditions is expected to similarly reduce opal production, increasing Si in surface waters along the WAP which could subsequently be exported to the Southern Ocean.

Measurement of dFe and nutrient drawdown indicate that WAP surface waters are not subject to Fe limitation, as all ratios are consistent with Fe-replete phytoplankton. This work identifies a strong source of Fe to deep waters from WAP shelf sediments, sufficient to prevent Fe-limitation based on upward nutrient fluxes alone. Both Fe and Ra analyses indicate that the shelf source of Fe is augmented by glacial sources during summer, providing Fe in excess of biological demand. As the supply of Fe is projected to increase in the future, while lower productivity will reduce Fe demand, the role of the WAP region as a net source of Fe to the Southern Ocean is expected to increase with continued climate change.

8.4 Future directions

The results, discussion and implications presented here identify several important aspects of biogeochemical cycling and phytoplankton productivity along the WAP. However, this analysis also highlights areas where additional study would aid in addressing outstanding questions and uncertainty:

Additional records of phytoplankton assemblages from low-chl years at the RaTS site would be extremely useful in assessing interannual variability in diatom communities under these conditions. This is particularly the case with regards to the suggested reduced species richness, as well as for validating low-chl indicator assemblages.

Combining the results of this study with regional circulation models would be of use in constraining the flux of (micro)nutrients from WAP shelf waters into the ACC. This would allow for a more robust estimate of the potential for excess Si and Fe to enhance productivity away from the shelf.

Better constraining vertical fluxes of Fe, and reducing the uncertainty in flux estimates for glacial Fe would give a better picture of relative Fe supply terms. This in turn would improve estimates of the potential future increases to the WAP Fe inventory.

Additional Ra surveys in the same location would be helpful in quantifying intraseasonal and interannual variability in Ra activities and flux estimates (particularly of ^{227}Ac, an indicator of UCDW), which could subsequently be used to improved projections of future change.

Finally, similar records at multiple WAP sites would be beneficial in comparing latitudinal trends in phytoplankton, diatoms, and macro- and micro-nutrient cycling. A key strength of the dataset presented here is the high-resolution seasonal coverage, which is absent from the spatially extensive studies conducted by ships. Time-series data from other locations would allow a more detailed assessment of how the northern versus southern regions of the WAP are responding to changing environmental conditions, and help in predicting how these systems will continue to respond in the future. Such data could also be used to assess Si and Fe budgets over a greater spatial scale, by accounting for regional differences in glacial fluxes or productivity.

8.5 References

ARDELAN, M.V., HOLM-HANSEN, O., HEWES, C.D., REISS, C.S., SILVA, N.S., DULAIOVA, H., STEINNES, E. & SAKSHAUG, E. 2010. Natural iron enrichment around the Antarctic Peninsula in the Southern Ocean. *Biogeosciences*, **7**, 11–25.

ARRIGO, K.R., DUNBAR, R.B., LIZOTTE, M.P. & ROBINSON, D.H. 2002. Taxon-specific differences in C/P and N/P drawdown for phytoplankton in the Ross Sea, Antarctica. *Geophysical Research Letters*, **29**, 1938, 10.1029/2002GL015277.

ARRIGO, K.R., WORTHEN, D., SCHNELL, A. & LIZOTTE, M.P. 1998. Primary production in Southern Ocean waters. *Journal of Geophysical Research*, **103**, 15587–15600.

ASPER, V. & SMITH, W.O., Jr. 1999. Particle Fluxes during austral spring and summer in the southern Ross Sea, Antarctica. *Journal of Geophysical Research*, **104**, 5345–5359.

ATKINSON, A., SIEGEL, V., PAKHOMOV, E. & ROTHERY, P. 2004. Long-term decline in krill stock and increase in salps within the Southern Ocean. *Nature*, **432**, 100–103.

BOYD, P.W., ARRIGO, K.R., STRZEPEK, R. & VAN DIJKEN, G.L. 2012. Mapping phytoplankton iron utilization: Insights into Southern Ocean supply mechanisms. *Journal of Geophysical Research*, **117**, 1–18, 10.1029/2011JC007726.

BRZEZINSKI, M., JONES, J.L. & DEMAREST, M.S. 2005. Control of silica production by iron and silicic acid during the Southern Ocean Iron Enrichment Experiment (SOFeX). *Limnology and Oceanography*, **50**, 810–824.

BRZEZINSKI, M.A., PRIDE, C.J., FRANCK, V.M., SIGMAN, D.M., SARMIENTO, J.L. & MATSUMOTO, K. 2002. A switch from $Si(OH)_4$ to NO_3 depletion in the glacial Southern Ocean. *Geophysical Research Letters*, **29**, 10.1029/2001GL014349.

DE BAAR, H.J.W. & DE JONG, J.T.M. 2001. Distributions, sources and sinks of iron in seawater. *In* Turner, D. & Hunter, K., *eds. The biogeochemistry of iron in seawater*. Chichester: John Wiley & Sons Ltd., 123–253.

DE JONG, J., SCHOEMANN, V., LANNUZEL, D., CROOT, P., DE BAAR, H. & TISON, J.-L. 2012. Natural iron fertilization of the Atlantic sector of the Southern Ocean by continental shelf sources of the Antarctic Peninsula. *Journal of Geophysical Research*, **117**, 1–25, 10.1029/2011JG001679.

DITULLIO, G.R., GREBMEIER, J.M., ARRIGO, K.R., LIZOTTE, M.P., ROBINSON, D.H., LEVENTER, A., BARRY, J.P., VANWOERT, M.L. & DUNBAR, R.B. 2000. Rapid and early export of *Phaeocystis antarctica* blooms in the Ross Sea, Antarctica. *Nature*, **404**, 595–598.

DUCKLOW, H.W., BAKER, K., MARTINSON, D.G., QUETIN, L.B., ROSS, R.M., SMITH, R.C., STAMMERJOHN, S.E., VERNET, M. & FRASER, W. 2007. Marine pelagic ecosystems: the West Antarctic Peninsula. *Philosophical Transactions of the Royal Society B: Biological Sciences*, **362**, 67–94, 10.1098/rstb.2006.1955.

DUCKLOW, H.W., FRASER, W., KARL, D.M., QUETIN, L.B., ROSS, R.M., SMITH, R.C., STAMMERJOHN, S.E., VERNET, M. & DANIELS, R.M. 2006. Water-column processes in the West Antarctic Peninsula and the Ross Sea: Interannual variations and foodweb structure. *Deep Sea Research Part II: Topical Studies in Oceanography*, **53**, 834–852, 10.1016/j.dsr2.2006.02.009.

DUNBAR, R.B., LEVENTER, A.R. & MUCCIARONE, D.A. 1998. Water column sediment fluxes in the Ross Sea, Antarctica: Atmospheric and sea ice forcing. *Journal of Geophysical Research*, **103**, 30741–30759.

FREW, R.D., HUTCHINS, D.A., NODDER, S., SANUDO-WILHELMY, S., TOVAR-SANCHEZ, A., LEBLANC, K., HARE, C.E. & BOYD, P.W. 2006. Particulate iron dynamics during FeCycle in subantarctic waters southeast of New Zealand. *Global Biogeochemical Cycles*, **20**.

GERRINGA, L.J.A., ALDERKAMP, A.-C., LAAN, P., THURÓCZY, C.-E., DE BAAR, H.J.W., MILLS,

M.M., VAN DIJKEN, G.L., VAN HAREN, H. & ARRIGO, K.R. 2012. Iron from melting glaciers fuels the phytoplankton blooms in Amundsen Sea (Southern Ocean) Iron biogeochemistry. *Deep-Sea Research Part II*, **71-76**, 16–31, 10.1016/j.dsr2.2012.03.007.

HENLEY, S.F. 2012. *Climate-induced changes in carbon and nitrogen cycling in the rapidly warming Antarctic coastal ocean*. PhD Thesis: University of Edinburgh.

HOFFMANN, L.J., PEEKEN, I. & LOCHTE, K. 2008. Iron, silicate, and light co-limitation of three Southern Ocean diatom species. *Polar biology*, **31**, 1067–1080, 10.1007/s00300-008-0448-6.

HOFMANN, E.E., KLINCK, J.M., LASCARA, C.M. & SMITH, D.A. 1996. Water mass distribution and circulation west of the Antarctic Peninsula and including Bransfield Strait. *Antarctic Research Series: Foundations for ecological research west of the Antarctic Peninsula*, **70**, 61–80.

HOLETON, C.L., NEDELEC, F., SANDERS, R., BROWN, L., MOORE, C.M., STEVENS, D.P., HEYWOOD, K.J., STATHAM, P.J. & LUCAS, C.H. 2005. Physiological state of phytoplankton communities in the Southwest Atlantic sector of the Southern Ocean, as measured by fast repetition rate fluorometry. *Polar biology*, **29**, 44–52, 10.1007/s00300-005-0028-y.

HOMOKY, W.B., SEVERMANN, S., MCMANUS, J., BERELSON, W.M., RIEDEL, T.E., STATHAM, P.J. & MILLS, R.A. 2012. Dissolved oxygen and suspended particles regulate the benthic flux of iron from continental margins. *Marine Chemistry*, **134-135**, 59–70, 10.1016/j.marchem.2012.03.003.

LAM, P.J., BISHOP, J.K.B., HENNING, C.C., MARCUS, M.A., WAYCHUNAS, G.A. & FUNG, I.Y. 2006. Wintertime phytoplankton bloom in the subarctic Pacific supported by continental margin iron. *Global Biogeochemical Cycles*, **20**, 10.1029/2005GB002557.

LANCELOT, C., DE MONTETY, A., GOOSSE, H., BECQUEVORT, S., SCHOEMANN, V., PASQUER, B. & VANCOPPENOLLE, M. 2009. Spatial distribution of the iron supply to phytoplankton in the Southern Ocean: a model study. *Biogeosciences*, **6**, 2861–2878.

LANCELOT, C., HANNON, E., BECQUEVORT, S., VETH, C. & DE BAAR, H.J.W. 2000. Modeling phytoplankton blooms and carbon export production in the Southern Ocean: dominant controls by light and iron in the Atlantic sector in Austral spring 1992. *Deep-Sea Research I*, **47**, 1621–1662.

LEBLANC, K., HARE, C.E., BOYD, P.W., BRULAND, K.W., SOHST, B., PICKMERE, S., LOHAN, M.C., BUCK, K., ELLWOOD, M. & HUTCHINS, D.A. 2005. Fe and Zn effects on the Si cycle and diatom community structure in two contrasting high and low-silicate HNLC areas. *Deep Sea Research Part I: Oceanographic Research Papers*, **52**, 1842–1864, 10.1016/j.dsr.2005.06.005.

LOEB, V., SIEGEL, V., HOLM-HANSEN, O., HEWITT, R., FRASER, W., TRIVELPIECE, W. & TRIVELPIECE, S. 1997. Effects of sea-ice extent and krill or salp dominance on the Antarctic food web. *Nature*, **387**.

MARTINSON, D.G., STAMMERJOHN, S.E., IANNUZZI, R.A., SMITH, R.C. & VERNET, M. 2008. Western Antarctic Peninsula physical oceanography and spatio-temporal variability. *Deep-Sea Research II*, **55**, 1964–1987, 10.1016/j.dsr2.2008.04.038.

MEREDITH, M.P., VENABLES, H.J., CLARKE, A., DUCKLOW, H., ERIKSON, M., LENG, M.J., LENAERTS, J.T.M. & VAN DEN BROEKE, M.R. *In press*. The freshwater system west of the Antarctic Peninsula: spatial and temporal changes. *Journal of Oceanography*.

MEREDITH, M.P., WALLACE, M.I., STAMMERJOHN, S.E., RENFREW, I.A., CLARKE, A., VENABLES, H.J., SHOOSMITH, D.R., SOUSTER, T. & LENG, M.J. 2010. Changes in the freshwater composition of the upper ocean west of the Antarctic Peninsula during the first decade of the 21st century. *Progress In Oceanography*, **87**, 127–143, 10.1016/j.pocean.2010.09.019.

MONTES-HUGO, M., DONEY, S.C., DUCKLOW, H.W., FRASER, W., MARTINSON, D.,

STAMMERJOHN, S.E. & SCHOFIELD, O. 2009. Recent Changes in Phytoplankton Communities Associated with Rapid Regional Climate Change Along the Western Antarctic Peninsula. *Science*, **323**, 1470–1473, 10.1126/science.1164533.

PLANQUETTE, H., FONES, G.R., STATHAM, P.J. & MORRIS, P.J. 2009. Origin of iron and aluminium in large particles (>53 μm) in the Crozet region, Southern Ocean. *Marine Chemistry*, **115**, 31–42, 10.1016/j.marchem.2009.06.002.

PLANQUETTE, H., SANDERS, R.R., STATHAM, P.J., MORRIS, P.J. & FONES, G.R. 2011. Fluxes of particulate iron from the upper ocean around the Crozet Islands: A naturally iron-fertilized environment in the Southern Ocean. *Global Biogeochemical Cycles*, **25**, 1–12, 10.1029/2010GB003789.

REIGSTAD, M. & WASSMANN, P. 2007. Does *Phaeocystis* spp. contribute significantly to vertical export of organic carbon? *Biogeochemistry*, **83**, 217–234.

SAVIDGE, D.K. & AMFT, J.A. 2009. Circulation on the West Antarctic Peninsula derived from 6 years of shipboard ADCP transects. *Deep Sea Research Part I: Oceanographic Research Papers*, **56**, 1633–1655, 10.1016/j.dsr.2009.05.011.

VAUGHAN, D.G., MARSHALL, G.J., CONNOLLEY, W.M., PARKINSON, C., MULVANEY, R., HODGSON, D.A., KING, J.C., PUDSEY, C.J. & TURNER, J. 2003. Recent rapid regional climate warming on the Antarctic Peninsula. *Climatic Change*, **60**, 243–274.

VENABLES, H.J., CLARKE, A. & MEREDITH, M.P. *In press*. Wintertime controls on summer stratification and productivity at the western Antarctic Peninsula. *Limnology and Oceanography*.

VERITY, P.G., BRUSSAARD, C.P., NEJSTGAARD, J.C., VAN LEEUWE, M.A., LANCELOT, C. & MEDLIN, L.K. 2007. Current understanding of *Phaeocystis* ecology and biogeochemistry, and perspectives for future research. *Biogeochemistry*, **83**, 311–330, 10.1007/s10533-007-9090-6.

WALSH, J.J., DIETERLE, D.A. & LENES, J. 2001. A numerical analysis of carbon dynamics of the Southern Ocean phytoplankton community: the roles of light and grazing in e!ecting both sequestration of atmospheric CO_2 and food availability to larval krill. *Deep-Sea Research I*, **48**, 1–48.

ZHOU, M., NIILER, P.P. & HU, J.-H. 2002. Surface currents in the Bransfield and Gerlache Straits, Antarctica. *Deep-Sea Research I*, **49**, 267–280.

Section 9: Appendices

Appendix A2.1: Sampling dates

Table A2.1: List of sampling dates from the two field seasons studied here. Dates where sampling was performed at multiple depths (0–25 m) are indicated as "Depth profile" type sampling, and dates of radium sample collection are noted.

Summer 2008			Summer 2009		
Sample	Date	Type	Sample	Date	Type
801	04/12/2008		901	02/12/2009	
802	08/12/2008		902	07/12/2009	Depth profile
803	12/12/2008		903	10/12/2009	
804	15/12/2008		904	15/12/2009	
805	18/12/2008			16/12/2009	Sea-ice
806	27/12/2008		906	21/12/2009	
807	30/12/2008	Depth profile	907	22/12/2009	
808	04/01/2009		908	24/12/2009	
809	07/01/2009	Depth profile	909	28/12/2009	Depth profile
810	12/01/2009	Depth profile	910	30/12/2009	
811	13/01/2009		911	04/01/2010	Depth profile
812	15/01/2009	Depth profile	912	07/01/2010	
813	19/01/2009		913	13/01/2010	Depth profile
814	22/01/2009		914	16/01/2010	
815	26/01/2009		915	18/01/2010	Depth profile
816	29/01/2009	Depth profile	916	21/01/2010	
817	02/02/2009		917	23/01/2010	Depth profile
818	05/02/2009		919	27/01/2010	Depth profile
819	09/02/2009		920	30/01/2010	
820	12/02/2009	Depth profile	921	02/02/2010	
821	18/02/2009		922	06/02/2010	
822	23/02/2009		923	12/02/2010	Depth profile
823	26/02/2009			13/02/2010	Radium
824	02/03/2009			14/02/2010	Radium
825	05/03/2009	Depth profile	924	15/02/2010	Depth profile
826	11/03/2009		925	18/02/2010	
827	14/03/2009	Depth profile	926	22/02/2010	Depth profile
			927	25/02/2010	
				25/02/2010	Radium
			928	01/03/2010	Depth profile
			929	04/03/2010	
			930	10/03/2010	Depth profile
			931	15/03/2010	
			932	18/03/2010	Depth profile

Appendix A2.2: Statistical analysis of seasonal chlorophyll

Chlorophyll concentrations were compared between seasons to investigate differences between years of the same chl type (*i.e.* 2004 and 2005; both high-chl seasons), and between seasons with different chl dynamics (*i.e.* 2006 and 2008; an intermediate- and a low-chl season, respectively). All [chl] measurements for each summer bloom period (as defined in section 2.4.1) were compared by season (year) and by season type (*i.e.* high-, intermediate- or low-chl). Analysis of variance was performed on each type of grouping (by season and by season type), and both ANOVA results indicated significant variation between groups (*p*-values of 1.28×10^{-15} and 2.2×10^{-16}, respectively; Fig A2.2.1, a and c). Post-hoc pair-wise comparisons (Tukey test) were done to determine which of the groups were distinct, and results of these analyses are shown in Figure A2.2.1 (b and d). Both low-chl seasons were distinct from both the high-chl seasons, as well as 2006 (an intermediate-chl year).

When grouped at the season-type level, differences between all three types were statistically significant (Fig A2.2.1d). This analysis includes even the [chl] measurements from early and late in the growing period, where [chl] is just beginning to increase or falling to winter levels, and thus is very low in all seasons. Consideration of only mid-summer chl would result in more marked differences between the season types, but differences are clear even when the entire summer period is included, suggesting that the season-type groups used here reflect distinct conditions and comparison between these groups can be used to investigate the mechanisms leading to such different chl conditions.

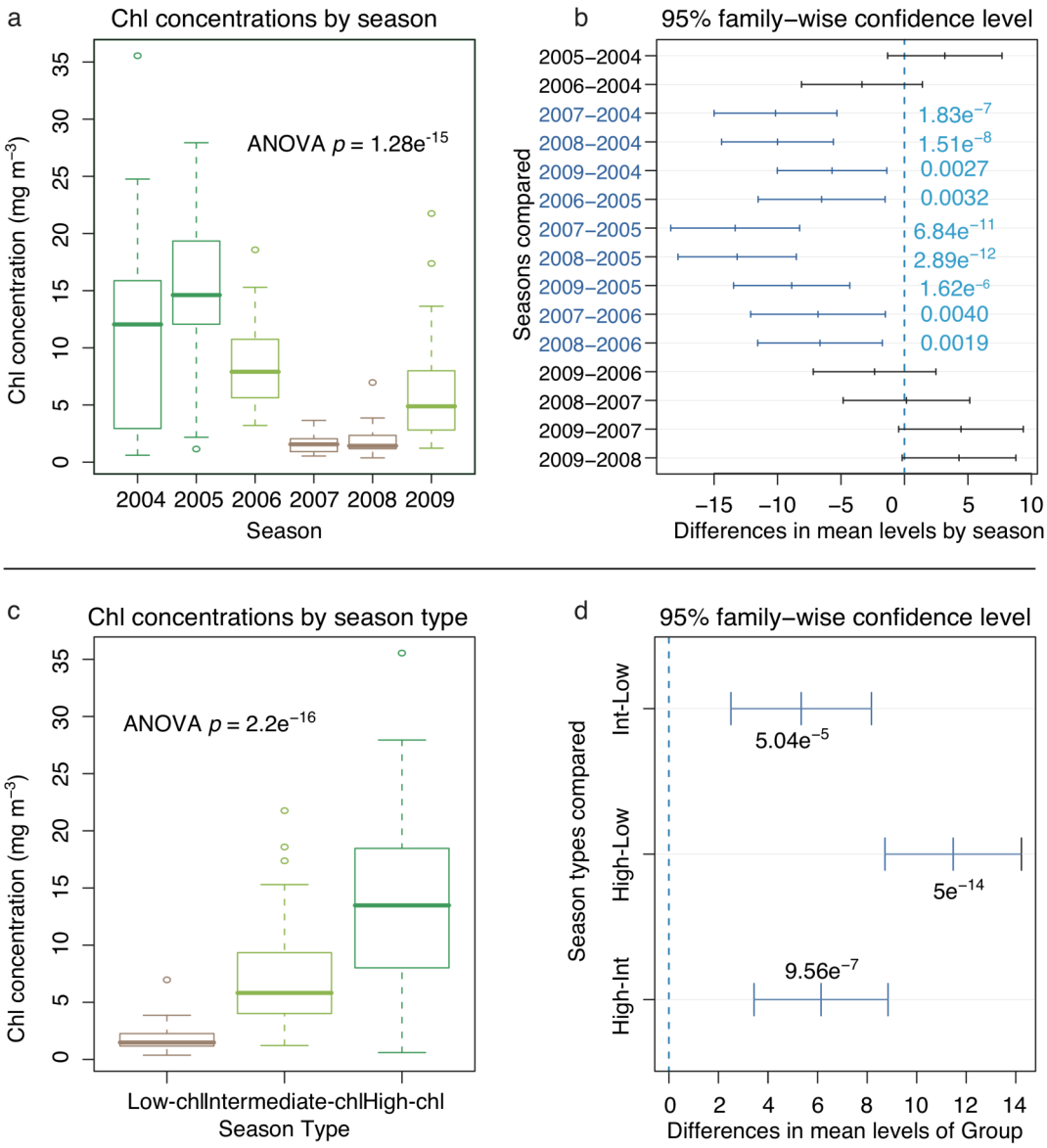

Figure A2.2.1: Boxplots visualising population distribution of [chl] measurements, grouped by season (a) and by season type (c). In both cases the high-chl seasons are shown in dark green, intermediate-chl in light green, and low-chl in brown. Analysis of variance (ANOVA) was done for both groupings. *P*-values for ANOVA tests are shown on the plots and in both cases are highly significant ($p < 0.05$). Tukey test post-hoc pair-wise comparisons were then performed to identify where groups differed. Confidence intervals for Tukey-test comparisons are shown in (b) and (d), by season and by season type respectively. Confidence levels which do not overlap the zero line denote comparisons between statistically different groups, which is shown on the plots by blue lines and text (*i.e.* blue denotes a difference between groups, black denotes that groups are not statistically different).

Appendix A3.1: Evaluation of biomass concentration estimates

Diatom assemblages from the summers of 2004 and 2005 have been described previously in Annett *et al*. (2010), but only one further season was available for comparison of absolute cell abundances. As such, only relative species composition has been presented, as insufficient data was available to establish the reliability of absolute biomass concentration estimates. Thus the biomass estimates from all seasons are compared here to show that the data from the early two seasons are in keeping with those from later years, and are robust reflections of biomass trends.

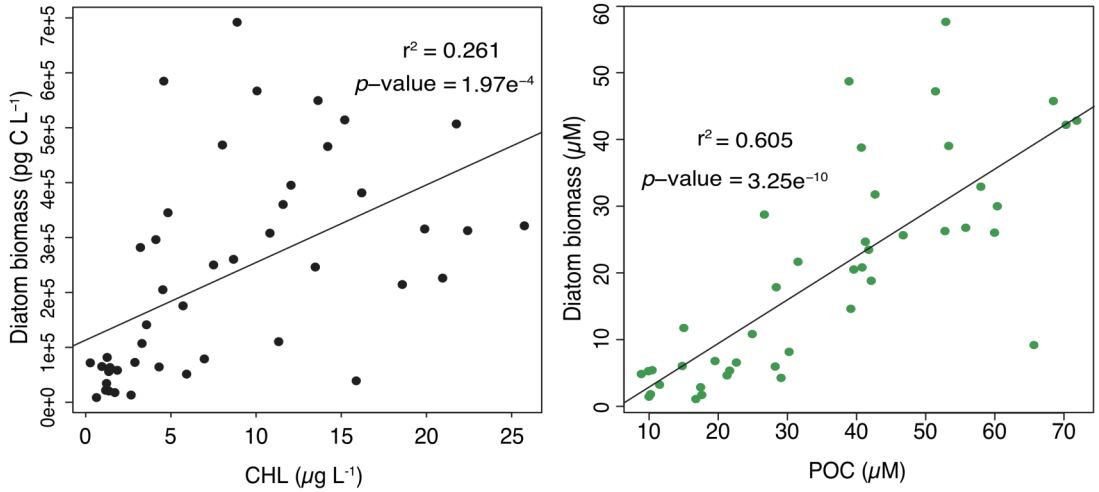

Figure A3.1: Relationship between estimated diatom biomass and (a) [chl] (from BAS data), and (b) particulate organic carbon (POC). In plot (b), diatom biomass concentrations (pg C L^{-1}) have been converted to units of μmol L^{-1} to facilitate comparison with POC. Lines given are for linear best-fit regressions, and r^2 and *p*-values indicated for each correlation. Data are for all 5 seasons for which samples are available.

Figure A3.1 shows the estimated diatom community biomass versus both [chl] and POC. A one to one relationship for biomass:chl would not be expected due to several factors. Within the diatom community, interspecific variation in C:chl ratios and changes in species' size distributions would act to decouple this relationship. Additionally, contributions from non-diatom phytoplankton, while

shown to be low over the course of a season, are not zero and may be significant in individual samples, further weakening the biomass:chl relationship.

Although weak, a significant correlation was found between estimated diatom community biomass and chl concentrations ($r^2 = 0.261$, p-value $= 2.0 \times 10^{-4}$). Broad patterns such as lower [chl] in summer 2008 are clearly reflected in biomass records. As well, it can be seen that intra-annual variations in estimated diatom biomass, although at lower resolution, follow the same trends as those of chl concentrations. This is taken as evidence that the estimates of diatom biomass presented here are reliable reflections of diatom-dominated phytoplankton production in Ryder Bay, as are chlorophyll concentrations, although the two proxies are subject to slightly different sets of influences. In contrast, there is a strong correlation between diatom biomass and POC, which is even more statistically significant than for [chl] ($r^2 = 0.605$, p-value $= 3.3 \times 10^{-10}$). There is one sample where very high POC does not correspond to high biomass. This sample is from 4 January 2007, when cell counts were performed using settling chambers. Any agitation of the settling chamber could have resuspended many of the cells, resulting in falsely low cell abundances. When this outlier is discounted from the data, the strength of the correlation increases dramatically ($r^2 = 0.697$; p-value $<2.1 \times 10^{-12}$). The strong, significant correlation found here indicates a high degree of confidence that trends in diatom biomass reflect POC, to an even higher degree than chl. This is to be expected as biomass is estimated in terms of cellular carbon rather than chlorophyll. Biomass estimated from cell counts is ~70% of that measured on filters, which reflects a source of POC in addition to viable diatom cells. While this offset is significant, it is consistent with some POC present in non-diatom phytoplankton and/or detrital material. The offset is also systematic, as can be seen by the strong correlation (r^2 ~0.7) between biomass and POC, and so trends in either parameter can be used as equivalent proxies for diatom-dominated productivity at this site. As such, we are confident that the estimated biomass concentrations in seawater are valid reflections of diatom biomass variations in the water column, and not affected by issues of preservation or distribution which could bias abundance calculations.

Appendix A4.1: Diatom cell measurements, surface area, volume and biomass

Table A4.1.1: Mean values of linear measurements (µm), surface area (SA; μm^2), biovolume (V; μm^3), surface area to volume ratio (SA:V; $\mu m^2\ \mu m^{-3}$) and carbon biomass (pg C $cell^{-1}$) of phytoplankton species observed in this study. D = diatmeter; P = perivalvar axis; A = apical axis; T = transapical axis. Shapes (Sh) were used to estimate volume from linear dimensions: C = cylinder, DC = double cone, EP = ellipse based prism, PB = rectangular box, RRP = rounded rectangular prism, S = sphere and Com = complex.

Taxon *Species*	D	P	A	T	Sh	SA	V	SA:V	Biomass
Diatoms									
Actinocyclus actinochilus	36	17			C	4000	17000	0.235	883.5
Asteromphalus hookeri	58	7			C	6500	18000	0.361	1032.3
Banquisia belgicae		25	105	10	RB	2700	6600	0.409	463.8
Berkeleya spp	13	105			D	3700	6700	0.552	433.8
Chaetoceros neglectus		11	9.0	8.7	EP	550	1300	0.423	111.7
C. simplex		4.7	4.7	2.1	EP	94	75	1.253	11.5
C. socialis		8.7	7.5	16	EP	600	830	0.723	82.9
C. subgenus *Hyalochaeta* resting spores		5	3	3	EP	59	32	1.844	5.40
C. atlanticus		18	12	11	EP	1100	3700	0.297	270.2
C. convolutus		19	12	7	EP	850	2500	0.340	211.2
C. criophilus		18	13	7	EP	860	2600	0.331	214.1
C. dichaeta		26	13	12	EP	430	560	0.768	61.2
C. flexuosus		6.0	3.2	20	EP	2000	6400	0.313	457.7
Corethron pennatum	47	149			C	25000	250000	0.100	5477.2
Dactylisolen cf. *antarcticus*	50	*			C	160	2000	0.080	65.0
Ephemera planamembranacea		3	60	8	EP	930	1140	0.816	121.0
Eucampia antarctica var. *antarctica*					Com	9100	29000	0.314	1767.1
Fragilariopsis curta		3.8	12	4.1	RRP	190	140	1.357	20.2
F. cylindrus		3.1	10	2.2	RRP	75	20	3.750	3.55

Taxa *Species*	D	P	A	T	Sh	SA	V	SA:V	Biomass
Fragilariopsis kerguelensis		4.2	19	4.8	EP	340	300	1.133	39.8
F. obliquecostata		3.5	21	3.3	RRP	310	250	1.240	33.8
F. ritscheri		4.4	21	4.3	EP	350	310	1.129	41.0
F. sublinearis		3.9	22	3.5	RRP	340	290	1.172	38.6
F. vanheurkii		3.2	53	2.6	RRP	450	220	2.045	30.2
Haslea trompii		12	90	7	EP	3200	6200	0.516	384.8
Membraneis challengeri		6	59	17	EP	2400	4700	0.511	298.1
Minidiscus chilensis	5.8	4.3			C	120	120	1.000	19.1
Navicula directa		5.9	65	5	EP	1300	1500	0.867	162.2
N. gelida		5	16	3	EP	230	190	1.211	26.5
N. glaciei		4	22	3	EP	290	210	1.381	28.9
Odontella weissflogii		66	49	30	EP	10500	76000	0.138	2317.8
Porosira glacialis	31		14		C	2900	10700	0.271	649.5
P. pseudodenticulata	29		17		C	2900	10700	0.271	649.5
Proboscia alata	14	200			C	9000	29000	0.310	1752.1
P. inermis	12	248			C	9700	29000	0.335	1861.5
P. truncata	25	248			C	20500	122000	0.168	4031.9
Pseudogomphonema kamtschaticum		12	28	4	Com	500	450	1.111	57.1
Pseudo-nitzschia lineola		3.4	89.5	3.8	RB	1400	1300	1.077	147.1
P. turgidula		3.8	105	4.5	RB	1700	1700	1.000	186.9
Stellarima microtrias	52	21			C	7400	42000	0.176	1609.3
Thalassiosira ambigua	16	8			C	800	1600	0.500	153.1
T. antarctica	48	26			C	7600	47000	0.162	1677.2
T. dichotomica	12	5.9			C	380	500	0.760	54.8

Table A4.1.1 (continued):

Taxa *Species*	D	P	A	T	Sh	SA	V	SA:V	Biomass
T. gracilis var. *gracilis*	17	6.5			C	800	1500	0.533	111.2
T. gracilis var. *expecta*	15	6.4			C	680	1200	0.567	95.4
T. gravida	14	7.8			C	660	1200	0.550	93.3
T. lentiginosa	72	30			C	14500	116000	0.125	3168.1
T. ritscheri	49	24			C	5600	45000	0.124	1357.5
Thalassiothrix antarctica		*	6	6	RB	24	36	0.667	4.73
Silicoflagellates									
Distephanus speculum	23				S	1700	6500	0.262	964.1
Dinoflagellates									
Gyrodinium lachryma	22	13			Com	560	1200	0.467	197.0
Podolampas antarctica	94	17			Com	2700	7600	0.355	1116.8
Polarella glacialis resting spores	9				½ S	200	190	1.053	34.8
Protoperidinium spp.	100	44			Com	21300	219000	0.097	26303.7
Protoperidinium, small spp.	40	29			Com	5300	18000	0.294	2511.6
Scripsiella troichoidea resting spores	8.6				S	230	330	0.697	58.5

(*) refers to dimensions that were often larger than the field of view, or species that were not found intact. In such cases a measurement was made of each fragment to calculate area and volume in each case, but the mean is not presented here as it does not reflect the average value of that axis.

Appendix A4.2: Diatom species abundances

Table A4.2.1: Cellular abundances of diatom species counted for this study (2008 and 2009) and from previous studies (2004 and 2005 data from Annett *et al*. 2010; 2006 data from Annett 2008). All values are in untils of cells L^{-1}.

Date	Banquisia	Odontella	Cocconeis	Chaetoceros	Hyalo.*	Phaeo.*	Corethron	Cylind.*	Dactyl*	Eucampia
2004-12-13	12672	19010	0	2430546	2411536	19010	0	0	0	0
2005-01-07	10528	99433	0	1231212	1223608	7604	0	0	1433	1755
2005-01-10	10077	77257	0	682313	667757	14556	0	0	0	99
2005-01-21	8957	192582	0	61108	55509	5599	0	0	2	1755
2005-02-12	5746	4309	0	30515	30515	0	0	0	479	479
2005-02-28	2060	1603	0	5797	0	5797	114	229	650	343
2005-12-23	94	37	0	717	690	27	0	0	0	19
2006-01-10	3542	17315	0	721126	720535	590	787	0	0	6296
2006-01-24	4294	9686	0	108738	104844	3894	200	0	0	5692
2006-02-10	1084	8172	559	10114	7585	2529	451	0	23	1174
2006-02-23	3451	4026	0	12138	9262	2876	575	0	0	288
2006-02-27	800	2999	0	0	0	0	800	0	0	200
2006-12-09	0	0	0	20229	14985	5245	2248	0	0	10115
2006-12-12	1883	1883	0	37665	28248	9416	3766	9416	0	0
2006-12-22	7800	4800	0	456713	440513	16200	4300	200	0	36200
2006-12-29	11288	7525	0	402610	364983	37627	3763	0	0	47034
2007-01-04	2193	0	0	46592	40015	6578	2193	0	0	15896
2007-01-08	4328	2164	0	367881	367881	0	4328	0	0	0
2007-01-11	4800	7400	0	522525	497925	24600	700	200	1	69900
2007-01-18	5589	2395	0	836118	822543	13574	798	1597	0	26350
2007-01-22	8195	3512	0	530674	521309	9366	585	3512	0	23999
2007-01-25	18793	25057	0	2573969	2542648	31321	6264	0	0	0
2007-01-31	11604	0	0	251549	247086	4463	0	893	0	4910

Table A4.2.1 (cont'd): Cellular abundances of diatom species counted for this study (2008 and 2009) and from previous studies (2004 and 2005 data from Annett *et al*. 2010; 2006 data from Annett 2008). All values are in untils of cells L^{-1}.

Date	Banquisia	Odontella	Cocconeis	Chaetoceros	Hyalo.*	Phaeo.*	Corethron	Cylind.*	Dactyl*	Eucampia
2008-12-04	879	0	0	45110	44817	293	11717	293	0	293
2008-12-18	1758	0	0	110506	110506	0	7030	0	0	0
2008-12-27	0	0	0	567686	567686	0	2636	0	0	0
2009-01-07	439	0	0	106771	106771	0	20	0	0	0
2009-01-26	659	0	0	439	439	0	1227	0	0	0
2009-02-26	1758	0	0	0	0	0	2197	0	0	0
2009-03-02	0	145	0	0	0	0	870	870	0	0
2009-12-07	3515	13621	0	0	0	5273	0	0	0	32954
2009-12-15	1318	220	1098	0	0	13621	2417	0	0	3515
2009-12-21	0	0	0	0	0	0	1845	0	0	0
2009-12-24	0	0	220	0	0	439	439	0	0	1098
2009-12-28	0	5712	0	0	0	1758	0	0	0	3735
2009-12-30	439	352	220	0	0	0	527	0	0	220
2010-01-07	0	352	0	0	0	1933	439	0	0	0
2010-01-16	0	1758	0	0	0	1758	0	879	0	3515
2010-01-23	0	4833	0	0	0	5932	0	439	0	10106
2010-01-27	0	10985	439	0	0	879	439	0	0	25484
2010-02-02	0	17136	0	0	0	4833	0	0	0	439
2010-02-12	0	25924	879	0	0	5273	0	0	0	38227
2010-02-15	0	26803	0	0	0	14060	0	0	0	27681
2010-02-22	0	21091	0	0	0	879	0	0	0	8348
2010-03-01	0	6737	0	0	0	2343	0	0	0	27385
2010-03-04	0	110	0	0	0	0	0	0	0	4394
2010-03-10	0	769	220	0	0	439	0	0	0	12522
2010-03-15	0	0	0	0	0	439	0	0	0	439

*Hyalo. = C. Hyalochaeta subgenus, Phaeo. = Phaeoceros subgenus, Cylind = Cylindrotheca, Dactyl. = Dactyliosolen

Table A4.2.1 (cont'd): Cellular abundances of diatom species counted for this study (2008 and 2009) and from previous studies (2004 and 2005 data from Annett *et al*. 2010; 2006 data from Annett 2008). All values are in untils of cells L^{-1}.

Date	Fragilariopsis*	F.curta gp	F.kerg gp*	F.rhombica	N.directa	N.gel gp*	Proboscia	P.alata	P.inermis	P.truncata
2004-12-13	1096365	1040241	56124	0	20820	0	2716	0	2716	0
2005-01-07	2162574	2139939	22635	0	4679	3509	5264	0	2924	2340
2005-01-10	2794144	2793947	17915	197	2239	3359	560	0	560	0
2005-01-21	333053	314550	11197	0	1120	0	3359	0	3359	0
2005-02-12	1296381	1268134	10533	0	958	5745	359	0	359	0
2005-02-28	184416	183738	678	0	3206	1468	7785	0	7327	458
2005-12-23	10430520	10430001	508	0	5	2172	30	0	27	3
2006-01-10	1041663	986512	38762	0	0	787	61193	0	60012	1181
2006-01-24	1333872	1288905	8321	200	1598	3497	61359	0	60410	949
2006-02-10	484980	464812	20168	0	542	181	113546	0	113140	406
2006-02-23	224411	199105	575	0	0	9262	186778	0	186778	0
2006-02-27	388284	377487	0	0	0	5598	160052	0	160052	0
2006-12-09	43455	26223	11988	0	3746	7492	1124	0	0	0
2006-12-12	175141	122410	0	0	22599	0	26365	0	0	0
2006-12-22	156597	82397	0	0	7600	4600	1700	0	0	0
2006-12-29	124170	71492	52678	0	7525	15051	0	0	0	0
2007-01-04	18637	10963	7674	0	1096	0	0	0	0	0
2007-01-08	95216	34624	60592	0	2164	4328	10820	0	0	0
2007-01-11	87128	33928	0	0	5400	2000	2600	0	0	0
2007-01-18	13574	11977	0	0	8783	1597	6388	0	0	0
2007-01-22	3512	3512	0	0	2341	585	2341	0	0	0
2007-01-25	281890	281890	0	0	12528	6264	0	0	0	0
2007-01-31	23209	22316	893	0	8927	893	893	0	0	0

*Fragiliariopsis = all species, F.kerg gp = F. kerguelensis group, N.gel gp = Navicula gelida group

Table A4.2.1 (cont'd): Cellular abundances of diatom species counted for this study (2008 and 2009) and from previous studies (2004 and 2005 data from Annett *et al*. 2010; 2006 data from Annett 2008). All values are in untils of cells L^{-1}.

Date	Fragiliariopsis	F.curta gp	F.kerg gp	F.rhombica	N.directa	N.gel gp	Proboscia	P.alata	P.inermis	P.truncata
2008-12-04	2050	879	1172	0	0	0	0	0	0	0
2008-12-18	2417	1098	1318	0	0	0	0	0	0	0
2008-12-27	21091	0	21091	0	0	879	0	0	0	0
2009-01-07	6151	6151	0	0	0	0	0	0	0	0
2009-01-26	106146	0	0	348	0	0	0	0	0	0
2009-02-26	879	0	879	0	0	0	0	0	0	0
2009-03-02	218962	580	290	0	16531	4640	0	0	0	0
2009-12-07	86998	44817	42181	0	1758	879	16697	879	5273	10545
2009-12-15	24825	20212	4614	0	1758	439	5492	0	1318	4174
2009-12-21	61075	50969	8788	1318	8348	0	2636	0	2636	0
2009-12-24	42035	38227	2050	1758	1318	3954	13401	0	11644	1758
2009-12-28	3515	1977	879	659	0	8348	22833	0	4598	18235
2009-12-30	40775	38227	1230	1318	3076	439	10326	220	8788	1318
2010-01-07	15818	13621	2197	0	439	879	20256	0	17795	2461
2010-01-16	41742	18454	22409	879	0	0	40423	0	26803	13621
2010-01-23	34711	32954	1758	0	439	439	51628	0	39545	12083
2010-01-27	80408	65908	14500	0	879	879	57999	0	55802	2197
2010-02-02	67226	65029	2197	0	439	0	39764	439	30098	9227
2010-02-12	30757	25484	5273	0	2636	0	35151	439	32515	2197
2010-02-15	16697	15818	879	0	2636	0	10106	0	10106	0
2010-02-22	164212	164212	0	0	2636	0	7030	0	7030	0
2010-03-01	1318	879	0	439	0	2197	435	0	435	0
2010-03-04	427303	425325	1977	0	0	0	1428	0	1318	110
2010-03-10	753327	750910	1977	439	659	439	110	0	110	0
2010-03-15	16697	16697	0	0	0	0	0	0	0	0

Table A4.2.1 (cont'd): Cellular abundances of diatom species counted for this study (2008 and 2009) and from previous studies (2004 and 2005 data from Annett *et al*. 2010; 2006 data from Annett 2008). All values are in untils of cells L^{-1}.

Date	Pseudonit*	Pseudog.	Rhizos*.	Thalas.*	Centrics	(v. smal)	(small)	(med)	(large)	Cosc.*
2004-12-13	74229	0	0	0	872786	413522	429808	13397	16059	0
2005-01-07	179564	0	0	0	371385	178089	178089	15207	0	0
2005-01-10	114206	0	0	0	7838	0	1120	2239	4479	0
2005-01-21	44787	0	1541	8	63878	18503	25221	8957	11197	0
2005-02-12	479	0	0	0	124594	58706	63494	1436	958	0
2005-02-28	6640	229	0	0	24936	6057	7202	10647	1030	0
2005-12-23	2127	0	0	0	1521018	760000	760935	19	64	0
2006-01-10	58635	0	0	8	421803	203228	216804	1771	0	0
2006-01-24	12881	399	0	32	108615	44787	60783	1398	1648	0
2006-02-10	1145	0	0	6	8986	2777	4945	451	813	0
2006-02-23	0	9262	0	4	0	0	0	0	0	0
2006-02-27	0	400	0	0	12796	6398	6398	0	0	0
2006-12-09	7492	0	0	7	61437	5245	14235	25474	14235	2248
2006-12-12	35781	0	0	24	120527	56497	28248	11299	24482	0
2006-12-22	308400	0	0	6	137294	9694	52600	41000	34000	0
2006-12-29	248339	0	0	85	346170	45153	127932	116644	56441	0
2007-01-04	9867	0	0	36	62489	6578	37274	7126	11511	0
2007-01-08	67084	0	0	60	194760	12984	142824	21640	17312	0
2007-01-11	44800	0	0	3	328188	19388	164600	75800	68400	0
2007-01-18	23156	0	0	10	69469	9582	27947	11179	20761	0
2007-01-22	56193	0	0	12	107118	8195	23414	26341	49169	0
2007-01-25	231776	0	0	31	676536	601365	37585	12528	25057	0
2007-01-31	63378	0	0	4	45525	8034	14282	9819	13390	0

*Pseudonit. = Pseudonitzschia spp., Pseudog. = Pseudogomphonema, Rhizos. = Rhizosolenia, Thalas. = Thalassiothrix and Trichotoxon, Cosc. = Coscinodiscus.

Table A4.2.1 (cont'd): Cellular abundances of diatom species counted for this study (2008 and 2009) and from previous studies (2004 and 2005 data from Annett *et al*. 2010; 2006 data from Annett 2008). All values are in untils of cells L^{-1}.

Date	Pseduonit.	Psedog.	Rhizos.	Thalas.	Centrics	(v. small)	(small)	(med)	(large)	Cosc.
2008-12-04	3515	0	0	0	20212	13182	7030	0	0	0
2008-12-18	0	879	0	0	11424	0	4833	2636	3954	0
2008-12-27	7909	0	0	0	20212	0	13182	1758	5273	0
2009-01-07	1758	0	0	0	6151	0	879	879	4394	0
2009-01-26	220	0	0	0	287088	278416	1575	6878	220	0
2009-02-26	0	0	0	0	439	439	0	0	0	0
2009-03-02	0	0	0	0	355850	352660	2610	290	290	0
2009-12-07	91392	0	879	0	386659	116877	163452	106331	0	0
2009-12-15	18015	879	439	2197	31636	12742	13182	5712	0	0
2009-12-21	0	0	0	439	2197	879	439	879	0	0
2009-12-24	14500	2417	1538	0	7909	4394	2636	879	0	0
2009-12-28	7030	1318	220	0	42181	6151	34711	439	879	0
2009-12-30	3515	439	176	0	3954	3954	0	0	0	0
2010-01-07	0	0	0	0	4394	2197	2197	0	0	0
2010-01-16	6151	879	0	0	7030	1758	1758	3515	0	0
2010-01-23	15379	439	0	0	23287	1758	4833	5273	11424	0
2010-01-27	28999	0	4833	1758	56241	3515	11424	1758	39545	0
2010-02-02	17136	439	0	0	97983	11863	12742	3515	69862	0
2010-02-12	18454	0	0	0	193330	2636	6151	55363	129179	0
2010-02-15	15818	0	0	1758	241662	10985	8788	117755	104134	0
2010-02-22	11424	879	0	0	154664	9666	12742	63272	68984	439
2010-03-01	586	0	0	0	35151	1465	1465	4101	28121	0
2010-03-04	220	0	220	220	24166	549	0	3515	20102	439
2010-03-10	0	879	0	0	2783	1098	1025	366	293	0
2010-03-15	0	439	0	0	1098	659	0	439	0	330

Appendix A4.3

Table A4.2: List of groups or species counted in determination of diatom community richness. Each category was given a score of present or absent, and the sum

	Category (Genus/group)	Species/group/subgenera
1	Chaet	Hyalochaeta subgenus
2	Chaet	Phaeoceros subgenus
3	Coerethron	inerme
4	Cocconeis	fasciolata
5	Cylindrotheca	all
6	Dactyliosolen	cf. antarctica
7	Eucampia	antarctica var. antarctica
8	Fragilariopsis	curta group (total)
9	Fragilariopsis	kerguelensis group (total)
10	Fragilariopsis	rhombica
11	Navicula	gelida/glaciei
12	Navicula	directa
13	Odontella	weisflogii
14	Proboscia	alata
15	Proboscia	inermis
16	Proboscia	truncata
17	Pseudogomophonema	kamtschaticum
18	Pseudonitzschia	all
19	Centric	very small
20	Cent	small
21	Cent	medium
22	Cent	large
23	Coscinodiscus	all
24	Thalassiothrix	antarctica, plus Trichotoxon reinboldii

Appendix A5.1: Analysis of biogenic opal concentration

A5.1.1 Biogenic opal extraction

Concentration of particulate biogenic Si (BSi) was determined using an adaptation of the double wet-alkaline digestion method outlined by Ragueneau & Treguer (1994), based on a method proposed by Brzezinski & Nelson (1989). Corrections were made for lithogenic contamination from Al:Si ratios as developed by Ragueneau *et al*. (2005).

Dried filters were covered with 4 mL of 0.2 M NaOH, as this concentration has been shown to minimise mineral silica leaching (Krausse *et al*. 1983). Filters were digested at 100 °C. A preliminary extraction was done over 8 h (Sample 915-10c in Figure A4.1.1) to investigate the suitability of the extraction concentration, temperature and time for these samples. The concentration of dissolved Si in the extraction solution increased linearly in a two-phase manner over the 8 h experiment. The first, fast phase of dissolution primarily reflects the breakdown of the more labile BSi fraction. The second, slower dissolution is from lithogenic Si (LSi) only, after the BSi is completely dissolved, although this dissolution occurs during the initial phase as well, increasing the apparent rate of dissolution above the true BSi dissolution rate. Rates of BSi and LSi dissolution were found to be constant, as evidence by the high linearity of each curve. By extending the regression of this line back to the origin, the lithogenic component can be accounted for, calculating the biogenic fraction of total Si, as illustrated in Figure A5.1.1.

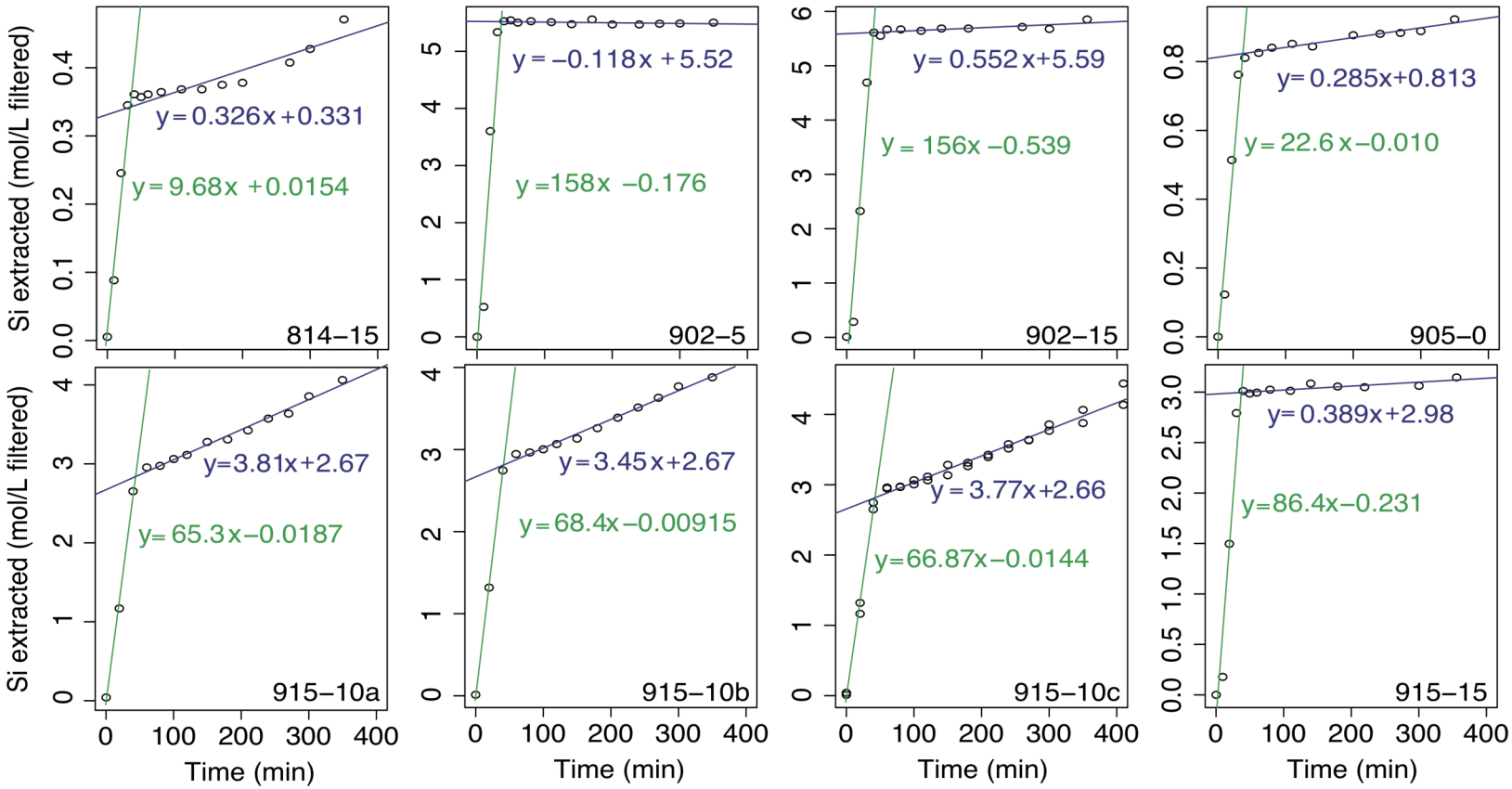

Figure A5.1.1: Trials of wet-alkaline extractions for BSi and LSi. All were done in 4 mL of 0.2 M NaOH. At each time point, two 50 µL samples were collected, diluted to 3 mL, and concentrations were measured using the spectrophotometric HACH method (see text). Equations give the rate of dissolution (for the fast (BSi) phase, in green; and for the slow (LSi) phase in blue; both in nmol/min) in the form y = mx + b, where m is the slope (rate) and b is the y-intercept. The value of the intercept of the blue curve equals the total BSi content. Total time for sample 915-10c was 8 h, and the regression is calculated from all values, but only the first 420 min are shown here.

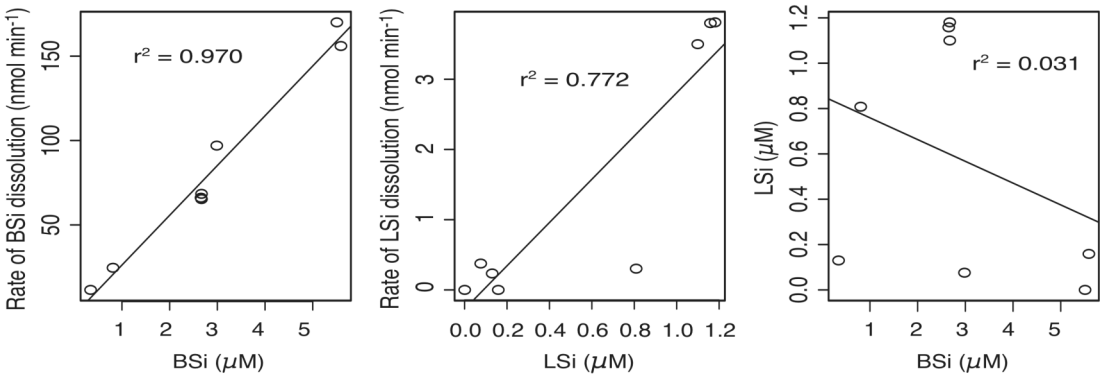

Figure A5.1.2: Correlations of dissolution rates versus extracted Si (BSi or LSi), and LSi versus BSi. Adjusted r^2 values are shown for each plot.

Table A5.1.a: Summary of BSi extraction trials. All experiments were monitored over at least 400 minutes.

Sample name	BSi (μM)	Rate of BSi dissolution (nmol min^{-1})	LSi (μM)	Rate of LSi dissolution (nmol min^{-1})
814-15	0.343	12	0.13	0.234
902-5	5.51	170	0	0
902-15	5.59	160	0.159	0
905-0	0.808	25	0.808	0.303
915-10a	2.67	65	1.18	3.8
915-10b	2.67	68	1.1	3.5
915-10c	2.66	66.1	1.16	3.8
915-15	2.99	97	0.076	0.376

Several additional trials of this type were done, for time periods up to 350 min to establish if any differences in rates of dissolution were present for high or low BSi content, and if the BSi:LSi ratio varied between samples or was constant. Results and summary of these trials are shown in Figure A5.1.2 and Table A5.1.1, respectively. From these it can be seen that the rate of BSi dissolution is positively correlated with total BSi (r^2 = 0.97), which could be expected as increasing one of the reactants will increase the rate of product formation provided the NaOH is available in excess. The same was true for the rate of LSi dissolution being a function of LSi content, although this relationship was weaker (r^2 = 0.77), possibly due to the lower LSi contents being near the resolution limit of the method. Total lithogenic content was not correlated with BSi, and thus the BSi:LSi is not constant

in this environment. This means that a simple correction for average LSi content per BSi, as was applicable for the study by Ragueneau & Tréguer (1994), was not applicable here.

This type of extraction is time- and labour-intensive, leading Ragueneau *et al*. (2005) to develop a method that uses only two sampling points, and is able to account for varying BSi:LSi ratios. A first extraction is done such that BSi will be completely dissolved, but minimising the amount of LSi that is also broken down. The extract solution is removed in full, and filters are then rinsed and dried to remove all remaining traces of BSi. A second extraction is performed which extracts only LSi. Si and Al are then analysed for both fractions, and the ratio of Al:Si in the lithogenic fraction of each sample is used to calculate the contribution from LSi in the first extraction of that sample, as Al from biogenic sources can be assumed to be negligible compared to the LSi fraction. Ragueneau *et al*. (2005) used extraction times of 40 min, but the trials done here showed that full dissolution of the biogenic fraction of Si was not always complete after 40 min, likely due to the higher [BSi] present in this study (Figure A5.1.1). For Ryder Bay samples with the highest suspended particulate matter concentrations, BSi was completely dissolved after 45.7 min, and 60 min was chosen to ensure complete dissolution.

At concentrations above ~50 ppm (1.4 mM), Si may be lost due to the formation of secondary precipitates. As the method of Ragueneau *et al*. (2005) uses 4 mL of NaOH, this was increased for certain samples in this study to prevent oversaturation due to the greater amounts of BSi present in surface waters. In samples with high chl *a* or SPM where extractions were anticipated to result in solutions of 1 mM Si or above, the volume was adjusted to 8 or 10 mL to avoid any Si loss through precipitation.

After extraction, the samples were centrifuged for 10 min at 2500 rpm and 2 mL of supernatant were removed for [Si] determination. The filters were then rinsed three times according to Ragueneau *et al*. (2005) and dried at 85 °C in a clean air supply. A second extraction was performed on the dried sample in the same manner in order to obtain an Al:Si ratio for lithogenic contamination.

Supernatants from the first and second extractions were analysed for [Si] and [Al] using the inductively coupled plasma optical emission spectrometer (ICP-OES;

see section A5.1.1.2). As BSi was fully dissolved after the first extraction (Figure A5.1.1), the second extraction was used to obtain Si:Al ratios ($Si:Al_2$) of any contaminating lithogenic material. Aluminium concentrations in the first extraction ($[Al]_1$) were assumed to come from lithogenic material, and $Si:Al_2$ was used to calculate the associated contribution of Si from lithogenic contamination (LSi_1) in the first extraction according to the equation:

$$LSi_1 = [Al]_1 \times (Si:Al_2) \quad (2)$$

For most samples the $Si:Al_2$ ratio was ~5.6 μmol:nmol, therefore any samples where $Si:Al_2$ exceeded 8 μmol:nmol were subjected to a third extraction to ensure that high Si:Al due to biogenic material remaining after the first extraction could be accounted for.

A5.1.2 Extracted Si and Al determination by ICP-OES

Concentrations of dissolved Si and Al were determined using a Varian VISTA Pro ICP–OES (Axial) in the School of Geosciences, University of Edinburgh (UK). The supernatants from wet-alkaline extractions were diluted to a final volume of 10 mL, acidified with 2% sub-boiled Aristar-grade HNO_3, and internal standards of In, Bi, Sc and Y added at concentrations of 10 ppm. Standards were prepared using serial dilutions of 1000 ppm solutions of Si, Al, Fe and Mn at the concentrations listed in Table A5.1.2, and additions of acid and internal standards were made as for samples. A background solution of NaOH plus HCl was added to each standard to mimic the concentrations of NaOH and HCl used in the extraction and neutralisation steps, to eliminate any matrix effects from the high Na content. Samples were run using an AutoAnalyser and 5 replicate peak measurements for each element. Regression of the standard calibration curves were highly linear, with r^2 values above 0.95 for each element measured. All BSi results are presented in μM: μmol particulate Si extracted per L of seawater filtered.

Table A5.1.2: Concentrations of Si and metals in standards used for ICP-OES analysis. Low-Si standards were used for the second (primarily lithogenic) extraction, while high-Si standards were needed for the much greater Si concentrations in the first (primarily biogenic) extraction. All standards had internal standards (In, Bi, Sc, Y), a background solution and acid (HNO_3) added at the same concentrations as in the samples.

Standard	Si (ppm)	Al (ppm)	Fe (ppm)	Mn (ppm)
Low-Si1	0.01	0.01	0.01	0.01
Low-Si2	0.1	0.1	0.1	0.1
Low-Si3	1	0.3	0.3	0.3
Low-Si4	1.8	0.6	0.6	0.6
High-Si1	1	0.01	0.01	0.01
High-Si2	5	0.1	0.1	0.1
High-Si3	10	0.3	0.3	0.3
High-Si4	15	0.6	0.6	0.6

Appendix A5.2: Dissolved Si concentrations – Dataset comparison

As part of the RaTS programme, [Si_d] is monitored at 15 m in Ryder Bay throughout the year. These records (courtesy of BAS, Cambridge UK) are shown in Figure A5.2.1, and display considerable sample-to-sample variability on top of a typical pattern of seasonal drawdown during austral summer. While longer-term records are provided for context (2004-2010), this discussion focuses on detailed analysis of the 2008 and 2009 seasons only (Figure A5.2.1b), when additional records are available for comparison.

Concentrations in winter 2008 averaged 51.8 μM, and the following summer (summer 2008) average concentration was 44.2 μM. Concentrations were initially very low (<30 μM), but display high variability with no observable trend, such that very little overall drawdown occurred (average drawdown for the 2008 growing seasons ~ -0.078 μM d^{-1}, *i.e.* a slight overall *increase* throughout the summer), consistent with very low biological activity suggested by low chlorophyll concentrations (*see* Chapter 2). Concentrations in winter 2009 averaged 60.9 μM, with a trend of decreasing concentration apparent in summer 2009. The calculated average drawdown for the summer 2009 season is ~0.118 μM d^{-1}, although this does not include the peak in Si_d in late October, which would give a much greater value of ~0.280 μM d^{-1}, in both cases significantly different to the lack of trend in summer 2008. Additionally, the data from both seasons indicate considerable variability around the trends, suggesting alternating periods of drawdown and resupply resulting in cumulative inputs and use much greater than reflected by the seasonal averages alone.

For both seasons (2008 and 2009), there is a poor match between data from long-term monitoring and the concentrations measured in this study. It is suggested here that differences may be due to handling and transport of samples, which in the case of long-term (BAS) records involves freezing of samples. If freezing is

relatively slow, [Si_d] in the remaining liquid can increase, and at high concentrations Si precipitates will form, which will not be redissolved by normal analysis methods.

Samples collected for this study in summer 2009 displayed relatively gradual changes in concentration over the time-series, in contrast to records from 2008 and the long-term monitoring programme data. These gradual changes, and the good agreement with Si collected for isotopic analysis by precipitation suggest that these data are robust. For 2008, both data sets showed considerable intersample variations, although these variations were not consistent between the data sets. In addition, the Si yield for isotopic analysis was in some cases greater than that predicted from the concentration measurement, indicating that the [Si_d] was erroneously low, as would result from freezing. As such, it is likely that some of the 2008 samples for [Si_d] were unintentionally frozen at some point during storage or transport. In chapter 5, these samples have been excluded from the data set, and only samples where both datasets agreed within 10% are displayed. The disagreement between the two data sets is consistent with only some samples being affected by slow freezing.

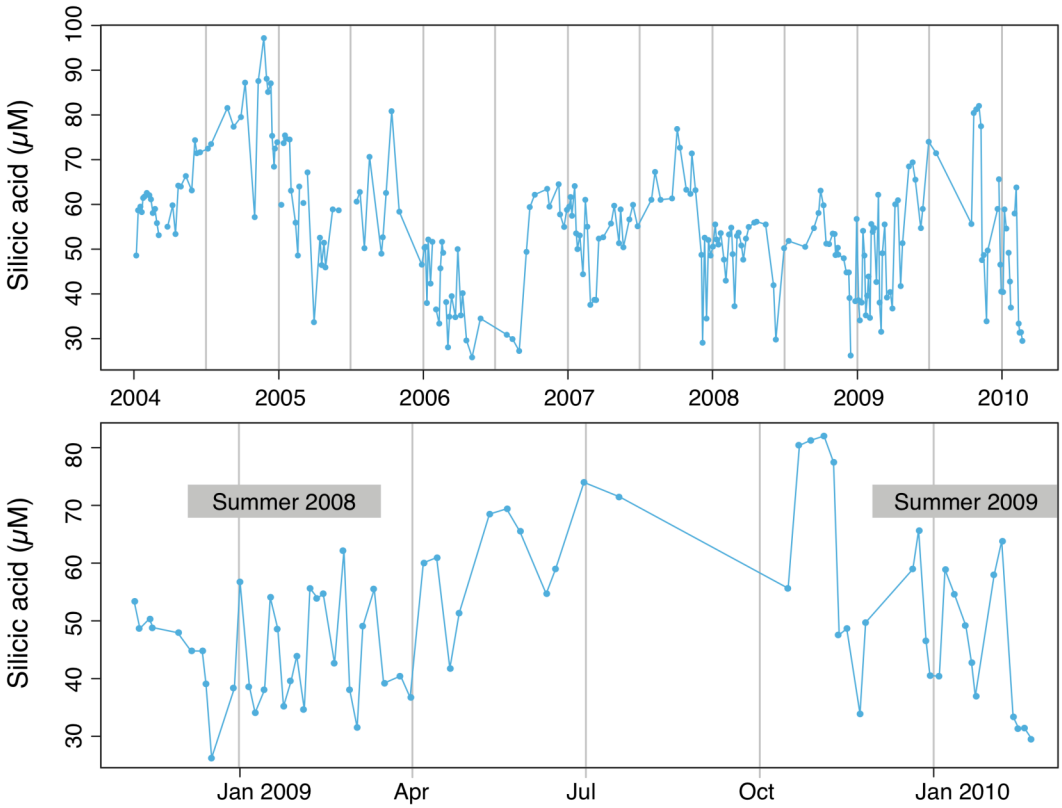

Figure A5.2.1: BAS Sid data for 6 years (2004 – 2010 top) and 2008-2010 only (bottom).

Given the lack of correlation between [Si_d], between both data sets and with $\delta^{30}Si_d$ in 2008, we cannot rule out that control of $\delta^{30}Si_d$ was subject to different processes in 2008, indicating that at times $\delta^{30}Si_d$ does not reflect [Si_d]. This would be interesting in terms of what it might mean for the processes involved and remains a possibility that cannot be ruled out, although given the obvious uncertainty in [Si_d] analysis that year, this is not the most probable explanation. While the analysis here suggests that BAS monitoring data are more robust in 2008, due to the relatively high intersample variability and irregular agreement with the data set from this study, analysis of Si cycling and isotopic variation is restricted to the more reliable 2009 data.

Table A5.2.1: Concentrations and trends in concentrations of silicic acid at the RaTS site during the study period. Both the BAS data set and results from this study are shown. Samples were only collected for this study during the summer growing season, therefore winter values are denoted by "no data" (nd) and winter to summer trends are not available (na). The average [Si_d] for summer 2009 includes samples through 18/3/10, but BAS data is only available through 22/2/10. Only the period for which both data sets are complete was used for the calculation of drawdown trends, to allow comparison between the two sets of data.

	BAS data	This study	
Average [Si_d]			
Winter 2008	58.1	nd	
Summer 2008	44.2 ± 9.4	54.9 ± 5.1	4/12/08 – 16/3/09
Winter 2009	60.9	nd	
Summer 2009	46.0 ± 12	45.2 ± 4.6	2/12/09 – 18/3/10
Slope (drawdown)			Dates
Summer 2008	-0.0781	0.147	4/12/08 – 16/3/09
r^2	0.064	0.643	
Summer 2009	0.118	0.112	2/12/09 – 22/2/10
r^2	0.0894	0.454	
Including winter 2008	-0.0684	na	13/9/08 – 30/3/09
r^2	0.171		
Including winter 2009	0.2796	na	22/10/09 – 22/2/10
r^2	0.4305		

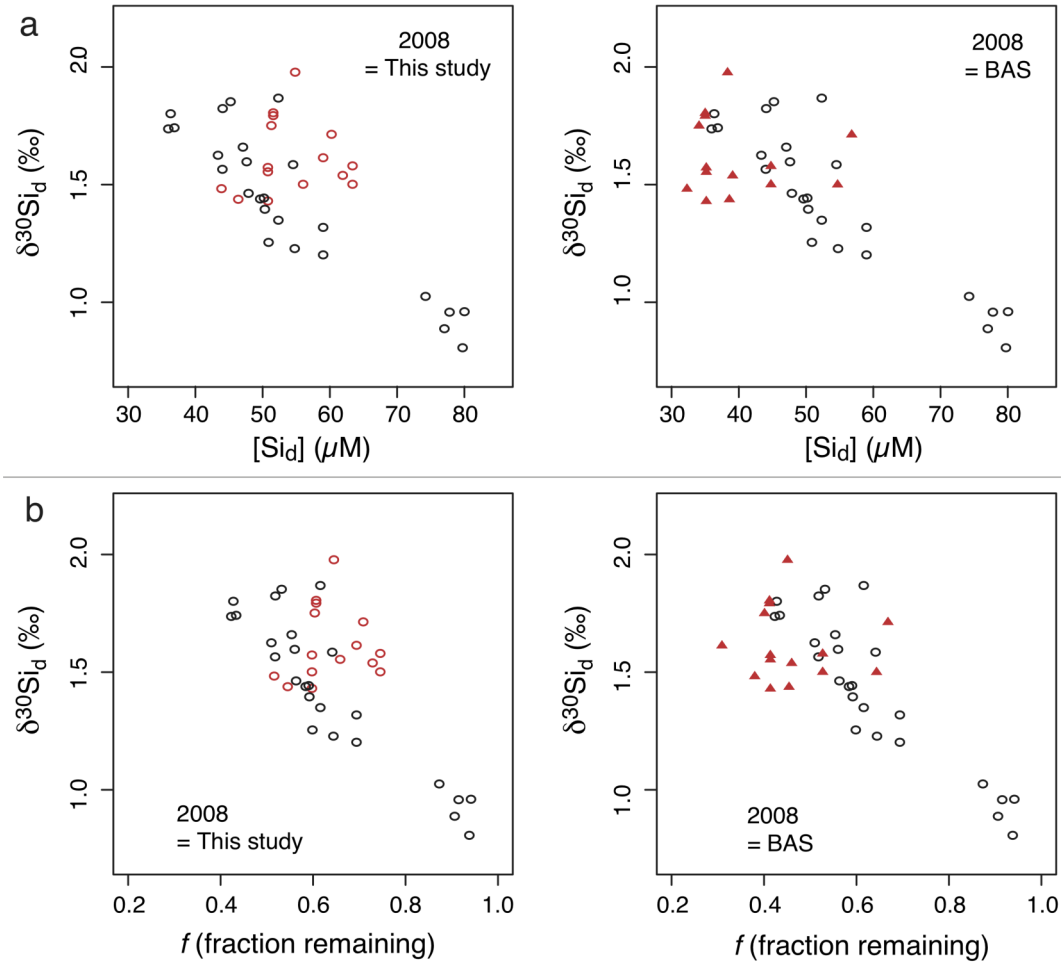

Figure A5.2.2: (a) $\delta^{30}Si_d$ versus $[Si_d]$ for both data sets, and (b) $\delta^{30}Si_d$ versus f for both data sets. In all plots, 2009 data is shown in black. Data from 2008 from this study is shown as red circles, while data from the RaTS programme for 2008 is shown as red triangles. The small range of values in 2008 result in no overall trend in the data, and both datasets show outliers compared to the 2009 data.

Appendix A6.1: Published manuscript "Use of radium isotopes to estimate mixing rates and trace sediment inputs to surface waters in northern Marguerite Bay (Antarctic Peninsula)"

Source: Annett, A.L., S.F Henley, P. van Beek, M. Souhaut, R. Ganeshram, H.J. Venables, M.P. Meredith, W. Geibert. (2012) Use of radium isotopes to estimate mixing rates and trace sediment inputs to surface waters in northern Marguerite Bay, Antarctic Peninsula. *Antarctic Science*. doi:10.1017/S0954102012000892. Published by Cambridge University Press.

Antarctic Science page 1 of 12 *(2012)* © Antarctic Science Ltd 2012 doi:10.1017/S0954102012000892

Use of radium isotopes to estimate mixing rates and trace sediment inputs to surface waters in northern Marguerite Bay, Antarctic Peninsula

AMBER L. ANNETT[1], SIAN F. HENLEY[1], PIETER VAN BEEK[2], MARC SOUHAUT[2], RAJA GANESHRAM[1], HUGH J. VENABLES[3], MICHAEL P. MEREDITH[3] and WALTER GEIBERT[1,4]

[1]*School of GeoSciences, University of Edinburgh, Edinburgh EH9 3JW, UK*
[2]*Laboratoire d'Etudes en Geophysique et Oceanographie Spatiales (CNRS/UPS/IRD/CNES), Observatoire Midi Pyrénées, Toulouse, France*
[3]*British Antarctic Survey, NERC, High Cross, Madingley Road, Cambridge CB3 0ET, UK*
[4]*Scottish Association for Marine Science (SAMS), Scottish Marine Institute, Oban, UK*
amber.annett@ed.ac.uk

Abstract: In the western Antarctic Peninsula region, micronutrient injection facilitates strong plankton blooms that support productive food webs, unlike large areas of the low-productivity Southern Ocean. We use naturally occurring radioisotopes of radium to constrain rates of chemical fluxes into Ryder Bay (a small coastal embayment in northern Marguerite Bay), and hence to evaluate possible sources of sediment-derived micronutrients and estimate sediment-ocean mixing rates. We present the first coupled, short-lived radium isotope (^{223}Ra and ^{224}Ra) measurements from Antarctic waters, both present at very low activities (mean 0.155 and 3.21 dpm m^{-3}, respectively), indicating much lower radium inputs than in other coastal environments. Longer-lived ^{228}Ra activity was also lower than existing nearshore values, but higher than open ocean waters, indicating some degree of coastal radium input on timescales exceeding the week-to-month range reflected by ^{223}Ra and ^{224}Ra. Using a simple diffusion model along a shore to mid-bay transect, effective horizontal eddy diffusivity estimates ranged from 0.22–0.83 m^2 s^{-1} from ^{223}Ra and ^{224}Ra, respectively, much lower than already-low mixing estimates for the Southern Ocean. Significant radium enrichment and much faster mixing (18 m^2 s^{-1}) was found near a marine-terminating glacier and consequently any sediment-derived micronutrient inputs in this location are more probably dominated by glacial processes than groundwater, land runoff, or marine sediment sources.

Received 28 April 2012, accepted 13 August 2012

Key words: actinium-227, glacial inputs, horizontal eddy diffusivity, land-ocean interface, Radium Delayed Coincidence Counter (RaDeCC), Ryder Bay

Introduction

The western Antarctic Peninsula (WAP), a region of high phytoplankton production supporting a large and productive food web, is currently undergoing the most pronounced recent rapid regional warming in the southern hemisphere (Vaughan *et al*. 2003). Average air temperature on the WAP has increased at a rate of 3.6 ± 1.4°C per century, several times the global average (Vaughan *et al*. 2003). The majority of glaciers in the region are retreating, and the rate of this retreat is accelerating (Cook *et al*. 2005). At sea, an increase of > 1°C has been recorded in the surface waters in summer, decreasing to near zero at 100 m depth (Meredith & King 2005). There has also been a significant reduction in sea ice duration, with trends of later advance and earlier retreat in the Marguerite Bay area (Stammerjohn *et al*. 2008).

Unique in its proximity to the Antarctic Circumpolar Current (ACC), the WAP is subject to frequent incursions of Circumpolar Deep Water (CDW), which transports heat, salt and nutrients (Klinck 1998) onto the shelf, thereby influencing water mass properties and productivity along the WAP. Martinson *et al*. (2008) showed increasing trends in ocean heat content over the shelf, consistent with an increase in frequency of CDW incursions, believed to be at least partially driven by changes in atmospheric circulation (Martinson *et al*. 2008, Meredith *et al*. 2010). The observed changes in glacial retreat are also consistent with warmer waters, as it has been shown that the temperature of marine waters can significantly impact the melt rates of marine-terminating glaciers (Pritchard *et al*. 2012).

From a biological perspective, a key influence on primary productivity along the WAP is stratification, as a more stable water column provides higher average light levels to cells in near-surface waters, thus encouraging phytoplankton growth (Venables *et al*. in press). Changes in freshwater inputs, heat content, and the associated changes in sea ice cover can affect stratification, and

therefore productivity in this region. Indeed, phytoplankton dynamics already show changes linked to sea ice cover and stratification in both the northern and southern regions of the WAP (Montes-Hugo *et al.* 2009). In addition to light, growth of phytoplankton in Southern Ocean waters can be further limited by availability of micronutrients, primarily iron (Hoffmann *et al.* 2008). Freshwater inputs (surface runoff, glacial meltwater and groundwater) are clearly important to biological production due to their role in stratification, but are also a potential source of micronutrients such as iron (Raiswell 2011), an element known to limit phytoplankton productivity in large regions of the Southern Ocean.

To address these topics, radium (Ra) in seawater was measured at a coastal Antarctic site at the WAP. Radium is produced continuously in both continental and deep sea sediments by the decay of the particle reactive element thorium (Th). Radium occurs naturally in seawater as four radioisotopes: the short-lived isotopes ^{223}Ra and ^{224}Ra (half-life ($t_{1/2}$) = 11.435 days and $t_{1/2}$ = 3.66 days, respectively), and the long-lived ^{226}Ra and ^{228}Ra ($t_{1/2}$ = 1600 years and $t_{1/2}$ = 5.75 years, respectively). Radium Delayed Coincidence Counting (RaDeCC), a radon (Rn) detection system proposed for use with Ra isotopes by Moore & Arnold (1996), allows measurement of ^{223}Ra and ^{224}Ra in the field, as well as activity of progenitor radionuclides (actinium (^{227}Ac) and $^{224}Ra_{supported}$ (= ^{228}Th), respectively) following the decay of the short-lived isotopes.

The information obtained by RaDeCC analysis covers isotopes of different half-lives, as well as of different sources. The concentration of Ra isotopes is highest at sediment margins due to the Th source, and decreases away from these margins due to dilution and radioactive decay. In the case of ^{227}Ac, the dominant source is deep water, open ocean sediments, where low sediment accumulation rates and deep overlying water columns lead to higher accumulation of the parent isotope than in shallow shelf settings (Geibert *et al.* 2002). The different sources and decay rates can be exploited to detect and differentiate multiple inputs (e.g. for different groundwater reservoirs) as well as to estimate rates of the processes affecting these inputs on different timescales. In the last two decades, the short-lived isotopes of Ra have been used in the Southern Ocean to investigate coastal mixing rates and eddy diffusivity coefficients (Charette *et al.* 2007), water mass pathways (van Beek *et al.* 2008), iron inputs (Dulaiova *et al.* 2009) and terrigenous material from icebergs (Shaw *et al.* 2011).

The aim of this study was to use Ra isotopes to further constrain the sources of surface water in Ryder Bay and the extent to which they interact with sediments, while establishing a baseline against which any future change in Ra distributions may be interpreted. These Ra radioisotopic data are the most southerly (67°34.02'S) reported to date. The relative importance of surface water sources, marine and glacial sediment interaction, and the timescales on which mixing processes occur will aid in understanding not only oceanographic processes and local circulation patterns, but also trace metal availability in a region of very rapid change (Wallace *et al.* 2008, Meredith *et al.* 2010).

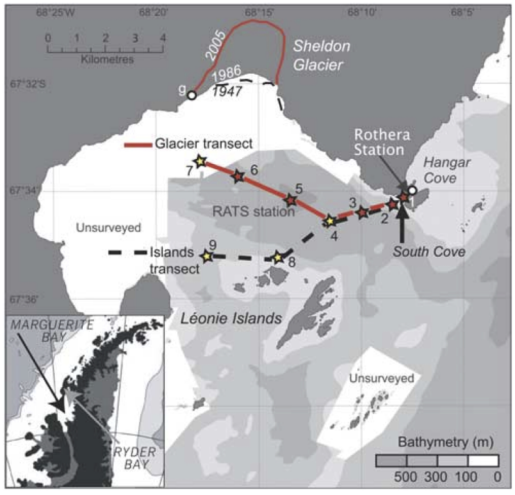

Fig. 1. Station numbers and locations in Ryder Bay. Red stations sampled 13–14 February, yellow stations sampled 25 February. Maximum depth is 520 m (at station 5, which is also the Rothera Oceanographic and Biological Time Series monitoring site). Station 1 is within South Cove, and is adjacent to the British Antarctic Survey's Rothera Research Station. Also shown is the edge of Sheldon Glacier, and the point used for glacially-derived mixing rates (denoted by "g").

Background

Study site and oceanographic context

Ryder Bay is a shallow (maximum *c.* 500 m) coastal embayment at the northern end of Marguerite Bay (Adelaide Island; Fig. 1), and is subject to processes that influence physical and biogeochemical conditions along the coastal WAP region (e.g. seasonal ice cover, glacial inputs). Largely representative of Marguerite Bay (Clarke *et al.* 2008), it is the site of the Rothera Oceanographic and Biological Time Series (RaTS) programme conducted by the British Antarctic Survey at nearby Rothera Research Station. This programme has monitored water column conditions and biological activity year-round in Ryder Bay since 1997 (Clarke *et al.* 2008). The accessibility of the RaTS site and long-term environmental dataset make this an ideal location for investigating mixing rates and sediment interaction in coastal WAP waters, in the context of understanding cycling of glacial- and marine sediment-derived micronutrients.

The oceanography of the Marguerite Bay region, and the WAP more broadly, differs from other Antarctic shelf regions in its large fluxes of glacial meltwater from land and proximity to the ACC (Clarke *et al*. 2008). In Ryder Bay, use of oxygen isotopes has identified meteoric (glacial and snow) water as the dominant source of the freshwater inputs to Antarctic Surface Water (AASW) during summer, as opposed to melting sea ice (Meredith *et al*. 2010). The contribution of this meteoric water to the surface mixed layer varies annually, but is typically 2–6%, compared with maximum 2% sea ice meltwater (Meredith *et al*. 2010). As such, the glacial influence in Ryder Bay surface waters is likely to be near the upper limit of the range relevant to the WAP (Clarke *et al*. 2008, and references therein).

Water masses along the WAP, as well as in Marguerite Bay and Ryder Bay, are well described (e.g. Clarke *et al*. 2008, Meredith *et al*. 2010). Briefly, the dominant water mass at depth derives from warm (>1.0°C), high-nutrient CDW, which intrudes onto the continental shelf in relatively unmodified form (Martinson *et al*. 2008) due to the local absence of an Antarctic Slope Front (Klinck 1998). While CDW can be divided into upper (UCDW) and lower (LCDW) water masses, LCDW is present only in deep troughs (Moffat *et al*. 2008) and it is UCDW that dominates above the continental shelf. Upward mixing of UCDW provides heat and macronutrients to the near-surface layers, and studies indicate that this mixing occurs primarily in coastal and shallow regions (Howard *et al*. 2004, Wallace *et al*. 2008). Above the UCDW, surface waters cool and gain salt during sea ice formation in autumn and winter, resulting in a seasonally deep mixed layer. The remnant of this persists into summer as a temperature minimum layer at depths around 100 m, termed winter water (WW). During summer, this WW layer is capped at the surface by lighter waters that have been warmed by insolation and freshened by meltwater, producing AASW.

Methods

Sample collection and processing

Samples for RaDeCC analysis were collected from a small boat using a 12 V impeller pump attached to acid-cleaned (10% HCl) silicon tubing. The tubing was rinsed with at least 25 l of seawater before collecting an appropriate volume (110–180 l) of seawater from 10 m depth into clean 20 l containers. Five samples were collected on 13 and 14 February 2010, along a transect from shore to the RaTS site, which is located *c.* 2 km from shore in Ryder Bay (station 5; Fig. 1). Mixing rates derived from RaDeCC measurements along this line were used to assess the potential of sediment-derived nutrient sources for near-surface productivity at this site. Following this transect, four additional samples were collected on 25 February 2010, in order to investigate potential input signals from nearby islands and Sheldon Glacier. Sampling transects are shown in Fig. 1.

Samples were slowly (*c.* 200 ml min^{-1}; van Beek *et al*. 2008) passed through a column filled with *c.* 20 g loosely-packed MnO_2-impregnated acrylic fibre, which quantitatively adsorbs Ra from seawater (97% extraction for samples up to 400 l; Moore 2008). The Mn-fibre was then rinsed with Milli-Q water (Millipore systems) to remove salts and particles. Excess water was removed by squeezing, and a moisture to fibre ratio of 0.3–1 g_{H2O}:g_{fibre} was maintained in order to maximize movement of Rn from the columns to the counting chambers.

Columns were then introduced into the RaDeCC system, following full sample preparation and processing procedures as described by Moore (2008). Counting was performed for as long as possible whilst still allowing all samples from a single sampling event to be analysed within a two day period. Counting time averaged 1000 min per sample, and in all cases exceeded 400 min.

Raw counts were corrected as described by Garcia-Solsona *et al*. (2008) and Moore (2008), and converted to ^{223}Ra and ^{224}Ra activities in decays per minute (dpm) using the efficiencies measured for each scintillation chamber (*c.* 0.35 and 0.60, respectively). Detector efficiency was monitored using standards obtained from the International Atomic Energy Agency (Monte Carlo, Monaco) and prepared at LEGOS, OMP (Toulouse, France), according to published methods (Dimova *et al*. 2008, Moore 2008, Scholten *et al*. 2010). Standards were measured several times throughout the duration of the study to monitor detector efficiency. Problems have been reported with decay of ^{227}Ac standards (≤ 12%; Scholten *et al*. 2010) in the first *c.* 50 days after preparation, although we were unable to assess this for our standards due to the timing of preparation and measurement. As this would affect only absolute (not relative) activities and are within the error reported here, this effect is not considered further.

All samples were measured at least four times in order to correct for interference from longer-lived Ra isotopes. Initial counting was done as soon after collection as possible, and samples were re-counted after 8, 21, and >90 days to correct for interference from ^{224}Ra, ^{224}Ra supported by ^{228}Th, and ^{227}Ac, respectively.

Estimation of error followed the equations of Garcia-Solsona *et al*. (2008), with minor changes to the error propagation in correcting for long-lived isotopes. In our case, the third and fourth counts were used to estimate ^{228}Th and ^{277}Ac, respectively. Interference from these sources was assumed to be constant and therefore not corrected for time since sample collection. Ingrowth of ^{228}Th from ^{228}Ra was not accounted for, as this contributed <1% of ^{228}Th in all cases. These long-lived interferences

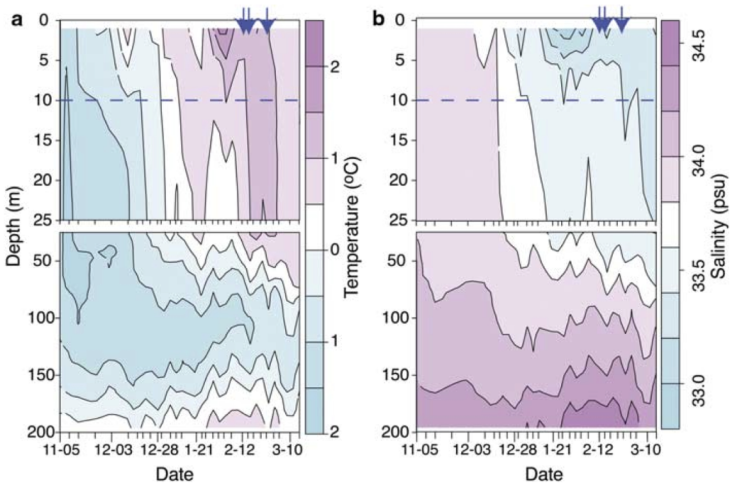

Fig. 2. a. Temperature, and **b.** salinity at station 5 (Rothera Oceanographic and Biological Time Series monitoring site). The top 25 m is expanded in the top plots. Arrows show dates of sampling, and dashed line marks sampling depth (10 m). Data courtesy of BAS.

were subtracted from the time-corrected first counts according to the formula:

$$A_{ex} = A_1 \cdot e^{-\lambda t} - A_{3/4}, \quad (1)$$

where A_{ex} is the excess activity (at the time of collection), A_1 is the activity measured in the first count, $A_{3/4}$ is the activity measured during the third or fourth count, λ is the decay constant of ^{223}Ra or ^{224}Ra, and t is the time between collection and the first count. Error combination followed the standard formula:

$$\Delta A_{ex}^2 = (\Delta A_1 \cdot e^{-\lambda t})^2 + \Delta A_{3/4}^2, \quad (2)$$

where Δ denotes the absolute error of each term. Note that reported ^{227}Ac has not been corrected for activity supported by ^{231}Pa. Assuming ^{231}Pa to be *c.* 0.1 dpm m^{-3} (determined by Geibert *et al.* (2002) for surface waters south of the Antarctic Polar Front), the corrected $^{227}Ac_{ex}$ would be 0.1 dpm m^{-3} less than the numbers shown here.

Gamma counting

Once the analyses using RaDeCC were performed, the Mn-fibres were ashed (16 h at 820°C) and transferred into sealed vials for gamma counting, following Charette *et al.* (2001). Radium isotopes adsorbed on MnO_2 ash were analysed using low-background gamma-ray spectrometry at the underground laboratory of Ferrières (LAFARA, LAboratoire de mesure des FAibles RAdioactivités) located in the French Pyrénées, 100 km from Toulouse (van Beek *et al.* 2010, van Beek *et al.* in press). Radium-228 activities were determined using the 338, 911 and 969 keV peaks of ^{228}Ac. Uncertainties reported for ^{228}Ra activities are errors due to counting statistics (one standard deviation).

Results

Oceanographic context

Seasonal records of water column conditions are available for station 5 (the RaTS Site) as part of the

Table I. Station details and short-lived radium activities from Radium Delayed Coincidence Counter (RaDeCC) analysis. As sample collection occurred on two occasions, station superscript "b" denotes samples from the second sampling event. Distances given are to the nearest shoreline for each individual station. For glacial stations, distances are given to a point on the edge of Sheldon Glacier (denoted in the table by *, location shown on Fig. 1).

Station	Latitude	Longitude	Water column depth (m)	Distance (km)	Sample volume (l)	$^{223}Ra_{ex}$ (dpm m^{-3})	$^{224}Ra_{ex}$ (dpm m^{-3})
1	-67.569	-68.133	15	0.01	163.7	0.643 ± 0.35	14.6 ± 0.84
2	-67.570	-68.137	100	0.28	153.7	0.248 ± 0.23	2.95 ± 0.43
3	-67.573	-68.167	400	0.90	168.6	0.039 ± 0.14	1.12 ± 0.22
4^b	-67.575	-68.190	450	1.70	109.7	bdl	0.762 ± 0.26
5	-67.567	-68.234	520	2.00	125.1	0.006 ± 0.16	0.463 ± 0.19
6	-67.562	-68.267	320	*5.55	177.0	bdl	4.48 ± 0.58
7^b	-67.557	-68.297	300	*4.25	113.4	0.277 ± 0.25	2.13 ± 0.44
8^b	-67.589	-68.258	150	5.50	107.0	0.209 ± 0.31	2.33 ± 0.55
9^b	-67.583	-68.300	160	1.80	114.1	0.204 ± 0.16	0.066 ± 0.223

bdl = below detection limit.

Table II. Progenitor isotope activities from Radium Delayed Coincidence Counter (RaDeCC) analysis (^{228}Th and ^{227}Ac) and gamma spectroscopy (^{228}Ra). Also shown are ratios of ^{228}Ra:^{227}Ac. As in Table I, station superscript "b" denotes samples from the second sampling event. All activities are given in dpm m^{-3}.

Station	^{228}Th	^{227}Ac	^{228}Ra	^{228}Ra:^{227}Ac
1	3.40 ± 0.26	0.271 ± 0.14	22.4 ± 1.4	82 ± 47
2	2.69 ± 0.25	0.400 ± 0.14	13.0 ± 0.95	33 ± 14
3	bdl	0.338 ± 0.12	19.2 ± 1.3	57 ± 24
4^{b}	0.430 ± 0.12	0.378 ± 0.19	17.5 ± 1.3	46 ± 27
5	0.776 ± 0.14	0.383 ± 0.15	19.8 ± 1.5	52 ± 24
6	3.02 ± 0.28	0.052 ± 0.072	39.5 ± 2.1	760 ± 1090
7^{b}	1.83 ± 0.26	0.897 ± 0.22	17.1 ± 1.3	19 ± 6
8^{b}	2.59 ± 0.28	0.437 ± 0.20	16.8 ± 1.6	38 ± 21
9^{b}	0.764 ± 0.14	0.059 ± 0.10	13.0 ± 1.2	220 ± 400

bdl = below detection limit.

RaTS monitoring programme (British Antarctic Survey, Cambridge, UK). Upper layer temperature and salinity data indicate a typical seasonal progression from well-mixed wintertime waters in November (with temperatures < 0°C and comparatively high salinity) to more stratified summer conditions characterized by warmer surface waters (> 1°C) and significant freshening due to meltwater input (salinity as low as *c.* 33.1; Fig. 2). Beneath the summertime surface layer, the WW layer is apparent as a temperature minimum at *c.* 100 m depth, with properties largely dictated by those of the previous winter mixed layer.

From these temperature and salinity records, it can be seen that physical conditions between the two sampling events were very similar, implying that no significant upwelling or mixing events occurred (such as might be expected during, for example, strong weather events), and that any lateral advection occurred within a relatively uniform water mass. We therefore interpret stations from both transects on the assumption that differences chiefly reflect steady-state diffusive and advective processes.

Short-lived isotopes

Activity of ^{223}Ra$_{ex}$ (below detection limit (bdl)–0.649 dpm m^{-3}) is considerably lower than that of ^{224}Ra$_{ex}$ (0.066–14.6 dpm m^{-3}), although both isotopes show very similar trends (Table I). Very low activities were found in the central, deep area of Ryder Bay (stations 3, 4 and 5; depth > 300 m; hereafter "mid-bay"), on average 0.023 and 0.076 dpm m^{-3} for ^{223}Ra$_{ex}$ and ^{224}Ra$_{ex}$, respectively. The most pronounced enrichment is seen at station 1, nearest the shore (in South Cove, alongside Rothera Station) and in shallowest water depth (< 30 m). This high activity decreases with distance from the shore, through stations 1–5. An enrichment is also seen in the sample nearest the Léonie Islands group (station 8), which is sustained in ^{223}Ra$_{ex}$ at station 9, but not in ^{224}Ra$_{ex}$. The two samples taken from nearer to Sheldon Glacier (stations 6 and 7) exhibit higher activities of ^{224}Ra$_{ex}$ relative to mid-bay samples. This enrichment is also seen in ^{223}Ra$_{ex}$ at station 7, although station 6 ^{223}Ra$_{ex}$ was below detection limits.

Many of the values reported here, especially those from central Ryder Bay, are below the detection limits estimated by Moore (2008) for RaDeCC analysis (0.2 and 0.5 total collected dpm for ^{223}Ra and ^{224}Ra, respectively). However, the background activity measured with our RaDeCC system was much lower than all samples analysed (mean 3% and 9% of raw counts for 219 and 220 channels, respectively) and reproducibility was good (*c.* 20% standard deviation for three consecutive readings). Furthermore, samples from similar areas display much less variation than the error of individual samples (see Discussion). Therefore we consider our results above the detection limit of RaDeCC analysis, except in the three cases noted in Table I.

Parent isotopes

The average activity of ^{227}Ac is lower than that of ^{228}Th (^{227}Ac: 0.052–0.897 dpm m^{-3}; ^{228}Th: bdl–3.40 dpm m^{-3}; Table II), in keeping with the relationship between the daughter nuclides (^{223}Ra$_{ex} < ^{224}$Ra$_{ex}$). The spatial distribution of ^{228}Th is similar to that of ^{223}Ra$_{ex}$ and ^{224}Ra$_{ex}$, with marked enrichment near Rothera station (South Cove, stations 1 and 2) and nearest the islands (station 8). As with ^{224}Ra$_{ex}$, the increase in ^{228}Th near station 8 is not seen at station 9, slightly further from land and in deeper water.

The distribution of ^{227}Ac shows very different trends from the short-lived Ra isotopes. The highest activity reported (0.897 ± 0.217 dpm m^{-3}) is at station 7, nearest Sheldon Glacier, with all other stations displaying less than half of this value. Excluding station 7, the trends of ^{227}Ac are roughly opposite to those of the Ra suite, with mid-bay stations displaying high values (0.37 ± 0.02 dpm m^{-3}), and nearshore stations (1, 2, 8, 9) having slightly lower activities of 0.29 ± 0.17 dpm m^{-3}, although these are not statistically different to mid-bay waters.

Long-lived Ra isotopes

The long-lived Ra isotope ^{228}Ra shows slightly different trends from the short-lived isotopes (Table II). Station 1 again shows enrichment, although this is minor compared with the enrichment seen in ^{223}Ra$_{ex}$, ^{224}Ra$_{ex}$ and ^{228}Th. Stations 3–5 show relatively consistent values (*c.* 17.5 dpm m^{-3}) but, in contrast to other Ra isotopes, station 2 displays lower activity than the mid-bay stations. The highest ^{228}Ra activity was measured at station 6, coincident with a peak (although not to maximum activity) of ^{228}Th.

Due to the different sources of each radioisotope, ratios such as ^{228}Ra:^{227}Ac can be helpful in distinguishing between different source waters. Station 6 shows a peak

in the ratio of ^{228}Ra:^{227}Ac (Table II). A second peak is seen at station 9, and a minimum at station 7, although these latter variations are driven by the activity of ^{227}Ac, and within error these ratios are not significantly different from the average for other stations.

Discussion

Radium sources to Ryder Bay

From the activities of $^{223}Ra_{ex}$ and $^{224}Ra_{ex}$ along both transects, we identify sources near South Cove, the Léonie Islands, and Sheldon Glacier. Station 1, with the shallowest water depth and short distance from shore, would be expected to exhibit the greatest activity, and indeed shows strong enrichment in $^{223}Ra_{ex}$, $^{224}Ra_{ex}$ and ^{228}Th.

Radium-223, in excess of that supported by decay of dissolved ^{227}Ac, is produced from the decay of ^{227}Th, which is strongly bound to sediments. Thus $^{223}Ra_{ex}$ displays a strong source along any interface (land-water or sediment-water). A clear enrichment in $^{223}Ra_{ex}$ is evident at station 1 (Table I), to values of 0.65 dpm m^{-3}. To our knowledge, these are the first coupled short-lived Ra isotope activities reported for Antarctic waters. The only published $^{223}Ra_{ex}$ activities from coastal Southern Ocean waters are 0.42–5.2 dpm m^{-3}, from waters within 2.6 km of the sub-Antarctic Iles Crozet (Charette *et al.* 2007), generally higher than the range for this study (bdl–0.65 dpm m^{-3}) but in keeping with activity in our South Cove sample. Further offshore from Iles Crozet, however, $^{223}Ra_{ex}$ dropped to 0.02–0.19 dpm m^{-3} (*c.* 12 km from shore; Charette *et al.* 2007), in close agreement with the values reported here for distances of 0.5–2 km.

As with $^{223}Ra_{ex}$, $^{224}Ra_{ex}$ shows a strong signal of enrichment from sediments due to its Th progenitor. The decay of ^{228}Ra, present mainly in the dissolved phase, produces ^{228}Ac, which quickly decays ($t_{1/2}$ = 6.15 h) to ^{228}Th. This ^{228}Th is rapidly scavenged and slowly releases ^{224}Ra from sediments. In coastal areas, ^{228}Th may also be sourced from the surrounding rock in addition to its production within the water column, and indeed this terrigenous source is much greater than the marine source. Published values for $^{224}Ra_{ex}$ range from 3.1–47 dpm m^{-3} (Iles Crozet; Charette *et al.* 2007) and 8–17 dpm m^{-3} (coastal Antarctic Peninsula surface waters; Dulaiova *et al.* 2009). Only station 1 of the Ryder Bay samples falls within this range (14.6 dpm m^{-3}), although other nearshore samples clearly show this land-interface signal.

This shore-derived signal is transported offshore, and stations 2 and 8, both at similar distances from the shoreline (South Cove and Leonie Islands, respectively) and at similar depths, display very similar activities of all nuclides measured here (Tables I & II). Station 9 also shows some enrichment in $^{223}Ra_{ex}$ relative to mid-bay samples, which does not appear in the other isotopes. This could be explained by slow mixing such that ^{224}Ra, with its shorter half-life,

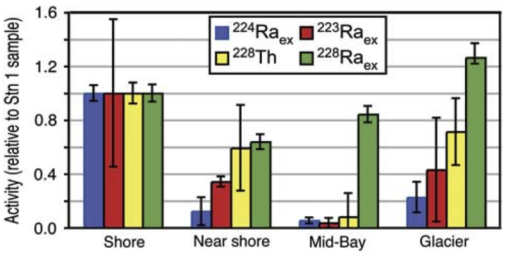

Fig. 3. Radium activities grouped by location type, and relative to the highest measured activity (in all cases at station 1 (shore), error bars show sample uncertainty). Nearshore stations: 2, 8 and 9. Mid-bay stations: 3, 4 and 5. Glacier stations: 6 and 7. Error bars on nearshore, mid-bay and glacier stations represent one standard deviation, except in the case of $^{223}Ra_{ex}$ at the glacier station where sample error is shown because only one sample was above the detection limit.

would decay more quickly than ^{223}Ra during a given period of mixing. Additionally, the difference in signal between these two isotopes may be small, as the errors on $^{223}Ra_{ex}$ are relatively large due to the much lower activity of this isotope and sampling constraints preventing the collection of larger volume samples. This signal of higher activities in the nearshore sampling locations is consistent with a Ra source from surrounding rocks, and/or production of Ra in shallow marine sediments.

Notably, there are also enrichment signals towards Sheldon Glacier which, in the case of $^{224}Ra_{ex}$, ^{228}Th and ^{228}Ra, are very high given the distance from land at these stations. Glacial flour, subglacial and/or surface meltwater flows, or sediment/seawater interaction beneath the ice shelf could all potentially act as sources for Ra enrichment near Sheldon Glacier. While we are unable to discriminate here between these processes, it is probable that the signal is at least partly derived from the glacier (and entrained terrigenous material) itself. Shaw *et al.* (2011) reported $^{224}Ra_{ex}$ activities of *c.* 1.2–9.4 dpm m^{-3} in surface waters near free-drifting icebergs in the Weddell Gyre, showing that glacial material alone can account for a highly significant $^{224}Ra_{ex}$ enrichment in the absence of any bottom sediments.

There is some variability between the activities at stations 6 and 7, although records of δ^{18}O (Meredith *et al.* in press) in water samples at the RaTS site indicate similar proportions of meteoric (glacial/snow) water in the water column on both sampling days. Thus we infer that glacial sources of Ra are highly variable, as might be expected given the potential for different processes (ice melt versus subglacial sediment-water mixing) to contribute terrigenous material, in addition to potential differences in the composition of that material. Additionally, small-scale flow filaments could contribute to different Ra activity being collected from these two stations,

Table III. Mean (range) activities for short-lived Ra isotopes ($^{223}Ra_{ex}$ and $^{224}Ra_{ex}$) and their parent isotopes (^{227}Ac and $^{228}Th/^{228}Ra$). Ranges of activities reported from similar environments are also given for comparison. All activities are given in dpm m^{-3}.

Source	Location	$^{223}Ra_{ex}$	$^{224}Ra_{ex}$	^{227}Ac	^{228}Th	^{228}Ra
This study	Ryder Bay	0.155 (bdl–0.649)	3.21 (0.066–14.6)	0.335 (0.052–0.897)	1.68 (bdl–3.40)	19.8 (13.0–39.5)
Dulaiova *et al*. 2009	Surface, coastal Antarctic Peninsula		(8–17)			(10–20)
Charette *et al*. 2007	Inshore (to 12.5 km), Iles Crozet	(0.02–5.2)	(1.4–47)			(8.9–41)
Van Beek *et al*. 2008	Surface, offshore Iles Kerguelen					(0.4–3.9)
Geibert *et al*. 2002	Surface waters, UCDW			(0.1–0.5)		
Shaw & Moore 2002	Surface, offshore South Shetland Islands			0.20		
Hanfland 2002	Surface, shelf waters Antarctic Peninsula and Weddell Sea					(2–20)
Moore 2000a[a], Moore & Arnold 1996b	Typical coastal values	22.4[a] (4.6–300)[b]	144[a] (4.9–660)[b]			

[a] From the South Atlantic Bight.
[b] From the Mississippi and Atchafalaya River mixing zones, and Tampa Bay, Florida (for samples with salinity > 27 parts per thousand).
bdl = below detection limit.

even if sediment composition were invariant. Despite this variability, the average activities at stations nearest Sheldon Glacier show a clear signal of all four Ra nuclides (Fig. 3). "Glacier" stations exhibit statistically higher $^{224}Ra_{ex}$ and ^{228}Th than mid-bay samples (3.30 dpm m^{-3} vs 0.78 dpm m^{-3}, $P = 0.0344$; 0.24 vs 0.027, $P = 0.050$; respectively, two-sample *t*-tests). The two glacier stations show very different $^{223}Ra_{ex}$ activities, consistent with high variability of glacial sources. One sample is below the detection limit, but activity nearest the glacier (0.277 dpm m^{-3}, station 7) is an order of magnitude higher than the mid-bay average of 0.023 dpm m^{-3}, indicating an intermittent but significant glacial source of $^{223}Ra_{ex}$, as with ^{224}Ra.

Trends in ^{228}Ra are also consistent with a glacial source, as station 6 displays pronounced enrichment to an activity approximately twofold higher than at station 1 (Table II). While variable, average ^{228}Ra was 28.3 dpm m^{-3} near the glacier, compared to 18.9 dpm m^{-3} in mid-bay stations, although this difference was not statistically significant ($P = 0.236$). The highly significant enrichment at station 6 leads to elevated ^{228}Ra:^{227}Ac ratios (Table II) compared to all other stations, suggestive of a distinct water source that is enriched in ^{228}Ra. This enrichment, coupled with the very low ^{227}Ac activity (produced in deep ocean sediments - see below) indicates a terrestrial source, consistent with glacial meltwater. In keeping with its much longer half-life ($t_{1/2} = 5.75$ years), the distribution of ^{228}Ra shows less variability between the different location types than the shorter-lived isotopes. Due to its long half-life, variations in ^{228}Ra activity within Ryder Bay must reflect dilutive processes, rather than decay during advection which is seen in the shorter-lived isotopes. The increase in ^{228}Ra activity near the glacier is consistent with an input of enriched water to the surface, as by a thin lens of glacial meltwater. Even a modest extent of mixing with the underlying water column would then dilute this signal due to the very small relative volume of a thin meltwater lens, in accordance with the lower values of ^{228}Ra in mid-bay stations.

Deep water renewal

Activities of the short-lived isotopes of Ra and their progenitors are low compared to many coastal areas (Table III). Few studies have examined Ra isotopes in Southern Ocean locations, but the scarce data suggest that as a whole the Southern Ocean displays low Ra activity, except for ^{226}Ra (Hanfland 2002) which decays much more slowly ($t_{1/2} = 1600$ years). Reported activities for ^{223}Ra and ^{224}Ra in coastal areas of the Antarctic Peninsula (Dulaiova *et al*. 2009) and Iles Crozet (Charette *et al*. 2007), as well as waters offshore of Iles Kerguelen (van Beek *et al*. 2008) are higher on average than those reported here, but the ranges overlap in all cases.

For coastal waters, the activities of short-lived Ra isotopes reported here are extremely low. Studies from the Iles Crozet and South Shetland Islands (Charette *et al*. 2007, Dulaiova *et al*. 2009) reported similar, very low ranges compared to locations outside the Southern Ocean. The South Atlantic Bight, for example, displays inshore Ra activities of 22.4 and 144 dpm m^{-3} ($^{223}Ra_{ex}$ and $^{224}Ra_{ex}$, respectively; Moore 2000a) - up to four orders of magnitude higher than those in Ryder Bay. However, even other Southern Ocean samples, when compared by distance from shore, have high activity compared to Ryder Bay. As such, the $^{223}Ra_{ex}$ and $^{224}Ra_{ex}$ activities in Ryder Bay are among the lowest reported for an inshore (< 5 km) setting.

Activities are especially low in the case of mid-Ryder Bay samples, where mean $^{223}Ra_{ex}$ was 0.023 dpm m^{-3}, and that of $^{224}Ra_{ex}$ was 0.76 dpm m^{-3}. Activity of $^{223}Ra_{ex}$ offshore from Iles Crozet is reported as 0.02–0.19 dpm m^{-3} (*c.* 12 km from shore; Charette *et al*. 2007), and the Ryder Bay values are in keeping with the lower limit of this range despite being significantly closer to shore. Low values of $^{224}Ra_{ex}$ were also observed in Southern Ocean surface waters: Dulaiova *et al*. (2009) reported $^{224}Ra_{ex}$ activities of 2–4 dpm m^{-3} above the continental shelf, while Drake Passage/ACC waters were found to contain no $^{224}Ra_{ex}$. The activities measured here for mid-Ryder Bay samples are in keeping with offshore waters, suggesting limited input from sediment-water interaction, coastal runoff or submarine groundwater discharge. Taken together, the activities of both short-lived Ra isotopes in central Ryder Bay suggest an open ocean source for surface waters, with slow diffusion of Ra enrichment derived from interfaces (sediment-water and land-water).

The distribution of ^{227}Ac is very different from that of short-lived Ra species. Actinium-227 is produced from decay of ^{231}Pa, which itself is produced from ^{235}U, an isotope with a near-uniform distribution throughout the global ocean. Upon production, ^{231}Pa is rapidly scavenged, and builds up in slowly-accumulating deep sea sediments (Geibert *et al*. 2002). Thus the deep sea is a major source for the more soluble ^{227}Ac which diffuses out of the sediment into the overlying bottom water. Geibert *et al*. (2002) showed that UCDW and LCDW can be distinguished based on their ^{227}Ac activities, with the deeper LCDW having higher activity. However, Shaw & Moore (2002) showed that in surface waters of the Southern Ocean, enrichment of ^{227}Ac can also be seen in continental shelf and coastal regions due to decay of terrigenous ^{235}U in shelf sediments: a global dataset of ^{227}Ac by delayed coincidence counting has demonstrated that ^{227}Ac is supplied to some extent by coastal environments (Geibert & Vöge 2008).

The ^{227}Ac values reported here, with the exception of station 7, show highest activities in mid-bay samples (0.37 ± 0.02 dpm m^{-3}). The higher activity at station 7 may be due to a glacial source with extremely high spatial and temporal variability, as is indicated by the Ra isotopes. However, since there is no definitive single explanation for the higher values at station 7, we restrict discussion of ^{227}Ac data to mid-bay stations. Most sites along the islands transect are within error of the mid-bay samples, and significant variations in ^{227}Ac activity would not be expected, as the very long half-life of ^{227}Ac (21.77 years) vastly exceeds the timescale relevant to circulation in Ryder Bay.

The mean mid-bay ^{227}Ac activity of 0.37 dpm m^{-3} is somewhat higher than those reported by Shaw & Moore (2002) for open Drake Passage surface waters (0.13–0.23 dpm m^{-3}), and even for on-shelf sites around the South Shetland Islands and South America (0.20–0.27 dpm m^{-3}). The greater activity may either reflect interaction with the continental shelf or slope, or ^{227}Ac-rich source waters. Geibert *et al*. (2002) studied ^{227}Ac with depth in the Weddell Gyre and Drake Passage, finding that UCDW was characterized by $^{227}Ac_{ex}$ activities of 0.2–0.4 dpm m^{-3} (equivalent to ^{227}Ac *c.* 0.43–0.75 dpm m^{-3}). Waters in the Drake Passage were found to have slightly lower activities, with surface water reported at 0.10–0.27 dpm m^{-3} (Shaw & Moore 2002) and UCDW (*c.* 500 m) ^{227}Ac activity measured as 0.37 dpm m^{-3} (supplemental data from Geibert *et al*. (2002); we compare ^{227}Ac activities rather than $^{227}Ac_{ex}$ to avoid introducing any uncertainty arising from an estimation of the ^{231}Pa correction for our data). The values measured in Ryder Bay, especially the mid-bay stations, are in better agreement with the ^{227}Ac of subsurface (500 m) Drake Passage waters than surface waters. Current understanding of regional circulation is that Marguerite Bay is subject to frequent but irregular incursions of UCDW at depth via Marguerite Trough (Martinson *et al*. 2008, Moffat *et al*. 2009), with CDW being the ultimate source of waters in Marguerite Bay and Ryder Bay. This water mixes up into the WW and AASW layers, with mixing expected to occur primarily in coastal and shallow regions (Wallace *et al*. 2008). Additionally, $\delta^{18}O$ data at station 5 indicates that $>96\%$ of the water at 15 m comes from CDW during the sampling period (Meredith *et al*. in press). The lack of enrichment in Ryder Bay ^{227}Ac relative to UCDW values indicates very little continental shelf input of ^{227}Ac.

However, ^{228}Ra is higher than expected for open-ocean UCDW, indicating some recent interaction of the water mass with sediments, which also has the potential to contribute some ^{227}Ac. Activity of ^{228}Ra for Antarctic Polar Front and ACC waters has been reported as 0.25–2 dpm m^{-3} (see Charette *et al*. 2007). Our measurements are an order of magnitude higher than these open water values, but consistent with surface waters near Iles Crozet (8.9–41 dpm m^{-3}; Charette *et al*. 2007) and in the Weddell Gyre (21–32 dpm m^{-3}; Rutgers van der Loeff 1994). Despite being higher than more oceanic regions, the activities measured here are still much lower than temperate coastal areas (e.g. 75–246 dpm m^{-3} in the South Atlantic Bight; Moore 2000a), suggesting relatively minor ^{228}Ra inputs relative to river-influenced locations.

The elevated ^{227}Ac and ^{228}Ra activities in Ryder Bay can be explained by a combination of the UCDW source water and modest interaction with the continental shelf or shelf-break. Indeed, the path of UCDW from the ACC onto the WAP shelf is consistent with a shelf-break or margin source, which has been proposed as a major contributor to oceanic micronutrient budgets (e.g. Jeandel *et al*. 2011). While ^{228}Ra indicates some continental shelf interaction, there is no observed enrichment in ^{227}Ac relative to offshore UCDW, which is as expected for a shelf setting. Relatively shallow depths (*c.* 500 m) allow for limited ^{231}Pa production, and a high rate of sediment accumulation on

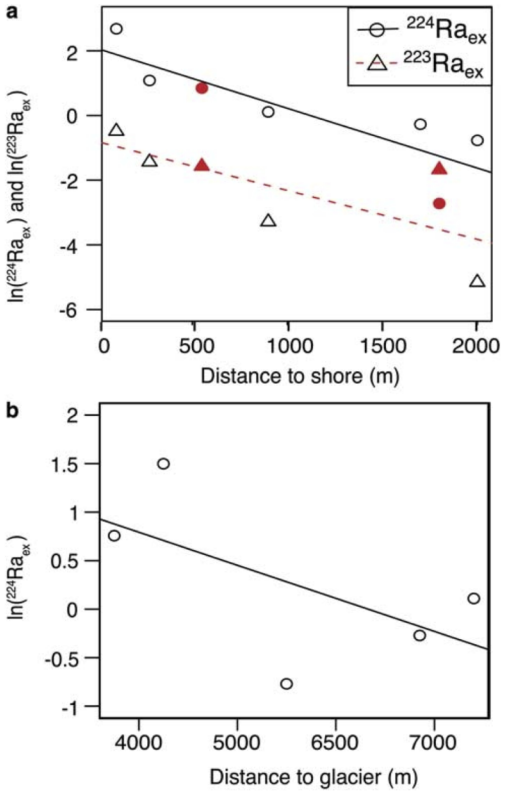

Fig. 4. a. Determination of effective eddy diffusivity coefficients (k_h) based on activity of $^{223}Ra_{ex}$ and $^{224}Ra_{ex}$ versus distance for the islands transect. Due to the semi-enclosed nature of Ryder Bay, distance was measured to nearest land (including the islands), to better reflect a source of Ra in sediments which would be present along the entire shoreline, rather than solely at a fixed point such as South Cove. Shown are all stations along the islands transect as well as station 5 (the Rothera Oceanographic and Biological Time Series site). Filled symbols are those stations nearest the Léonie Islands group (stations 8 and 9); stations 1–5 are shown as open symbols. **b.** Effective eddy diffusivity coefficients (k_h) from $^{224}Ra_{ex}$ for the glacier transect. Glacier transect distances are relative to a point on the edge of Sheldon Glacier (indicated in Fig. 1), included are stations 3–7.

the shelf will dilute ^{231}Pa in sediments, leading to low ^{227}Ac release. The ^{227}Ac activities also suggest negligible inputs from coastal or land sources. However, without depth profile samples it is not possible here to quantify ^{227}Ac from terrigenous sources versus UCDW. We suggest that future work assessing ^{227}Ac activities in deeper waters could aid in constraining the extent of UCDW incursions integrated over several years.

Mixing rates within Ryder Bay

Short-lived Ra isotopes have previously been used to estimate horizontal eddy diffusivity in other Southern Ocean waters (Charette *et al*. 2007). If the distribution of Ra can be described by diffusion, as opposed to advection, then a one-dimensional diffusion model can be used to calculate eddy diffusion coefficients (k_h) along an onshore-offshore transect, as developed by Moore (2000a). In this case, activity can be expressed according to the equation:

$$A_x = A_o \cdot e^{-x\sqrt{\lambda/k_h}}, \quad (3)$$

where A_x and A_o are the activities at distance x (from shore) and at the source ($x = 0$), respectively, and λ is the decay constant. From this equation, if $\ln(A_x)$ is plotted versus distance (x), the slope (m) can be expressed as follows:

$$m = \sqrt{\lambda/k_h}. \quad (4)$$

Thus the decay constant and slope from the $\ln(A_x)$ versus distance plot can be used to calculate k_h (Moore 2000a). This estimate of eddy diffusivity does not solely reflect eddy diffusion, and significant advection will result in a non-linear relationship, either concave (onshore advection) or convex (offshore) (see Dulaiova *et al*. 2009). Thus, provided the data display a reasonably linear fit, the k_h can be considered an "effective" horizontal eddy diffusion coefficient giving an estimate of offshore mixing (Charette *et al*. 2007). For transects from South Cove into central Ryder Bay, the k_h values determined for this study are $1.0\,m^2\,s^{-1}$ for $^{224}Ra_{ex}$ ($0.64\,m^2\,s^{-1}$ if island stations are included) and $0.13\,m^2\,s^{-1}$ for $^{223}Ra_{ex}$ ($0.31\,m^2\,s^{-1}$ if island stations are included; Fig. 4).

As Ryder Bay is enclosed on three sides, a simple diffusion model may be inadequate to represent the pattern of circulation in Ryder Bay, and the data here are unlikely to fulfil the assumption that activity decreases to zero at some distance. However, while there are significant potential caveats in the determination of k_h here, the semi-enclosed nature of Ryder Bay should contribute to higher Ra activities in mid-bay stations than if the only Ra source was a point source (i.e. station 1), which would result in the calculated mixing rates being overestimates. As a result, the overall magnitude of mixing suggested here ($\leq 1.0\,m^2\,s^{-1}$) is worthy of note.

This range of eddy coefficients from the islands transect ($0.13–1.0\,m^2\,s^{-1}$) is much lower than the $6.6–39\,m^2\,s^{-1}$ range estimated by Charette *et al*. (2007). Both of these k_h estimates are extremely low in comparison to those estimated for other coastal regions (e.g. $360–420\,m^2\,s^{-1}$ for the South Atlantic Bight; Moore 2000a) including the northern Antarctic Peninsula ($596–63\,000\,m^2\,s^{-1}$; Dulaiova *et al*. 2009). This strongly supports very slow diffusion from the margins to the centre of the bay, implying that mid-bay waters are sourced predominantly from more open ocean or

deep waters, with very little influence from land-water exchange. Any sedimentary source of micronutrients (e.g. iron), would thus be expected to be very low in central Ryder Bay, and probably Marguerite Bay as well, and to occur via sediment-water interaction before the modified UCDW enters Ryder Bay. However, as noted above, ^{228}Ra is higher than in open ocean surface waters, and the longer $t_{1/2}$ reflects the longer timescale of the postulated sediment interaction. This interaction is probably on the order of several months to several years before the water enters Ryder Bay, while the very low short-lived Ra isotope activities reflect little or no input on the scale of one week to one month.

In addition to mixing rates, short-lived Ra measurements can also be used to estimate the length of time a water parcel has been isolated from the Ra source. Ratios of $^{224}Ra_{ex}$:^{228}Ra were used to estimate ages in mid-bay samples, following Moore (2000b) and Dulaiova *et al*. (2009). Taking the activity ratio at station 1 as the source end-member, stations 3–5 display Ra ages of 13, 14 and 18 days, respectively. The very low rates of horizontal transport determined above are consistent with these age estimates, as studies in other regions have found younger ages for water much farther offshore (e.g. Ra age of approximately seven days up to 150 km offshore; Dulaiova *et al.* 2009).

Similar evaluation of k_h was performed for the glacier transect. As Sheldon Glacier terminates over a large area at the northern end of Ryder Bay, distances were measured from an arbitrarily chosen point on the nearest ice-edge (shown in Fig. 1). As the calculation for k_h depends on the slope of the plot versus x, only relative distances are taken into account, such that the absolute distance between source and sample does not affect the estimated k_h. Due to the two values bdl for $^{223}Ra_{ex}$, only $^{224}Ra_{ex}$ activity was used to assess k_h, giving an estimate of 18 $m^2 s^{-1}$ for mixing between the area around Sheldon Glacier and mid-Ryder Bay (Fig. 4). In agreement, ages derived using station 7 ratios as a source (0.5 and 8 days, for stations 6 and 5, respectively), are considerably lower than those calculated for sediment sources. That the k_h estimate for glacial mixing is an order of magnitude greater than the estimates for the islands transect may reflect the nature of the underlying dispersive processes. If the enrichment signal derives from glacial meltwater as postulated, this would be present in a shallow freshwater lens at the surface. This water could be differentially affected by processes that induce horizontal mixing at the surface (potentially atmospherically-forced; i.e. wind, inertial currents etc.), in addition to overall horizontal mixing occurring in the water column. This may potentially account for the faster effective horizontal diffusivity of a glacier-derived signal compared to that from sediments.

Previous studies have combined estimates of k_h with ^{228}Ra gradients to estimate offshore fluxes of ^{228}Ra (see Dulaiova *et al*. 2009). Following this approach, we used the islands transect stations, plus the RaTS site, to assess the gradient of ^{228}Ra away from shore in Ryder Bay, which gave a slope of 0.61 ± 2.0 dpm m^{-3} km^{-1}. There was considerable scatter in the data and the r^2 value for the regression (^{228}Ra vs distance to nearest land) was very low (0.18). To obtain an upper estimate for ^{228}Ra flux, we used an upper limit of the ^{228}Ra-gradient slope plus error (2.6 dpm m^{-3} km^{-1}) multiplied by the highest value estimated for k_h (1.0 m^{-2} s^{-1}; from $^{224}Ra_{ex}$ data along this transect), which gives a ^{228}Ra flux of 230 dpm m^{-2} d^{-1}. While there is a high degree of uncertainty in this calculation, reflected in the standard error of the slope, the magnitude of this upper ^{228}Ra flux estimate is relatively low compared to other Southern Ocean locations. For example, the ^{228}Ra flux calculated by Charette *et al*. (2007) around Iles Crozet is 1630–9660 dpm m^{-2} d^{-1}. The estimate for Livingston Island (South Shetland Islands) is 31 900 dpm m^{-2} d^{-1}, although the estimate for Elephant Island (South Shetland Islands) is very low (15.8 dpm m^{-2} d^{-1}, Dulaiova *et al.* 2009). We suggest that location plays a large role in determining fluxes: low values are found in Ryder Bay (coastal Antarctic), high values near Iles Crozet (sub-Antarctic islands), and the large range of the Dulaiova *et al*. (2009) study at the northern tip of the western Antarctic Peninsula may include regions with both Antarctic and sub-Antarctic characteristics. Our analysis shows that land-ocean inputs are low in the Antarctic environment, and as such ice-ocean fluxes may dominate in these regions.

Analysis by Cochran & Krishnaswami (1980) determined that bioturbation is the dominant process contributing to sedimentary ^{228}Ra flux, and as such our very low upper estimate of ^{228}Ra flux may indicate a relatively low amount of bioturbation in Ryder Bay and/or the sediments underlying the path of water entering Ryder Bay. Marine surveys around Rothera Research Station report high abundances of benthic organisms and largely bare rock substrates (Smale *et al*. 2008). Thus, it is more probable that the low Ryder Bay fluxes reflect comparatively low amounts of sediments in shallow (mixed-layer) waters, as opposed to scarcity of bioturbating organisms. Frequent scouring by icebergs, as is the case in shallow waters of Ryder Bay (Smale *et al*. 2008), or the very steep sides of the bay, may also contribute to low amounts of sediment.

Conclusions

Here we present short-lived Ra isotope activities in a shallow embayment on the western Antarctic Peninsula, and the activities of their progenitor isotopes. These measurements are the most southerly to date. The activities of both $^{223}Ra_{ex}$ and $^{224}Ra_{ex}$ were low compared to other coastal Southern Ocean locations, and extremely low compared to those reported for low latitude regions.

Waters near Sheldon Glacier show a clear enrichment signal in $^{223}Ra_{ex}$, $^{224}Ra_{ex}$, and ^{228}Ra. Although seawater-sediment interaction underneath the ice is also a potential source for this enrichment, material entrained within the ice itself is a more likely source, as other studies have found.

The mid-bay activities resemble relatively open water, indicating very little interaction with sediment-water or land-water interfaces, although elevated ^{228}Ra indicates some continental shelf influence over timescales on the order of several months to years. The high activities of ^{227}Ac reflect that the ultimate source for Ryder Bay surface waters is UCDW, which is known to intrude onto the WAP shelf episodically.

Horizontal mixing rates between mid-bay and shore waters are significantly slower than those reported for other coastal areas, consistent with relatively high Ra ages for such an environment. Given the slow mixing rates and extremely low short-lived Ra activities for a relatively shallow coastal environment, sediment interaction and coastal runoff are therefore not likely to be a major source of micronutrients to Ryder Bay. The mixing rate estimate for glacial to mid-bay waters, however, is more than an order of magnitude greater than those for non-glacial samples, indicating that glacially influenced waters represent a more dispersive source of terrestrial material (and any associated micronutrients) in coastal areas.

Acknowledgements

The authors would like to thank the Rothera Research Station marine staff, in particular Danny Edmunds, for help with sample collection, and the British Antarctic Survey for logistical support. Jan Scholten at the International Atomic Energy Agency in Monaco kindly provided standards, and helpful discussion regarding methodology. The editor (L. Padman) and two anonymous reviewers provided valuable comments to improve the manuscript. This work was supported by an Antarctic Science Bursary, Collaborative Gearing Scheme funding (through the National Environment Research Council, UK), the British Council-EGIDE ALLIANCE/Franco-British Research Partnership Programme, an NSERC scholarship and the University of Edinburgh.

References

Charette, M.A., Buesseler, K.O. & Andrews, J.E. 2001. Utility of radium isotopes for evaluating the input and transport groundwater-derived nitrogen to a Cape Cod estuary. *Limnology and Oceanography*, **46**, 465–470.

Charette, M.A., Gonneea, M.E., Morris, P.J., Statham, P., Fones, G., Planquette, H., Salter, I. & Garabato, A.N. 2007. Radium isotopes as tracers of iron sources fuelling a Southern Ocean phytoplankton bloom. *Deep-Sea Research II*, **54**, 1989–1998.

Clarke, A., Meredith, M.P., Wallace, M.I., Brandon, M.A. & Thomas, D.N. 2008. Seasonal and interannual variability in temperature, chlorophyll and macronutrients in northern Marguerite Bay, Antarctica. *Deep-Sea Research II*, **55**, 1988–2006.

Cochran, J.K. & Krishnaswami, S. 1980. Radium, thorium, uranium and ^{210}Pb in deep-sea sediments and sediment pore waters from the north equatorial Pacific. *American Journal of Science*, **280**, 849–889.

Cook, A.J., Fox, A.J., Vaughan, D.G. & Ferrigno, J.G. 2005. Retreating glacier fronts on the Antarctic Peninsula over the past half-century. *Science*, **308**, 541–544.

Dimova, N., Dulaiova, H., Kim, G. & Burnett, W.C. 2008. Uncertainties in the preparation of ^{224}Ra Mn fiber standards. *Marine Chemistry*, **109**, 220–225.

Dulaiova, H., Ardelan, M.V., Henderson, P.B. & Charette, M.A. 2009. Shelf-derived iron inputs drive biological productivity in the southern Drake Passage. *Global Biogeochemical Cycles*, 10.1029/2008GB003406.

Garcia-Solsona, E., Garcia-Orellana, J., Masqué, P. & Dulaiova, H. 2008. Uncertainties associated with ^{223}Ra and ^{224}Ra measurements in water via a Delayed Coincidence Counter (RaDeCC). *Marine Chemistry*, **109**, 198–219.

Geibert, W. & Vöge, I. 2008. Progress in the determination of ^{227}Ac in sea water. *Marine Chemistry*, **109**, 238–249.

Geibert, W., Rutgers van der Loeff, M.M., Hanfland, C. & Dauelsberg, H.-J. 2002. Actinium-227 as a deep-sea tracer: sources, distribution and applications. *Earth and Planetary Science Letters*, **198**, 147–165.

Hanfland, C. 2002. *Radium-226 and radium-228 in the Atlantic sector of the Southern Ocean*. PhD thesis, University of Bremen, 135 pp.

Hoffmann, L.J., Peeken, I. & Lochte, K. 2008. Iron, silicate, and light co-limitation of three Southern Ocean diatom species. *Polar Biology*, **31**, 1067–1080.

Howard, S.L., Hyatt, J. & Padman, L. 2004. Mixing in the pycnocline over the western Antarctic Peninsula shelf during Southern Ocean GLOBEC. *Deep-Sea Research II*, **51**, 1965–1979.

Jeandel, C., Peucker-Ehrenbrink, B., Jones, M.T., Pearce, C.R., Oelkers, E.H., Godderis, Y., Lacan, F., Aumont, O. & Arsouze, T. 2011. Ocean margins: the missing term in oceanic element budgets? *Eos Transactions*, **92**, 217–224.

Klinck, J. 1998. Heat and salt changes on the continental shelf west of the Antarctic Peninsula between January 1993 and January 1994. *Journal of Geophysical Research*, **103**, 7617–7636.

Martinson, D.G., Stammerjohn, S.E., Iannuzzi, R.A., Smith, R.C. & Vernet, M. 2008. Western Antarctic Peninsula physical oceanography and spatio-temporal variability. *Deep-Sea Research II*, **55**, 1964–1987.

Meredith, M.P. & King, J.C. 2005. Rapid climate change in the ocean west of the Antarctic Peninsula during the second half of the 20th century. *Geophysical Research Letters*, 10.1029/2005GL024042.

Meredith, M.P., Venables, H.J., Clarke, A., Ducklow, H.J., Erickson, M., Leng, M.J., Lenaerts, J.T.M. & van den Broeke, M.R. In press. The freshwater system west of the Antarctic Peninsula: spatial and temporal changes. *Journal of Climate*.

Meredith, M.P., Wallace, M.I., Stammerjohn, S.E., Renfrew, I.A., Clarke, A., Venables, H.J., Shoosmith, D.R., Souster, T. & Leng, M.J. 2010. Changes in the freshwater composition of the upper ocean west of the Antarctic Peninsula during the first decade of the 21st century. *Progress in Oceanography*, **87**, 127–143.

Moffat, C., Owens, B. & Beardsley, R.C. 2009. On the characteristics of Circumpolar Deep Water intrusions to the west Antarctic Peninsula continental shelf. *Journal of Geophysical Research*, 10.1029/2008JC004955.

Moffat, C., Beardsley, R.C., Owens, B. & van Lipzig, N. 2008. A first description of the Antarctic Peninsula coastal current. *Deep-Sea Research II*, **55**, 277–293.

Montes-Hugo, M., Doney, S.C., Ducklow, H.W., Fraser, W., Martinson, D., Stammerjohn, S.E. & Schofield, O. 2009. Recent changes in phytoplankton communities associated with rapid regional climate change along the western Antarctic Peninsula. *Science*, **323**, 1470–1473.

Moore, W.S. 2000a. Determining coastal mixing rates using radium isotopes. *Continental Shelf Research*, **20**, 1993–2007.

Moore, W.S. 2000b. Ages of continental shelf waters determined from ^{223}Ra and ^{224}Ra. *Journal of Geophysical Research*, **105**, 22 117–22 122.

Moore, W.S. 2008. Fifteen years experience in measuring ^{224}Ra and ^{223}Ra by delayed-coincidence counting. *Marine Chemistry*, **109**, 188–197.

Moore, W.S. & Arnold, R. 1996. Measurement of ^{223}Ra and ^{224}Ra in coastal waters using a delayed coincidence counter. *Journal of Geophysical Research*, **101**, 1321–1329.

PRITCHARD, H.D., LIGTENBERG, S.R.M., FRICKER, H.A., VAUGHAN, D.G., VAN DEN BROEKE, M.R. & PADMAN, L. 2012. Antarctic ice sheet loss driven by basal melting of ice shelves. *Nature*, **484**, 502–505.

RAISWELL, R. 2011. Iceberg-hosted nanoparticulate Fe in the Southern Ocean mineralogy, origin, dissolution kinetics and source of bioavailable Fe. *Deep-Sea Research II*, **58**, 1364–1375.

RUTGERS VAN DER LOEFF, M.M. 1994. ^{228}Ra and ^{228}Th in the Weddell Sea. *In* JOHANNESSEN, O.M., MUENCH, R.D. & OVERLAND, J.E., *eds. The polar oceans and their role in shaping the global environment.* The Nansen centennial volume. *Geophysical Monograph Series*, **85**, 177–186.

SCHOLTEN, J.C., PHAM, M.K., BLINOVA, O., CHARETTE, M.A., DULAIOVA, H. & ERIKSSON, M. 2010. Preparation of Mn-fiber standards for the efficiency calibration of the delayed coincidence counting system (RaDeCC). *Marine Chemistry*, **121**, 206–214.

SHAW, T.J. & MOORE, W.S. 2002. Analysis of ^{227}Ac in seawater by delayed coincidence counting. *Marine Chemistry*, **78**, 197–203.

SHAW, T.J., RAISWELL, R., HEXEL, C.R., VU, H.P., MOORE, W.S., DUDGEON, R. & SMITH, K.L. 2011. Input, composition, and potential impact of terrigenous material from free-drifting icebergs in the Weddell Sea. *Deep-Sea Research II*, **58**, 1376–1383.

SMALE, D.A., BARNES, D.K.A., FRASER, K.P.P. & PECK, L.S. 2008. Benthic community response to iceberg scouring at an intensely disturbed shallow water site at Adelaide Island, Antarctica. *Marine Ecology Progress Series*, **355**, 85–94.

STAMMERJOHN, S.E., MARTINSON, D.G., SMITH, R.C., YUAN, X. & RIND, D. 2008. Trends in Antarctic annual sea ice retreat and advance and their relation to El Niño–Southern Oscillation and Southern Annular Mode variability. *Journal of Geophysical Research*, 10.1029/2007JC004269.

VAN BEEK, P., SOUHAUT, M. & REYSS, J.-L. 2010. Measuring the radium quartet (^{226}Ra, ^{228}Ra, ^{224}Ra, ^{223}Ra) in water samples using gamma spectrometry. *Journal of Environmental Radioactivity*, **101**, 521–529.

VAN BEEK, P., BOURQUIN, M., REYSS, J-L., SOUHAUT, M., CHARETTE, M.A. & JEANDEL, C. 2008. Radium isotopes to investigate the water mass pathways on the Kerguelen Plateau (Southern Ocean). *Deep-Sea Research II*, **55**, 622–637.

VAN BEEK, P., SOUHAUT, M., LANSARD, B., BOURQUIN, M., REYSS, J-L., JEAN, P. & VON BALLMOOS, P. In press. LAFARA: A new underground laboratory in the French Pyrénées for ultra low-level gamma-ray spectrometry. *Journal of Environmental Radioactivity*.

VAUGHAN, D.G., MARSHALL, G.J., CONNOLLEY, W.M., PARKINSON, C., MULVANEY, R., HODGSON, D.A., KING, J.C., PUDSEY, C.J. & TURNER, J. 2003. Recent rapid regional climate warming on the Antarctic Peninsula. *Climatic Change*, **60**, 243–274.

VENABLES, H.J., CLARKE, A. & MEREDITH, M.P. In press. Wintertime controls on summer stratification and productivity at the western Antarctic Peninsula. *Limnology and Oceanography*.

WALLACE, M.I., MEREDITH, M.P., BRANDON, M.A., SHERWIN, T.J., DALE, A. & CLARKE, A. 2008. On the characteristics of internal tides and coastal upwelling behaviour in Marguerite Bay, west Antarctic Peninsula. *Deep-Sea Research II*, **55**, 2023–2040.